UNIVERSITY OF CALIFORNIA, SAN DIEGO

The Physiological Basis of BOLD Functional MRI

A dissertation submitted in partial satisfaction of the requirements for the degree of Doctor of Philosophy

in

Bioengineering with a Specialization in Multi-Scale Biology

by

Valerie Ewing McClintock Griffeth

Committee in charge:

Professor Gabriel Silva, Chair
Professor Richard Buxton, Co-Chair
Professor James Brewer
Professor David Dubowitz
Professor Andrew McCulloch

2013

The Dissertation of Valerie Ewing McClintock Griffeth is approved, and it is acceptable in quality and form for publication on microfilm and electronically:

_____

_____

_____

_____
Co-Chair

_____
Chair

University of California, San Diego

2013

DEDICATION

For Mimi, an inspiration and the great oak of our family.

EPIGRAPH

"We live on an island surrounded by a sea
of ignorance. As our island of knowledge
grows, so does the shore of our ignorance."

John Archibald Wheeler

"Careful. We don't want to learn anything from this."

Bill Watterson

TABLE OF CONTENTS

LIST OF ABBREVIATIONS

ASE	Asymmetric spin echo
ASL	Arterial spin labeling,
BCP	BOLD constrained perfusion
BOLD	Blood oxygenation level dependent
CASL	Continuous arterial spin labeling
CBF	Cerebral blood flow
CBV	Cerebral blood volume
CBVv	Venous cerebral blood volume
$CMRO_2$	Cerebral metabolic rate of oxygen metabolism
DBM	Detailed biophysical model of the BOLD response
fMRI	Functional magnetic resonance imaging
GCM	Generalized calibration model
GLM	General linear model
GRE	Gradient recalled echo
Hct	Hematocrit,
MEG	Magnetoencephalography
OEF	Oxygen extraction fraction
$P_{a/v}O_2$	Arterial/venous partial pressure of oxygen
PASL	Pulsed arterial spin labeling
PCASL	Pseudo-continuous arterial spin labeling
PET	Positron emission tomography
$P_{ET}O_2/CO_2$	Partial end-tidal pressure of oxygen/carbon dioxide
SaO_2	Arterial hemoglobin saturation
SvO_2	Venous hemoglobin saturation
TE	Echo time
TRUST	T_2-relaxation under spin tagging
VASO	Vascular space occupancy
VERVE	Venous refocusing for volume estimation

LIST OF SYMBOLS

A	Scaling parameter of the heuristic model
α	Davis model parameter
α_T	Grubb's exponent relating the total CBV change to the CBF change
α_v	Exponent relating the venous CBV change to the CBF change
β	Davis model parameter
$\Delta\chi$	Magnetic field susceptibility of fully deoxygenated blood
[dHb]	Blood concentration of deoxyhemoglobin
$\langle \mathrm{dHb} \rangle$	Content of deoxyhemoglobin in a voxel
E_0	Baseline oxygen extraction fraction
$\varepsilon_{a,c,v}$	Baseline intravascular (arterial/capillary/venous) to tissue signal ratio
f	CBF normalized to baseline
Hct	Hematocrit
λ	Intravascular to extravascular spin density ratio
M	Scaling parameter of the Davis model
σ	Fraction of arteriolar blood reflecting venous saturation
ϕ_T	Exponent relating the total CBV change to CBF change in the DBM
ϕ_v	Exponent relating the venous CBV change to CBF change in the DBM
n	Ratio of fractional changes in CBF to $CMRO_2$
r	$CMRO_2$ normalized to baseline
R_2^*	Signal decay rate
V_I	Total CBV fraction
$\omega_{A/a/v}$	Arterial/arteriolar/venous fraction of baseline CBV
Y_{off}	Hemoglobin saturation producing equal blood-tissue susceptibility

LIST OF FIGURES

LIST OF TABLES

ACKNOWLEDGEMENTS

I would like to thank Dr. Richard Buxton for the many hours we spent discussing how to make functional MRI into a clinical tool able to make quantitative measurements in patient populations. His guidance has been invaluable on many drafts of papers and fellowship grants, and his perspective on offering dissenting opinion without alienating readers has been of immeasurable importance. I am grateful to him for making the last five years so enjoyable that I never wanted to leave. Without his tireless enthusiasm and passion for research, I already would have graduated from medical school.

I would also like to acknowledge Aaron Simon, Nicholas Blockley, Farshad Moradi and David Dubowitz for their numerous and thoughtful suggestions for improving my experiments, data analysis and manuscripts. Finally, I would like to acknowledge everyone at the UCSD Keck Center for fMRI for not giving away my desk when I would disappear for weeks at a time.

Chapter 1, in full, is a reprint of the material as it appears in Neuroimage 2011. Griffeth, VEM and Buxton, RB (2011). A theoretical framework for estimating cerebral oxygen metabolism changes using the calibrated-BOLD method: Modeling the effects of blood volume distribution, hematocrit, oxygen extraction fraction, and tissue signal properties on the BOLD signal. Neuroimage 58: 198-212. The dissertation author was the primary investigator and author of this paper.

Chapter 2, in full, has been submitted for publication and is the material as it may appear in PLoS ONE 2013. Griffeth, VEM and Buxton, RB (2013). A new functional MRI approach for investigating modulations of brain oxygen metabolism. PLoS ONE. The dissertation author was the primary investigator and author of this paper.

Chapter 3, in full, is a reprint of the material as it appears in Neuroimage 2011. Griffeth, VEM and Buxton, RB (2011). Prospects for quantitative fMRI: investigating the effects of caffeine on baseline oxygen metabolism and the response to a visual stimulus in humans. Neuroimage 57: 809-816. The dissertation author was the primary investigator and author of this paper.

Chapter 4, in part, is currently being prepared for submission for publication of the material. Griffeth VEM, Simon AB, Buxton RB. Effect of watching a complex movie on blood flow and oxygen metabolism coupling as well as fMRI signal variability in the human visual cortex. The dissertation author is the primary investigator and author of this material.

Chapter 5, Section A, in full, is a reprint of material as it appears in NMR Biomed 2012. Blockley, NP, VEM Griffeth, Simon AB, Buxton RB (2012). A review of calibrated blood oxygenation level-dependent (BOLD) methods for the measurement of task-induced changes in brain oxygen metabolism. NMR Biomed. The dissertation author was a supporting investigator and author of this material.

Chapter 5, Section B, in full, is a reprint of material as it appears in Neuroimage 2012. Blockley, NP, VEM Griffeth, Buxton RB (2012). A general analysis of calibrated BOLD methodology for measuring $CMRO_2$ responses: comparison of a new approach with existing methods. Neuroimage 60: 279-89. The dissertation author was a supporting investigator and author of this material.

Chapter 5, Section C, in full, is a reprint of material as it appears in Neuroimage 2013. Blockley NP, Griffeth VEM, Germuska MA, Bulte DP, Buxton RB. (2013). An analysis of the use of hyperoxia for measuring venous cerebral blood volume: Comparison of the existing

method with a new analysis approach. Neuroimage 72: 33-40. The dissertation author was a supporting investigator and author of this material.

Chapter 5, Section D, in full, is a reprint of material as it appears in PLoS ONE 2013. Simon AB**,** Griffeth VEM, Wong EC, Buxton RB (2013). A novel method of combining blood oxygenation and blood flow sensitive magnetic resonance imaging techniques to measure the cerebral blood flow and oxygen metabolism responses to an unknown neural stimulus. PLoS ONE 8: e54816. The dissertation author was a supporting investigator and author of this material.

VITA

2004	Bachelor of Arts, Vassar College
2013	Doctor of Philosophy, University of California, San Diego
2015	Doctor of Medicine, University of California, San Diego

PUBLICATIONS

Griffeth, V.E., Perthen, J.E., Buxton, R.B. Prospects for quantitative fMRI: investigating the effects of caffeine on baseline oxygen metabolism and the response to a visual stimulus in humans. Neuroimage, 2011. 57(3):809-16.

Griffeth, V.E. and Buxton, R.B. A theoretical framework for estimating cerebral oxygen metabolism changes using the calibrated-BOLD method: Modeling the effects of blood volume distribution, hematocrit, oxygen extraction fraction, and tissue signal properties on the BOLD signal. Neuroimage, 2011. 58(1): 198-212.

Blockley, N. P., V. E. Griffeth, Simon, A.B., and Buxton, R.B. "A review of calibrated blood oxygenation level-dependent (BOLD) methods for the measurement of task-induced changes in brain oxygen metabolism." NMR Biomed, 2012.

Blockley, N.P., V.E. Griffeth, and Buxton, R.B. A general analysis of calibrated BOLD methodology for measuring $CMRO_2$ responses: comparison of a new approach with existing methods. Neuroimage, 2012. 60(1): 279-89.

Blockley, N.P., Griffeth, V.E., Germuska, M.A., Bulte, D.P., Buxton, R.B. An analysis of the use of hyperoxia for measuring venous cerebral blood volume: Comparison of the existing method with a new analysis approach. Neuroimage, 2013. 72C:33-40.

Simon, A.B., Griffeth, V.E., Wong, E.C., Buxton, R.B. A novel method of combining blood oxygenation and blood flow sensitive magnetic resonance imaging techniques to measure the cerebral blood flow and oxygen metabolism responses to an unknown neural stimulus. PLoS One, 2013. 8(1):e54816.

Griffeth, V.E., Blockley, N.P., Simon, A.B. and Buxton, R.B. (in press). A simplified model for the blood oxygenation level dependent (BOLD) effect for estimating brain oxygen metabolism changes. PLOS Biology.

FIELDS OF STUDY

Major field: Bioengineering (Specialization in Multi-Scale Biology)

Studies in Functional MRI
Professor Richard Buxton

Studies in Exercise Physiology
Professor Susan Hopkins

ABSTRACT OF THE DISSERTATION

The Physiological Basis of BOLD Functional MRI

by

Valerie Ewing McClintock Griffeth

Doctor of Philosophy in Bioengineering with a Specialization in Multi-Scale Biology

University of California, San Diego, 2013

Professor Gabriel Silva, Chair
Professor Richard Buxton, Co-Chair

Functional magnetic resonance imaging (fMRI) is an exciting technology, and researchers have used it to give us beautiful maps of the brain performing a multitude of tasks. A non-invasive tool that can be safely applied in humans, fMRI also has the potential to go beyond a simple mapping tool by providing insight into the physiology underlying neural activity, particularly the cerebral metabolic rate of oxygen ($CMRO_2$), which is an indicator of the underlying neural activity. The blood oxygenation level dependent (BOLD) signal is the main fMRI signal, but a major concern with BOLD is the inability to quantitatively relate it to underlying physiological changes. This is because the BOLD signal depends not only on oxygen metabolism changes but also on cerebral blood flow (CBF) and the baseline state of the brain. However by performing simultaneous measurements of CBF and BOLD in response to a

stimulus and also in response to inhaled CO_2 for calibration, quantitative measurements of $CMRO_2$ can be made using a simple mathematical model to relate the data. One measure commonly reported is the ratio of the CBF change to the $CMRO_2$ change, commonly known as the CBF-$CMRO_2$ coupling parameter, *n*. In this work, I explore the physiological basis of the BOLD signal *in situ* by developing a detailed biophysical model of the BOLD signal and optimizing the simple mathematical model used for data analysis. I also present a new heuristic model of the BOLD signal that suggests a new, straightforward "ratio" method for the analysis of combined BOLD and CBF measurements.

I applied the optimized simple model to study the effects of caffeine on the physiological response of the brain to a visual stimulus and found that caffeine increases the absolute $CMRO_2$ change to the same stimulus by 61% suggesting increased neuronal excitability. Using the detailed biophysical method, I also demonstrate that the ratio method accurately determines when CBF-$CMRO_2$ coupling in response to a stimulus differs between two stimuli using only the measured BOLD and CBF signals. Finally I demonstrate a new method for BOLD calibration that is more reliable than the inhaled CO_2 method.

INTRODUCTION

Importance of the problem: Accurately interpreting BOLD fMRI

Functional magnetic resonance imaging (fMRI) has had wide ranging impact on modern science in fields as diverse as medicine, neuroscience, psychology, and economics. Extraordinary pictures of brain activity produced by this technique have provided neurosurgeons with the ability to avoid functionally important areas of the brain during operations to remove tumors [1] while also producing fascinating insights, such as the conclusion that the brain processes social pain in a similar manner as physical pain [2]. However use of fMRI has been limited to mapping neural activity, while wider application of the technique has been hindered by the inability to precisely quantify signal changes in a physiological manner. So while the scientific literature on fMRI using the blood oxygenation level-dependent (BOLD) signal is growing rapidly, there remain difficulties in interpreting this complex signal. For this reason, the full potential of fMRI as a probe of altered brain function in disorders or in response to drugs has not been realized.

The problem of interpreting the BOLD response in fMRI studies

A major concern with fMRI is the inability to quantitatively relate the BOLD signal to the underlying physiological changes. The BOLD signal results from changes in local deoxyhemoglobin content [3], and so depends on the relative changes in cerebral blood flow (CBF), cerebral blood volume (CBV) and the cerebral metabolic rate of oxygen ($CMRO_2$), and on the baseline metabolic state. This complexity of the signal leads to a fundamental problem in interpreting the magnitude of the BOLD response: for example, what does it mean if the magnitude of the BOLD response in the visual cortex is unchanged after an intervention such as caffeine? Does this mean caffeine does not change the neurological response to a visual

stimulus or is it that the BOLD response does not detect the combined changes of CBF and $CMRO_2$? Because of this complexity, BOLD fMRI has had limited clinical applications to date, confined instead to mapping where CBF changes. While the complex sensitivity of the BOLD signal to CBF and $CMRO_2$ creates difficulty in interpretation, it also offers the possibility of calculating changes in $CMRO_2$ from combined BOLD and CBF measurements. This quantitative fMRI approach offers the potential to broaden fMRI from a mapping tool into a true probe of brain function in health and disease.

Improving scientific knowledge: Significance of $CMRO_2$

Using changes in the BOLD signal as a gauge of changes in neural activity has often been proposed, but this correlation is not straightforward. Similarly one cannot simply interpret the BOLD response as a reflection of CBF, because it is strongly modulated by the $CMRO_2$ response. An additional complication is that different aspects of neural activity may separately drive changes in CBF and $CMRO_2$. Still, fluctuations in $CMRO_2$ likely provide a much more accurate reflection of neural activity than changes in CBF or the BOLD signal alone since aerobic metabolism of glucose is the primary metabolic fuel for energy production in the human brain [4]. Recent research has shown that changes in $CMRO_2$ are expected to reflect the underlying energy requirement of evoked neural activity [5], which is primarily the energy cost of pumping ions against their gradient at neuronal synapses [6,7]. The ability to accurately and non-invasively measure $CMRO_2$ is of importance as changes in cerebral metabolism have been associated with many common illnesses such as stroke, Alzheimer's Disease, Parkinson's disease, schizophrenia [8,9], depression [10], obsessive compulsive disorder [11], bipolar disorder [12,13], and alcohol abuse [14]. Therefore by improving our ability to non-invasively determine $CMRO_2$ dynamics, we may also unlock the ability to greatly expand our knowledge of these diseases and our ability to treat them.

A new research paradigm: Quantitative fMRI

In most fMRI experiments, the BOLD signal is not absolutely quantifiable and is relative to the baseline state of the brain. This creates difficulty when comparing the BOLD signal between conditions in which the baseline state changes, which may occur as the result of disease [15] or due to administration of a drug such as caffeine [16,17] or acetazolamide [18]. The relative and complex nature of the BOLD signal has limited the application of this technique to qualitative mapping of changes in blood oxygenation, while determining how neural activity changes between different conditions has been much more difficult to achieve reliably. The dual-echo spiral arterial spin labeling (ASL) pulse sequence [19] quantifies the BOLD signal by allowing direct measurement of the absolute transverse relaxation rate (R_2^*), which is the physical parameter underlying the BOLD effect. Simultaneously, this pulse sequence also provides absolute measurements of CBF thereby permitting examination of changes in both the baseline state and evoked responses. By combining these simultaneous measurements of BOLD and CBF, the calibrated-BOLD experiment permits calculation of $CMRO_2$ and quantitative comparisons of activation changes. The utility of this approach to studies of drugs and disease has been shown previously [16,18,20]. Here we will further the applications of quantitative BOLD fMRI through detailed modeling of the BOLD signal, by proposing new acquisition methods and analysis techniques, and finally by applying these advances to studies on the effects of caffeine and simple versus complex visual stimuli on the coupling of CBF and $CMRO_2$.

Conceptual changes: Tools for Quantitative fMRI

The sensitivity of the BOLD signal to CBF, CBV, and $CMRO_2$ creates some difficulty in interpreting the signal, but it also offers the possibility of estimating changes in $CMRO_2$ when measurements of BOLD and CBF are combined. The calibrated-BOLD approach

proposed by Davis et al. [21] does just this with the goal of estimating the $CMRO_2$ change during brain activation; it combines measurements of BOLD and CBF responses to activation and hypercapnia while approximating CBV from CBF by a power-law relationship [22]. Yet the Davis model has been routinely criticized as being oversimplified.

Results summary

In my first three years of graduate work I developed a detailed biophysical model of the BOLD response (DBM) to address criticisms of the Davis model, examine how inaccurate this simple model could be under various conditions, and suggest possible improvements in order to make calculations of $CMRO_2$ changes more accurate. Although we found that in most cases the Davis model is quite accurate, we were able to make minor improvements by optimizing the two associated parameters, α and β [17]. This change improved the ability of the Davis model to estimate changes in $CMRO_2$ while maintaining the same mathematical form of the model. These refinements had little impact in typical regions of CBF-$CMRO_2$ coupling, but significant impact on $CMRO_2$ estimates associated with when changes in CBF and $CMRO_2$ occur in opposite directions.

I used this improved Davis model to analyze the effects of caffeine on the BOLD response. Although the BOLD response to a visual stimulus was not significantly altered by caffeine, the more detailed measurements with the combined ASL/BOLD acquisition showed that there were large underlying changes in both the baseline state and in the $CMRO_2$ response to the stimulus, but that these factors tended to cancel, resulting in no change in the BOLD response [17]. In fact the baseline shift in physiology due to caffeine involved a decrease in CBF and an increase in $CMRO_2$. This suggests that these methodological improvements will be essential in expanding calibrated BOLD to the study of drugs and diseases in which the coupling of CBF and $CMRO_2$ may not be typical.

Using the detailed BOLD model, I have also developed a heuristic model of the BOLD response [23]. While this model performs as well as the Davis model when applied to calibrated-fMRI data, the real advantage of this model is that it provides a physiological basis for the ratio method, which is an approach for determining whether the neurophysiological response to two stimuli within the same ROI changes by comparing only measured BOLD and CBF signals. This approach is advantageous, because it does not require a separate experiment in order to determine a calibration parameter [23].

I used this method to examine whether the neurophysiological response to a flickering checkerboard differs from the response to a more naturalistic and engaging stimulus such as brief movie clips in primary visual cortex. I found that while the coupling of blood flow and oxygen metabolism does not change between the stimulus types, the movie stimulus does provoke a more variable response when compared to the baseline state. I was the principal investigator and author on the projects thus far discussed.

The DBM of the BOLD response has permitted further examination of the calibrated BOLD fMRI methodology. Currently one of two approaches is most commonly used to calculate the calibration parameter necessary to determine changes in the $CMRO_2$ stimulus response from combined BOLD and CBF data: hypercapnia or hyperoxia respiratory challenge. In two recent publications, the limitations of these two approaches were examined and a new approach using the reversible transverse relaxation rate (R_2') was proposed [24,25]. The results from the simulation study indicates that the new R_2' calibration method works reasonably well [24]. Meanwhile the hyperoxia approach to calibration is unreliable, because hematocrit and baseline oxygen extraction fraction must be assumed, but variability in these parameters has a significant effect on the measurement. Hypercapnia calibration is the most reliable method

particularly when the venous blood volume change with activation is unknown. For these two manuscripts I was a supporting investigator and author.

Further examination of the hyperoxia respiratory challenge using the DBM shows that rather than being a reliable measurement of the calibration parameter, hyperoxia challenge is in fact a good way to measure changes in venous cerebral blood volume (CBVv) and more specifically deoxyhemoglobin containing blood volume [26]. A previous analysis technique to relate BOLD signal changes to CBVv based on dynamic contrast agent experiments had significant uncertainty, but in a new analysis we found a direct relationship between the BOLD signal change and CBVv. For this manuscript I was a supporting investigator and author.

In an additional application of the DBM, we recently developed a novel method for improving dynamic measurements of CBF and $CMRO_2$ [27]. This technique makes it possible to test for changes in blood flow and oxygen metabolism coupling when the stimulus is unknown. Previous measurements of this coupling have relied on block design experiments in which measurements can be repeated then averaged to improve precision and decrease signal noise. This approach instead improves CBF measurement precision using the relationship between BOLD and CBF and information contained in simultaneously acquired BOLD and ASL signals in a method termed BOLD Constrained Perfusion (BCP) estimation. For this manuscript I was a supporting investigator and author.

In total this work improves our understanding of fMRI and of the BOLD signal, which results from the complex interaction of the baseline brain state with changes in CBF, CBV and $CMRO_2$. Notably a major limitation of measuring the BOLD signal alone is that the data is inherently qualitative, but by combining with additional measurements of CBF and the

calibration parameter we can quantitatively measure changes in $CMRO_2$ and the coupling of blood flow and oxygen metabolism.

References

1. Tomczak RJ, Wunderlich AP, Wang Y, Braun V, Antoniadis G, et al. (2000) fMRI for preoperative neurosurgical mapping of motor cortex and language in a clinical setting. J Comput Assist Tomogr 24: 927-934.

2. Eisenberger NI, Lieberman MD, Williams KD (2003) Does rejection hurt? An FMRI study of social exclusion. Science 302: 290-292.

3. Ogawa S, Menon RS, Tank DW, Kim S-G, Merkle H, et al. (1993) Functional brain mapping by blood oxygenation level - dependent contrast magnetic resonance imaging: a comparison of signal characteristics with a biophysical model. Biophysical J 64: 803-812.

4. Greene AE, Todorova MT, Seyfried TN (2003) Perspectives on the metabolic management of epilepsy through dietary reduction of glucose and elevation of ketone bodies. J Neurochem 86: 529-537.

5. Lin AL, Fox PT, Hardies J, Duong TQ, Gao JH (2010) Nonlinear coupling between cerebral blood flow, oxygen consumption, and ATP production in human visual cortex. Proc Natl Acad Sci U S A 107: 8446-8451.

6. Attwell D, Laughlin SB (2001) An energy budget for signaling in the grey matter of the brain. J Cereb Blood Flow Metab 21: 1133-1145.

7. Attwell D, Iadecola C (2002) The neural basis of functional brain imaging signals. Trends Neurosci 25: 621-625.

8. Hoyer S, Oesterreich K (1975) Blood flow and oxidative metabolism of the brain in patients with schizophrenia. Psychiatr Clin (Basel) 8: 304-313.

9. Gur RE, Resnick SM, Alavi A, Gur RC, Caroff S, et al. (1987) Regional brain function in schizophrenia. I. A positron emission tomography study. Arch Gen Psychiatry 44: 119-125.

10. Videbech P, Ravnkilde B, Pedersen AR, Egander A, Landbo B, et al. (2001) The Danish PET/depression project: PET findings in patients with major depression. Psychol Med 31: 1147-1158.

11. Baxter LR, Jr., Phelps ME, Mazziotta JC, Guze BH, Schwartz JM, et al. (1987) Local cerebral glucose metabolic rates in obsessive-compulsive disorder. A comparison with rates in unipolar depression and in normal controls. Arch Gen Psychiatry 44: 211-218.

12. Brooks JO, 3rd, Wang PW, Strong C, Sachs N, Hoblyn JC, et al. (2006) Preliminary evidence of differential relations between prefrontal cortex metabolism and sustained attention in depressed adults with bipolar disorder and healthy controls. Bipolar Disord 8: 248-254.

13. Yatham LN, Maj M (2010) Bipolar disorder : clinical and neurobiological foundations. Chichester, UK: Wiley.

14. Volkow ND, Hitzemann R, Wang GJ, Fowler JS, Burr G, et al. (1992) Decreased brain metabolism in neurologically intact healthy alcoholics. Am J Psychiatry 149: 1016-1022.

15. D'Esposito M, Deouell LY, Gazzaley A (2003) Alterations in the BOLD fMRI signal with ageing and disease: a challenge for neuroimaging. Nat Rev Neurosci 4: 863-872.

16. Perthen JE, Lansing AE, Liau J, Liu TT, Buxton RB (2008) Caffeine-induced uncoupling of cerebral blood flow and oxygen metabolism: a calibrated BOLD fMRI study. Neuroimage 40: 237-247.

17. Griffeth VE, Perthen JE, Buxton RB (2011) Prospects for quantitative fMRI: Investigating the effects of caffeine on baseline oxygen metabolism and the response to a visual stimulus in humans. Neuroimage 57: 809-816.

18. Brown GG, Eyler Zorrilla LT, Georgy B, Kindermann SS, Wong EC, et al. (2003) BOLD and perfusion response to finger-thumb apposition after acetazolamide administration: differential relationship to global perfusion. J Cereb Blood Flow Metab 23: 829-837.

19. Wong EC, Buxton RB, Frank LR (1998) Quantitative imaging of perfusion using a single subtraction (QUIPSS and QUIPSS II). Magn Reson Med 39: 702-708.

20. Ances BM, Liang CL, Leontiev O, Perthen JE, Fleisher AS, et al. (2009) Effects of aging on cerebral blood flow, oxygen metabolism, and blood oxygenation level dependent responses to visual stimulation. Hum Brain Mapp 30: 1120-1132.

21. Davis TL, Kwong KK, Weisskoff RM, Rosen BR (1998) Calibrated functional MRI: mapping the dynamics of oxidative metabolism. Proc Natl Acad Sci USA 95: 1834-1839.

22. Grubb RL, Raichle ME, Eichling JO, Ter-Pogossian MM (1974) The effects of changes in $PaCO_2$ on cerebral blood volume, blood flow, and vascular mean transit time. Stroke 5: 630 - 639.

23. Griffeth VE, Blockley NP, Simon AB, Buxton RB (2013) A simplified model for the blood oxygenation level dependent (BOLD) effect for estimating brain oxygen metabolism changes. PLoS One.

24. Blockley NP, Griffeth VE, Buxton RB (2012) A general analysis of calibrated BOLD methodology for measuring CMRO2 responses: comparison of a new approach with existing methods. Neuroimage 60: 279-289.

25. Blockley NP, Griffeth VE, Simon AB, Buxton RB (2012) A review of calibrated blood oxygenation level-dependent (BOLD) methods for the measurement of task-induced changes in brain oxygen metabolism. NMR Biomed.

26. Blockley NP, Griffeth VE, Germuska MA, Bulte DP, Buxton RB (2013) An analysis of the use of hyperoxia for measuring venous cerebral blood volume: Comparison of the existing method with a new analysis approach. Neuroimage 72: 33-40.

27. Simon AB, Griffeth VE, Wong EC, Buxton RB (2013) A novel method of combining blood oxygenation and blood flow sensitive magnetic resonance imaging techniques to measure the cerebral blood flow and oxygen metabolism responses to an unknown neural stimulus. PLoS One 8: e54816.

CHAPTER 1

Contents lists available at ScienceDirect

NeuroImage

journal homepage: www.elsevier.com/locate/ynimg

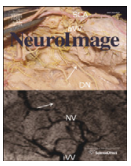

A theoretical framework for estimating cerebral oxygen metabolism changes using the calibrated-BOLD method: Modeling the effects of blood volume distribution, hematocrit, oxygen extraction fraction, and tissue signal properties on the BOLD signal

Valerie E.M. Griffeth [a], Richard B. Buxton [b,*]

[a] Department of Bioengineering, and Center for Functional Magnetic Resonance Imaging, University of California, San Diego, CA 92093, USA
[b] Department of Radiology, and Center for Functional Magnetic Resonance Imaging, University of California, San Diego, CA 92093, USA

ARTICLE INFO

Article history:
Received 11 January 2011
Revised 23 May 2011
Accepted 28 May 2011
Available online 6 June 2011

Keywords:
Blood oxygenation level dependent
Cerebral blood flow
Cerebral metabolic rate of oxygen
Mathematical modeling
Functional MRI

ABSTRACT

Calibrated blood oxygenation level dependent (BOLD) imaging, a technique used to measure changes in cerebral O_2 metabolism, depends on an accurate model of how the BOLD signal is affected by the mismatch between changes in cerebral blood flow (CBF) and cerebral metabolic rate of O_2 ($CMRO_2$). However, other factors such as the cerebral blood volume (CBV) distribution at rest and with activation also affect the BOLD signal. The Davis model originally proposed for calibrated BOLD studies (Davis et al., 1998) is widely used because of its simplicity, but it assumes CBV changes are uniformly distributed across vascular compartments, neglects intravascular signal changes, and ignores blood-tissue signal exchange effects as CBV increases and supplants tissue volume. More recent studies suggest that venous CBV changes are smaller than arterial changes, and that intravascular signal changes and CBV exchange effects can bias estimated $CMRO_2$. In this paper, recent experimental results for the relationship between deoxyhemoglobin and BOLD signal changes are integrated in order to simulate the BOLD signal in detail by expanding a previous model to include a tissue compartment and three blood compartments rather than only the venous blood compartment. The simulated data were then used to test the accuracy of the Davis model of calibrated BOLD, demonstrating that the errors in estimated $CMRO_2$ responses across the typical CBF–$CMRO_2$ coupling range are modest despite the simplicity of the assumptions underlying the original derivation of the model. Nevertheless, the accuracy of the model can be improved by abandoning the original physical meaning of the two parameters α and β and treating them as adjustable parameters that capture several physical effects. For a 3 Tesla field and a dominant arterial volume change with activation, the accuracy of the Davis model is improved with new values of $\alpha = 0.14$ and $\beta = 0.91$.

Introduction

Functional magnetic resonance imaging (fMRI) is widely used for mapping spatial and temporal patterns of brain activity. The most common measurement is the blood oxygenation level dependent (BOLD) signal, which results from changes in local deoxyhemoglobin content (Ogawa et al., 1993). When the brain is activated, an unexpected physiological phenomenon occurs: local cerebral blood flow (CBF) increases much more than the cerebral metabolic rate of oxygen ($CMRO_2$) (Fox and Raichle, 1986), decreasing both local oxygen extraction fraction and local deoxyhemoglobin content. Deoxyhemoglobin is paramagnetic and creates magnetic field distortions within and around blood vessels, thereby decreasing the MR signal. Thus decreased blood deoxyhemoglobin content results in the basic BOLD effect of increased MR signal with neural activation. However, interpreting relative levels of BOLD signal change in terms of neural activity is difficult due to the BOLD signal's complex dependence on changes in cerebral blood volume (CBV) in addition to CBF and $CMRO_2$. Although this sensitivity of the BOLD signal to multiple factors creates some difficulty in interpreting the signal, it also offers the possibility of estimating changes in $CMRO_2$ when BOLD and CBF measurements are combined.

The calibrated-BOLD approach proposed by Davis et al. (1998) does just this; it combines measurements of CBF and BOLD responses to

Abbreviations: BOLD, (blood oxygenation level dependent); CBF, (cerebral blood flow); $CMRO_2$, (cerebral metabolic rate of oxygen); CBV, (cerebral blood volume); fMRI, (functional magnetic resonance imaging); *OEF*, (oxygen extraction fraction); *Hct*, (hematocrit); V_i, (intravascular volume); R_{2E}^*, (intrinsic extravascular signal decay rate); S_AO_2, (arterial O_2 saturation); ω_v, baseline venous CBV fraction; ϕ_v, exponent relating venous CBV changes to CBF; TE, echo time; λ, intravascular to extravascular spin density ratio.

* Corresponding author at: University of California, San Diego, 9500 Gilman Dr. MC 0677, La Jolla, CA 92093-0677, USA. Fax: +1 858 822 0605.
E-mail address: rbuxton@ucsd.edu (R.B. Buxton).

1053-8119/$ – see front matter © 2011 Elsevier Inc. All rights reserved.
doi:10.1016/j.neuroimage.2011.05.077

neural activation and hypercapnia stimulation with the goal of estimating the $CMRO_2$ change during brain activation. Changes in O_2 metabolism are important as they are expected to reflect the underlying energy requirement of evoked neural activity (Lin et al., 2010). This multimodal imaging approach combining BOLD and CBF measurements requires a theoretical framework that accurately describes how the BOLD signal depends on changes in CBF, $CMRO_2$ and CBV. The Davis model is one such framework and has been used in nearly all subsequent applications of calibrated BOLD. As originally derived, this nonlinear model essentially describes the extravascular signal change with the assumption that it depends on both the change in venous oxygenation and the change in venous CBV. These changes in turn are related to alterations in CBF and $CMRO_2$ in an equation involving two parameters, α and β. The parameter β was originally meant to describe a nonlinear MR signal dependence on venous oxygenation, reflecting the idea that deoxyhemoglobin has a weaker effect on the signal change in the smallest vessels compared to larger veins because of the effects of diffusion (Ogawa et al., 1993). Similarly, the parameter α was meant to be the exponent in a power law relationship between blood flow and venous blood volume. Finally, there is an overall scaling parameter M, typically determined by a separate hypercapnia experiment, that depends on the amount of deoxyhemoglobin present in the baseline state and details of the image acquisition. The calibration step with hypercapnia uses the same model to determine M, and requires two assumptions: hypercapnia changes CBF but not $CMRO_2$ (Chen and Pike, 2010; Jones et al., 2005; Sicard and Duong, 2005) and CBV has the same dependence on CBF in the activation and hypercapnia experiments.

However, the Davis model is potentially oversimplified: it only considers extravascular signal changes and leaves out intravascular contributions to the BOLD signal (Boxerman et al., 1995); it neglects the possibility that changes in deoxyhemoglobin containing CBV (capillary and venous) may be proportionally smaller than the arterial CBV changes (Chen and Pike, 2009a; Hillman et al., 2007; Kim et al., 2007; Kim and Kim, 2006); and volume exchange effects were neglected, ignoring the possibility that differences in the intrinsic signal between blood and tissue may change the overall signal upon neural activation (Buxton et al., 2004; Leontiev and Buxton, 2007; Obata et al., 2004). To clarify the assumptions involved, we retain α as a parameter in the Davis model, but define the exponent representing the relationship between CBV and CBF as ϕ. The original assumption setting $\alpha = \phi = 0.38$ based on experiments in non-human primates (Grubb et al., 1974) assumes that CBV changes are proportionally equal for all blood compartments. The second parameter was assumed to be $\beta = 1.5$, based on Monte Carlo simulations of only the extravascular signal dependence on deoxyhemoglobin at 1.5 T (Davis et al., 1998).

Previous models of the BOLD effect have sought to address these deficiencies. Buxton et al. (1998), with corrections and improvements by Obata et al. (2004), incorporated intravascular signal changes and volume exchange effects by modeling the BOLD signal change as a volume-weighted sum of signal from two compartments: intravascular (venous) and extravascular. More recent models have directly addressed the issue of relating CBV changes to CBF by incorporating direct measurements of CBV in calculating $CMRO_2$ (Donahue et al., 2009; Lin et al., 2008; Lu et al., 2004). These studies used the VASO technique to measure changes in total CBV, but this approach requires two additional assumptions: (1) an absolute baseline CBV value must be assumed to derive the fractional change in CBV necessary for use in the Davis model, and (2) the venous CBV change is assumed to be proportional to the total CBV change measured with VASO. Moving beyond steady-state modeling of BOLD, other approaches have sought to incorporate transient dynamics of CBV (Kim and Kim, 2010b), deoxyhemoglobin (Mandeville et al., 1999), and $CMRO_2$ (Buxton, 2010; Hyder et al., 2010) or explain the coupling and uncoupling of CBF and $CMRO_2$ (Friston et al., 2000; Zheng et al., 2010) that underlies the BOLD signal.

The focus of this work was to model the steady-state BOLD signal and examine how it can be combined with measurements of CBF in order to calculate $CMRO_2$ more accurately. To do so, we followed the approach taken by Uludag et al. (2009) in which the Obata–Buxton model (Buxton et al., 1998; Obata et al., 2004) was expanded to not only include intravascular signal changes but also volume exchange effects. We did not linearize the model, because we were concerned that intravascular signal changes are actually quite large and would therefore violate the linearization assumption. Based on the knowledge that the BOLD signal is primarily a result of changes in the local deoxyhemoglobin content, we modeled the BOLD response as the volume-weighted sum of signals from four compartments: an extravascular tissue compartment and three blood compartments separated into arteries, capillaries and veins to allow for differences in the blood volume distribution between the three blood compartments at baseline ($\omega_{a,c,v}$) and the fractional changes with activation ($\phi_{a,c,v}$). This detailed analytic steady-state BOLD prediction model (the "detailed model") allows for arbitrary changes in CBF and $CMRO_2$ as well as arbitrary coupling of CBV and CBF. We do not explicitly examine transient aspects of the BOLD signal, and instead focus on approximate steady-state conditions, corresponding to typical calibrated BOLD applications using block design stimulus presentations. Furthermore, we make no assumptions about the relationship between CBF and $CMRO_2$ responses. Instead, CBF and $CMRO_2$ are varied independently allowing examination of the full range of BOLD effects. Finally within our model, we include the ability to alter hematocrit (Hct), baseline O_2 extraction fraction (OEF_0), echo time (TE), the intrinsic intravascular to extravascular signal ratio (λ), the intrinsic extravascular signal decay rate (R^*_{2E}), and arterial O_2 saturation (S_AO_2) in order to more accurately model the BOLD effect and increase our understanding of the relationship between BOLD, CBF and $CMRO_2$.

We addressed the following questions using the detailed model:

1. By allowing α and β to be free parameters, can the Davis model be optimized to improve its performance in calculating changes in oxygen metabolism?
2. How large are the errors in oxygen metabolism calculations associated with using the Davis model (with either the original or with optimized values for the parameters α and β), and do these errors vary for different coupling ratios of CBF and $CMRO_2$ changes?
3. How sensitive are $CMRO_2$ calculations to variations of the physiological state, particularly the blood volume distribution at baseline and the balance of arterial and venous CBV changes with activation?
4. If the assumptions underlying the hypercapnia calibration experiment (no effect on $CMRO_2$ and the same relationship between CBF and CBV as during neural activation) are incorrect, how will this impact calculations using the Davis model?

Our primary finding is that despite the oversimplifications of the Davis model, the same mathematical form of the Davis model with corrections to α and β adequately captures the behavior of the much more complex physiology described by the detailed model. The classic Davis model is reasonably accurate for most activation experiments in which both CBF and $CMRO_2$ increase in parallel, without optimization of α and β provided that M is accurately measured. However, studies of the response to drugs such as caffeine have shown more divergent effects, lowering CBF and possibly increasing $CMRO_2$, which leads to inaccuracies in calculations by the original Davis model. Parameter optimization improves the accuracy of the Davis model across the full range of potential CBF and $CMRO_2$ responses. By permitting α and β to be free parameters, though, their physical interpretation becomes complicated in that they no longer correspond to their original meaning. While variation of many of the physiological parameters has a strong effect on the magnitude of the BOLD response, this effect is adequately captured in the scaling parameter M, so that Davis model estimates of $CMRO_2$ change remain relatively accurate even with fixed α and β. The primary physiological parameters for which this is not true are related to CBV,

both the baseline distribution between compartments and the balance between arterial and venous changes. Additional errors due to assumptions about the hypercapnia calibration are largest when the CBF change is much larger than the $CMRO_2$ change. These results emphasize the necessity of accurately determining how CBV distributes with activation and also the importance of measuring M values accurately for each subject. In this paper, our focus is on the Davis model, and its ability to calculate $CMRO_2$ changes from BOLD and CBF data, because the Davis model is particularly well-suited for the calibrated BOLD experiment. In future studies, we will examine the effects of hypoxia and the accuracy of other models in predicting the BOLD signal.

Theory

The Davis model for calibrated-BOLD is presented and the associated assumptions are analyzed. A detailed four-compartment model for the BOLD response is developed and implemented using Matlab. Note that upper case variables describe absolute quantities (e.g., F is CBF, the blood inflow to the arteriolar compartment in units of ml blood/ml tissue-sec, and V_a is the arteriolar blood volume fraction in units of ml blood/ml tissue), while lower case variables represent the same quantity normalized to its baseline value (e.g., f and v_a are dimensionless and equal to 1 at rest). Similarly, Δ denotes an absolute change while δ specifies a percent change from the baseline state.

The Davis model

With this nomenclature in mind, the Davis model relates f and normalized $CMRO_2$, r, to the percent change in the BOLD signal (δS) using the following equation:

$$\delta S = M\left[1-f^{\alpha}\left(\frac{r}{f}\right)^{\beta}\right] \tag{1}$$

As originally derived, the mathematical form in the brackets represents the idea that the signal is modulated both by changes in the volume of blood containing deoxyhemoglobin (modeled with the first term in f relating CBV to CBF by a power law) and also by the magnetic susceptibility of the blood (modeled by the second term in r and f).

The r/f term models the susceptibility effect due to a change of deoxyhemoglobin concentration in the venous blood. The parameter β was introduced based on Monte Carlo simulations of water molecule diffusion around magnetized vessels to describe how the signal depends on the susceptibility. This dependence is expected to differ between large and small vessels because of the effects of diffusion on the extravascular signal change near the smaller vessels. The typical value used is $\beta = 1.5$ (Davis et al., 1998), although it has been argued that the value should be reduced at higher magnetic field strengths (Boxerman et al., 1995; Chiarelli et al., 2007b; Ogawa et al., 1993).

The third parameter, M, essentially lumps together a number of effects that modulate the magnitude of the BOLD response, including aspects of local brain physiology and image acquisition parameters. In particular, M varies with the amount of deoxyhemoglobin present in the baseline state. It is typically calculated from an additional experiment using combined BOLD and CBF measurements obtained in response to hypercapnic stimulation. This assumes there is no change in $CMRO_2$ ($r = 1$) and that CBV with activation (AC) and with hypercapnia (HC) changes in the same way in response to CBF changes ($\phi_{HC} = \phi_{AC}$) as noted above.

Development of a detailed model of the BOLD response

The calibrated BOLD methodology depends on an accurate model of how the BOLD signal is related to the mismatch between CBF and $CMRO_2$, which is often expressed as the coupling parameter, n, defined as the ratio of the fractional changes (e.g., a 50% increase in CBF accompanied by a 20% increase in $CMRO_2$ would be $n = 2.5$). The model presented here, following the approach by Uludag et al. (2009), separates the signal into four compartments: one extravascular and three intravascular. Previous models have included multiple compartments to varying degrees (Blockley et al., 2009; Donahue et al., 2009; Obata et al., 2004). The Davis model considers only the extravascular compartment, neglects blood volume exchange effects, and assumes CBV changes are uniformly distributed across vascular compartments. The Obata model (Obata et al., 2004) explicitly includes both intravascular and extravascular components, however it only includes exchange effects with venous CBV thereby neglecting significant changes occurring in the arterial vasculature. More recent models examined effects of both arterial and venous compartments on the BOLD signal, but neglected effects of the capillary compartment (Donahue et al., 2009; Lin et al., 2008). These models also do not account for differing dependencies of arterial and venous CBV on CBF, variable baseline distribution of CBV, differences in the intravascular to extravascular proton density, and baseline extravascular signal decay rate constant (R^*_{2E}).

The basic signal equation for the detailed model is derived in the Appendix with the result shown in Eqs. (2) and (3):

$$\delta S = H\left[(1-V_I)e^{-TE\cdot\Delta R^*_{2E}} + \varepsilon_A V_A e^{-TE\cdot\Delta R^*_{2A}} + \varepsilon_C V_C e^{-TE\cdot\Delta R^*_{2C}} + \varepsilon_V V_V e^{-TE\cdot\Delta R^*_{2V}}\right] - 1 \tag{2}$$

where

$$H = 1 \Big/ \left(1 - V_{I,0} + \varepsilon_A V_{A,0} + \varepsilon_C V_{C,0} + \varepsilon_V V_{V,0}\right) \tag{3}$$

Here, V denotes the volume fractions of the individual compartments (E = extravascular, I = intravascular, A = arterial, C = capillary, and V = venous). Baseline is denoted by the subscript "0" (V_0). The parameter ε is the signal ratio at baseline of an intravascular volume to extravascular volume (e.g. ε_v is the signal ratio in the experiment between equal volumes of venous blood and extravascular tissue). TE is the echo time of the MR measurement, and ΔR_2^* is the change in the MR signal relaxation rate with the stimulus for each of the four compartments, three intravascular and one extravascular.

Volume fractions were determined by examining a range of total baseline intravascular volume fractions ($V_{I,0}$) and fractional distributions (ω) as shown in Table 1. Changes in total CBV were modeled as in Grubb et al. (1974) by assuming a power law relationship to CBF with exponent ϕ. Distributions of ΔCBV to the compartments containing deoxyhemoglobin were calculated separately using different exponents (ϕ_c and ϕ_v) for capillary and venous ΔCBV respectively. Ranges of ϕ and ϕ_v were examined while ϕ_c was assumed to be half of ϕ_v reflecting small changes in capillary CBV (Stefanovic et al., 2008). Arterial ΔCBV was calculated as the remainder of total ΔCBV after subtraction of capillary and venous ΔCBV. Next, a range of hemoglobin saturations (SO_2) was studied for each vascular compartment: venous O_2 saturation (S_VO_2) was calculated from S_AO_2 across a range of f, r, and OEF_0; capillary O_2 saturation (S_CO_2) was calculated as a weighted sum of S_AO_2 and S_VO_2. Values of R_2^* for the blood and tissue compartments were calculated based on relationships from the literature, which incorporate the effects of Hct, SO_2, baseline OEF and CBF. Eqs. (2) and (3) thereby allow us to simulate the BOLD signal across a wide range of physiological states.

Simulations and results

Following the outline presented in Fig. 1, we determined a set of typical physiological values for the detailed model inputs (Table 1), and used this simulation to optimize the Davis model parameters α and β. Next, we used the detailed model to simulate changes to the BOLD activation and hypercapnia responses as the physiological parameters vary. The focus of the simulations was to test the accuracy of $CMRO_2$

Table 1
Parameters defining the standard physiology. Values without a marker are assumed. Values marked with † are calculated using the assumed values in the detailed model at $\delta CBF = 50\%$ and $\delta CMRO_2 = 20\%$.

Variable	Standard value (range tested)	Description
TE	32 ms (20–40 ms)	Echo time
$V_{l,0}$	0.05 (0.01–0.15)	Total blood volume fraction at baseline (Roland et al., 1987)
ω_a	0.2	Arterial fraction of baseline total blood volume (Weber et al., 2008)
ω_c	0.4 (0.6–0.2)	Capillary fraction of baseline total blood volume (Weber et al., 2008)
ω_v	0.4 (0.2–0.6)	Venous fraction of baseline total blood volume (Weber et al., 2008)
ϕ	0.38 (0.3–0.65)	Grubb's constant relating CBF to total CBV (Grubb et al., 1974)
ϕ_c	0.1 (0–0.33)	Exponent relating CBF to capillary CBV (Stefanovic et al., 2008)
ϕ_v	0.2 (0–0.65)	Exponent relating CBF to venous CBV (Chen and Pike, 2009a)
$V_a(t)$	0.016	†Arterial blood volume with activation
$V_c(t)$	0.021	†Capillary blood volume with activation from Grubb relation and ϕ_c
$V_v(t)$	0.022	†Venous blood volume with activation from Grubb relation and ϕ_c
OEF_0	0.4 (0.25–0.65)	Resting oxygen extraction fraction (Marchal et al., 1992)
κ	0.4	Fraction of capillary blood considered to be "arterial" (Tsai et al., 2003)
S_AO_2	0.98	Arterial oxygen saturation (Schutz, 2001)
S_cO_2	0.74	†Capillary oxygen saturation at baseline (Eq. (A8))
S_vO_2	0.59	†Venous oxygen saturation at baseline (Eqs. (A6) and (A7))
Hct	0.44 (0.25–0.65)	Resting hematocrit of arteries and vein (Gustard et al., 2003)
Hct_c	0.33 (0.19–0.49)	†Resting hematocrit of capillaries calculated from Hct (Sakai et al., 1985)
A^*	21.2 s^{-1}	†Constant term in quadratic dependence of intravascular R_2^* on Hct for arteries and vein (Zhao et al., 2007)
A_C^*	19.7 s^{-1}	†Constant term in quadratic dependence of intravascular R_2^* on Hct for capillaries (Zhao et al., 2007)
C^*	174.7 s^{-1}	†Quadratic term in quadratic dependence of intravascular R_2^* on Hct for arteries and vein (Zhao et al., 2007)
C_C^*	142.7 s^{-1}	†Quadratic term in quadratic dependence of intravascular R_2^* on Hct for capillaries (Zhao et al., 2007)
$R_{2A}^*(0)$	21.3 s^{-1}	†Resting arterial rate of signal decay (Eq. (A5)) (Zhao et al., 2007)
$R_{2c}^*(0)$	28.9 s^{-1}	†Resting capillary rate of signal decay (Eq. (A5)) (Zhao et al., 2007)
$R_{2V}^*(0)$	50.9 s^{-1}	†Resting venous rate of signal decay (Eq. (A5)) (Zhao et al., 2007)
$R_{2E}^*(0)$	25.1 s^{-1}	Resting extravascular rate of signal decay (Perthen et al., 2008)
ΔR_{2A}^*	0 s^{-1}	†Change in arterial signal decay rate with activation (Eq. (A9))
ΔR_{2C}^*	−3.1 s^{-1}	†Change in capillary signal decay rate with activation (Eq. (A9))
ΔR_{2V}^*	−10.2 s^{-1}	†Change in venous signal decay rate with activation (Eq. (A9))
ΔR_{2E}^*	−0.4 s^{-1}	†Change in extravascular signal decay rate (Eq. (A10): (Ogawa et al., 1993)
λ	1.15 (0.9–1.3)	Intravascular to extravascular spin density ratio determined experimentally
ε_a	1.30	†Ratio of baseline intravascular arterial to extravascular signal (Eq. (A2))
ε_c	1.02	†Ratio of baseline intravascular capillary to extravascular signal (Eq. (A2))
ε_v	0.50	†Ratio of baseline intravascular venous to extravascular signal (Eq. (A2))
γ	2.68×10^8	Gyromagnetic ratio of protons
$\Delta\chi$	2.64×10^{-7}	Susceptibility of fully deoxygenated blood (Spees et al., 2001)
B_0	3 T	Magnetic field strength
$SO_{2,off}$	0.95	Blood saturation for equal tissue–blood susceptibility (Spees et al., 2001)

estimates from the calibrated BOLD experiment using the Davis model, although the effect of different physiological parameters (e.g., hematocrit) on the BOLD response is interesting in itself. Here, we are essentially asking the question of whether the simple calibration step accurately captures the variability of the BOLD response due to variation in particular physiological parameters.

Producing simulated BOLD data for a standard subject

For imaging parameters, we assumed a 3 T system with TE = 32 ms. For the standard subject, the total intravascular volume fraction at rest was assumed to be $V_{l,0} = 0.05$ (Roland et al., 1987). The fractional distribution of CBV at baseline (ω) between arteries, capillaries and veins was assumed to be $\omega_a = 0.2$, $\omega_c = 0.4$ and $\omega_v = 0.4$ consistent with intra-cortical measurements of CBV distribution (Weber et al., 2008). The exponent relating f to total v was assumed to be $\phi = 0.38$ ($f = v^{\phi}$) as in Grubb et al. (1974). The venous CBV was assumed to change by a smaller fraction than the total CBV change, with the exponent $\phi_v = 0.2$ relating normalized venous volume (v_v) to f (Chen and Pike, 2009a). The capillary volume change exponent was assumed to be half of ϕ_v ($\phi_v = 0.1$) (Stefanovic et al., 2008). Arterial ΔCBV was then calculated to be the remainder of total ΔCBV resulting in an effective $\phi_a = 1.1$ at $f = 1.5$.

Venous oxygenation at baseline was determined from Eq. (A7) (Appendix) assuming $S_AO_2 = 98\%$ (Schutz, 2001) and $OEF_0 = 0.4$ (Marchal et al., 1992). Activation S_VO_2 was determined across a range of f and r using Eqs. (A6) and (A7) (Appendix). Capillary oxygen saturation was calculated from S_AO_2 and S_VO_2 using Eq. (A8) with $\kappa = 0.4$ effectively giving a slightly greater weight to venous blood (Tsai et al., 2003). *Hct* was set to 0.44, and the baseline tissue relaxation rate constant (R_{2E}^*) was assumed to be 25.1 s^{-1} based on previous 3 T studies from our group (Perthen et al., 2008). Changes in R_2^* were calculated using Eqs. (A9) and (A10). Table 1 includes the full list of standard parameter values and resulting intermediaries such as values of R_2^* associated with each compartment.

The intravascular to extravascular intrinsic signal ratio was experimentally determined using a GE Signa Excite 3-T whole-body system with a body transmit coil and an 8-channel receive-only head coil. Two subjects were imaged using a high-resolution flow-compensated spoiled-GRASS protocol with TR/TE/α = 4000 ms/5.4 ms/10°. Images were viewed using AFNI (Cox, 1996). Intravascular measurements were taken from the sagittal sinus while extravascular measurements were taken from the visual cortex gray matter. The spin density ratio was then calculated from the signal ratio to be 1.15. This fraction allows calculation of the intrinsic intravascular to extravascular signal ratio using Eq. (A2) (Appendix). For arteries, capillaries and veins, this resulted in intrinsic signal ratios of $\varepsilon_A = 1.30$, $\varepsilon_C = 1.02$, and $\varepsilon_V = 0.50$ (Table 1). With these values, volume exchange effects will add to the BOLD response for arterial changes, subtract from the BOLD response for venous changes, and have little effect for capillary changes.

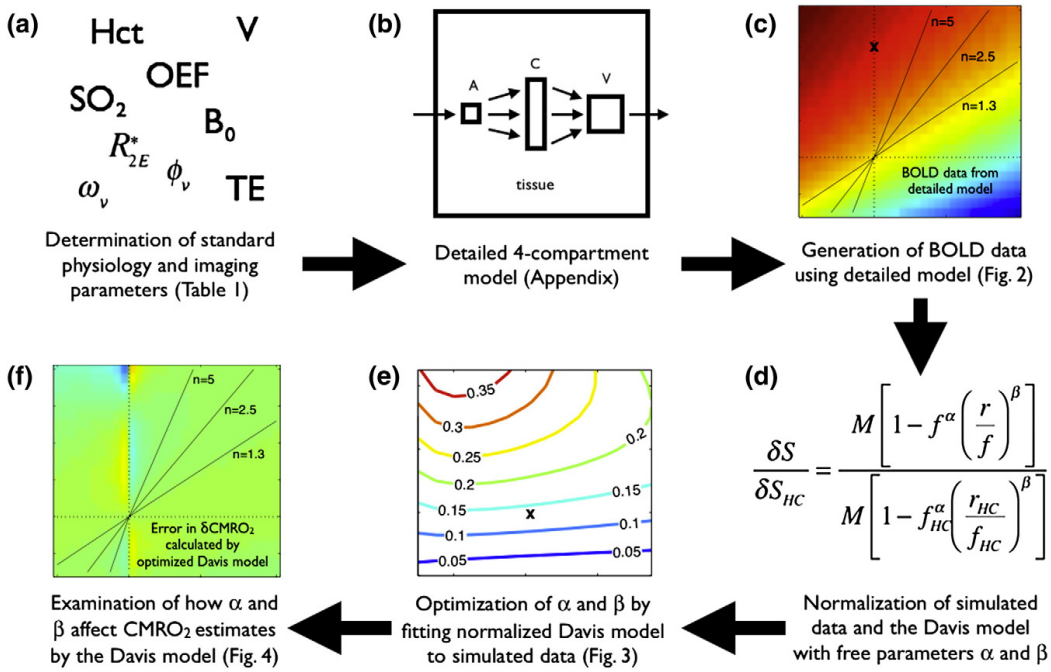

Fig. 1. Work flow diagram showing development and implementation of the detailed model. (a) A standard physiological set was defined including blood volume fractions, hemoglobin content and saturation, tissue properties and signal acquisition parameters (Table 1). (b) Following the approach used by Uludag et al. (2009), a detailed four-compartment model was developed (Appendix). (c) BOLD data were generated using this detailed model. (d) The BOLD signal simulated for the standard reference physiology was normalized to the signal at $f_{HC}=1.6$ and $r_{HC}=1.0$ (δS_{HC}). This is the simulated hypercapnia (HC) signal. The Davis model equation was similarly normalized in order to reduce the number of free parameters from three including M down to two (α and β). (e) Non-linear parameter optimization was performed using the Matlab function fmincon. The BOLD signal produced by the optimized Davis model is now shown. (f) By analyzing BOLD data generated using the detailed model, the efficacy of the Davis model was determined by its ability to calculate $CMRO_2$ changes accurately.

Optimization of the Davis model

Numerical simulations

For this standard set of parameters, the detailed 4-compartment model was used to calculate the BOLD signal for arbitrary changes in CBF (f) and $CMRO_2$ (r) (Fig. 2a). In the current simulations, f was varied from 0.7 to 1.8 and r was varied from 0.8 to 1.4. BOLD hypercapnic calibration was simulated for $f=1.6$ and $r=1$ (marked by 'x' on Fig. 2); this is a typical CBF change measured for 5% CO_2 inhalation (Ances et al., 2009; Perthen et al., 2008). Optimization of α and β of the Davis model was performed by normalizing the simulated BOLD data to the simulated hypercapnic BOLD signal. The Davis model equation was similarly normalized to this hypercapnia (subscript HC) value of δS_{HC} and $f_{HC}=1.6$ thereby eliminating the scaling parameter, M (Fig. 1d). Using the Matlab function fmincon, non-linear parameter optimization of α and β was performed using this simulated and normalized BOLD signal associated with the standard subject. Fitting was performed across the entire δCBF–$\delta CMRO_2$ plane thereby making α and β insensitive to specific values and coupling ratios of blood flow and oxygen metabolism.

Simulation results

The optimized values of $\alpha=0.14$ and $\beta=0.91$ are designated the "optimized" parameters while the original values of $\alpha=0.38$ and $\beta=1.5$ are designated the "classic" parameters. The Davis models associated with these parameters are similarly notated. The BOLD surfaces predicted with the Davis model using the optimized and classic parameter values are shown in Fig. 2b and c. The classic Davis model predicts a modest systematic difference in the BOLD signal while the optimized Davis model produces a signal nearly identical to that of the detailed model. We also performed this optimization of α and β for large ranges of the detailed model inputs: $\phi_v=0$–0.65, $\omega_v=0.2$–0.6, $R^*_{2E}=15$–$45\ s^{-1}$, $\lambda=0.9$–1.3, $Hct=0.25$–0.65, and $OEF_0=0.25$–0.65 (Fig. 3). Of these physiologic variables, the best-fit value of α shows the strongest dependence on ϕ_v (Fig. 3a) while β shows the strongest dependence on ω_v (Fig. 3b). The fitted α and β showed somewhat weaker dependence on tissue properties and baseline deoxyhemoglobin content (Fig. 3c–f). Optimized α is approximately linearly dependent on these parameters. Simultaneously, β shows quadratic dependence on baseline CBV distribution (ω_v) and linear dependence on ϕ_v, the tissue parameters (R^*_{2E} and λ), and the baseline deoxyhemoglobin content parameters (Hct and OEF_0). α and β are much less dependent on the other inputs to the detailed model (see supplementary data, Fig. S1).

Error in $\delta CMRO_2$ calculations associated with the Davis model α and β

Numerical simulations

Given the classic and optimized values for α and β, we then tested the primary question related to the calibrated BOLD experiment: how large are the errors in estimation of $CMRO_2$ change when using the Davis model, and does this depend on the particular combination of CBF and $CMRO_2$ changes? For the second part of the question, we were particularly interested in three combinations of CBF/$CMRO_2$ coupling, which we can characterize by the coupling ratio n: $\delta CBF/\delta CMRO_2$. The

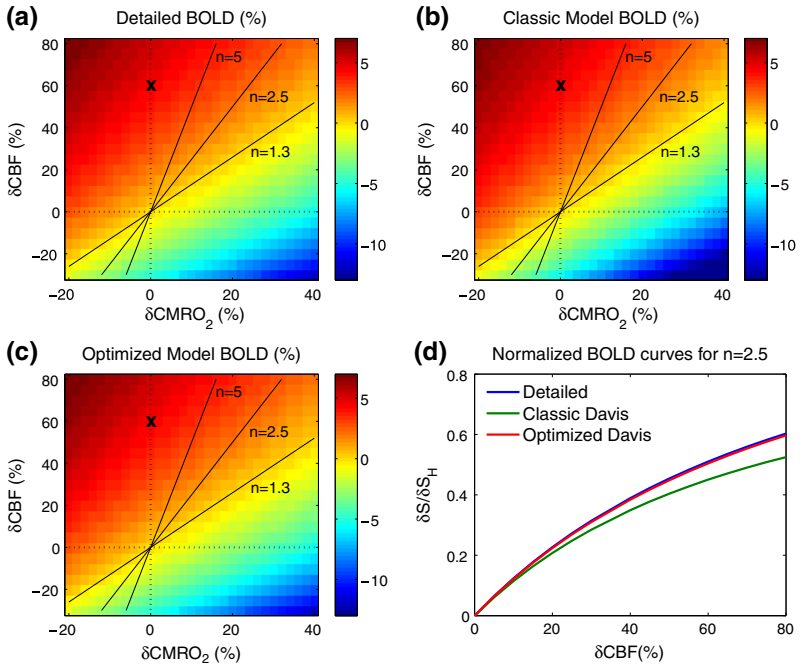

Fig. 2. Simulated BOLD response using the three models (detailed, classic Davis and optimized Davis). Dashed lines correspond to δCBF = 0% and δCMRO$_2$ = 0%. Solid lines represent the coupling parameters $n = 1.3$, $n = 2.5$, and $n = 5$. The line for $n = 1.3$ is approximately where the BOLD signal is 0. The 'x' marks the assumed response for an ideal hypercapnia calibration experiment. (a) BOLD response simulated by the detailed model. (b) BOLD response simulated by the classic Davis model. The contours are similar, although there is a very slight difference in the slope, and a general underestimation of the BOLD signal most apparent in the bottom right corner where flow is decreased and O_2 metabolism is increased. (c) BOLD response simulated by the optimized Davis model closely matches the simulation by the detailed model. (d) Normalized BOLD signals at n = 2.5 for the three models. Normalizing the BOLD signal to the simulated hypercapnia BOLD signal removes dependence on M in the Davis models and shows that the classic Davis model (green) underestimates the BOLD signal. In contrast, the optimized Davis model (red) fits the simulated data from the detailed model (blue) very well.

first is in the region $n = 2.5$ (δCBF = 50%, δCMRO$_2$ = 20%), corresponding to activation results in a number of calibrated BOLD studies using the classic Davis model (Perthen et al., 2008; Stefanovic et al., 2004). The second is $n = 5$ (δCBF = 50%, δCMRO$_2$ = 10%), a higher ratio that some PET studies have found (Ito et al., 2005). The third was motivated by studies of the effects of caffeine, which lowers CBF and raises CMRO$_2$ (δCBF = −25%, δCMRO$_2$ = 30%, $n = -0.8$) (Griffeth et al., 2011). In these simulations we assumed that hypercapnia changes only CBF, with no effect on CMRO$_2$. To simulate the calibrated BOLD experiment, M values for both the classic and optimized Davis models were determined using Eq. (1) and the BOLD response from the detailed model at $f_{HC} = 1.6$ and $r_{HC} = 1.0$ (marked with an 'x' in Fig. 2a). This results in values of $M = 11.1$ and $M = 14.9$ for the classic and optimized Davis models respectfully. Using these values for M, The two Davis models were then compared in their ability to accurately predict δCMRO$_2$ from the simulated BOLD and CBF data by comparing the percent error from actual δCMRO$_2$. Errors in δCMRO$_2$ estimates by both models were determined using Eq. (4):

$$\xi = \frac{\delta CMRO_2^{\text{Estimated}} - \delta CMRO_2^{\text{Detailed}}}{\delta CMRO_2^{\text{Detailed}}} \quad (4)$$

Simulation results

Errors in estimated δCMRO$_2$ are displayed across the δCBF–δCMRO$_2$ plane in Fig. 4. Note that both δCMRO$_2$ and ξ are percentages, although δCMRO$_2$ is the percent change in absolute CMRO$_2$ while ξ is the percent error relative to the actual percent change (e.g., if true δCMRO$_2$ is 10% and the estimated δCMRO$_2$ is 15%, the percent error is ξ = 50%). Errors for specific combinations of δCBF and δCMRO$_2$ are listed in Table 2. It is clear that the classic Davis model using α = 0.38 and β = 1.5 systematically underestimates δCMRO$_2$ (Fig. 4a and Table 2, column 1). Along the coupling parameter contours of $n = 2.5$ and $n = 5$, this underestimation is close to −10%. Specifically for $n = 2.5$ (δCBF = 50% and δCMRO$_2$ = 20%), the classic Davis model underestimates δCMRO$_2$ by −9.8% such that it reports a change of 18.0% when it is actually 20%. Even for a much larger value of the coupling parameter such as $n = 5.0$ (δCBF = 50% and δCMRO$_2$ = 10%), the Davis model is only −6.9% in error. Yet, the optimized model improves the accuracy of CMRO$_2$ calculations. For δCBF = 50% and δCMRO$_2$ = 20%, the Davis model with optimized parameters predicts δCMRO$_2$ = 19.7% (ξ = −1.3%) while for a higher coupling of δCBF = 50% and δCMRO$_2$ = 10%, the optimized model returns δCMRO$_2$ = 9.8% (ξ = −2.5%). For the region with decreased CBF (−25%) but increased CMRO$_2$ (30%) the error using the classic model was ξ = −38.0% while with the optimized model it was reduced to −1.2%.

Error in δCMRO$_2$ calculations due to physiological variation

Numerical simulations

The previous simulations showed that the Davis model with optimized α and β works well for estimating δCMRO$_2$ for the

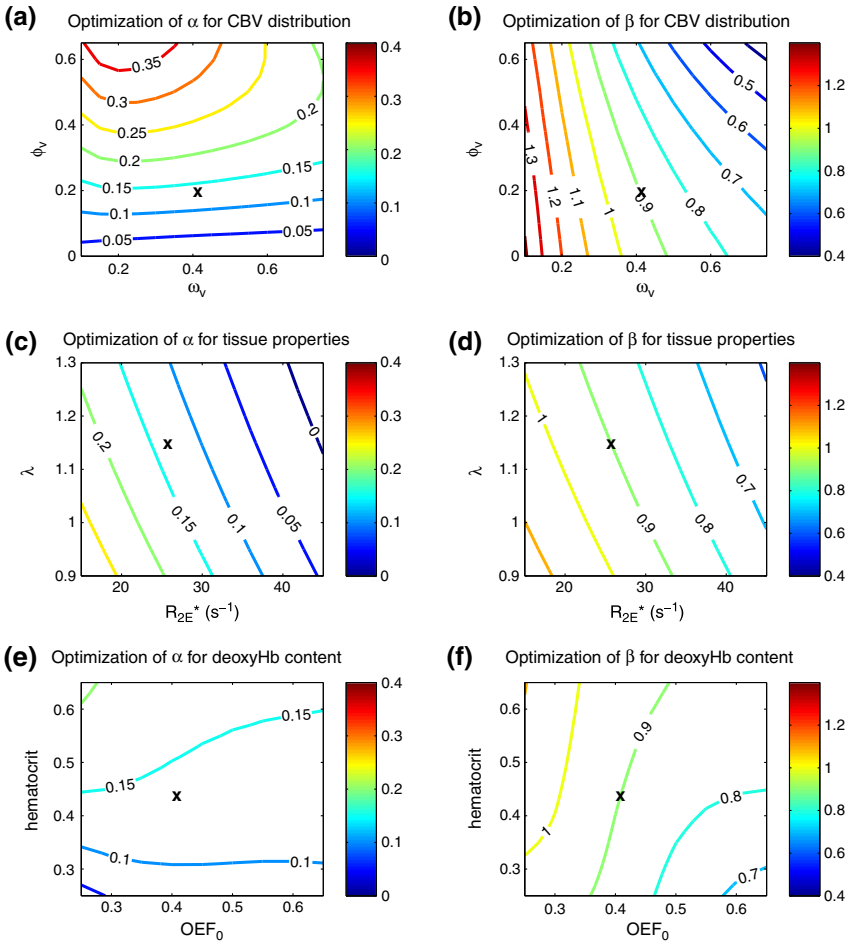

Fig. 3. Dependence of Davis model α and β on CBV distribution, tissue properties, and hemoglobin content and saturation. 'x' marks the location defined by the standard parameter set where $\alpha = 0.14$ and $\beta = 0.91$ are the best-fit values. Physiological inputs to the detailed model with the highest impact on the calibrated BOLD experiment were varied in pairs to determine their effect on optimization of the Davis model α and β. (a) CBV distribution at baseline (ω_v) has only a small impact on optimization of α while CBV distribution with activation (ϕ_v) has the biggest effect on optimized α. The relationship between α and ϕ_v is mostly linear based on the spacing of contour lines especially for $\phi_v < 0.4$ and $\omega_v < 0.4$. (b) Variation in ω_v has the largest effect on the optimized β. This relationship is more nonlinear since the spacing of the contour lines grows as ω_v increases. ω_v has a much smaller impact on ω. (c–d) Tissue properties R'_{2E} and λ have a smaller impact on optimization of α and β. The relationship between these tissue properties and the parameters appears to be mostly linear. (e–f) Hematocrit and baseline oxygen extraction fraction are shown to have an even smaller effect on α and β.

physiological parameter set defined in Table 1. In practice there is likely to be substantial variation of these parameters across subjects even for a healthy population. As described in section 3.2, we found that the optimal values of α and β do depend on these physiological parameters, and in a typical experiment there will not be sufficient information available to adjust the values of α and β. The important question for the calibrated BOLD method is then: if we adopt the values of α and β optimized for our "best guess" at the underlying physiology (Table 1), how large are the errors in the estimate of $\delta CMRO_2$ if these physiological parameters vary? To assess the errors in the estimation of $\delta CMRO_2$ we varied the value of each physiological parameter in the detailed model and then simulated the calibrated BOLD experiment to measure $\delta CMRO_2$ with either the classic or optimized Davis models. The physiological parameters were varied over the following ranges: $\phi_v = 0$–0.65, $\omega_v = 0.2$–0.6, $R^*_{2E} = 15$–$45\ s^{-1}$, $\lambda = 0.9$–1.3, $Hct = 0.25$–0.65, $OEF_0 = 0.25$–0.65, $V_{i,0}$ (0.01–0.1), ϕ (0.3–0.65), TE (20–40 ms), and λ (0.9–1.3). A range for ϕ_c (0–0.3) was also examined but found to have little effect on calculations of $\delta CMRO_2$. Therefore, ϕ_c was assumed to be equal to half of ϕ_v consistent with small changes to capillary volume during activation. Simulated hypercapnia calibration was repeated for each variation in order to calculate M; note the classic value of M is similar to what is typically calculated for experimental data using the Davis model (Fig. 5). The impact of the physiological variations was assessed for two scenarios of combined CBF and $CMRO_2$ change: $n = 2.5$ and $n = -0.8$ simulating the effects of caffeine. Both of these combinations were analyzed with the two Davis models to determine how accurate the models' estimates of $\delta CMRO_2$ would be, i.e. how close to $\delta CMRO_2 = 20\%$ or 30% (Table 2).

Simulation results

For $n = 2.5$, varying ϕ_v in the range of 0–0.65 has the largest impact on $\delta CMRO_2$ estimates with the classic model estimating $\delta CMRO_2 = 15.0$–

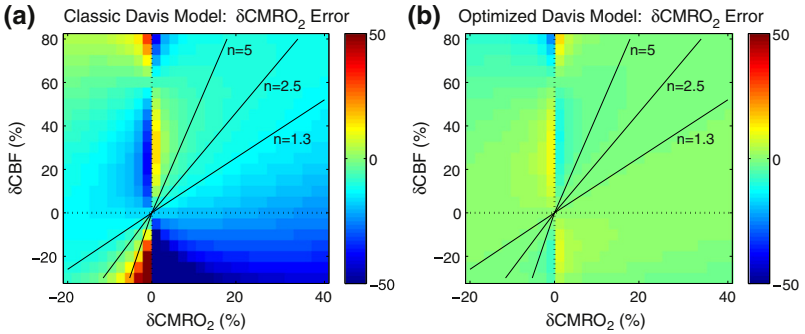

Fig. 4. Percent error (ξ) in $\delta CMRO_2$ calculations using the classic and optimized Davis model parameter sets. (a) Using the classic Davis model, $\delta CMRO_2$ is consistently underestimated as indicated by the turquoise areas along the $n = 2.5$ and $n = 5$ coupling parameter lines. (b) The optimized parameters of $\alpha = 0.14$ and $\beta = 0.91$ produce much more accurate estimates of $\delta CMRO_2$ across the entire expanse examined. This is apparent from the green coloring across the majority of the δCBF–$\delta CMRO_2$ plane corresponding to zero error. Errors around $\delta CMRO_2 = 0$ are artifacts of division by a small number.

30.0% and the optimized model estimating $\delta CMRO_2 = 16.2$–34.2% (Fig. 6a). Variations in $\delta CMRO_2$ calculations produced by *Hct*, ω_v, and R^*_{2E} were secondary, while the smallest impacts on $\delta CMRO_2$ calculations were produced by altering $V_{I,0}$ and ϕ (see supplementary data, Table S1 for exact ranges). This was despite very large ranges of $V_{I,0}$ (0.01 to 0.1 while literature values are typically about 0.05) and ϕ (0–0.65). At $n = -0.8$, ϕ_v again had a significant influence. However, at this combination of δCBF and $\delta CMRO_2$, R^*_{2E} in the range of 15–45 s^{-1} produced the largest variance while ω_v in the range 0.2–0.6 also had a sizeable effect (Fig. 6b). Meanwhile, the impact of λ and OEF_0 was greater than that of *Hct* and *TE*. ϕ still had very little impact.

As it was determined that the venous CBV change (ϕ_v) had the biggest impact on the accuracy of the Davis model, we more closely examined how variations in ϕ_v affected the Davis model for the cases of $\phi_v = 0$, 0.2, 0.38, and 0.65. Again, the hypercapnia experiment was simulated using BOLD data from the detailed model to calculate *M* for each case. We then analyzed the simulated BOLD data associated with the standard subject across the δCBF–$\delta CMRO_2$ plane for each value of ϕ_v using the two Davis models. Using Eq. (4), we calculated the percent error associated with each point in the *f*–*r* plane (Fig. 7). As expected, the optimized Davis model fits best at $\phi_v = 0.2$, but overestimates changes in $CMRO_2$ if $\phi_v = 0.38$ or 0.65, and underestimates changes in $CMRO_2$ when $\phi_v = 0$. Although not shown, the classic Davis model fits the simulated data for $\phi_v = 0.38$ somewhat better but is still not as accurate as the optimized model at $\phi_v = 0.2$.

To address the finding by Lin et al. (2008) that $\phi = 0.65$ with activation, we examined in more detail how this would affect $\delta CMRO_2$ calculations. We repeated the process used to produce Fig. 7 for both the classic and optimized Davis models but set $\phi = 0.65$ rather than $\phi = 0.38$ and combined this with the same four values of ϕ_v. The images for $\phi = 0.65$ are not shown, since they are practically identical to those in Fig. 7 ($\phi = 0.38$). This was expected due to the minimal impact ϕ had on $\delta CMRO_2$ calculations as shown in Fig. 6. This suggests that the venous volume change, rather than the overall volume change, is the key physiological parameter that determines the accuracy of the Davis model estimates of $\delta CMRO_2$.

Potential error in δCMRO₂ calculations associated with hypercapnia calibration

Numerical simulations

The hypercapnia calibration process assumes that inhalation of low levels of CO_2 (typically ~5%) does not affect $CMRO_2$ in the brain. In calculations up to this point, we assumed our method of calibration was accurate, but more recent experiments on hypercapnia calibration suggest that inhalation of 5% CO_2 decreases $CMRO_2$, with recent estimates giving this decrease between −13% and −26% (Bolar et al., 2010; Xu et al., 2011) for CBF changes of 55% and 32% respectively. To simulate this, we calculated the hypercapnic BOLD signal from the detailed model simulation for $f_{HC} = 1.6$ and r_{HC} varied from 0.8 to 1.1, but we calculated *M* from Eq. (1) assuming $r_{HC} = 1$. Additionally, the dependence of CBV on CBF may differ between neural activation and hypercapnia (Chen and Pike, 2010). To simulate this error, we took the hypercapnic BOLD signal from the detailed model simulation for

Table 2
Error in $\delta CMRO_2$ and *n* as calculated by the classic and optimized Davis models for the standard subject as defined in Table 1. While the optimized Davis model is best for all couplings of δCBF and $\delta CMRO_2$, the classic Davis model with the true value of *M* also produces reasonable estimates of $\delta CMRO_2$ around $n = 2.5$ and $n = 5.0$. Calculations using the classic Davis model parameters with a biased *M* (as might be determined from a hypercapnia calibration) are also given, and at $n = 2.5$ this model is also quite accurate. However, the classic Davis model with the biased *M* is not accurate for $n = 5.0$ or $n = -0.8$. Even the classic model with the true *M* is not accurate for $n = -0.8$.

	Classic α and β	Optimized α and β	Classic α and β
			Biased *M* ($r_{HC} = 0.9$)
Typical functional activation (fMRI): ($n = 2.5$)	$\delta CMRO_2 = 18.0\%$	$\delta CMRO_2 = 19.7\%$	$\delta CMRO_2 = 21.0\%$
$\delta CBF = +50\%$	$\xi = -9.8\%$	$\xi = -1.3\%$	$\xi = 5.1\%$
$\delta CMRO_2 = +20\%$	$n = 2.8$	$n = 2.5$	$n = 2.4$
Typical functional activation (PET): ($n = 5.0$)	$\delta CMRO_2 = 9.3\%$	$\delta CMRO_2 = 9.8\%$	$\delta CMRO_2 = 13.9\%$
$\delta CBF = +50\%$	$\xi = -6.9\%$	$\xi = -2.5\%$	$\xi = 38.9\%$
$\delta CMRO_2 = +10\%$	$n = 5.4$	$n = 5.1$	$n = 3.6$
Typical response to caffeine (fMRI): ($n = -0.8$)	$\delta CMRO_2 = 18.6\%$	$\delta CMRO_2 = 29.6\%$	$\delta CMRO_2 = 12.7\%$
$\delta CBF = -25\%$	$\xi = -38.0\%$	$\xi = -1.2\%$	$\xi = -57.7\%$
$\delta CMRO_2 = +30\%$	$n = -1.3$	$n = -0.8$	$n = -2.0$

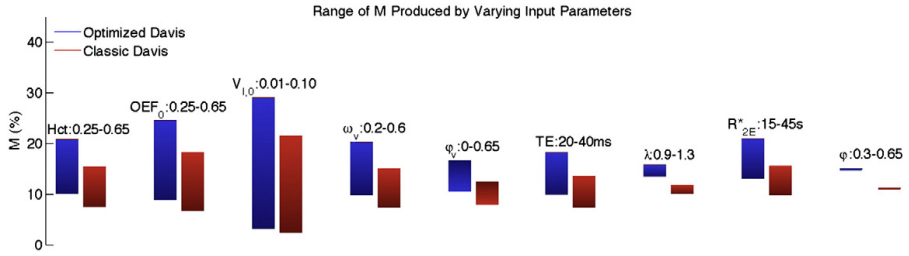

Fig. 5. Range of M for classic and optimized Davis models as input parameters vary. (The parameters are: Hct = hematocrit, OEF_0 = baseline O_2 extraction fraction, $V_{I,0}$ = baseline CBV fraction, ω_v = baseline venous CBV fraction, ϕ_v = exponent relating venous CBV changes to CBF, TE = echo time, λ = intravascular to extravascular spin density ratio, R^*_{2E} = intrinsic extravascular signal decay rate, and ϕ = exponent relating total CBV changes to CBF.) Values for M associated with the standard physiology for the two models are classic $M = 11.1$ and optimized $M = 14.9$. Note the gradient of the bars corresponds to the ranges of the input parameters; the lowest values of the inputs are associated with the dark end of the bars and the highest values are associated with the light end of the bars. Specifically note the large variation in M due to $V_{I,0}$. Also as expected doubling TE approximately doubles calculated M. There is much smaller variation in M for ϕ_v, but sizeable variation in M due to Hct, OEF_0, and ω_v, consistent with the dependence of M on baseline deoxyhemoglobin-containing blood volume and deoxyhemoglobin concentration. Finally, the tissue relaxation rate constant, R^*_{2E} also has a noticeable impact on M as expected.

$f_{HC} = 1.6$ and $r_{HC} = 1.0$ but varied ϕ_{vHC} from 0 to 0.4. Again, we analyzed this signal using Eq. (1) to calculate M but still using $\alpha = 0.14$ and $\beta = 0.91$, which were optimized for $\phi_{vHC} = 0.2$.

Simulation results

For the standard subject, the true M for the classic Davis model was determined to be 11.1%, but if hypercapnia calibration decreases $CMRO_2$ by −10% ($r_{HC} = 0.9$) the scaling parameter would be overestimated ($M = 13.3\%$). We repeated the calculation of $\delta CMRO_2$ for this biased M using the classic Davis model at the three values of n (2.5, 5.0 and −0.8). We found the error in $\delta CMRO_2$ to be remarkably small at $n = 2.5$ and $\delta CMRO_2 = 20\%$ (21.0%, $\xi = 5.1\%$) such that the systematic error in M tends to correct systematic error in the classic α and β. At $n = 5.0$ and $\delta CMRO_2 = 10\%$, this is not the case. This value of M leads to large error in $\delta CMRO_2$ (13.9%, $\xi = 38.9\%$) and underestimate of $n = 3.6$ (Table 2). At $n = -0.8$ and $\delta CMRO_2 = 30\%$ instead of correcting the error associated with the classic α and β, the hypercapnia M magnified the error and grossly underestimated $\delta CMRO_2$ (12.7%, $\xi = -57.7\%$) (Table 2). Errors associated with biases due to both non-iso-metabolic hypercapnia calibration and concurrent variation of all other input parameters as in the previous section followed a similar systematic pattern of error (supplementary data, Table S1). The errors in $\delta CMRO_2$ for different degrees of $CMRO_2$ change with hypercapnia are shown in Fig. 8a.

If the relationship between CBV and CBF between activation and hypercapnia experiments changes, this also leads to bias in M. One study suggested that ϕ_{vHC} is less than ϕ_v due to activation (0.15 versus

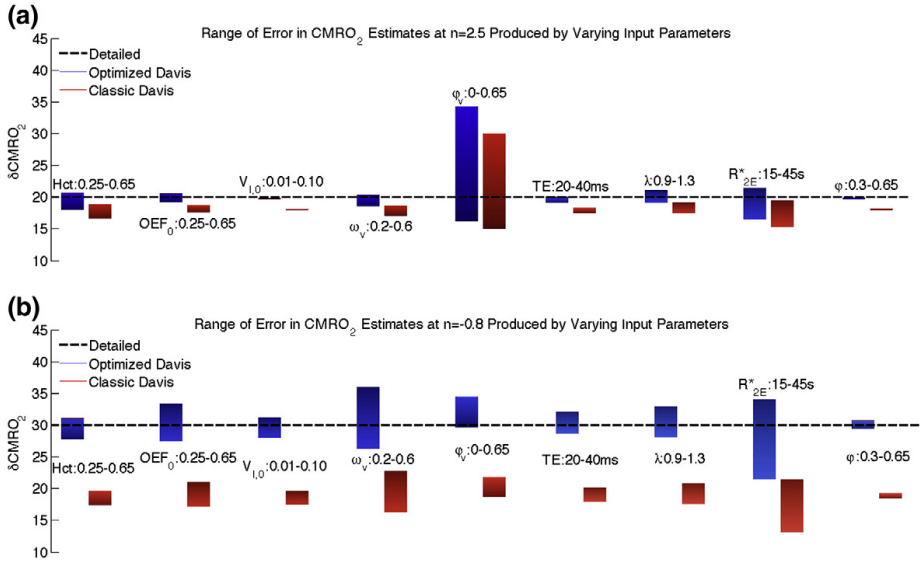

Fig. 6. Range of error in estimated $\delta CMRO_2$ due to single parameter variation. The nine input parameters to the detailed model again were altered around the standard values in Table 1 (see Introduction or Fig. 5 caption for parameter definitions). (a) At $n = 2.5$ ($\delta CBF = 50\%$) the classic Davis model shows a systematic underestimation of $\delta CMRO_2$ from the true value of 20.0% to 18.0% ($\xi = -9.8\%$). The optimized Davis model yields a more accurate estimate of $\delta CMRO_2$. Altering ϕ_v has the largest impact on the Davis model estimation (classic: 15.0–30.0%, max $\xi = 50.1\%$ and optimized: 16.2–34.2%, max $\xi = 71.0\%$). Variations in Hct, ω_v, and R^*_{2E} also have sizeable although much smaller effects on both models (see Table S1 for exact ranges). Variations due to $V_{I,0}$, TE, and ϕ are exceptionally small and are accounted for by the scaling parameter. The pattern of error at $n = 5.0$ is similar to the pattern of error for $n = 2.5$. (b) In the case of $n = -0.8$, ω_v and baseline R^*_{2E} have the largest effect on $\delta CMRO_2$ calculations followed by OEF_0, λ, and ϕ_v. The other parameters all also have a larger impact on $\delta CMRO_2$ calculations around this coupling of CBF and $CMRO_2$ suggesting that the mathematical form of the Davis model is not as reliable in this area of CBF–$CMRO_2$ coupling.

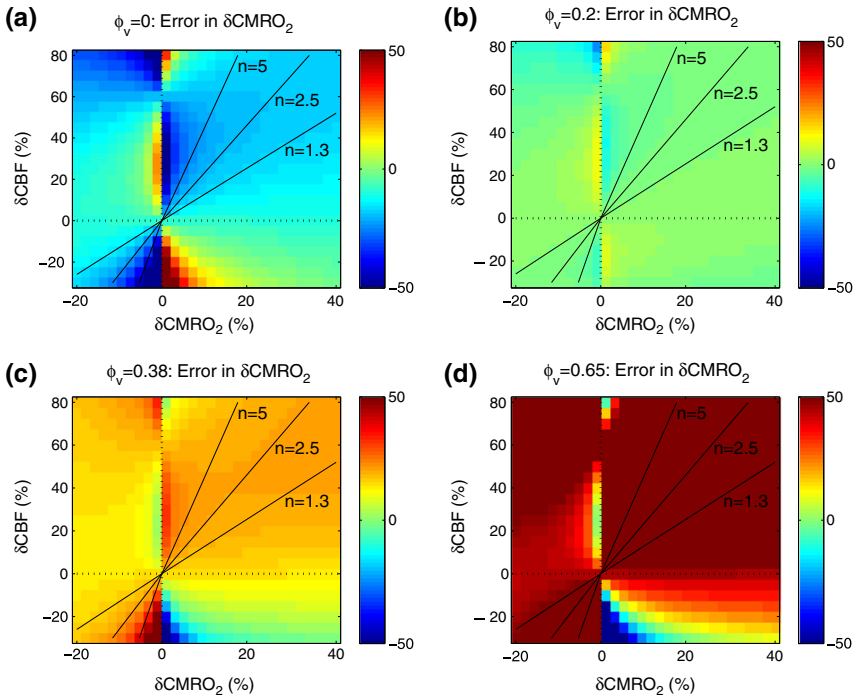

Fig. 7. Percent error in δCMRO$_2$ calculations using the optimized Davis model parameters ($\alpha = 0.14$ and $\beta = 0.91$) as the venous CBV change with activation (ϕ_v) is varied. (a) For $\phi_v = 0$, none of the total ΔCBV is distributed to the veins or capillaries. In this case the optimized Davis model underestimates CMRO$_2$. (b) As noted, recent research suggests ϕ_v is lower than total ϕ such that some δCBV distributes to the capillaries and veins, but most goes to the arteries. This plot is identical to Fig. 2b, and as expected due to the parameter optimization it shows that the modified Davis model provides a more accurate estimate of δCMRO$_2$ when most CBV distributes to the arteries. (c) When $\phi_v = 0.38$, ΔCBV distributes equally to all compartments, and in this case the optimized Davis model overestimates CMRO$_2$. (d) If venous CBV changes are much larger, such that $\phi_v = 0.65$, the optimized Davis model grossly overestimates δCMRO$_2$. This is consistent with the findings of Lin et al. (2008).

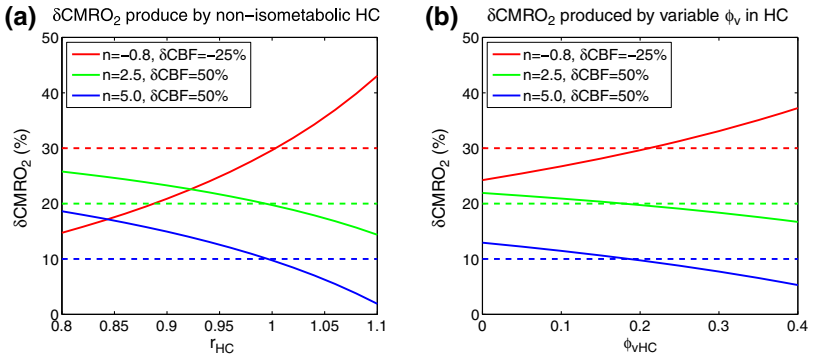

Fig. 8. Systematic error in δCMRO$_2$ calculations using the optimized Davis model due to errors in assumptions related to the effects of hypercapnia. Dashed lines represent true δCMRO$_2$. r_{HC} is the normalized change in δCMRO$_2$ due to hypercapnia (HC), normally assumed to be zero. ϕ_{vHC} is the exponent relating venous CBV to CBF for HC, normally assumed to be equal to the corresponding value for activation (0.2 in these calculations). (a) Deviation from the assumption that hypercapnia is iso-metabolic produces large errors in δCMRO$_2$ calculations. A decrease in cerebral O_2 metabolism with hypercapnia as some studies suggest will result in M being overestimated. This results in CMRO$_2$ being overestimated for $n = 2.5$ (green) and $n = 5.0$ (blue) and underestimated for $n = -0.8$ (red). Interestingly when using the classic Davis model, Table 2 (column 3) shows that this bias in M allows for some correction due to the bias introduced by the classic parameters. (b) If the relationship between CBV and CBF between activation and hypercapnia experiments changes, this also leads to bias in the estimation of CMRO$_2$. One study suggested that ϕ_{vHC} is less than ϕ_v due to activation (0.15 versus 0.23 respectively) (Chen and Pike, 2010). Again, this would overestimate δCMRO$_2$ calculations associated with $n = 2.5$ and $n = 5.0$ and underestimate δCMRO$_2$ for $n = -0.8$.

0.23 respectively) (Chen and Pike, 2010). If this is the case, then this would again lead to M being overestimated ($M = 11.4\%$). This error is much lower than the error associated with $r_{HC} = 0.9$, although it would result in $\delta CMRO_2$ calculations associated with $n = 2.5$ and $n = 5.0$ also being overestimated while for $n = -0.8$ $\delta CMRO_2$ will be underestimated (Fig. 8b).

Discussion

The calibrated BOLD method introduced by Davis and colleagues (Davis et al., 1998) offers one of the best noninvasive tools currently available for measuring changes in oxygen metabolism in the human brain with good spatial and temporal resolution. Estimating the fractional $CMRO_2$ change between two states (e.g., baseline/activation or pre/post drug administration) requires three things: measurement of both the CBF and BOLD signal differences; a mathematical model of how the BOLD response depends on δCBF and $\delta CMRO_2$; and a calibration experiment to determine an overall scaling factor for the BOLD response (M). Here, we examined the accuracy of these latter two requirements as they relate to the Davis model. This simple model describes the BOLD response as a function of δCBF and $\delta CMRO_2$ with three parameters: M, α and β. It has become the standard model for the calibrated BOLD experiment, with α and β assumed to have fixed values of $\alpha = 0.38$ and $\beta = 1.5$. M is determined from a hypercapnia experiment, with the assumption that mild hypercapnia alters CBF but not $CMRO_2$. In this paper we have analyzed the accuracy of the Davis model with a specific focus on the expected errors in the estimate of $\delta CMRO_2$ in the calibrated BOLD experiment. We developed a detailed analytical four-compartment model of the BOLD signal for a magnetic field strength of 3 T that includes a number of physiological parameters that could potentially affect the BOLD response, including hematocrit, oxygen extraction fraction, cerebral blood volume, and the distribution of blood volume changes between arterial and venous vessels as CBF changes.

Our detailed model of the BOLD response is an expanded version of other modeling approaches, which have sought to improve upon our physiologic understanding of the dependence on changes in blood volume and deoxyhemoglobin (Blockley et al., 2009; Buxton, 2009; Lin et al., 2008; Obata et al., 2004; Stephan et al., 2007; Uludag et al., 2009). However, the way we have used the model in the current study is somewhat different. Although the detailed model is much more complete than the simple Davis model, models such as this are difficult to adapt directly to the calibrated BOLD experiment because there are too many unknown variables. The power of the Davis model is its simplicity, with many potential physiologic sources of variability lumped into a single scaling parameter M that is measured individually. Despite the number of physiological variables that affect the BOLD signal, the surface of BOLD signal as a function of δCBF and $\delta CMRO_2$ is relatively smooth, so it is plausible that a simpler mathematical form such as the Davis model can provide a reasonably accurate approximation. To that end, we improved the Davis model by allowing α and β to be free parameters and performing non-linear parameter optimization to find the values that best fit the BOLD signal generated by the detailed model. By generating simulated data for a wide range of physiological conditions, we were able to test the ability of the Davis model, with either the classic or optimized values of α and β, to accurately calculate changes in $\delta CMRO_2$. We examined the impact of both variations in the underlying physiology and systematic errors related to the assumptions about the effects of hypercapnia in the calibration experiment. In analyzing such errors it is important to note that they are not uniform for all combinations of δCBF and $\delta CMRO_2$, and here we looked in detail at three values of the coupling ratio n ($\delta CBF/\delta CMRO_2$): $n = 2.5$ and $n = 5$, corresponding to a range of values reported for stimulus responses, and $n \sim -0.8$, a value we recently found for the effects of caffeine (lowered CBF but raised $CMRO_2$).

The key results are as follows:

1. The simulated data from the detailed model predict an M value close to what is typically observed, supporting the assumptions and parameter values underlying the model.
2. The Davis model fits this simulated data very well if α and β are allowed to be free parameters, although this requires that one abandon the physical meaning of these parameters as they were originally derived.
3. If there is physiological variation from the standard physiology used to optimize α and β, then the error expected in $\delta CMRO_2$ calculations is largest for variation in the venous CBV at baseline and the venous CBV change with activation.
4. If hypercapnia reduces $CMRO_2$, or produces smaller the venous volume changes for the same CBF relative to activation, then $\delta CMRO_2$ will be overestimated for the activation response but underestimated for the caffeine response.

These results are discussed in detail below.

The Davis model scaling parameter is simulated well by the detailed model

For the values of α and β optimized to the standard physiology defined in Table 1, the classic Davis model analysis of the simulated data results in $M = 11.1\%$. In comparison, using the classic parameters and correcting for TE, a sampling of published hypercapnia M values range from 7.0 to 14.1 (Chiarelli et al., 2007b; Hoge et al., 1999; Mark et al., 2011; Perthen et al., 2008; Stefanovic et al., 2006). This demonstrates that the detailed model reasonably simulates the BOLD signal. The simulations also show that the exact value of M varies significantly with variation of the baseline physiological parameters, particularly those parameters affecting total baseline deoxyhemoglobin including Hct, OEF_0, $V_{l,0}$ and ω_v (see Fig. 5), emphasizing the importance of experimentally measuring M in the calibrated-BOLD experiment. In fact, variation in published M values may be due to physiological variation between subjects and regions of interest. Particularly, regional variation in baseline CBV fraction ($V_{l,0}$) (Chugh et al., 2009) may account for differences in M between the motor cortex and visual cortex in the above referenced papers. For this reason, using a theoretical estimate of M for a standard set of physiological conditions is likely to introduce significant error in the estimation of $CMRO_2$ (Lin et al., 2008).

Optimization of Davis model parameters, α and β improves fit to simulated data

Despite the restrictive assumptions that went into its derivation, the errors in the estimate of $\delta CMRO_2$ using the classic Davis model are modest for most activation experiments. The classic Davis model with an accurately determined M systematically underestimates $\delta CMRO_2$ by about -10% (see Fig. 4). Even for a much higher value $n = 5.0$, the Davis model with the true M value underestimates $\delta CMRO_2$ by only -6.9%. However, for more unusual combinations of CBF and $CMRO_2$ change the errors can be quite a bit larger. For example, for $n = -0.8$ (increased $CMRO_2$ but decreased CBF) the error balloons to -38.0%. Using the parameter values $\alpha = 0.14$ and $\beta = 0.91$, optimized for the standard set of physiological parameters defined in Table 1, these errors are reduced, particularly for $n = -0.8$ where the optimized Davis model returns an error of only -1.2%.

A $CBF/CMRO_2$ coupling ratio described by $n = -0.8$ may at first glance seem physiologically unreasonable, but in fact such changes may occur in response to a drug, as we recently found for caffeine. In that study, δCBF was found to decrease by -27% (Perthen et al., 2008). Combined with analysis of the BOLD signal using the classic parameters and a hypercapnia calibrated M, a trend toward increased $CMRO_2$ was found ($\delta CMRO_2 = 13.3\%$, $p = 0.067$). Yet further analysis

of this data using the optimized model parameters and hypercapnia calibrated M revealed a significant metabolism increase due to caffeine ($\delta CMRO_2 = 21.8\%$, $p = 0.030$) (Griffeth et al., 2011). If the hypercapnia calibration is in error (see discussion below), with hypercapnia actually lowering $CMRO_2$, the true $CMRO_2$ change with caffeine may be as high as 30%.

As a consequence of this approach of optimizing α and β, we can neither identify α as simply the exponent relating CBV to CBF, nor can we strictly relate R_2^* to deoxyhemoglobin concentration using β as in the original derivation of the Davis model. Instead, α and β are effectively capturing several sources of variation arising in the detailed model, and they should just be regarded as fitting parameters. Keeping this in mind, optimal values of α and β depend on the physiologic parameters chosen for the standard state. For example, we included in our standard state the finding that relative CBV changes are larger for arteries than for capillaries and veins (Hillman et al., 2007; Kim et al., 2007; Chen and Pike, 2009a). Our finding of $\alpha = 0.14$ after parameter optimization is consistent with this smaller venous CBV change (smaller ϕ_v), but α is still not equal to ϕ_v implying that it is dependent on other parameters as well. Indeed, baseline CBV distribution and tissue properties also have large impacts on α and β (Fig. 3). As more data becomes available on the true nature of the physiology, this figure will allow for α and β to be appropriately adjusted. For example, this figure shows that α is most affected by and tracks linearly with ϕ_v such that when the assumed value of this parameter is increased, the optimized α determined by this process of non-linear parameter optimization also increases (e.g. $\phi_v = 0.38$ produces an optimized $\alpha = 0.24$ and $\beta = 0.84$).

Similarly, in the original Davis model derivation, β was used to relate extravascular R_{2E} to the concentration of deoxyhemoglobin, which is proportional to the ratio of O_2 fractions in activation and baseline. This ratio in turn is equal to the ratio r/f. Classically, the exponent β depended on the diameter of the vessels involved in signal creation, with $\beta = 1$ for large vessels and $\beta = 2$ for small vessels (Ogawa et al., 1993). In the Monte Carlo simulations performed by Davis et al. (1998), β was determined to be 1.5 for $B_0 = 1.5$ T. At 3 T, the large vessel component of the susceptibility difference will dominate such that β at 3 T should be smaller (Boxerman et al., 1995; Chiarelli et al., 2007b). Fig. 3 shows that the optimized value of β is affected by a variety of CBV and tissue parameters. Combined with the finding that α tracks with but is not equal to ϕ_v, this confirms that the Davis model is an oversimplification that does not model influences of the BOLD signal in a straightforward manner. Instead, the two parameters of the Davis model effectively capture multiple factors affecting the BOLD signal beyond what they were originally intended to model. Therefore, one should avoid using experimentally determined values of ϕ_v and β within the Davis model and instead perform more detailed parameter optimizations that capture the full range of physical and physiological factors that affect the BOLD signal.

Variation in CBV distribution has largest effect on the accuracy of the Davis model

Given the optimized values of α and β for the state defined in Table 1, it is important to determine the errors in $\delta CMRO_2$ that will result when this model is applied but the underlying physiology differs from this standard state. Despite the limitations of the Davis model, the fact that it relies on a calibration step to measure the variable scaling parameter, M, gives it a distinct advantage as this potentially allows for the absorption of many variable baseline factors, such as $V_{I,0}$, TE, Hct and OEF_0. That is, variation of a physiological variable that only scales the magnitude of the BOLD response, regardless of the exact values of δCBF and $\delta CMRO_2$, will not affect the estimate of $\delta CMRO_2$ provided M is accurately measured. For example, Fig. 6 shows that $V_{I,0}$, Hct, TE and ϕ do not have a large impact on $\delta CMRO_2$ calculations. Even large variations in $V_{I,0}$ cause only small deviations in the range of calculated $\delta CMRO_2$ (Supplementary data, Table S1).

The physiological parameters that are not captured well by M, and so are likely to produce the largest errors in the estimation of $CMRO_2$ changes, are the venous CBV at baseline, the venous CBV change, R_{2E}^* and to a lesser extent OEF_0. These parameters may vary with brain region, stimulus type or duration, between subjects, and in health and disease. For example although Rostrup et al. (2005) found the relationship between changes in CBF and CBV to be constant across the brain, other groups have found variation in regional baseline CBV (Chugh et al., 2009) and in the temporal dynamics of CBV distribution in vessels as they dilate in response to a stimulus (Kim and Kim, 2010b). There is also evidence of CBV changing with disease (Guckel et al., 2007). In addition to differences in CBV, regional differences have been found in OEF_0 and R_{2E}^* (He and Yablonskiy, 2007), and inter-subject differences have been found in baseline CBF (Ances et al., 2009).

To address this physiologic variation, we varied the basic parameter values over wide ranges and calculated the error in estimated $\delta CMRO_2$. The change in venous CBV with activation (ϕ_v) is the most important factor in reliably estimating $\delta CMRO_2$ around $n = 2.5$. Recent research has suggested that arterial changes dominate venous change (Chen and Pike, 2009a; Hillman et al., 2007; Kim et al., 2007; Kim and Kim, 2006), but additional studies are needed to precisely quantify the relationship between venous CBV and CBF. Particularly, it is important to define how CBV changes are distributed dynamically, whether this changes with stimulus duration and type, and whether the relationship between CBV and CBF depends on brain region (Kim and Kim, 2010a,b). Any of these considerations could alter ϕ and/or ϕ_v thereby affecting optimization of the Davis model parameters and $CMRO_2$ calculations.

For $n = 2.5$, baseline venous volume fraction (ω_v) is secondarily important while for $n = -0.8$ accurate knowledge of ω_v and R_{2E}^* becomes much more significant, even more so than ϕ_v. In this regime of strong uncoupling (decreased CBF with increased $CMRO_2$), baseline CBV, intravascular to extravascular spin density ratio, and baseline oxygen extraction also have sizeable although smaller effects on $\delta CMRO_2$ calculations (Fig. 6b). As with ϕ_v, additional research is needed to confirm the normal range of OEF_0, $V_{I,0}$, and λ. However, it is possible to measure R_{2E}^* and λ in individual subjects and may soon be possible to reliably measure OEF_0 using MR techniques (Chen and Pike, 2009b; Lu and Ge, 2008; Qin et al., 2011). As our knowledge of these values increases, we will be able to increase the accuracy of our model.

The importance of an accurate knowledge of ϕ_v is emphasized in Fig. 7, which shows how accurate the optimized model is as ϕ_v increases from 0 to 0.2, 0.38 and 0.65. The Davis model optimized for $\phi_v = 0.2$ estimates $\delta CMRO_2$ very well at this value but overestimates $\delta CMRO_2$ if $\phi_v = 0.38$ or 0.65, and underestimates $\delta CMRO_2$ for $\phi_v = 0$. We also examined the effect of setting total $\phi = 0.65$ as found by Lin et al. using VASO (2008) and found it has little effect compared to $\phi = 0.38$ if $\phi_v = 0.2$ remains unchanged. However if this volume change is distributed equally to the compartments such that $\phi_v = 0.65$, then the optimized Davis model will overestimate $\delta CMRO_2$ in agreement with the results of Lin et al. (2008) and mirroring Fig. 7d. Yet, the VASO technique used in the study of Lin et al. specifically measures changes in total CBV rather than venous CBV. Therefore to apply VASO data to the Davis model, it must be assumed that venous CBV changes in the same way as total CBV. Furthermore, a value for baseline CBV must be assumed in order to translate absolute volume changes into fractional changes, which are necessary for calculating the power-law relationship between CBF and CBV. Both assumptions may lead to ϕ_v being overestimated. Specifically, experimental findings of larger changes on the arterial side do not support the large venous CBV changes associated with $\phi_v = 0.65$, although more experiments are needed to confirm this. A previous study also examined whether the assumption that venous CBV changes are similar to total CBV changes would affect $CMRO_2$ calculations (Kim et al., 1999). This study reported that the effects are minimal as long as a multiplicative term involving deoxyhemoglobin

and volume changes is small. However, this may not be the case in all activation experiments, and furthermore this model assumes that changes in R_2^* are small and only includes venous blood volume, neglecting the effects of arterial and capillary blood volume.

Violations of hypercapnia calibration assumptions lead to errors in M and $\delta CMRO_2$

In our initial calculations, we assumed that we could accurately measure M in order to explore the effects of physiologic variation. Recent research has suggested methods other than hypercapnia for more reliably measuring M. This is an active area of research, although one method gaining popularity is hyperoxia (Chiarelli et al., 2007b; Mark et al., 2011). To this point, though, most calibrated BOLD experiments have used hypercapnia to measure the scaling parameter M by assuming $CMRO_2$ is not changed by CO_2 inhalation (Chen and Pike, 2010; Jones et al., 2005; Sicard and Duong, 2005), but there is some controversy about this assumption (Kliefoth et al., 1979; Xu et al., 2011; Zappe et al., 2008). If hypercapnia in fact decreases $CMRO_2$ then this process would tend to overestimate M. At larger values of CBF–$CMRO_2$ coupling, this produces large errors in $\delta CMRO_2$ calculations and underestimates n. Interestingly, this underestimation of n is larger for bigger values of n. This may account for some of the discrepancies between fMRI and PET data in studies reporting larger values of n. For example, one PET study found values of n between 5 and 6 in the somatosensory cortex (Fox and Raichle, 1986) while an fMRI experiment found values closer to $n = 3$–4 (Chiarelli et al., 2007a). One area of CBF–$CMRO_2$ coupling particularly sensitive to M is decreased CBF and increased $CMRO_2$ as produced by caffeine. Here, overestimates of M will tend to underestimate $\delta CMRO_2$, and it is in this area that error in both M and the parameters α and β have the largest impact on $\delta CMRO_2$ calculations (Fig. 4).

Another assumption of hypercapnia calibration is that CBV changes in different compartments are the same for activation and hypercapnia. As Fig. 8 shows, error due to differences in relative CBV changes between activation and hypercapnia followed a pattern similar to violations of the iso-metabolic assumption. If ϕ_{vHC} is less than ϕ_v (Chen and Pike, 2010), then M and $\delta CMRO_2$ will be overestimated. If ϕ_{vHC} is more than ϕ_v, then the opposite pattern of errors is apparent. Even with the systematic error in M due to changes in CBV distribution and $\delta CMRO_2$ with hypercapnia, the Davis model is surprisingly accurate, especially close to $n = 2.5$. This is likely due to the calibration process. Even with the inaccuracies of calibration, some self-correction of errors occurs when the same, albeit incomplete, model is used to analyze both the hypercapnia and activation data.

Future work

In this paper we have used the detailed model of the BOLD effect to assess and improve the accuracy of the calibrated BOLD method. The detailed model can also be used to address more basic questions of which physiological changes dominate the BOLD effect. Total deoxyhemoglobin, influenced by blood volume and concentration, is the most important factor. Previous models have included to different degrees separate terms for CBV (to model exchange effects) and deoxyhemoglobin concentration in blood (to model the intrinsic signal change of blood). The detailed model includes these effects and others as above, and it can be used to evaluate additional models (Buxton, 2009; Obata et al., 2004; Stephan et al., 2007).

Finally, an area of future application of the detailed model is to analyze potential errors in $CMRO_2$ determination when hyperoxia is used for calibration. Hyperoxia was introduced as an alternative to hypercapnia as a way to avoid uncertainties due to the iso-metabolic assumption of the hypercapnia calibration, and because hyperoxia is more tolerable than hypercapnia (Chiarelli et al., 2007b). However, the hyperoxia calibration makes some additional assumptions such as baseline OEF, and the impact of these assumptions can be tested with the current model. The hyperoxia approach also does not have the same self-correcting behavior as hypercapnia. The difference is that hypercapnia and activation both involve CBF changes and associated assumptions about how CBV is altered. In contrast when using hyperoxia calibration, only the activation part of the experiment depends on the CBF change, and hyperoxia just manipulates deoxyhemoglobin content. For this reason, calibrated BOLD using hyperoxia is likely to be more sensitive to inaccuracies in the modeling of how CBV depends on CBF. All of these effects will be evaluated with the detailed model in future work.

Conclusions

The detailed model of the BOLD response developed here provides a theoretical framework for analyzing a number of questions related to the interpretation of the BOLD response. Here, we focused on improving the accuracy of the calibrated BOLD method to estimate changes in $CMRO_2$. Despite the simplicity of the Davis model, and the restrictive assumptions of the original derivation, the mathematical form of the model nevertheless provides a reasonably accurate approximation for this complex phenomenon. The accuracy of the model is improved by using optimized values of the parameters α and β calculated from the detailed model. It is important to recognize, though, that the optimized parameter values no longer correspond to the physiological effects they were originally introduced to model and should be treated simply as fitting parameters. As new experimental data becomes available, particularly an accurate understanding of the venous CBV change with activation, these optimized values can be revised based on the calculations presented here for the detailed model.

Supplementary materials related to this article can be found online at doi:10.1016/j.neuroimage.2011.05.077.

Acknowledgments

We thank Farshad Moradi, Aaron Simon, and David Dubowitz for discussion, and Nic Blockley for confirmation of results as well as comments on the approach. This research was supported by funding from NIH grant NS-36722, NRSA grant HL-7089, NIGMS MSTP training grant GM7198 and HHMI-NIBIB Interfaces grant EB-9380.

Appendix A

The MR signal is a volume-weighted average of signals from extravascular and intravascular compartments (Buxton et al., 1998; Obata et al., 2004), and we assume that contributions from the different compartments combine linearly. The intravascular component can be further segmented into arterial, capillary and venous compartments denoted by the subscripts A, C and V respectively. The subscript I denotes the sum of all intravascular compartments. The subscript E denotes the extravascular compartment. We use the subscript 0 to denote the baseline state. Here we are assuming a static model, but ultimately we will apply this model dynamically, requiring a more detailed knowledge of how the different compartments change over time. S is the total signal while $S_{E,A,C,V}$ is the signal intensity of a voxel containing only the designated component, and $V_{E,A,C,V}$ is the corresponding volume fraction of that component. The net signal is then:

$$S = V_E S_E + V_A S_A + V_C S_C + V_V S_V \tag{A1}$$

The intrinsic signal for each compartment can be modeled as an exponential decay dependent on the transverse relaxation rate, R_2, and the signal at the theoretical $TE = 0$, which in general will depend on the spin density and the longitudinal relaxation time constant T_1. Assuming T_1 does not change with activation, such that the signal at

$TE=0$ does not change, then the following equality is formed describing the intrinsic signal ratio of blood:

$$\varepsilon_{(A,C,V)} = \frac{S_{(A,C,V),0}}{S_{E,0}} = \lambda \frac{e^{-TEi R^*_{2(A,C,V)}}}{e^{-TEi R^*_{2E}}} \tag{A2}$$

λ is the effective intravascular to extravascular spin density ratio, or the signal ratio when $TE=0$, and this was assumed to have the same value for each of the intravascular compartments. The value of λ was determined experimentally to be 1.15 (Producing simulated BOLD data for a standard subject section). Since BOLD is a fractional signal change, it can be expressed as $\delta S = \frac{S-S(0)}{S(0)} = \frac{\Delta S}{S(0)}$. Noting $V_E = 1-V_A-V_C-V_V = 1-V_I$, it follows that:

$$\delta S = H\left[(1-V_I)e^{-TE\cdot\Delta R^*_{2E}} + \varepsilon_A V_A e^{-TE\cdot\Delta R^*_{2A}} + \varepsilon_C V_C e^{-TE\cdot\Delta R^*_{2C}} + \varepsilon_V V_V e^{-TE\cdot\Delta R^*_{2V}}\right] - 1 \tag{A3}$$

Where

$$H = 1 \,/\, \left(1-V_{I,0} + \varepsilon_A V_{A,0} + \varepsilon_C V_{C,0} + \varepsilon_V V_{V,0}\right) \tag{A4}$$

The intravascular transverse relaxation rate constants were approximated for each compartment using a quadratic model dependent on *Hct* and SO_2 (Silvennoinen et al., 2003; Zhao et al., 2007):

$$\begin{aligned} &R^*_2 = A^* + C^*(1-SO_2)^2 \\ &\text{where} \\ &A^* = 14.87\cdot Hct + 14.686 \\ &C^* = 302.06\cdot Hct + 41.83 \end{aligned} \tag{A5}$$

The dependence of A* and C* on *Hct* was approximated using a linear fit of the experimental data for 3 T reported in Zhao et al. (2007).

The oxygen extraction fraction with activation was calculated from the normalized CBF and $CMRO_2$, which are variable inputs to the detailed model:

$$OEF = OEF_0 \frac{r}{f} \tag{A6}$$

Oxygen saturation for the venous compartment was determined from the arterial saturation and the oxygen extraction fraction:

$$S_V O_2 = S_A O_2 - OEF\cdot S_A O_2 \tag{A7}$$

Capillary oxygen saturation ($S_C O_2$) was calculated as an average of arterial and venous values with weighting κ:

$$S_C O_2 = \kappa\cdot S_A O_2 - (1-\kappa)\cdot S_V O_2 \tag{A8}$$

In calculating ΔR^*_2 values, the A^* terms cancel leaving dependence on *Hct* through C^* as well as SO_2 from both the baseline and activation states. The second term denoted by the subscript 0 is associated with the baseline state.

$$\Delta R^*_{2(A,C,V)} = C^*\left[\left(1-S_{(A,C,V)}O_2\right)^2 - \left(1-S_{(A,C,V)}O_{2,0}\right)^2\right] \tag{A9}$$

Note that SO_2 decreases from arteries to capillaries to veins, while capillary *Hct* is also 76% of the arterial value (Sakai et al., 1989).

Extravascular R^*_2 change was treated as a linear combination of the contributions from each of the vascular compartments calculated separately as determined by Ogawa et al. (1993). In general, R^*_2 is the sum of two components: the transverse relaxation rate in the presence of fully oxygenated blood (R_2) and the signal relaxation rate due to local field inhomogeneities including the effects of deoxygenated blood (R'_2). When calculating R^*_2, R_2 remains constant and therefore cancels leaving only the difference in R'_2 ($\Delta R^*_2 = R'_2(t) - R'_2(0)$), which was previously estimated using Monte Carlo simulations of water proton intravoxel phase dispersion. These experiments demonstrated that depending on vessel size, R^*_2 has either a linear or quadratic dependence on main magnetic field strength B_0, *Hct*, and SO_2 as well as purely linear dependence on blood volume fraction (V) (Ogawa et al., 1993):

$$\Delta R^*_{2E(A,C,V)} = \begin{cases} \frac{4\pi}{3}\Delta\chi\cdot Hct\cdot\gamma\cdot B_0\left[V_{(A,V)}\left(|SO_{2,off} - S_{A,V}O_2|\right) - V_{(A,V),0}\left(|SO_{2,off} - S_{A,V}O_{2,0}|\right)\right] \\ 0.04(\Delta\chi\cdot Hct\cdot\gamma\cdot B_0)^2\left[V_C\left(|SO_{2,off} - S_C O_2|\right)^2 - V_{C,0}\left(|SO_{2,off} - S_C O_{2,0}|\right)^2\right] \end{cases} \tag{A10}$$

Note that $\Delta\chi$ is the susceptibility of blood with fully deoxygenated blood, γ is the gyromagnetic ratio of protons, and $SO_{2,off}$ is the O_2 saturation that produces no magnetic susceptibility difference between blood and tissue. Total extravascular ΔR^*_2 is then the sum of these three blood compartment contributions.

References

Ances, B.M., Liang, C.L., Leontiev, O., Perthen, J.E., Fleisher, A.S., Lansing, A.E., Buxton, R.B., 2009. Effects of aging on cerebral blood flow, oxygen metabolism, and blood oxygenation level dependent responses to visual stimulation. Hum. Brain Mapp. 30, 1120–1132.

Blockley, N.P., Francis, S.T., Gowland, P.A., 2009. Perturbation of the BOLD response by a contrast agent and interpretation through a modified balloon model. NeuroImage 48, 84–93.

Bolar, D.S., Rosen, B.R., Evans, K.C., Sorensen, A.G., Adalsteinsson, E., 2010. Depression of cortical gray matter $CMRO_2$ in awake humans during hypercapnia. Proceedings of the ISMRM, Stockholm, p. 516.

Boxerman, J.L., Hamberg, L.M., Rosen, B.R., Weisskoff, R.M., 1995. MR contrast due to intravascular magnetic susceptibility perturbations. Magn. Reson. Med. 34, 555–566.

Buxton, R.B., 2009. Modeling the effects of changes in arterial blood volume on the BOLD signal. Proceedings of the ISMRM, Honolulu.

Buxton, R.B., 2010. Interpreting oxygenation-based neuroimaging signals: the importance and the challenge of understanding brain oxygen metabolism. Front Neuroenergetics 2, 8.

Buxton, R.B., Wong, E.C., Frank, L.R., 1998. Dynamics of blood flow and oxygenation changes during brain activation: the balloon model. Magn. Reson. Med. 39, 855–864.

Buxton, R.B., Uludag, K., Dubowitz, D.J., Liu, T.T., 2004. Modeling the hemodynamic response to brain activation. NeuroImage 23 (Suppl 1), S220–S233.

Chen, J.J., Pike, G.B., 2009a. BOLD-specific cerebral blood volume and blood flow changes during neuronal activation in humans. NMR Biomed. 22, 1054–1062.

Chen, J.J., Pike, G.B., 2009b. Human whole blood T2 relaxometry at 3 Tesla. Magn. Reson. Med. 61, 249–254.

Chen, J.J., Pike, G.B., 2010. MRI measurement of the BOLD-specific flow–volume relationship during hypercapnia and hypocapnia in humans. NeuroImage 53, 383–391.

Chiarelli, P.A., Bulte, D.P., Gallichan, D., Piechnik, S.K., Wise, R., Jezzard, P., 2007a. Flow–metabolism coupling in human visual, motor, and supplementary motor areas assessed by magnetic resonance imaging. Magn. Reson. Med. 57, 538–547.

Chiarelli, P.A., Bulte, D.P., Wise, R., Gallichan, D., Jezzard, P., 2007b. A calibration method for quantitative BOLD fMRI based on hyperoxia. NeuroImage 37, 808–820.

Chugh, B.P., Lerch, J.P., Yu, L.X., Pienkowski, M., Harrison, R.V., Henkelman, R.M., Sled, J.G., 2009. Measurement of cerebral blood volume in mouse brain regions using micro-computed tomography. NeuroImage 47, 1312–1318.

Cox, R.W., 1996. AFNI: software for analysis and visualization of functional magnetic resonance neuroimages. Comput. Biomed. Res. 29, 162–173.

Davis, T.L., Kwong, K.K., Weisskoff, R.M., Rosen, B.R., 1998. Calibrated functional MRI: mapping the dynamics of oxidative metabolism. Proc. Natl. Acad. Sci. U. S. A. 95, 1834–1839.

Donahue, M.J., Blicher, J.U., Ostergaard, L., Feinberg, D.A., MacIntosh, B.J., Miller, K.L., Gunther, M., Jezzard, P., 2009. Cerebral blood flow, blood volume, and oxygen metabolism dynamics in human visual and motor cortex as measured by whole-brain multi-modal magnetic resonance imaging. J. Cereb. Blood Flow Metab. 29, 1856–1866.

Fox, P.T., Raichle, M.E., 1986. Focal physiological uncoupling of cerebral blood flow and oxidative metabolism during somatosensory stimulation in human subjects. Proc. Natl. Acad. Sci. U. S. A. 83, 1140–1144.

Friston, K.J., Mechelli, A., Turner, R., Price, C.J., 2000. Nonlinear responses in fMRI: the Balloon model, Volterra kernels, and other hemodynamics. NeuroImage 12, 466–477.

Griffeth, V.E.M., Perthen, J.E., Buxton, R.B., 2011. Prospects for quantitative fMRI: investigating the effects of caffeine on baseline oxygen metabolism and the response to a visual stimulus in humans. Neuroimage (Electronic publication ahead of print).

Grubb, R.L., Raichle, M.E., Eichling, J.O., Ter-Pogossian, M.M., 1974. The effects of changes in $PaCO_2$ on cerebral blood volume, blood flow, and vascular mean transit time. Stroke 5, 630–639.

Guckel, F.J., Brix, G., Hennerici, M., Lucht, R., Ueltzhoffer, C., Neff, W., 2007. Regional cerebral blood flow and blood volume in patients with subcortical arteriosclerotic encephalopathy (SAE). Eur. Radiol. 17, 2483–2490.

Gustard, S., Williams, E.J., Hall, L.D., Pickard, J.D., Carpenter, T.A., 2003. Influence of baseline hematocrit on between-subject BOLD signal change using gradient echo and asymmetric spin echo EPI. Magn. Reson. Imaging 21, 599–607.

He, X., Yablonskiy, D.A., 2007. Quantitative BOLD: mapping of human cerebral deoxygenated blood volume and oxygen extraction fraction: default state. Magn. Reson. Med. 57, 115–126.

Hillman, E.M., Devor, A., Bouchard, M.B., Dunn, A.K., Krauss, G.W., Skoch, J., Bacskai, B.J., Dale, A.M., Boas, D.A., 2007. Depth-resolved optical imaging and microscopy of vascular compartment dynamics during somatosensory stimulation. NeuroImage 35, 89–104.

Hoge, R.D., Atkinson, J., Gill, B., Crelier, G.R., Marrett, S., Pike, G.B., 1999. Investigation of BOLD signal dependence on cerebral blood flow and oxygen consumption: the deoxyhemoglobin dilution model. Magn. Reson. Med. 42, 849–863.

Hyder, F., Sanganahalli, B.G., Herman, P., Coman, D., Maandag, N.J., Behar, K.L., Blumenfeld, H., Rothman, D.L., 2010. Neurovascular and neurometabolic couplings in dynamic calibrated fMRI: transient oxidative neuroenergetics for block-design and event-related paradigms. Front Neuroenergetics 2.

Ito, H., Ibaraki, M., Kanno, I., Fukuda, H., Miura, S., 2005. Changes in cerebral blood flow and cerebral oxygen metabolism during neural activation measured by positron emission tomography: comparison with blood oxygenation level-dependent contrast measured by functional magnetic resonance imaging. J. Cereb. Blood Flow Metab. 25, 371–377.

Jones, M., Berwick, J., Hewson-Stoate, N., Gias, C., Mayhew, J., 2005. The effect of hypercapnia on the neural and hemodynamic responses to somatosensory stimulation. NeuroImage 27, 609–623.

Kim, T., Kim, S.G., 2006. Quantification of cerebral arterial blood volume using arterial spin labeling with intravoxel incoherent motion-sensitive gradients. Magn. Reson. Med. 55, 1047–1057.

Kim, T., Kim, S.G., 2010a. Cortical layer-dependent arterial blood volume changes: improved spatial specificity relative to BOLD fMRI. NeuroImage 49, 1340–1349.

Kim, T., Kim, S.G., 2010b. Temporal dynamics and spatial specificity of arterial and venous blood volume changes during visual stimulation: implication for BOLD quantification. J. Cereb. Blood Flow Metab. 31 (5), 1211–1222.

Kim, S.G., Rostrup, E., Larsson, H.B.W., Ogawa, S., Paulson, O.B., 1999. Determination of relative $CMRO_2$ from CBF and BOLD changes: significant increase of oxygen consumption rate during visual stimulation. Magn. Reson. Med. 41, 1152–1161.

Kim, T., Hendrich, K.S., Masamoto, K., Kim, S.G., 2007. Arterial versus total blood volume changes during neural activity-induced cerebral blood flow change: implication for BOLD fMRI. J. Cereb. Blood Flow Metab. 27, 1235–1247.

Kliefoth, A.B., Grubb Jr., R.L., Raichle, M.E., 1979. Depression of cerebral oxygen utilization by hypercapnia in the rhesus monkey. J. Neurochem. 32, 661–663.

Leontiev, O., Buxton, R.B., 2007. Reproducibility of BOLD, perfusion, and CMRO(2) measurements with calibrated-BOLD fMRI. NeuroImage 35, 175–184.

Lin, A.L., Fox, P.T., Yang, Y., Lu, H., Tan, L.H., Gao, J.H., 2008. Evaluation of MRI models in the measurement of $CMRO_2$ and its relationship with CBF. Magn. Reson. Med. 60, 380–389.

Lin, A.L., Fox, P.T., Hardies, J., Duong, T.Q., Gao, J.H., 2010. Nonlinear coupling between cerebral blood flow, oxygen consumption, and ATP production in human visual cortex. Proc. Natl. Acad. Sci. U. S. A. 107, 8446–8451.

Lu, H., Ge, Y., 2008. Quantitative evaluation of oxygenation in venous vessels using T2-relaxation-under-spin-tagging MRI. Magn. Reson. Med. 60, 357–363.

Lu, H., Golay, X., Pekar, J.J., Van Zijl, P.C., 2004. Sustained poststimulus elevation in cerebral oxygen utilization after vascular recovery. J. Cereb. Blood Flow Metab. 24, 764–770.

Mandeville, J.B., Marota, J.J.A., Ayata, C., Zaharchuk, G., Moskowitz, M.A., Rosen, B.R., Weisskoff, R.M., 1999. Evidence of a cerebrovascular post-arteriole Windkessel with delayed compliance. J. Cereb. Blood Flow Metabol. 19, 679–689.

Marchal, G., Rioux, P., Petit-Taboue, M.-C., Sette, G., Travere, J.-M., LePoec, C., Courtheoux, P., Derlon, J.-M., Baron, J.-C., 1992. Regional cerebral oxygen consumption, blood flow, and blood volume in healthy human aging. Arch. Neurol. 49, 1013–1020.

Mark, C.I., Fisher, J.A., Pike, G.B., 2011. Improved fMRI calibration: precisely controlled hyperoxic versus hypercapnic stimuli. NeuroImage 54, 1102–1111.

Obata, T., Liu, T.T., Miller, K.L., Luh, W.M., Wong, E.C., Frank, L.R., Buxton, R.B., 2004. Discrepancies between BOLD and flow dynamics in primary and supplementary motor areas: application of the balloon model to the interpretation of BOLD transients. NeuroImage 21, 144–153.

Ogawa, S., Menon, R.S., Tank, D.W., Kim, S.-G., Merkle, H., Ellerman, J.M., Ugurbil, K., 1993. Functional brain mapping by blood oxygenation level — dependent contrast magnetic resonance imaging: a comparison of signal characteristics with a biophysical model. Biophys. J. 64, 803–812.

Perthen, J.E., Lansing, A.E., Liau, J., Liu, T.T., Buxton, R.B., 2008. Caffeine-induced uncoupling of cerebral blood flow and oxygen metabolism: a calibrated BOLD fMRI study. NeuroImage 40, 237–247.

Qin, Q., Grgac, K., van Zijl, P.C., 2011. Determination of whole-brain oxygen extraction fractions by fast measurement of blood T(2) in the jugular vein. Magn. Reson. Med. 65, 471–479.

Roland, P.E., Eriksson, L., Stone-Elander, S., Widen, L., 1987. Does mental activity change the oxidative metabolism of the brain? J. Neurochem. 7, 2373–2389.

Rostrup, E., Knudsen, G.M., Law, I., Holm, S., Larsson, H.B., Paulson, O.B., 2005. The relationship between cerebral blood flow and volume in humans. NeuroImage 24, 1–11.

Sakai, F., Nakazawa, K., Tazaki, Y., Ishii, K., Hino, H., Igarashi, H., Kanda, T., 1985. Regional cerebral blood volume and hematocrit measured in normal human volunteers by single-photon emission computed tomography. J. Cereb. Blood Flow Metab. 5, 207–213.

Sakai, F., Igarashi, H., Suzuki, S., Tazaki, Y., 1989. Cerebral blood flow and cerebral hematocrit in patients with cerebral ischemia measured by single-photon emission computed tomography. Acta Neurol. Scand. Suppl. 127, 9–13.

Schutz, S.L., 2001. Oxygen saturation monitoring by pulse oximetry, In: Lynn-McHale, D.J., Carlson, K.K. (Eds.), AACN procedure manual for critical care, 4th ed. Elsevier Saunders, St. Louis, Mo.

Sicard, K.M., Duong, T.Q., 2005. Effects of hypoxia, hyperoxia, and hypercapnia on baseline and stimulus-evoked BOLD, CBF, and $CMRO_2$ in spontaneously breathing animals. NeuroImage 25, 850–858.

Silvennoinen, M.J., Clingman, C.S., Golay, X., Kauppinen, R.A., van Zijl, P.C., 2003. Comparison of the dependence of blood R2 and R2* on oxygen saturation at 1.5 and 4.7 Tesla. Magn. Reson. Med. 49, 47–60.

Spees, W.M., Yablonskiy, D.A., Oswood, M.C., Ackerman, J.J., 2001. Water proton MR properties of human blood at 1.5 Tesla: magnetic susceptibility, T(1), T(2), T*(2), and non-Lorentzian signal behavior. Magn. Reson. Med. 45, 533–542.

Stefanovic, B., Warnking, J.M., Pike, G.B., 2004. Hemodynamic and metabolic responses to neuronal inhibition. NeuroImage 22, 771–778.

Stefanovic, B., Warnking, J.M., Rylander, K.M., Pike, G.B., 2006. The effect of global cerebral vasodilation on focal activation hemodynamics. NeuroImage 30, 726–734.

Stefanovic, B., Hutchinson, E., Yakovleva, V., Schram, V., Russell, J.T., Belluscio, L., Koretsky, A.P., Silva, A.C., 2008. Functional reactivity of cerebral capillaries. J. Cereb. Blood Flow Metab. 28, 961–972.

Stephan, K.E., Weiskopf, N., Drysdale, P.M., Robinson, P.A., Friston, K.J., 2007. Comparing hemodynamic models with DCM. NeuroImage 38, 387–401.

Tsai, A.G., Johnson, P.C., Intaglietta, M., 2003. Oxygen gradients in the microcirculation. Physiol. Rev. 83, 933–963.

Uludag, K., Muller-Bierl, B., Ugurbil, K., 2009. An integrative model for neuronal activity-induced signal changes for gradient and spin echo functional imaging. NeuroImage 48, 150–165.

Weber, B., Keller, A.L., Reichold, J., Logothetis, N.K., 2008. The microvascular system of the striate and extrastriate visual cortex of the macaque. Cereb. Cortex 18, 2318–2330.

Xu, F., Uh, J., Brier, M.R., Hart Jr., J., Yezhuvath, U.S., Gu, H., Yang, Y., Lu, H., 2011. The influence of carbon dioxide on brain activity and metabolism in conscious humans. J. Cereb. Blood Flow Metab. 31, 58–67.

Zappe, A.C., Uludag, K., Logothetis, N.K., 2008. Direct measurement of oxygen extraction with fMRI using 6% CO_2 inhalation. Magn. Reson. Imaging 26, 961–967.

Zhao, J.M., Clingman, C.S., Narvainen, M.J., Kauppinen, R.A., van Zijl, P.C., 2007. Oxygenation and hematocrit dependence of transverse relaxation rates of blood at 3 T. Magn. Reson. Med. 58, 592–597.

Zheng, Y., Pan, Y., Harris, S., Billings, S., Coca, D., Berwick, J., Jones, M., Kennerley, A., Johnston, D., Martin, C., Devonshire, I.M., Mayhew, J., 2010. A dynamic model of neurovascular coupling: implications for blood vessel dilation and constriction. Neuroimage 52 (3), 1135–1147.

Supplementary Information

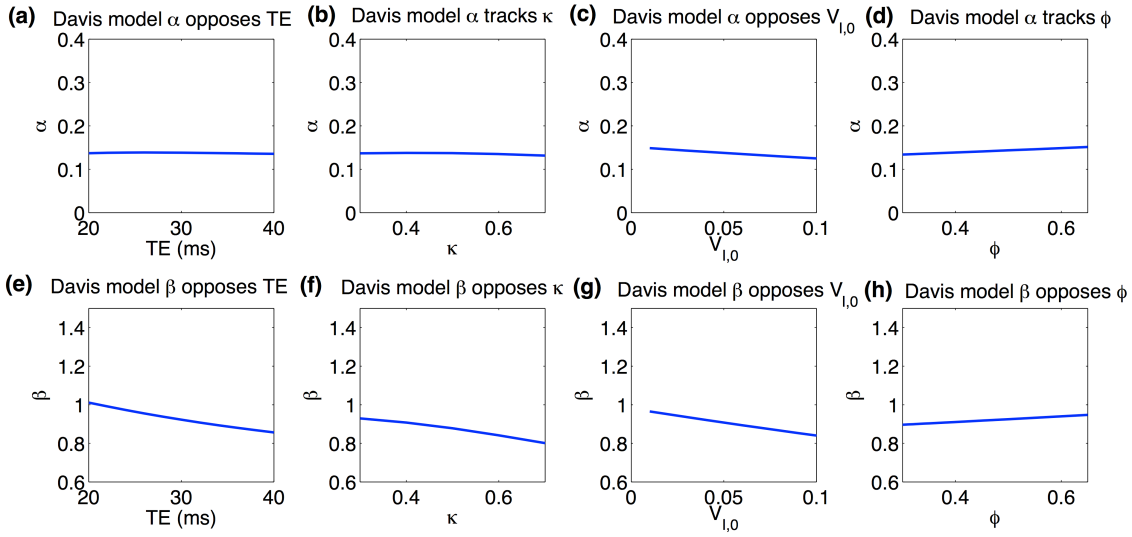

Supplementary Figure S1.1.9. Dependence of Davis model α and β on $V_{I,0}$, λ, TE, ϕ.

Optimization of Davis model parameters α and β was performed using the Matlab fmincon function. (a-d) Davis model a has a negative correlation to λ and a weak positive correlation to ϕ while not showing a strong dependence on VI,0 or TE. (e-h) Davis model β has a negative correlation to VI,0, λ and TE and a positive correlation to ϕ.

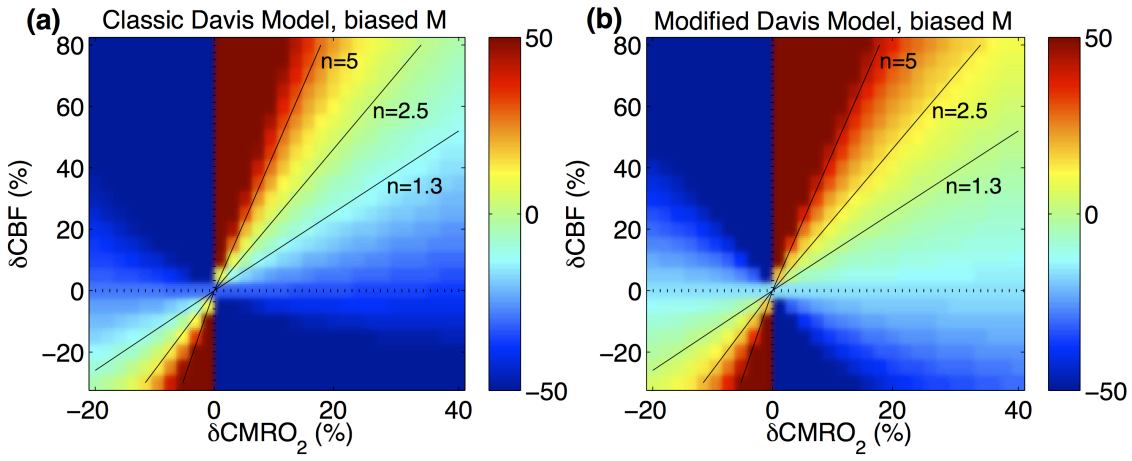

Supplementary Figure S2.1.10. Percent error (ξ) in $\delta CMRO_2$ calculations using the classic and optimized Davis model parameter sets but with biased *M*.

The hypercapnia calibration is often criticized for its assumption that 5% CO_2 inhalation does not change oxygen metabolism. Recent experiments have shown that this calibration method may in fact decrease $CMRO_2$ by 10%. If this is the case, *M* will be biased resulting in biased calculations of $\delta CMRO_2$ as shown. (a) $\delta CMRO_2$ appears to be correctly determined close to n=2.5 by the classic Davis model with *M* biased as noted. (b) The optimized parameters of α=0.14 and β=0.91 combined with a biased *M* produce accurate estimates of $\delta CMRO_2$ around n=1.3.

Supplementary Table S1.1.3. Range of variation and error due to input parameters.

The first three rows of errors are for a typical activation experiment with ΔCBF=50% and $\Delta CMRO_2$=25% (n=2). The second three rows of errors are for a simulated caffeine experiment with ΔCBF=-25% and $\Delta CMRO_2$=30% (n=-0.8). ξ is the fractional error and the ranges listed are associated with the minimum and maximum values respectively of each input parameter.

		ϕ_v	ω_v	*Hct*	*OEF*	$V_{1,0}$	ϕ	TE	R2*E	λ
	Range:	0-0.65	0.2-0.6	0.25-0.65	0.25-0.65	0.01-0.1	0.3-0.65	20-40 ms	15-45 s^{-1}	0.9-1.3
	Std value:	0.2	0.4	0.44	0.4	0.05	0.38	32 ms	25.1 s^{-1}	1.15
Classic α and β True *M*	*F*=50% *R*=20% *n*=2.5	15.0-30.0 (max ξ=50.1)	17.0-18.6 (max ξ=-15.1)	16.5-18.8 (max ξ=-17.5)	17.6-18.7 (max ξ=-12.2)	18.0-18.1 (max ξ=-10.0)	18.0-18.2 (max ξ=-10.0)	17.4-18.3 (max ξ=-12.8)	19.5-15.2 (max ξ=-24.0)	19.2-17.5 (max ξ=-12.7)
Optimized α and β True *M*		16.2-34.2 (max ξ=71.0)	18.5-20.4 (max ξ=-7.4)	18.0-20.6 (max ξ=-10.2)	19.2-20.6 (max ξ=-4.1)	19.7-19.8 (max ξ=-1.5)	19.7-19.9 (max ξ=-1.5)	19.0-20.1 (max ξ=-4.8)	21.5-16.5 (max ξ=-17.7)	21.1-19.1 (max ξ=5.3)
Classic α and β Hypercapnia *M*		18.0-31.4 (max ξ=57.0)	19.9-21.6 (max ξ=7.9)	19.5-21.8 (max ξ=8.9)	20.5-21.8 (max ξ=8.9)	21.0-21.1 (max ξ=5.4)	21.0-21.2 (max ξ=5.8)	20.4-21.3 (max ξ=6.6)	22.5-18.2 (max ξ=12.3)	22.1-20.5 (max ξ=10.6)
Classic α and β True *M*	*F*=-25% *R*=30% *n*=-0.8	18.6-21.7 (max ξ=-38.1)	22.7-16.3 (max ξ=-45.8)	17.3-19.6 (max ξ=-42.3)	21.0-17.1 (max ξ=-42.9)	19.6-17.4 (max ξ=-41.9)	18.4-19.3 (max ξ=-38.6)	20.2-17.9 (max ξ=-40.5)	21.5-13.0 (max ξ=-56.5)	20.8-17.5 (max ξ=-41.7)
Optimized α and β True *M*		29.6-34.4 (max ξ=14.7)	35.9-26.1 (max ξ=19.8)	27.7-31.1 (max ξ=-7.6)	33.3-27.4 (max ξ=-11.0)	31.2-27.9 (max ξ=-7.0)	29.3-30.7 (max ξ=2.4)	32.0-28.5 (max ξ=6.8)	34.0-21.4 (max ξ=-28.7)	33.0-28.0 (max ξ=9.9)
Classic α and β Hypercapnia *M*		13.6-11.8 (max ξ=-60.6)	16.7-10.5 (max ξ=-65.0)	12.1-13.2 (max ξ=-59.6)	14.9-11.1 (max ξ=-63.0)	13.6-11.6 (max ξ=-61.2)	12.5-13.2 (max ξ=-58.2)	14.3-11.9 (max ξ=-60.2)	14.6-8.8 (max ξ=-70.8)	14.2-11.9 (max ξ=-60.2)

Acknowledgements

Chapter 1, in full, is a reprint of the material as it appears in Neuroimage 2011. Griffeth, VEM and Buxton, RB (2011). A theoretical framework for estimating cerebral oxygen metabolism changes using the calibrated-BOLD method: Modeling the effects of blood volume distribution, hematocrit, oxygen extraction fraction, and tissue signal properties on the BOLD signal. Neuroimage 58: 198-212. The dissertation author was the primary investigator and author of this paper.

CHAPTER 2

A simplified model for the blood oxygenation level dependent (BOLD) effect for estimating brain oxygen metabolism changes

Abstract

Functional MRI (fMRI) using the blood oxygenation level dependent (BOLD) signal is a common technique in the study of brain function. The BOLD signal is sensitive to the complex interaction of physiological changes including cerebral blood flow (CBF), cerebral blood volume (CBV), and cerebral oxygen metabolism ($CMRO_2$). A primary goal of quantitative fMRI methods is to combine BOLD imaging with other measurements (such as CBF measured with arterial spin labeling) to derive information about $CMRO_2$. This requires an accurate mathematical model to relate the BOLD signal to the physiological and hemodynamic changes; the most commonly used of these is the Davis model. Here, we propose a new nonlinear model that is straightforward and shows heuristic value in clearly relating the BOLD signal to blood flow, blood volume and the blood flow-oxygen metabolism coupling ratio. The model was tested for accuracy against a more detailed model adapted for magnetic fields of 1.5, 3 and 7T. The mathematical form of the heuristic model suggests a new ratio method for comparing combined BOLD and CBF data from two different stimulus responses to determine whether CBF and $CMRO_2$ coupling differs. The method does not require a calibration experiment or knowledge of parameter values as long as the exponential parameter describing the CBF-CBV relationship remains constant between stimuli. The method was found to work well for 1.5 and 3T, but is prone to systematic error at 7T. If more specific information regarding changes in $CMRO_2$ is required, then with accuracy similar to that of the Davis model the heuristic model can be applied to calibrated BOLD data at 1.5T, 3T and 7T. Both models

work well over a reasonable range of blood flow and oxygen metabolism changes but are less accurate when applied to a simulated caffeine experiment in which CBF decreases and $CMRO_2$ increases.

Introduction

Functional magnetic resonance imaging (fMRI) is commonly used to map patterns of brain activation based on blood oxygenation level dependent (BOLD) signal changes [1]. A neural stimulus rapidly causes a large increase in cerebral blood flow (CBF) that is not matched in magnitude by the change in the cerebral metabolic rate of oxygen ($CMRO_2$) [2]. This mismatch, defined as the coupling ratio n ($\Delta CBF/\Delta CMRO_2$), leads to an increase in blood oxygenation that in large part determines the magnitude of the BOLD response. The coupling ratio is of interest because it is not constant but rather depends on factors such as brain region, stimulus type, aging and alterations in the baseline state due to drugs such as caffeine [3-8]. The current paradigm for examining variability in n relies on the Davis model [9] to analyze combined BOLD and CBF data from two stimulus response experiments along with data from an additional calibration experiment. This is a complicated data acquisition, and the analysis is further complicated by the mathematical form of the Davis model, which tends to obscure an underlying simplicity in the relationship between BOLD, CBF and $CMRO_2$ [10].

Davis and colleagues introduced this model for the BOLD effect using it as the foundation for the calibrated BOLD method, and this work remains the basis for calibrated BOLD studies today [9]. In the Davis model the BOLD signal is a nonlinear function of fractional changes in CBF and $CMRO_2$, multiplied by a scaling parameter M. The factor M is a lumped parameter, which includes many variables that could scale the BOLD signal and depends on both aspects of the physiological baseline state (oxygen extraction fraction, venous blood volume, and hematocrit) and also on parameters of the data acquisition (magnetic field strength and the echo time) [10,11]. The essence of the calibrated BOLD method is that this scaling parameter, M, is measured in a separate experiment. In the original Davis method and still the most commonly used approach [12-22], the calibration experiment to calculate M

utilizes inhalation of a hypercapnic gas mixture to elicit BOLD and CBF responses with the assumption that CO_2 alters CBF but not $CMRO_2$ [23,24].

However, the original derivation of the Davis model neglected intravascular signal changes and volume exchange effects associated with changes in cerebral blood volume (CBV), including changes on the arterial side that are thought to be the dominant site of CBV changes [25,26]. Recently we developed a detailed biophysical model of the BOLD signal (DBM) [10], which includes all of these additional effects while also specifically modeling effects related to arterial, capillary and venous blood volume changes with activation. While this model is too detailed to apply routinely in the calibrated BOLD experiment because many of the physiological parameters are unknown, it provides the solid theoretical framework necessary for relating the underlying metabolic and hemodynamic changes to the measured signals.

We previously used this DBM to test the accuracy of the Davis model when applied to the analysis of calibrated BOLD data, finding that errors in the estimated $CMRO_2$ change were surprisingly modest given that important components of the BOLD effect were neglected in the original derivation [10]. Effectively, the Davis model parameters were providing an approximate description of the factors that were left out, beyond the parameters' original definition in the model, and thus complicating their interpretation in physiological terms. In addition, the choice of parameter values had a relatively weak effect on the accuracy of the estimated $CMRO_2$ change, provided the model employed was used consistently to calculate both M from the hypercapnia experiment and also the $CMRO_2$ change from the activation experiment. This observation suggested that the Davis model may be more complicated than it needs to be (despite the fact that important effects were missing from its original derivation). This prompted us to look for a model that would be both simpler mathematically and that would

explicitly include the effects left out of the Davis model allowing straightforward parameter interpretation.

Here we present a new, heuristic model of the BOLD response that is a pure nonlinear function of CBF scaled by a lumped factor, which includes the CBF/$CMRO_2$ coupling ratio n. Inspired by the simple mathematical form of this new model, we present a straightforward "*ratio method*" to test whether the blood flow-oxygen metabolism coupling ratio is the same for two stimuli using only a comparison of the BOLD and CBF response ratios. This method is independent of model parameters assuming they remain consistent across experimental states, and it does not rely on an additional calibration experiment. The reliability of the new method was tested using the DBM [10] and as a demonstration the model was used to analyze data from a recent study of visual stimulus contrast [27]. Application of this technique will expand our understanding of why the mismatch between blood flow and oxygen metabolism occurs by simplifying the approach for detecting variations in the coupling ratio for different stimuli from combined BOLD and CBF data.

When quantitative information about the $CMRO_2$ change is necessary, the heuristic model can also be used in the same way as the Davis model to analyze calibrated BOLD data. To examine the accuracy of the heuristic model in this application, we again used the DBM to simulate measurements of both stimulus responses and calibration responses for different combinations of physiological states. This assessment was complementary to our previous examination of the Davis model as we again compared the results against the "true" $CMRO_2$ change from the DBM [10]. This analysis demonstrates that the heuristic model has comparable accuracy to the Davis model.

Methods and Results

Modifications to the detailed biophysical model of the BOLD signal

The DBM includes effects of intravascular and extravascular signal changes, hematocrit (*Hct*), baseline oxygen extraction fraction (E_0), blood volume fractions for different vascular compartments, changes in these volumes as CBF changes, tissue signal properties and imaging parameters [10]. In the current work, an additional feature in which the arteries are split into two compartments (large arteries - *A* and arterioles - *a*) was added in order to allow for partial oxygen desaturation of the arterioles. For simplicity, the second arteriolar compartment was modeled as equal in size to the fully saturated compartment with their sum comparable in size to previous modeling for the total arterial compartment. Desaturation occurring in the arteriolar compartment was modeled as a weighted average of arterial and venous hemoglobin saturation (Table 1, σ=0-0.2).

To permit modeling of the effect of hyperoxia on the BOLD signal, we also updated the DBM to calculate compartmental oxygen saturation from oxygen partial pressures using the Severinghaus equation [28]. The arterial oxygen concentration was calculated first followed by the venous oxygen concentration using the E_0 and Eq (10-13) from Chiarelli et al. [29]. Venous oxygen saturation was then calculated using linear interpolation of the Severinghaus equation. Arteriolar saturation was calculated as noted in the previous paragraph and capillary saturation was calculated also using a weighted average of arteries and veins [10].

We also expanded the DBM to simulate the BOLD signal at 1.5T and 7T, since the original model was only for 3T. This required adjusting the DBM to include magnetic field specific echo time (TE) and baseline extravascular signal decay rate (R_2^*) (Table 2) [30]. Intravascular signal decay rates were again determined using a quadratic model fit to data

relating intravascular R_2^* to oxygen saturation. At 1.5T hematocrit-dependent values were calculated according to Silvennoinen et al. [31]. At 7T data from Blockley et al. [32] was used to determine intravascular R_2^* dependence on oxygen saturation independent of hematocrit. Changes in extravascular signal decay rates are linearly dependent on B_0, which was already included in the model [1]. Calculations of oxygenation and blood volume were performed as published previously [10].

Simple BOLD signal models

The new model, as derived in Appendix A, is:

$$BOLD(\%) = A\left(1 - 1/f\right)\left(1 - \alpha_v - 1/n\right) \quad (1)$$

Important terms in this model include the scaling parameter (A), CBF in the active state normalized to its value in the baseline state (f), the ratio of fractional changes in CBF and $CMRO_2$ (n), and the exponent relating the CBF change to the venous CBV change (α_v). One additional parameter of importance is r, which is $CMRO_2$ in the active state normalized to its value in the baseline state and is related to n and f through $n=(f-1)/(r-1)$. In the following we refer to Eq. (1) as the heuristic model, because it clearly shows the basic physiological factors that affect the BOLD response: it is driven by the CBF change, but strongly modulated by both the venous CBV change and the CBF/$CMRO_2$ coupling ratio. The parameter α_v is from the Grubb relationship, which relates the normalized venous CBV change (v) to f through the equation $v = f^{\alpha_v}$. For calculations using the heuristic model, we set α_v=0.2 as determined by Chen and Pike [33].

The two underlying assumptions of the heuristic model discussed and illustrated in the Appendix are: (1) The fractional BOLD signal change is directly proportional to the absolute change in total dHb content in a voxel (simulations for 1.5T, 3T and 7T are shown in Figure A1 and Supporting Figures S2-3); and (2) the fractional change in tissue concentration of total dHb is equal to the fractional change of venous dHb (Figure A2). Figure A3 examines the relationship between changes in CBF and $CMRO_2$ in comparison to changes in both the BOLD signal and dHb content. At first glance, these assumptions appear to be too restrictive for the full complexity of the BOLD response, so we used the DBM to explore the errors in these assumptions and the ultimate effect of using the heuristic model for estimation of $CMRO_2$ changes, which is discussed below.

Of note in the heuristic model is the non-linear dependence of the BOLD signal on the CBF change, which is reflected in the term incorporating *f*. This term reflects the ceiling effect on the BOLD response: very large increases in CBF will tend to produce the largest BOLD signals as $1/f$ and $1/n$ approach zero (Eq. B2). Physically this corresponds to a clearance of dHb from the vasculature. For changes in CBF approaching zero (f=1), the BOLD response is a linear reflection of the fractional $CMRO_2$ change as shown in Appendix B (Eq. B7): $BOLD(\%) = A(1-r)$.

The second term in the heuristic model relates the BOLD signal change to *n* while also incorporating the dependence of CBV on CBF. This term reflects that the largest BOLD signal will result from a large *n*, when the saturation of hemoglobin is maximized through a much lower oxygen metabolism change relative to the blood flow change (e.g. hypercapnia) [24,34,35]. This term also reflects that smaller changes in venous CBV relative to CBF (smaller α_v) will lead to larger BOLD signal changes. The physical interpretation of this is that a smaller increase in dHb containing blood volume leads to a larger BOLD signal, because any increase

in volume will increase the dHb content of a voxel in opposition to the oxygen extraction fraction decrease, which dominates the BOLD signal change.

For comparison, the Davis model expressed in the same terms is:

$$BOLD(\%) = M\left[1 - f^{\alpha-\beta}\left(\frac{f-1}{n}+1\right)^{\beta}\right] \quad (2)$$

The Davis model has two parameters, α and β, and the original values for these parameters as applied to 1.5T BOLD data were α=0.38 and β=1.5 [9]. In this analysis, we set α=0.2, consistent with recent data indicating that most blood volume change occurs in the arterioles [25,26,33]. As originally derived in the Davis model, β relates blood oxygenation to transverse relaxivity and is dependent on magnetic field strength (B_0). Recent studies based on previous modeling of this relationship have proposed adjusting β to reflect this B_0 dependence using the following values: β=1.5 at 1.5T, β=1.3 at 3T and β=1 at 7T [9,36,37]. We refer to the Davis model with these parameter values as the B_0-adjusted Davis models (e.g. the *1.5T-adjusted Davis model*).

We have also proposed previously treating α and β as free parameters in the Davis model, and designate the Davis model using these parameters as the B_0-"free parameter" Davis models [10]. This approach attempts to provide the best fit to the surface of BOLD change as a function of CBF and $CMRO_2$ change using the mathematical form of the Davis model, but divorcing the parameters a and b from their original physical definitions. The process of fitting these parameters involves assuming our best guess of the physiology (Tables 1 and 2) in order to simulate the BOLD signal for CBF changes between -40% and 80% and $CMRO_2$ changes between -20% and 40%. We then normalized both the Davis model and the simulated data using an idealized hypercapnia simulation (ΔCBF=60% and $\Delta CMRO_2$=0%). This removes the scaling parameter, *M*, from the equation leaving only α and β to be fitted. We discuss the impact of

these parameters in a later section while listing their values here: α=0.1 and β=1 at 1.5T, α=0.13 and β=0.92 at 3T, and α=0.3 and β=1.2 at 7T. These values are perhaps counterintuitive, but when treating α and β as free-parameters they lose their physiological meaning and instead simply provide the best fit of the model to the simulated data given the physiological assumptions. In other words our values for α should not be used as an indication of the relationship between CBV and CBF, and our values for β should not be used to describe the relationship between the magnetic susceptibility due to deoxyhemoglobin and R_2^*. In addition to the Davis model parameter set noted above, we also examined the impact of fixing β=1, which makes the form of the Davis model more analogous to that of the heuristic model.

The ratio method

The form of the heuristic model suggests a new method for analyzing combined BOLD-CBF data independent of the scaling parameter in order to determine whether *n* changes for responses to different stimuli from the same baseline state without requiring a calibration experiment. Because the flow response term is separate from the coupling ratio term, we can use Eq. (1) to directly compare whether two stimulus responses have the same flow-metabolism coupling. Denoting one stimulus as a reference ("ref") and the comparison stimulus as "x", we first create a null hypothesis that *n* is the same for the two stimuli (n_x=n_{ref}). Taking the ratio of Eq. (1) for the two stimulus responses makes a specific prediction for a nonlinear combination of measured BOLD and CBF responses that is independent of the model parameter values:

$$BOLD_x \Big/ BOLD_{ref} = \left(1 - 1/f_x\right) \Big/ \left(1 - 1/f_{ref}\right) \tag{3}$$

This method assumes that both A and α_v remain constant between the two stimulus responses. Under these conditions the exact values of A and α_v are not needed because this ratio is independent of the model parameters. Differences in n can then easily be detected using a sign rank test or similar statistical analysis comparing the measured BOLD ratio with the ratio predicted by the non-linear CBF terms for equal values of n in Eq (3).

To test the accuracy of this new method, we employed the DBM to simulate BOLD and CBF responses for a reasonable range of physiological and imaging parameters (Tables 1 and 2). A reference data set with n_{ref}=2 was produced and compared to n_x=1.8, n_x=2 and n_x=2.2 at 1.5T, 3T and 7T (Fig. 1A-C). These values of n are typical for fMRI activation experiments [7,9,11,18,27,38-40]. Data sets for each value of n contained 10,000 simulations. Previously published combined BOLD and CBF data associated with changes in visual stimulus contrast [27] were then examined using this method (Fig. 1D). A sign rank test was used to determine whether the flow ratio was statistically different than the BOLD ratio with results for p noted.

This approach works well for 1.5T and 3T (Fig. 1A-B) as stimulus responses with values of n_x not equal to n_{ref} are shown to have BOLD ratios that diverge from the non-linear CBF ratio. Additionally when $n_x = n_{ref}$, the BOLD ratios are shown to be approximately equal to the non-linear CBF ratios reflected in the blue dots falling along the dashed line of identity. This is most apparent on the inset histograms taken from additional simulations for which the non-linear CBF ratio was fixed to 0.5: at 1.5T there is a very small tendency to underestimate the BOLD ratio when $n_x = n_{ref}$, but there is good separation between the data otherwise (Fig. 1A). Similarly at 3T the blue dots representing $n_x = n_{ref}$ fall equally on either side of 0.5 and are separated from the data representing both $n_x > n_{ref}$ and $n_x < n_{ref}$ (Fig. 1B). In certain cases, this method can also be used to make inferences about changes in $CMRO_2$: when $n_x > n_{ref}$ but $\Delta CBF_x < \Delta CBF_{ref}$, then $\Delta CMRO_{2,x}$ must also be less than $\Delta CMRO_{2,ref}$. Similarly when $n_x < n_{ref}$

but $\Delta CBF_x > \Delta CBF_{ref}$, then $\Delta CMRO_{2,x}$ must also be more than $\Delta CMRO_{2,ref}$. Note that when $\left(1-1/f_x\right) > \left(1-1/f_{ref}\right)$ then $\Delta CBF_x > \Delta CBF_{ref}$.

This approach is less reliable at 7T where the BOLD signal is more sensitive to changes in dHb (Fig. 1C). Specifically, the ratio method fails by predicting a difference in n_x from n_{ref} when no difference exists as reflected in the blue dots deviating from the line of identify. In the case that ΔCBF_x is less than ΔCBF_{ref}, there is a tendency for this method to predict an increase in n_x relative to n_{ref}, and when ΔCBF_x is greater than ΔCBF_{ref}, there is a tendency for this method to predict a decrease in n_x relative to n_{ref}. From the inset histogram, this deviation of the data from the predicted BOLD ratio of 0.5 designated by the black bar is clearly apparent (Fig. 1C).

We also tested whether the coupling of CBF and $CMRO_2$ impacts the effectiveness of the ratio method. As suggested by the form of the heuristic model, the ratio method is most sensitive to $1/n$. By testing different values of n, we found that for positive coupling of CBF and $CMRO_2$ the ratio method is most effective when differences in $1/n$ are greater than 0.05. For n=2, this corresponds to n=1.8 or n=2.2. For n=4, this corresponds to n=3.3 or n=5 (Supporting Fig. S1). We examined a wide range of both positive and negative values of n, and included in Supporting Figure S1 n=-1 corresponding to a decrease in CBF and an increase in $CMRO_2$. A general pattern emerged from simulations across a broad range of coupling parameter values showing that the ratio method breaks down close to a coupling of n=1.3, which is frequently associated with the null point of the BOLD signal (data not shown). Specifically at 1.5T and 3T, the ratio method appears to fail for $0.75<n<1.5$. The limits at 7T extend somewhat higher such that the model fails for $0.75<n<2.25$. In addition to this limitation on the range of n that can be examined, these tests also revealed a systematic bias in the predicted BOLD signal ratio. For

positive *n*, any difference between the BOLD ratio and non-linear CBF ratio less than 0.02 should be viewed with caution and outside the ability of the ratio method to discriminate. For example, if the non-linear CBF ratio predicts a BOLD ratio of 0.5, any BOLD ratio between 0.48 and 0.52 should be considered to have the same *n*. For negative *n*, this difference is 0.04. These biases are likely due to error inherent to the use of the relatively simple heuristic model to describe the full complexity of the BOLD signal.

Having confirmed the accuracy of the ratio method for simulated data at 3T, we applied this approach to a study of 9 subjects comparing different levels of visual stimulus contrast [27]. Consistent with the results from the previous analysis using the Davis model, we found that the response to 1% contrast has a lower *n* than the response to 100% contrast ($p<0.01$) (Fig. 1D). The BOLD ratios at 4% and 9% contrast also fall below the prediction by the CBF ratios, but the results do not reach statistical significance. Assuming n_{ref}=2.3 at 100% contrast consistent with a previous calibrated-BOLD study [22], these ratio differences translate to *n* values of 1.66, 2.14 and 2.25 (with associated Cohen-*d* statistics of 0.6, 1.04 and 1.71) respectively.

Simulating the calibrated-BOLD experiment

Next we simulated a calibrated-BOLD experiment to compare the heuristic model to the B_0-adjusted Davis model [9] for accuracy in determining the $CMRO_2$ change at 3 magnetic field strengths. To examine the effects of various parameters on calculations of the $CMRO_2$ change, we used two ranges for *n* (*n*=2 and *n*=-1). Activation studies typically show increases in both CBF and $CMRO_2$ with *n* about equal to 2 [18,22,40]. In contrast, we found that caffeine as a stimulus decreased CBF and increased $CMRO_2$, with *n* about equal to -1 [7]. To determine the effectiveness of the simple models, this comparison required three steps: (1) using the detailed

model to simulate the hypercapnia response assuming $\Delta CBF=60\%$ and $\Delta CMRO_2=0\%$, (2) using the detailed model to simulate the stimulus response with $n=2$ ($\%\Delta CBF=50\%$ and $\%\Delta CMRO_2=25\%$) or the caffeine response with $n=-1$ ($\%\Delta CBF=-25\%$ and $\%\Delta CMRO_2=25\%$), and (3) using the B_0-adjusted Davis model and the heuristic model to analyze this data in order to calculate the $CMRO_2$ change in response to either the simulated stimulus or caffeine experiments. Inputs to the detailed model were varied individually over the ranges specified in Tables 1 and 2 to determine the effect on $\Delta CMRO_2$ calculations. Parameters other than the one specified were kept constant at the best guess values.

Figure 2 presents deviations from the DBM simulated $CMRO_2$ response when using the simple models at 1.5T, 3T and 7T. These results demonstrate that $\%\Delta CMRO_2$ calculated using the heuristic model is consistent with $\%\Delta CMRO_2$ produced by the Davis model. It shows that even for variation in multiple physiological inputs to the DBM (Tables 1 and 2), the heuristic model with $\alpha_v=0.2$ [33] predicts changes in $CMRO_2$ comparable to predictions by the B_0-adjusted Davis model at 1.5T, 3T and 7T. These simple models are both quite accurate at the typical coupling ratio of $n=2$, and at 3T there is a small underestimation bias of -6.4% error by the heuristic model compared to -2.1% for the Davis model (Fig. 2B). Both models are most sensitive to differences in α_v, reflecting the impact of ΔCBF and venous ΔCBV coupling. If α_v is allowed to vary across a range of 0.1-0.3 within the DBM while the assumptions about α_v in the heuristic and Davis models are kept constant, then the 3T-adjusted Davis model will predict $\%\Delta CMRO_2$ between 22.2% and 29.6% (for a true value of 25%, with a maximum error of 18.4% of that 25% change in $CMRO_2$) while the heuristic model predicts $\%\Delta CMRO_2$ between 21.5% and 28.5% (maximum error of ±14.0%). These results are consistent with the pattern found previously using slightly different values for α and β in the Davis model [10]. At 1.5T the same pattern of underestimating the $CMRO_2$ change at $n=2$ was found: for the 1.5T-

adjusted Davis model the underestimation bias was -4.5% and for the heuristic model the bias was -13.3% (Fig. 2A). At 7T the basic models both overestimate $\%\Delta CMRO_2$ with overall bias percent errors of 7.7% using the heuristic model and 2.9% using the Davis model (Fig. 2C). These patterns of bias due to parameter variation are consistent when values of n up to 6 ($\%\Delta CBF=60\%$) are examined (not shown).

These basic models are less accurate when used to analyze changes associated with caffeine consumption (Fig. 2D-F), which we modeled in the DBM as a -25% CBF decreases and 25% $CMRO_2$ increase. This is a slightly extreme test case of CBF/$CMRO_2$ coupling changes due to caffeine, since previous findings estimated a smaller $CMRO_2$ increase for this level of CBF decrease [7]. At both 1.5T and 3T, the models systematically underestimate this simulated change in $CMRO_2$. For example at 3T, the B_0-adjusted Davis model calculates a $CMRO_2$ increase of only 17.7% (error of -29.2%) while the heuristic model calculates 18.8% (error of -24.8%) (Fig. 2E). Of note at this value of flow-metabolism coupling, the Davis and heuristic models at 3T and 7T are most sensitive to variation in baseline dHb content as determined by ω_v and E_0, and less sensitive to changes in blood flow-blood volume coupling, α_v. At 1.5T the simple models are most sensitive to the intravascular/extravascular proton density ratio (λ) followed by tissue R_2^* while showing less overall sensitivity to parameter variability. At 7T the heuristic model is more accurate with an error bias of -1.6% while the Davis model overestimates $\%\Delta CMRO_2$ with an error of 15.2%. For this combination of B_0, CBF and $CMRO_2$, the magnitude of error bars is also much larger suggesting greater sensitivity to changes in dHb at 7T.

We also used this method of simulating the calibrated BOLD experiment to examine the efficacy of these simple models over a larger range of CBF and $CMRO_2$ combinations while keeping other physiology constant at our best guess (Tables 1 and 2). We included in this

comparison the Davis model with β=1 (Fig. 3). As an example at 3T and for our best guess of the physiology, the simulated hypercapnia BOLD signal was 4.6% for a 60% CBF increase producing the following estimates of the scaling parameters: B_0-adjusted, M_{HC}=11.4%; fixed β=1, M_{HC}=14.6%; and heuristic model A_{HC}=15.3%. For an activation resulting in %ΔCBF=25% and %Δ$CMRO_2$=10%, the BOLD signal was 1.3%, and in this case the estimates of the $CMRO_2$ change with activation were: 10.3% for the B_0-adjusted Davis model, 9.3% for the fixed β=1 Davis model, and 9.7% for the heuristic model. We also tested the impact of treating α and β as free fitting parameters within the Davis model to minimize error in $CMRO_2$ calculations, and using this model Δ$CMRO_2$ was estimated to equal 10.0%.

Most apparent from Figure 3 is the performance similarity of these models at different field strengths. Although subtle differences between the models exist, they all appear to function reasonably well for positive coupling of CBF and $CMRO_2$ changes, particularly at 3T. Across all field strengths, the B_0-"free parameter" Davis models perform the most consistently while the B_0-adjusted Davis models also perform well. While we had expected the heuristic model to perform with the most similarity to the Davis model with β=1, it in fact shares similarity to both the B_0-adjusted and β=1 Davis models. Notably, most of the models have difficulty correctly determining a $CMRO_2$ change when it is associated with a decrease in CBF, as in changes associated with caffeine consumption. The exception to this are the free parameter Davis models and surprisingly the heuristic model at 7T (Fig. 3D, H, J, L). The drawback to the free parameter Davis model is that it requires one to discard physiological meaning for the parameters α and β. Furthermore values for α and β would need to be updated as new information affecting the DBM becomes available. Specifically α no longer corresponds to blood volume changes alone, so updating the model as new information about the true venous CBV values becomes available is more complicated. Note this is also clear from the values of α

and β at 3T, which differ slightly from those published previously due to the inclusion of a desaturated arteriolar compartment here [10].

Calibrated BOLD analysis of experimental data

Using these two simple models, we examined experimental data by reanalyzing $CMRO_2$ changes in response to a visual stimulus pre- and post-caffeine as well as changes due to caffeine alone [7,22]. This data set was acquired on a GE Signa Excite 3T whole-body system using a spiral dual-echo ASL PICORE QUIPSS II pulse sequence [41]. Responses to 20s blocks of an 8Hz flickering checkerboard were measured pre- and post-caffeine. For complete details of the experiment see Perthen et al. [22]. Results were compared to the same data published previously so that in addition to the heuristic model we examined $\Delta CMRO_2$ calculations by the original Davis model (α=0.38 and β=1.5), 3T-adjusted Davis model (α=0.2 and β=1.3), and fitted free parameter Davis model (α=0.13 and β=0.92).

Results from this analysis using these models are shown in Table 3. The estimated values of $CMRO_2$ were similar for all the models with slight systematic differences consistent with the simulations in Figures 2 and 3. The small differences in $\%\Delta CMRO_2$ predictions reflect the similarity of these models in calculating changes in $CMRO_2$ when both blood flow and metabolism increase. In contrast, the models diverge when calculating the $CMRO_2$ response to caffeine alone ($n\approx$-1). While the 3T free parameter model calculated a $CMRO_2$ change of 21.7%, the heuristic model found 17.1%, the 3T-adjusted Davis model found 15.7%, and the original Davis model calculated 13.3% (Table 3). We anticipate that the free parameter values are most accurate in this area of CBF-$CMRO_2$ and that the other models all underestimate the $CMRO_2$ change for caffeine. This is consistent with our previous findings [10].

Scaling parameters and limits of the Davis and heuristic models

The above tests comparing the simple models have focused on the effects of physiological variation in properties such as CBV and hematocrit, and we can think of estimates of the scaling parameter (M or A) as the fitted value that best approximates the BOLD signal behavior over the defined physiological range. However, it is useful to also consider the limits implied by these mathematical expressions because the scaling parameter is often described in physical terms as the maximum possible BOLD signal produced when all dHb has been eliminated [9]. By this interpretation, one could in principle determine the scaling factor by extreme physiological manipulations to eliminate deoxyhemoglobin. This raises the basic question of whether these simple models remain accurate under these extreme physiological conditions. That is, is the scaling parameter in the model best thought of as an absolute physiological variable or as a fitting parameter that adjusts the mathematical form to be accurate over a normal physiological range?

To address this question we considered the limiting forms of the simple models and compared them with the limits calculated from the DBM. This is a somewhat subtle question because the elimination of dHb can be accomplished through two basic paths: a dramatic increase of CBF (perhaps augmented with hyperoxia), or a reduction of absolute $CMRO_2$ to zero. We considered both scenarios with the DBM. First we modeled the elimination of dHb based on the carbogen-10 experiments by Gauthier et al. [42] allowing CBF to increase by 200%, slightly more than their finding of 160% produced using combined visual stimulus with 10% hypercapnia. We then combined this increase in CBF with an increase in arterial oxygen partial pressure (PaO_2) up to 600 mmHg consist with about 90% inspired O_2 [29]. We also included a

simulation with ΔCBF=100% (f=2) and PaO_2=390 mmHg to mimic the actual findings from the carbogen-10 experiments [42]. No literature was found on the relationship of CBV to CBF as blood flow increases beyond typical physiological measurements to provide an empirical basis for modeling such effects within the DBM, so here we kept α_T and α_v constant at 0.38 and 0.2 respectively [33,43]. Second, to simulate oxygen metabolism cessation, the $CMRO_2$ input to the DBM was simply decreased to zero without altering CBF or any other input. While not physiologically plausible, this simulation mimics complete removal of all dHb without altering CBV.

Note that one complexity of extending the DBM to these extreme physiological cases is that we model the intravascular and extravascular susceptibility difference as being minimized at a hemoglobin saturation of 95% rather than 100% ($SO_{2,off}$=95%) based on the work of [44]. Specifically, this assumes that the susceptibility of tissue is equal to the susceptibility of plasma (an assumption that needs to be tested experimentally). This results in the maximum BOLD signal occurring at a hemoglobin saturation less than 100%. Since we are after a calibration factor that reflects a constant relationship between the BOLD signal and hemoglobin saturation, we chose to extrapolate to the theoretical maximum BOLD signal at 100% SvO_2 by projecting from the inflection point using the inverted slope of the BOLD signal for SvO_2 greater than 95% (Fig. 4, dashed line). We modeled these mechanisms using the DBM and plotted BOLD vs. venous hemoglobin saturation (SvO_2) in order to determine the most appropriate definition for the scaling parameters (Fig. 4).

At 1.5T the combined hyperoxia with CBF increase appears nearly identical to elimination of $CMRO_2$ as both approach a limit of 8.9%. At higher magnetic field strengths, these cases diverge as the increase in CBF leads to the displacement of tissue volume for blood volume, which has a smaller contribution to the signal at higher B_0. At 3T, elimination of

$CMRO_2$ results in a maximum signal of 13.2% while combined hyperoxia-CBF increase produces a signal of 12.5%. The simulated carbogen-10 experiment at 3T resulted in a signal of 8.0%, which is close to the actual finding of 7.5%. The difference between dHb elimination methods is even larger at 7T: decreasing $CMRO_2$ results in a maximum signal of 24.7%, but combined hyperoxia-CBF increase produces a maximum signal of 18.9%. The difference at 7T was expected, because increased CBF leads to increased CBV replacing tissue volume without contributing to the BOLD signal at the higher magnetic field strength [45].

The limits of the Davis and heuristic model can also be examined for these two conditions with interesting differences arising. At very large values of CBF the heuristic model predicts a signal that is less than the maximum BOLD signal: $A(1-\alpha_v)$ (Appendix B, Eq. B2) while the Davis model predicts that the BOLD signal will simply equal *M.* At 1.5T and 3T, Figure 4 suggests this decrease is too aggressive since in the DBM simulations α_v was assumed to equal 0.2, but at 7T the heuristic model appears to more accurately reflect behavior at this limit.

When absolute $CMRO_2$ is reduced to zero (r=0), the heuristic model predicts dependence of the BOLD signal on both CBF and α_v: $BOLD(\%) = A\left(1 - \alpha_v \cdot \Delta CBF / CBF\right)$ (Appendix Eq. B3). When the CBF change is small as in Figure 4, this limit becomes the scaling parameter, A. Under the same circumstances, the Davis model reduces to M with no dependence on α_v or CBF.

These results show that the maximum BOLD signal therefore is dependent on how elimination of dHb is achieved, and for both simple models there are discrepancies between the value of the scaling parameters and the physical limits of reducing deoxyhemoglobin. For this reason, it is better to think of the scaling parameter as a fitted value that makes the equations

accurate over a normal physiological range, rather than having a more absolute meaning as the maximum possible BOLD change.

Ethics Statement

The institutional review board at the University of California San Diego approved the study of human subjects in the previously published work [22,27], and written informed consent was obtained from all participants.

Discussion

In this study, we revisited basic modeling of the BOLD signal and derived a new simplified model that has heuristic value in clearly showing the physiological factors that affect the BOLD signal. The heuristic model demonstrates the non-linear dependence of the BOLD signal on cerebral blood flow found in previous studies [46,47], directly incorporates the flow-metabolism coupling parameter, n, and also incorporates the dependence of venous CBV on CBF through α_v. It was inspired by work with the much more detailed model [10], which appeared to produce a very smooth BOLD dependence on CBF and $CMRO_2$ suggesting that the parameters α and β of the Davis model may be over-fitting the data. The form of the heuristic model suggests a new method comparing BOLD signal ratios to non-linear ΔCBF ratios in order to determine whether flow-metabolism coupling varies with the stimulus. Using the previously developed DBM [10], we demonstated the effectiveness of the ratio method while

also showing that the accuracy of the heuristic model is comparable to the Davis model when applied in the calibrated BOLD experiment.

Ratio Method

The new approach to analyzing combined BOLD and CBF data is straightforward and relies only on measured data to determine whether *n* varies with the stimulus (i.e. different levels of visual stimulus contrast, frequencies of finger tapping, or level of drug administration). As an example, we used the method to reanalyze a previous study investigating how *n* varies with the contrast of a visual stimulus. In the original analysis the conclusion that *n* varies with stimulus contrast was based on many repeated tests using the Davis model with different values for *M*, α and β. Here using the ratio method, the same conclusion is reached in a more straightforward manner. It is not apparent from the Davis model that the comparison of the BOLD signal ratio to the non-linear CBF response ratio would work, but it is readily apparent from an examination of the heuristic model, which separates the CBF response from the coupling parameter term. An additional application of the ratio method could be in the study of brain diseases with altered vascular responses. For example in diseases resulting in reduced blood vessel compliance, increasing stimulus intensity may not result in the same increase in the CBF response seen in normal subjects resulting in a constant or decreasing *n* rather than increasing *n*.

There are two limitations of this method: both the scaling parameter and the relationship between CBF and CBV changes (α_v) must remain constant across the comparison. The requirement on the scaling parameter to remain constant essentially limits the technique to

a common region of interest and baseline state. For example, it is not possible using this method to compare flow-metabolism coupling in the visual cortex to that in the motor cortex.

An additional limitation emerges at 7T. Simulations using the DBM confirm that the approach works well for 1.5T and 3T with the non-linear CBF ratio accurately predicting the BOLD signal ratio in all cases (Fig. 1A-B), but at 7T the relationship between the ratios is not a reliable prediction of changes in *n*. Specifically if the *n*-values are in fact the same for two stimuli, the ratio method at 7T would incorrectly show that the stimulus with the stronger CBF response had a smaller value of *n*. Thus although the heuristic model works reasonably well when calculating $\%\Delta CMRO_2$ from calibrated BOLD data at all magnetic field strengths (Fig. 2 and 3), the ratio method is unreliable at 7T. A much smaller bias is evident at 1.5T, but this deviation from identity is small as demonstrated from the inset histogram (Fig. 1A).

Calibrated-BOLD using the heuristic model

As performed previously for just the Davis model, it is possible to calculate stimulus associated changes in $CMRO_2$ using the heuristic model when BOLD and CBF measurements are combined with a hypercapnia calibration. To test this we simulated both an ideal hypercapnia calibration as well as an activation experiment using the DBM demonstrating that both the heuristic model and the B_0-adjusted Davis model produce reasonable estimates of $\Delta CMRO_2$ (less than 15% error) for positive changes in CBF and $CMRO_2$ (Fig. 2A-C). At 1.5T and 3T both models slightly underestimate changes while they overestimate changes in $CMRO_2$ at 7T. As previously reported [10], the parameter having the largest impact on $CMRO_2$ calculations by both models and across B_0 is α_v, emphasizing the importance of accurately determining the venous CBV-CBF relationship for future calibrated BOLD studies. In terms of

the effect of other physiological parameters, an interesting standout at 1.5T is λ, which is the intravascular/extravascular proton density ratio. This alters the intravascular to extravascular signal intensity, a factor that is more important at lower B_0 where the intravascular signal due to lower intravascular signal decay rates has a relatively greater impact than at 3T and 7T. At 7T another interesting standout is α_T, which emphasizes the importance of total CBV changes at the higher magnetic field when deoxygenated blood generates a relatively weak signal so that increases in blood volume displace tissue without contributing to the BOLD signal leading to an overall signal decrease. Not shown here, the same pattern of error is found when using the B_0-"free parameters" in the Davis model, which is consistent with previous findings [10].

While both models are reasonably accurate for cases in which both CBF and $CMRO_2$ increase, the models are less accurate when CBF and $CMRO_2$ changes are in opposition (Fig. 2D-F). Specifically for the Davis model, the B_0-adjusted values of β underestimate $\Delta CMRO_2$ at 1.5T and 3T while overestimating it at 7T. The heuristic model also does not perform well at 1.5T and 3T in this region of CBF-$CMRO_2$ coupling, but interestingly it is much more accurate at 7T. This is consistent with findings in Figure 3 examining a broad range of CBF-$CMRO_2$ coupling for our best guess of physiology. Application of these models to experimental data showed a similar pattern of $CMRO_2$ changes estimated for a visual stimulus response with the simple models in agreement with the exception of the original Davis model (α=0.38 and β=1.5), which estimated a smaller $CMRO_2$ response (Table 3). Also consistent with the simulations, the caffeine $CMRO_2$ responses calculated by the basic models were more dissimilar: the original Davis model produced the lowest estimate, the B_0-adjusted Davis model and the heuristic model produced slightly higher estimates, and the free parameter Davis model produced the highest estimate (Table 3). The inaccuracy of the Davis model for this region of CBF and $CMRO_2$ coupling has been noted previously and can be overcome by treating α and β both as free

parameters in the Davis model then fitting to DBM simulations [10]. The drawback to this approach is that the parameters lose their physiological meaning and must be refitted when new information becomes available.

Examining a full complement of CBF and $CMRO_2$ changes, Figure 3 also shows that fixing $\beta=1$ decreased accuracy of the Davis model for the most common region of CBF-$CMRO_2$ coupling while there was also unexpected improvement in the region of CBF decrease and $CMRO_2$ increase. Although $\beta=1$ simplifies the Davis model in line with the simplicity of the heuristic model, it is still not obvious that the ratio method would work due to the interaction of the CBF and $CMRO_2$ terms.

The scaling parameter and additional comparison of the simple models

When simple models of the BOLD effect are used, the physical meaning of the scaling parameter (i.e., its relationship to underlying physiological variables) can become blurred. Here we considered the question of whether the scaling parameter is literally the maximum BOLD signal change that would occur if all of the deoxyhemoglobin was removed, or whether it functions as a fitting parameter that differs based on the mathematical form of the particular simple model, adjusting each to fit the data over the normal physiological range. From Figure 4, it is apparent that the maximum BOLD signal depends on whether dHb is eliminated by increasing CBF or decreasing $CMRO_2$. Additionally while the limit of the Davis model in both cases is M, the limit of the heuristic model is either A when $CMRO_2$ goes to zero or $A(1-\alpha_v)$ when CBF approaches infinity. Finally both simulations and experimental data show that hypercapnia determined values of the scaling parameter depend not only on the simple model used but also on the values of the parameters α, β and α_v [7,10]. Therefore to maximize

accuracy of the simple models and avoid ambiguity introduced by making the scaling parameter equivalent to the maximum BOLD signal, it is better to determine the scaling parameter from a calibration experiment, thereby providing a good fit of the simple models to the physiologically reasonable range of CBF and $CMRO_2$ changes.

Our simulations provide further evidence of this: although the B_0-adjusted Davis M_{HC} is smaller than the heuristic model A_{HC} at 3T, both simple models estimate $CMRO_2$ changes well (Fig. 2 and 3). Furthermore the difference in M_{HC} between the original and free parameter Davis models published previously [10] suggests strong covariance between the scaling parameter (M), α, and β in the Davis model. It is through the calibration process that the simple models become self-correcting, emphasizing that the value of the scaling parameter depends on the model used to calculate it rather than on the maximum BOLD response.

Future applications

A potentially useful feature of the heuristic model is that if the variation of n over time during an activation experiment is relatively small, the BOLD response becomes simply a scaled version of a pure non-linear function in CBF. In models relating the BOLD response to underlying physiology (e.g., as a component of dynamic causal modeling [46]), the ambiguities due to the baseline state and the $CBF/CMRO_2$ coupling ratio are combined into a single scaling parameter, simplifying the treatment of the forward model from neural responses to measured BOLD responses.

As shown recently, the heuristic model is also useful for improving the precision of the CBF response when simultaneous measurements of BOLD and CBF are acquired [48]. By isolating dependence of the BOLD signal on the non-linear CBF response, the unknown

parameters A, α_v and n that modulate the BOLD signal can be combined into a single factor. This property relating the underlying CBF fluctuations simply to the BOLD signal is used by the BOLD-Constrained Perfusion (BCP) method to dramatically improve the estimate of CBF fluctuations. Specifically, the heuristic model is used as a constraint in the minimization of the cost function, which incorporates the measured BOLD signal, the measured CBF signal, the true underlying BOLD and CBF signals, and noise.

Conclusions

The heuristic model was inspired by work with the detailed BOLD model and a desire to develop a simple analysis for detecting changes in flow-metabolism coupling from combined BOLD and blood flow data. The heuristic model is advantageous over previous models, because it simplifies the dependence of the BOLD signal on blood flow and flow-metabolism coupling and in doing so suggests the ratio method for analysis of combined BOLD and CBF data. This approach works very well at 1.5T and 3T, but does not appear to work at 7T when it predicts a change in n when no change is present. It is remarkable to note that when applied to calibrated BOLD data the heuristic model with only one fixed parameter has accuracy similar to the Davis model with parameters adjusted for the magnetic field strength. At 1.5T, 3T and 7T, the heuristic model produces consistent results for $\Delta CMRO_2$ at n=2, although they are slightly less accurate than the B_0-adjusted Davis model. This small difference is balanced by greater accuracy of the heuristic model when applied to a simulated analysis of the response to caffeine particularly at 7T, which is a somewhat surprising result given the simplicity of the heuristic model.

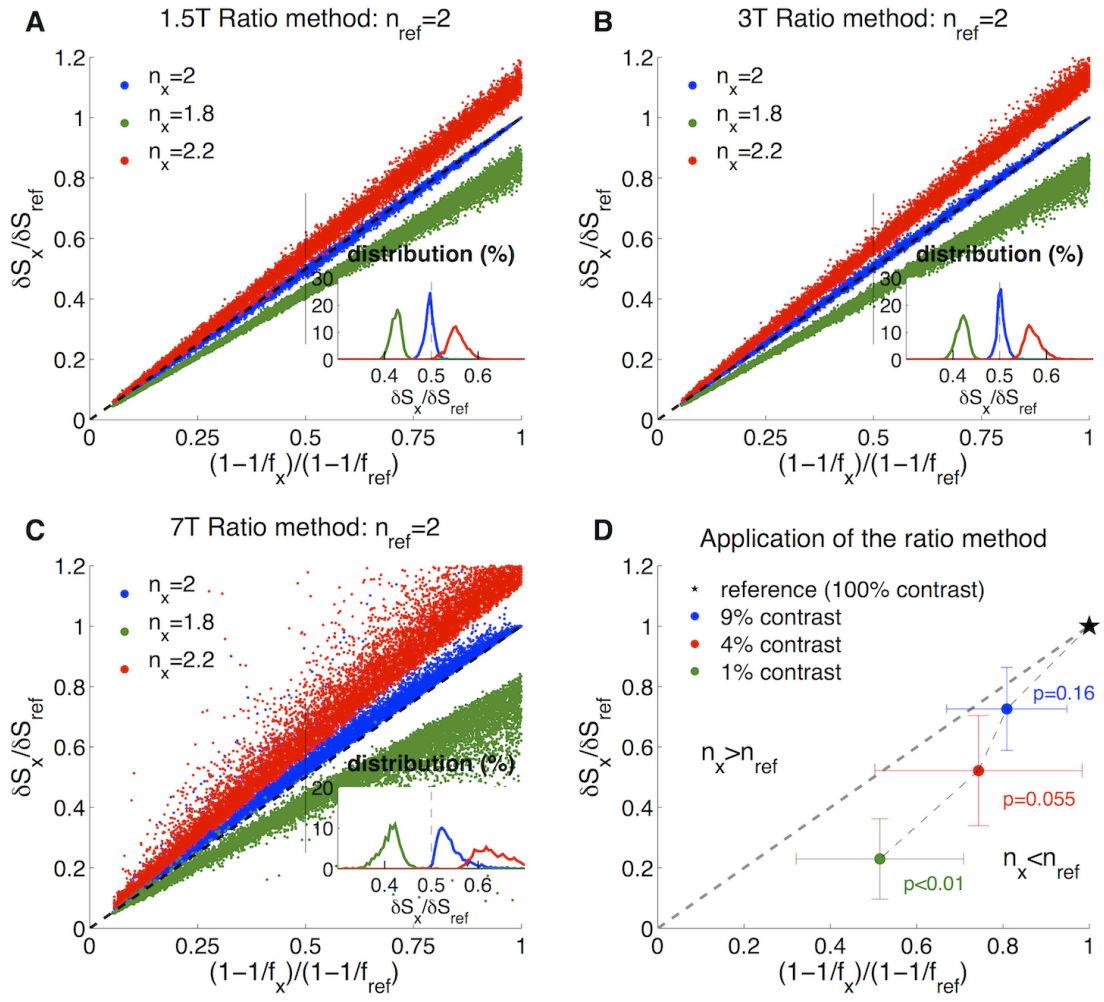

Figure 2.1. The ratio method for analysis of combined BOLD (δS) and CBF data.

The DBM was used to simulate BOLD data from changes in CBF and set values of *n*. 10,000 simulations were performed using the ranges for the model inputs noted in Tables 1 and 2. The data was compared to a reference of n_{ref}=2. Inset histograms show the distribution of δS ratios for a non-linear CBF ratio of 0.5. At 1.5T (A) and 3T (B), the ratio method separates the data well while predicting n_x=n_{ref} data will fall along the line of identity. At 7T (C), the ratio method does not perform as well, particularly for n_x=n_{ref} for which the data deviates from the line of identity. (D) Application of the ratio method to data examining the effect of visual stimulus contrast on the coupling of CBF and $CMRO_2$ in 9 subjects. 100% contrast flickering checkerboard was used as the reference with results showing that 1% contrast has a significantly lower *n*.

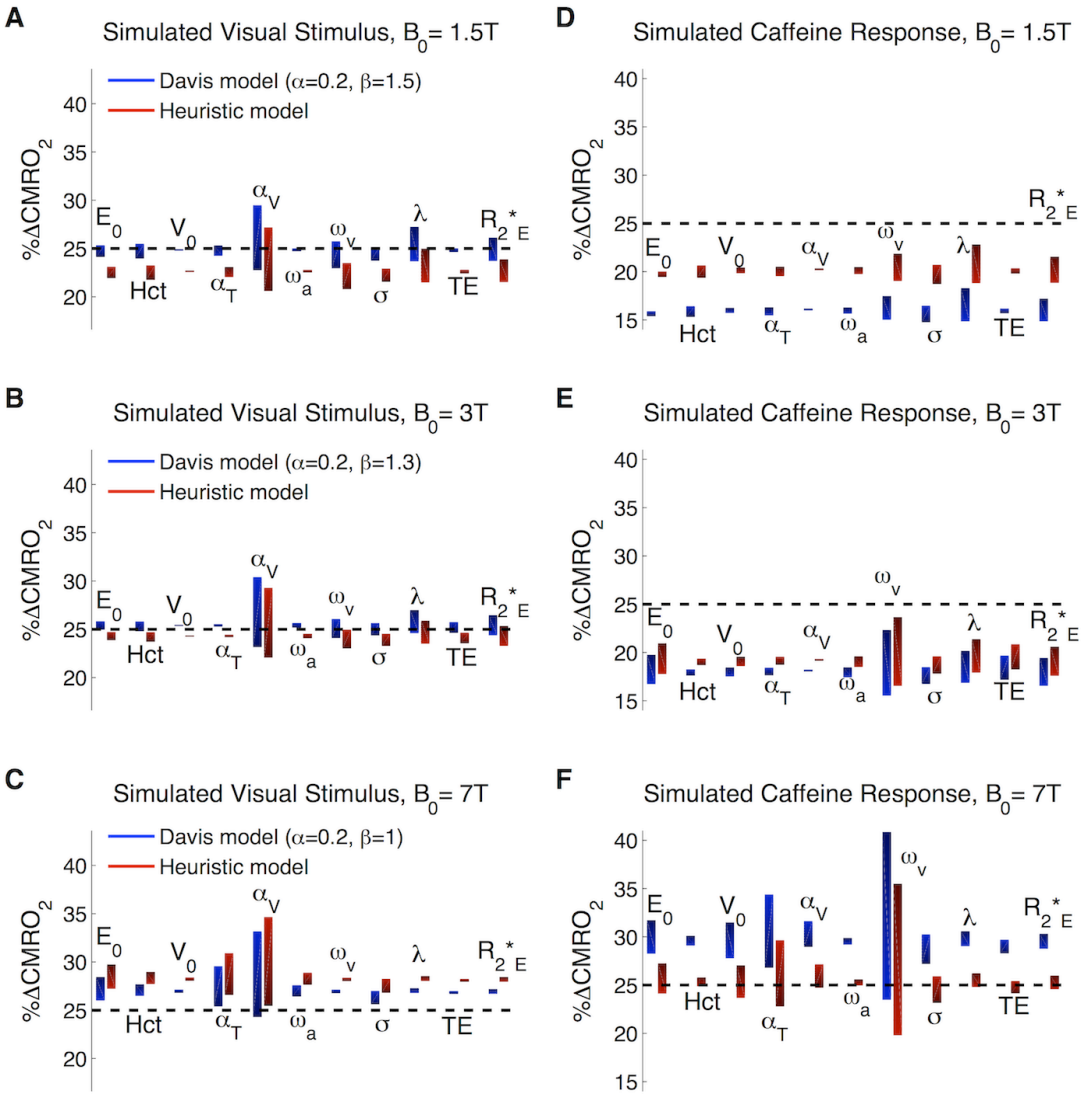

Figure 2.2. Heuristic vs. B_0-adjusted Davis model applied to the calibrated BOLD experiment: Estimating %ΔCMRO$_2$ calculation bias due to variability in physiological parameters.

Eleven input parameters to the detailed model were varied around reasonable values as defined in Tables 1 and 2 while other parameters were held constant at the best guess of physiology. The activation and ideal hypercapnia experiments were simulated for each of these physiological states at (A,B) 1.5T, (C,D) 3T and (E,F) 7T. The true CMRO$_2$ change with activation is shown as a dashed line, while the bars showing the range of calculated values is shaded from dark to light for increasing values of the associated physiological parameter. Davis model parameters α and β were adjusted for B_0 as noted in the figure. In the heuristic model, α_v=0.2 across all B_0. (A,C,E) Accuracy of the models at n=2 (%ΔCBF=50%) and variable B_0. (B,D,F) Accuracy of the models at n=-1 (%ΔCBF=-25%) and variable B_0. Note values for α and β in the Davis model are consistent for each B_0.

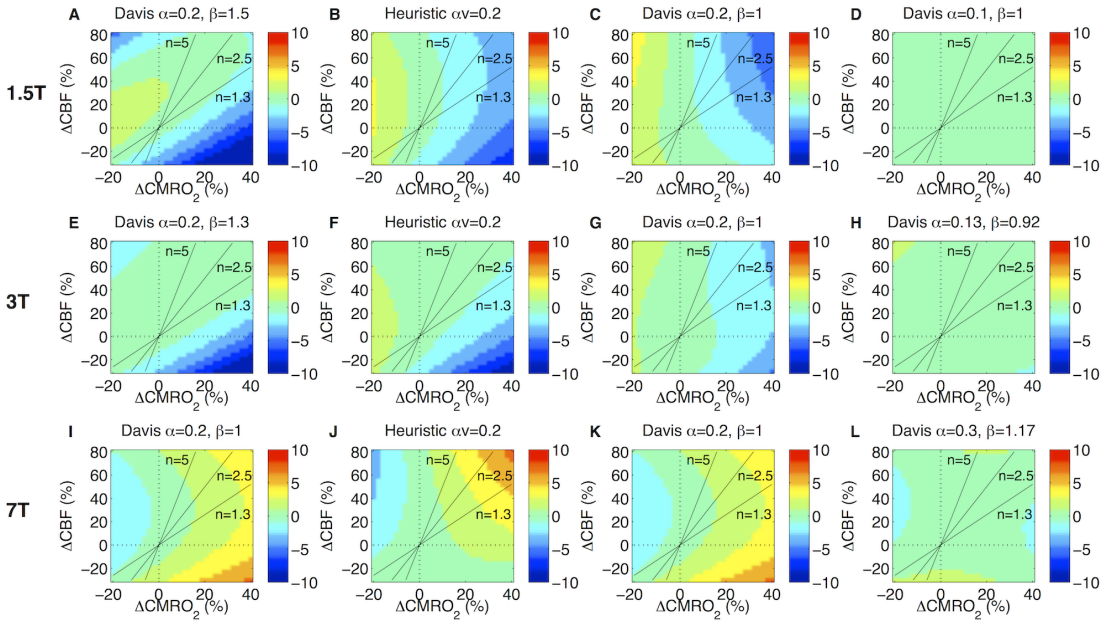

Figure 2.3. Absolute error in $\Delta CMRO_2$ calculations.

Simulated calibrated BOLD calculations were made for the best guess of physiology and imaging parameters noted in Tables 1 and 2. (A-D) Calculations in the absolute $\Delta CMRO_2$ error are shown at 1.5T for the 1.5T-adjusted Davis model, the heuristic model, the Davis model with α=0.2 and β=1, and the free parameter Davis model with α and β fitted as noted. Similar calculations are shown for 3T (E-H) and 7T (I-L).

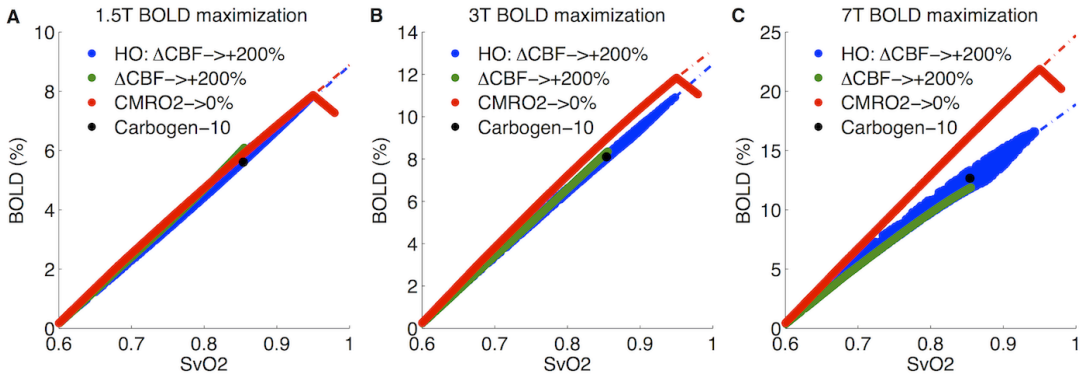

Figure 2.4. Simulating the maximum BOLD signal through dHb elimination.

The maximum BOLD signal results from complete elimination of dHb, which can be accomplished by increasing CBF, decreasing $CMRO_2$ and/or increasing PaO_2. Here the BOLD signal is shown as a function of SvO_2 at (A) 1.5T, (B) 3T, and (C) 7T. Three mechanisms of dHb reduction are included: hyperoxia combined with CBF increase (blue), CBF increase only (green) and $CMRO_2$ cessation (red). Also included is a simulation for ΔCBF=100% and PaO_2=390mmHg consistent with findings from Gauthier et al. [42].

Table 2.1. Input parameters to the detailed model.

Variable	Description	Best Guess	Reasonable Variation
V_0	Total baseline CBV fraction	0.05	0.03-0.07
ω_A	Arterial fraction of baseline CBV	0.1	0.05-0.15
ω_a	Arteriolar fraction of baseline CBV	0.1	0.05-0.15
ω_v	Venous fraction of baseline CBV	0.4	0.2-0.6
α_T	Grubb's constant relating total CBV to CBF	0.38	0.25-0.55
α_v	Exponent relating venous CBV to CBF	0.2	0.1-0.38
Hct	Resting hematocrit	0.44	0.37-0.5
E_0	Resting oxygen extraction fraction	0.4	0.3-0.5
σ	Fraction of arteriolar blood reflecting venous saturation	0.1	0-0.2
PaO_2	Arterial partial pressure of oxygen	104 mmHg	n/a
λ	Intravascular to extravascular spin density ratio	1.15	0.9-1.3

Table 2.2. Input parameter to the detailed model that are sensitive to B_0.

Variable	Description	Best Guess			Reasonable Variation		
		1.5T	3T	7T	1.5T	3T	7T
R_{2E}^*	Resting extravascular signal decay rate	11.6 s^{-1}	25.1 s^{-1}	35 s^{-1}	9-14 s^{-1}	20-30 s^{-1}	28-42 s^{-1}
TE	Echo time	50 ms	32 ms	25 ms	40-60 ms	20-40 ms	15-35 ms

Table 2.3. Comparing $\Delta CMRO_2$ calculations by different models.

			Heuristic[1]	B_0-adjusted[2]	Free parameter[3]	Original[4]
	ΔBOLD (%)	**ΔCBF (%)**	**$\Delta CMRO_2$ (%)**	**$\Delta CMRO_2$ (%)**	**$\Delta CMRO_2$ (%)**	**$\Delta CMRO_2$ (%)**
Pre-caffeine visual response	1.2±0.09	52.1±4.25	25.9±2.3	26.9±2.3	27.1±2.4	23.4±2.0
Post-caffeine visual response	1.2±0.07	57.0±3.57	36.6±2.2	37.0±2.3	36.5±2.4	32.0±2.0
Caffeine response	-6.3±1.1	-26.9±3.48	17.1±7.3	15.7±7.3	21.7±8.5	13.3±6.4

[1]Using the heuristic model proposed here with α_v=0.2, [2]Using the Davis model with α=0.2 and β=1.3; [3]Using the Davis model with α=0.13 and β=0.92; [4]Using the Davis model with α=0.38 and β=1.5

Appendix A

Derivation of the new model

Both the heuristic model and the Davis model are highly simplified mathematical expressions trying to capture a complex phenomenon. The main text describes tests of the accuracy of these simpler models against the DBM, which reflects our current knowledge of the BOLD signal and is the bottom-line test of the simpler models. Nevertheless, it is important to consider the basic ideas that motivated the proposed heuristic model, which can be derived from two assumptions. Neither of these assumptions is strictly true, and the DBM is used here to test each of these assumptions as the parameters in Tables 1 and 2 are varied.

Assumption 1: The fractional BOLD signal change is directly proportional to the absolute change in total deoxyhemoglobin (dHb) content in a voxel with slope m:

$$BOLD(\%) = -m \cdot \Delta\langle \mathrm{dHb} \rangle \tag{A1}$$

Here, $\langle \mathrm{dHb} \rangle$ ("dHb content") is total dHb per unit voxel volume and is dependent on both hemoglobin oxygen saturation and blood volume. $\langle \mathrm{dHb} \rangle_0$ is the dHb content in the baseline state. For our best guess of the physiology (Tables 1&2), this value is 0.11 mmol of dHb per liter of tissue volume assuming a hemoglobin monomer molecular weight of 16.1 kDa. In the seminal work of Ogawa and colleagues [1], they used Monte Carlo simulations to show that this assumption is true for the extravascular signal

change due to larger vessels for which diffusion is not important. Here using the detailed model, we tested whether this is still a reasonably accurate assumption when non-linear effects due to intravascular signal changes and extravascular signal changes around capillaries are incorporated; for 10,000 random combinations of %ΔCBF (-50% to 80%) and %ΔCMRO$_2$ (-30% to 50%), we examined the relationship between BOLD and $\langle dHb \rangle$ using our best guess of the physiology while also systematically varying these parameters as defined in Tables 1 and 2 (Appendix Fig. A1). We looked at the effects of varying baseline CBV fraction (V_0), the fraction of this CBV considered to be venous (ω_v), the coefficient relating venous CBV to CBF (α_v) and echo time (TE). We also examined whether a reasonable amount of combined variation in these parameters as defined in Tables 1 and 2 would have a different effect (App. Fig. A1D). Supporting Figures S2 and S3 show these simulations for 1.5T and 7T. The linearity of all these results suggests that Eq. (A1) is a reasonable assumption. This leads to the BOLD equation:

$$\frac{BOLD(\%)}{A} = -\frac{\Delta\langle \mathrm{dHb} \rangle}{\langle \mathrm{dHb} \rangle_0} \tag{A2}$$

Note, though, that the curves in Figure A1, while supporting an overall linear variation, have a certain thickness to them, indicating the limitations of this assumption. We consider the source of this effect below. In addition to those input parameters to the detailed model noted, we examined the others listed in Table 1; these results are not shown but are consistent with the first assumption.

Assumption 2: The fractional change in tissue concentration of total dHb is equal to the fractional change of venous dHb:

$$\frac{\Delta\langle \mathrm{dHb} \rangle}{\langle \mathrm{dHb} \rangle_0} = \frac{\Delta\langle \mathrm{dHb} \rangle_v}{\langle \mathrm{dHb} \rangle_{v,0}} \tag{A3}$$

Tests of this assumption using the DBM (in parallel to its use in producing Appendix Figure A1) are shown (Appendix Figure A2), suggesting that this assumption is accurate as well. We also examined the effect of varying the other parameters listed in Tables 1 and 2 (results not shown) without finding any noticeable effect on this relationship.

The first assumption defines the basic relationship between the BOLD signal and dHb, and the second assumption provides the link to the physiological parameters. We define f, v, and r respectively as CBF, venous CBV and $CMRO_2$ normalized to their baseline state values. Also E and E_0 are the oxygen extraction fractions in the active and baseline states such that E=dHb/Hb. Since in most cases $E/E_0 = r/f$ (from the definition of $CMRO_2$ with the notable exception of hyperoxia), the normalized change in venous dHb is:

$$\frac{\Delta\langle \mathrm{dHb} \rangle_v}{\langle \mathrm{dHb} \rangle_{v,0}} = \frac{\Delta CBV}{CBV_0} \cdot \frac{\Delta E}{E_0} = \frac{v \cdot r}{f} - 1 \tag{A4}$$

Combining equations [A2-A4], the BOLD equation becomes:

$$BOLD(\%) = M\left(1 - \frac{v \cdot r}{f}\right) \tag{A5}$$

We posit that the normalized change in $CMRO_2$ ($\Delta R/R_0$) and the normalized change in CBV ($\Delta V/V_0$) are small enough to justify first order approximation while the normalized change in CBF ($\Delta F/F_0$) is too large for such an approximation:

$$\begin{aligned} 1-\frac{v\cdot r}{f} &= 1-\frac{1}{f}\left(1+\frac{\Delta V}{V_0}\right)\left(1+\frac{\Delta R}{R_0}\right) \\ &\approx 1-\frac{1}{f}\left(1+\frac{\Delta V}{V_0}+\frac{\Delta R}{R_0}\right) \end{aligned} \tag{A6}$$

Defining the coupling parameter $n=(f\text{-}1)/(r\text{-}1)$ such that $\Delta R/R_0 = 1/n\cdot\Delta F/F_0$ and substituting for the approximation $\Delta V/V_0 = \alpha_v\cdot\Delta F/F_0$, which is the linearization of $v=f^{\alpha_v}$ leads to the following, which can be rearranged:

$$\begin{aligned} 1-\frac{v\cdot r}{f} &= 1-\frac{1}{f}\left(1+\alpha_v\frac{\Delta F}{F_0}+\frac{1}{n}\cdot\frac{\Delta F}{F_0}\right) \\ &\approx \frac{\left(1+\Delta F/F_0\right)F_0}{\left(1+\Delta F/F_0\right)F_0}-\frac{F_0}{\left(1+\Delta F/F_0\right)F_0}-\frac{\alpha_v\cdot\Delta F}{\left(1+\Delta F/F_0\right)F_0}-\frac{\Delta F}{n\left(1+\Delta F/F_0\right)F_0} \\ &\approx \frac{\Delta F/F_0}{1+\Delta F/F_0}-\frac{\alpha_v\cdot\Delta F/F_0}{1+\Delta F/F_0}-\frac{\Delta F/F_0}{n\left(1+\Delta F/F_0\right)} \\ &\approx \left(\frac{1+\Delta F/F_0}{1+\Delta F/F_0}-\frac{1}{1+\Delta F/F_0}\right)\left(1-\alpha_v-1/n\right) \\ &\approx \left(1-1/f\right)\left(1-\alpha_v-1/n\right) \end{aligned} \tag{A7}$$

The new model of the BOLD signal is therefore:

$$BOLD(\%) = A\left(1-1/f\right)\left(1-\alpha_v-1/n\right) \tag{A8}$$

As noted above, the primary source of error in this model likely arises from the thickness of the lines in Figure A1. While the overall behavior of the curves is linear,

the width of the curves contradicts the assumption that no change in $\Delta\langle \mathrm{dHb} \rangle$ produces no change in the BOLD signal. Specifically, a non-zero BOLD signal may occur even if there is no change in dHb content when an increase in CBF both decreases the blood concentration of dHb and also increases venous CBV. This would result in no extravascular signal change, but the decrease in dHb blood concentration would still produce a positive intravascular BOLD signal. Additionally there is exchange of blood and tissue volumes, which contributes to the signal change. For these reasons, a measured BOLD signal change could occur even when there is no change in total dHb content. The magnitude of this effect at 3T is illustrated (Appendix Figure A3) by showing curves of constant BOLD signal produced by the DBM in the plane of CBF and $CMRO_2$ changes with the best guess of the values for the physiological variables (Tables 1 and 2). Plotted with the curves of the BOLD signal is the curve of constant total dHb content, which departs from the null line of the BOLD signal as the CBF and $CMRO_2$ changes increase.

Appendix B: Limits of the simple models

Maximizing the BOLD signal through elimination of dHb

In order to maximize the BOLD signal in a particular subject, all dHb present in the baseline state must be eliminated. This can occur through increases in CBF or decreases in $CMRO_2$. These limits of the simple models are examined in order to elucidate their relationship to the maximum BOLD signal. The limits of the Davis model are straightforward. In the case of an infinite CBF change, the $f^{\alpha-\beta}$ term goes to zero:

$$\begin{aligned} BOLD(\%) &= M\left(1 - f^{\alpha-\beta} r^{\beta}\right) \\ &= M \end{aligned} \tag{B1}$$

When $CMRO_2$ approaches zero (r=0), the same solution is found such that in both instances the Davis model scaling parameter is equivalent to the maximum BOLD signal.

The heuristic model is also straightforward for the case of an infinite CBF change as both the $1/f$ and $1/n$ terms go to zero:

$$\begin{aligned} BOLD(\%) &= A\left(1 - 1/f\right)\left(1 - \alpha_v - 1/n\right) \\ &= A\left(1 - \alpha_v\right) \end{aligned} \tag{B2}$$

In the case that $CMRO_2$ approaches zero, the solution is slightly more complicated and depends on CBF, however if ΔCBF is small the limit simply becomes A:

$$
\begin{aligned}
BOLD(\%) &= A(1-1/f)(1-\alpha_v-1/n) \\
&= A\left(\frac{f-1}{f}\right)\left(1-\alpha_v-\frac{r-1}{f-1}\right) \\
&= A\left(\frac{f-1}{f}-\alpha_v\frac{f-1}{f}+\frac{1}{f}\right) \\
&= A\left[1-\alpha_v(1-1/f)\right] \\
&= A(1-\alpha_v\cdot\Delta CBF/CBF) \\
&= A
\end{aligned}
\tag{B3}
$$

The limit of the heuristic and Davis models as ΔCBF approaches zero

Starting with the Davis model and assuming changes in CBF and $CMRO_2$ are small, substitutions can be made for $f \rightarrow 1$ and n:

$$
\begin{aligned}
BOLD(\%) &= M\left[1-\left(\frac{\Delta R}{R_0}+1\right)^{\beta}\right] \\
&= M\left(1-\beta\cdot\frac{\Delta R}{R_0}-1\right) \\
&= M\cdot\beta\cdot\frac{\Delta R}{R_0}
\end{aligned}
\tag{B4}
$$

Starting with the heuristic model, substitutions can be made for f and n as follows:

$$
BOLD(\%) = A\left(1-\frac{F_0}{F_0+\Delta F}\right)\left(1-\alpha_v-\frac{F_0\cdot\Delta R}{R_0\cdot\Delta F}\right) \tag{B5}
$$

For small changes in flow, we can find the limit of the flow term using a first order approximation since the inverse of 1+x where x is a small number is 1-x. Additionally,

a number divided by ΔF as this term approaches zero will go to infinity overwhelming the finite 1-α_v term:

$$\begin{aligned} BOLD(\%) &= A\left(1-\frac{F_0}{F_0+(1+\Delta F/F_0)}\right)\left(1-\alpha_v-\frac{F_0\cdot\Delta R}{R_0\cdot\Delta F}\right) \\ &= A\left[1-(1-\Delta F/F_0)\right]\left(-\frac{F_0\cdot\Delta R}{R_0\cdot\Delta F}\right) \end{aligned} \tag{B6}$$

Solving for the BOLD signal leaves the following relationship:

$$BOLD(\%) = -A\frac{\Delta R}{R_0} \tag{B7}$$

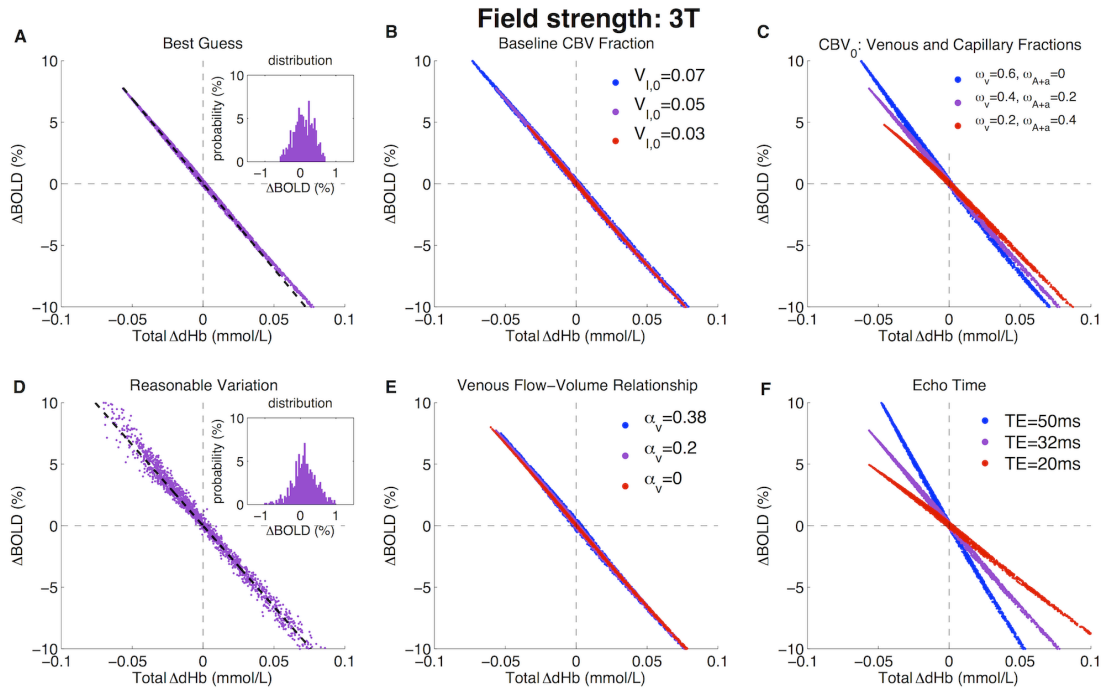

Appendix Figure A1.2.5. Relationship between the BOLD signal change and the total change in dHb content ($\Delta\langle \mathrm{dHb} \rangle$) at 3T.

Scatter plots were produced by independently varying ΔCBF (-50% to 80%) and $\Delta CMRO_2$ (-30% to 50%) within the specified ranges. Purple curves are identical in all subplots with the exception of (D) and represent the best guess physiological case (Tables 1 and 2). (A) For the best guess of physiological parameters, the relationship between the BOLD signal and $\Delta\langle dHb \rangle$ is linear, but there is a finite width to the curve. In this case, $\langle \mathrm{dHb} \rangle_0 = 0.11$ mmol of dHb per liter of tissue. For ΔBOLD between -3% and 3%, a fit to this line gives ΔBOLD(%)=-138* $\Delta\langle \mathrm{dHb} \rangle$. Inset is a histogram of ΔBOLD probability distribution around $\Delta\langle \mathrm{dHb} \rangle = 0 \pm 0.025$ mg/mL (i.e., variation in the BOLD signal that could result when there is no change in net tissue dHb). (D) Allowing a wider and still reasonable distribution of physiology (Tables 1 and 2, Reasonable Variation) produced more scatter in the relationship between ΔBOLD and $\Delta\langle \mathrm{dHb} \rangle$. For ΔBOLD between -3% and 3%, a fit to this line gives ΔBOLD=-133* $\Delta\langle \mathrm{dHb} \rangle$. Inset is a histogram of ΔBOLD probability distribution around $\Delta\langle \mathrm{dHb} \rangle = 0 \pm 0.025$mg/mL. The remaining panels show how the curve changes when one of the physiological variables is altered: (B) varying baseline CBV fraction; (C) varying baseline venous and capillary CBV fractions; (E) varying the exponent relating CBF and venous CBV; (F) altering TE.

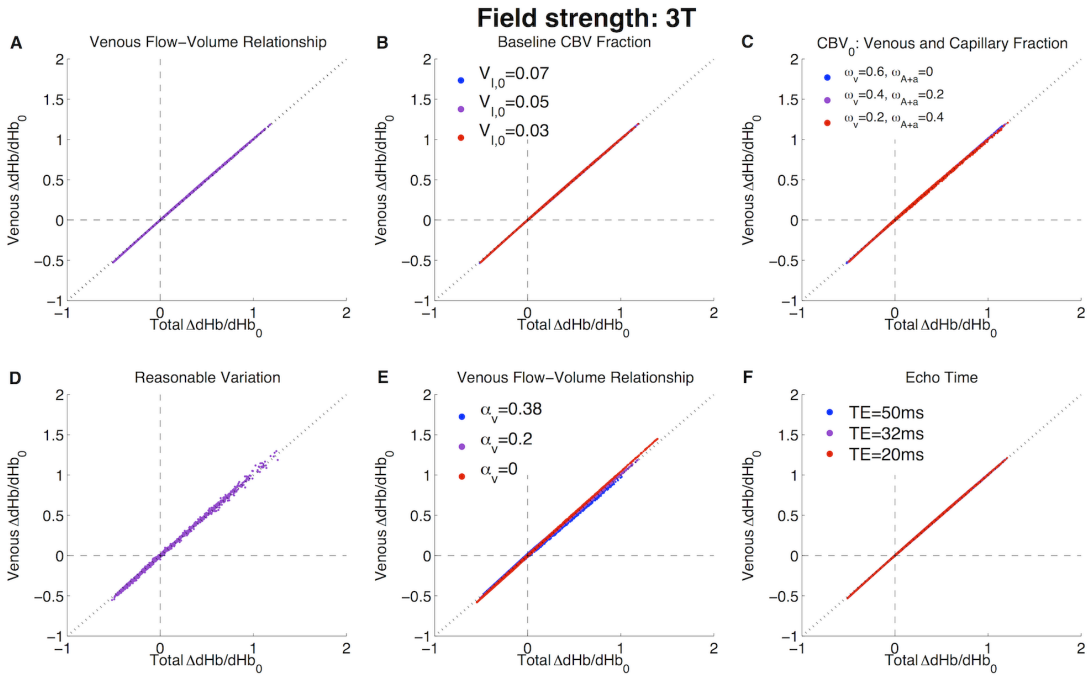

Appendix Figure A2.2.6. Relationship between the normalized venous change and normalized total change in dHb contents.

Scatter plots were produced as in Fig. A1 by independently varying ΔCBF (-50% to 80%) and $\Delta CMRO_2$ (-30% to 50%) within the specified ranges. Purple curves are identical in all subplots with the exception of (D) and represent the best guess physiological case (Tables 1 and 2). (D) Combined variation of the parameters within the reasonable ranges (Tables 1 and 2). The only physiological variable that created a slight deviation from the identity line is the venous flow-volume relationship expressed as α_v (E).

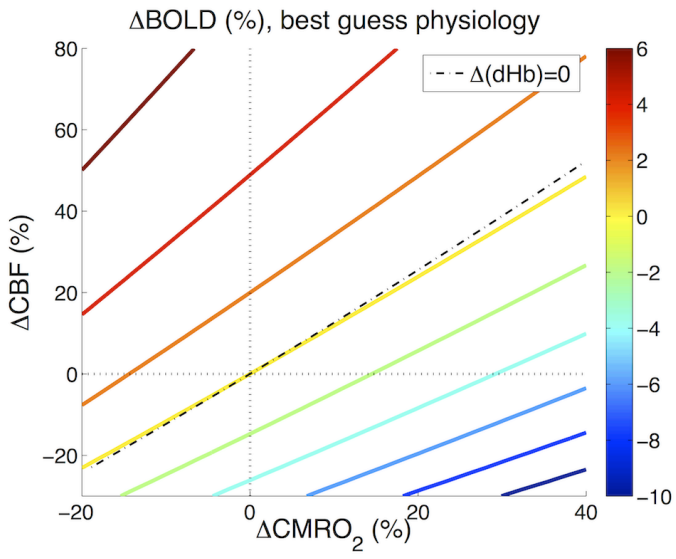

Appendix Figure A3.2.7. Comparing zero BOLD response to zero change in total dHb content.

This plot of the BOLD response as a function of changes in CBF and $CMRO_2$ was generated using our best guess of the physiological inputs to the DBM model at 3T (Tables 1 and 2). The color scale represents the BOLD signal as a percent change. The dot-dash line represents $\Delta\langle \mathrm{dHb} \rangle = 0$ while the solid orange line represents ΔBOLD=0%. For positive changes in CBF and $CMRO_2$, $\Delta\langle \mathrm{dHb} \rangle = 0$ is shown to be associated with a small positive BOLD signal. This is due to the intravascular effects of *dHb*: although the increase in CBV and decrease in *dHb* concentration combine to produce no change in total *dHb* content and no change in the extravascular signal, the intravascular signal decay rate decreases due to the decrease in *dHb* concentration.

Supplementary Information

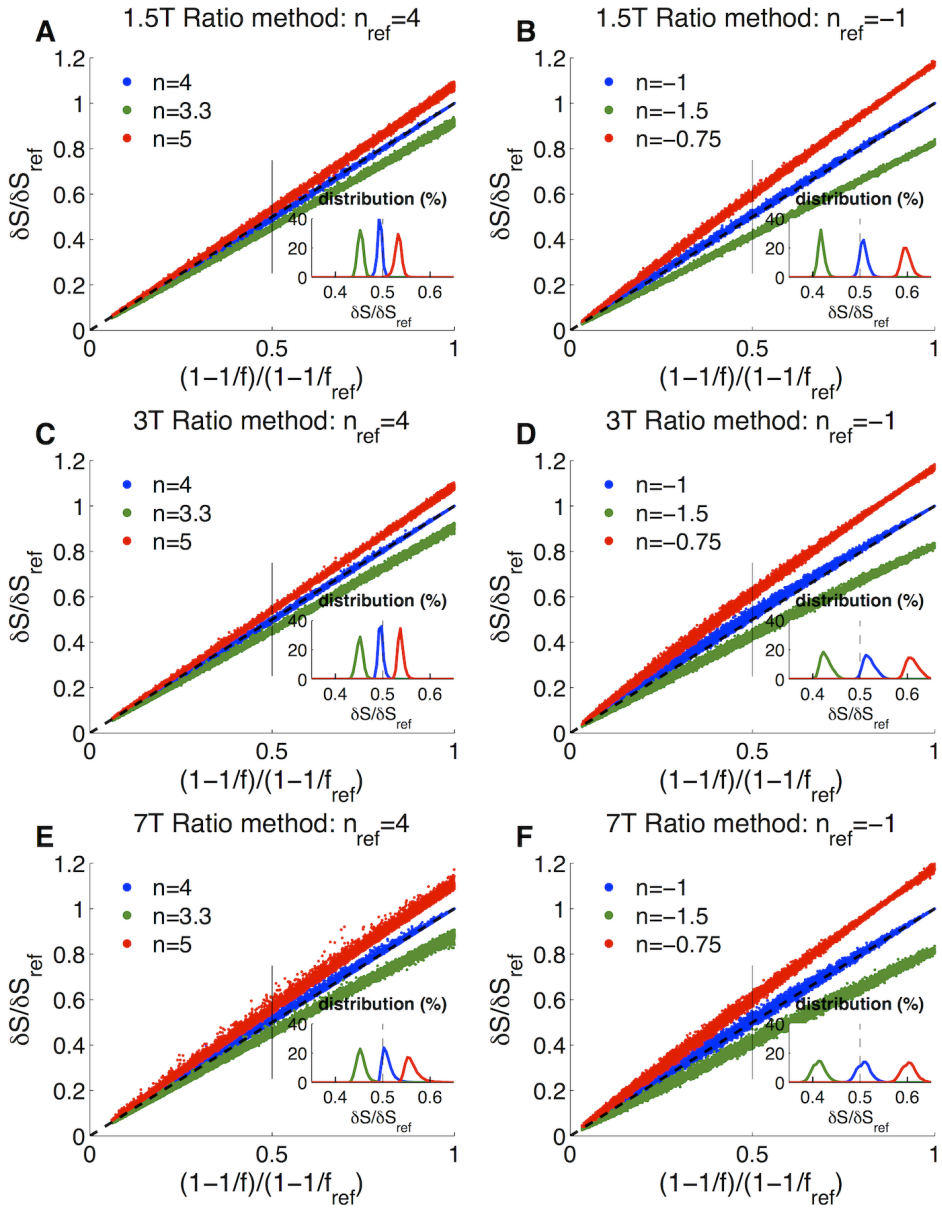

Supplementary Figure S1.2.8. The ratio method for analysis of combined BOLD (δS) and CBF data: effects of different *n*.

The DBM was used to simulate BOLD data from changes in CBF and set values of *n*. 10,000 simulations were performed using the ranges for the model inputs noted in Tables 1 and 2. The data was compared to a reference of n_{ref}=-1 or n_{ref}=4 at B_0=1.5T, 3T and 7T. Inset histograms show the distribution of δS ratios for a CBF ratio of 0.5. (A,C,E) For n_{ref}=4 at 1.5T (A) and 3T (C), the ratio method appears to work well, although the data is slightly more difficult to distinguish, which is expected due to the decreased sensitivity of the BOLD signal to *n* at higher values of *n*. At 7T (E), the approach is again biased when n_x=n_{ref}. At all three field strengths, the ratio method separates the data well for n_{ref}=-1, although there is bias in the n_x=n_{ref} data. (B,D,F).

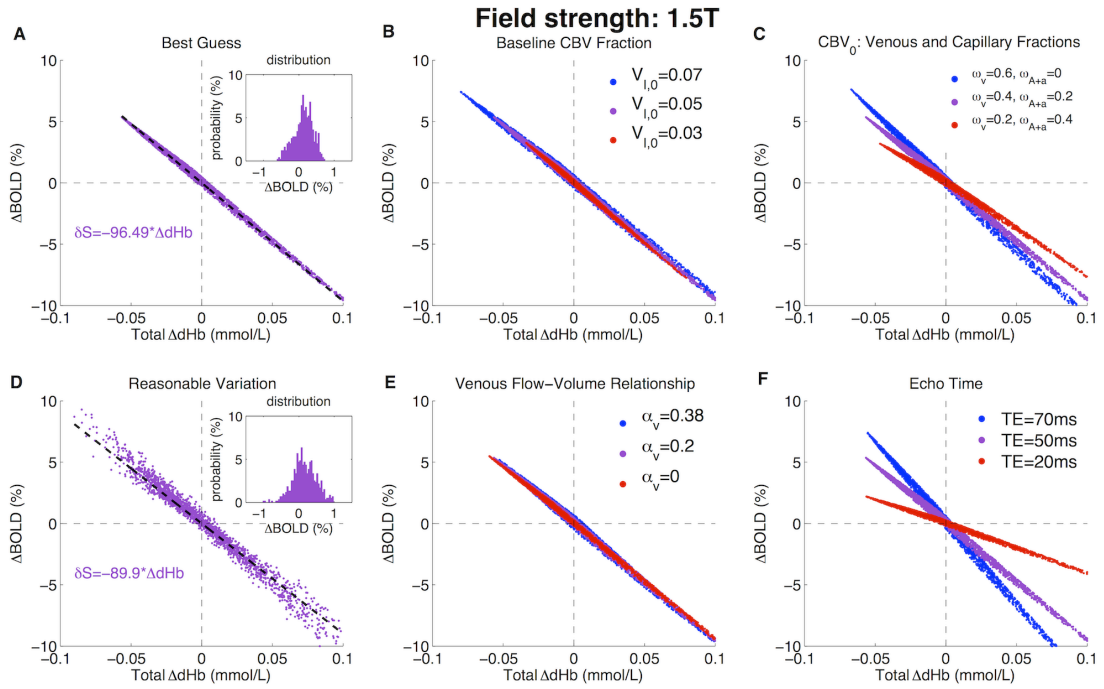

Supplementary Figure S2.2.9. Relationship between the BOLD signal change and the total $\Delta\langle \mathrm{dHb} \rangle$ at 1.5T.

Scatter plots were again produced by independently varying ΔCBF and $\Delta CMRO_2$. (A) For the best guess of physiology, the relationship between the BOLD signal and $\Delta\langle dHb \rangle$ is linear, but again there is a finite width to the curve. For ΔBOLD between -3% and 3%, a fit to this line gives ΔBOLD(%)=-96* $\Delta\langle dHb \rangle$. The inset is a histogram of ΔBOLD probability distribution around $\Delta\langle dHb \rangle$=0±0.025 mg/mL is similar to that at 3T As expected, the BOLD signal shows weaker dependence on the change in dHb content than at 3T (B-F).

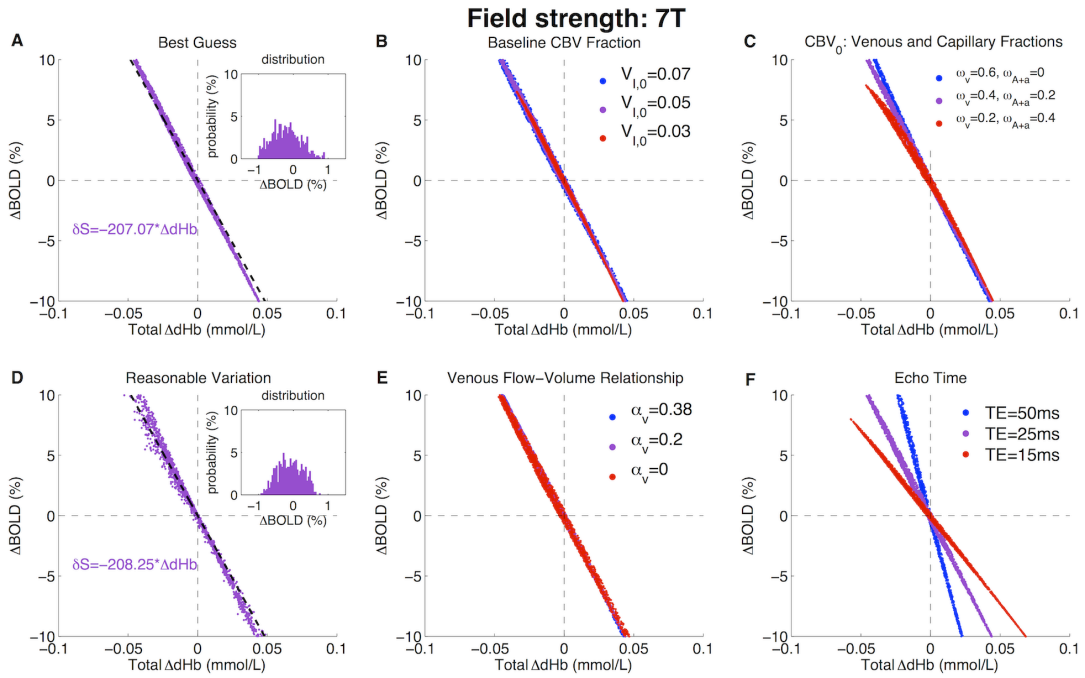

Supplementary Figure S3.2.10. Relationship between the BOLD signal change and the total $\Delta\langle \mathrm{dHb} \rangle$ at 7T.

(A) For the best guess of physiology, the relationship between the BOLD signal and $\Delta\langle \mathrm{dHb} \rangle$ is linear with a tighter distribution than at 3T or 7T. For ΔBOLD between -3% and 3%, a fit to this data gives ΔBOLD(%)=-207* $\Delta\langle \mathrm{dHb} \rangle$. As expected, the BOLD signal shows stronger dependence on the change in dHb content than at 3T (B-F).

Acknowledgements

Chapter 2, in full, has been submitted for publication and is the material as it may appear in PLoS ONE 2013. Griffeth, VEM and Buxton, RB (2013). A new functional MRI approach for investigating modulations of brain oxygen metabolism. PLoS ONE. The dissertation author was the primary investigator and author of this paper.

References

1. Ogawa S, Menon RS, Tank DW, Kim S-G, Merkle H, et al. (1993) Functional brain mapping by blood oxygenation level - dependent contrast magnetic resonance imaging: a comparison of signal characteristics with a biophysical model. Biophysical J 64: 803-812.

2. Fox PT, Raichle ME (1986) Focal physiological uncoupling of cerebral blood flow and oxidative metabolism during somatosensory stimulation in human subjects. Proc Natl Acad Sci USA 83: 1140-1144.

3. Ances BM, Leontiev O, Perthen JE, Liang C, Lansing AE, et al. (2008) Regional differences in the coupling of cerebral blood flow and oxygen metabolism changes in response to activation: Implications for BOLD-fMRI. Neuroimage 39: 1510-1521.

4. Donahue MJ, Blicher JU, Ostergaard L, Feinberg DA, MacIntosh BJ, et al. (2009) Cerebral blood flow, blood volume, and oxygen metabolism dynamics in human visual and motor cortex as measured by whole-brain multi-modal magnetic resonance imaging. J Cereb Blood Flow Metab 29: 1856-1866.

5. Ances BM, Liang CL, Leontiev O, Perthen JE, Fleisher AS, et al. (2009) Effects of aging on cerebral blood flow, oxygen metabolism, and blood oxygenation level dependent responses to visual stimulation. Hum Brain Mapp 30: 1120-1132.

6. Chen Y, Parrish TB (2009) Caffeine's effects on cerebrovascular reactivity and coupling between cerebral blood flow and oxygen metabolism. Neuroimage 44: 647-652.

7. Griffeth VE, Perthen JE, Buxton RB (2011) Prospects for quantitative fMRI: Investigating the effects of caffeine on baseline oxygen metabolism and the response to a visual stimulus in humans. Neuroimage 57: 809-816.

8. Moradi F, Buracas GT, Buxton RB (2012) Attention strongly increases oxygen metabolic response to stimulus in primary visual cortex. Neuroimage 59: 601-607.

9. Davis TL, Kwong KK, Weisskoff RM, Rosen BR (1998) Calibrated functional MRI: mapping the dynamics of oxidative metabolism. Proc Natl Acad Sci USA 95: 1834-1839.

10. Griffeth VE, Buxton RB (2011) A theoretical framework for estimating cerebral oxygen metabolism changes using the calibrated-BOLD method: modeling the effects of blood volume distribution, hematocrit, oxygen extraction fraction, and tissue signal properties on the BOLD signal. Neuroimage 58: 198-212.

11. Hoge RD, Atkinson J, Gill B, Crelier GR, Marrett S, et al. (1999) Investigation of BOLD signal dependence on cerebral blood flow and oxygen consumption: the deoxyhemoglobin dilution model. Magn Reson Med 42: 849-863.

12. Hoge RD, Atkinson J, Gill B, Crelier GR, Marrett S, et al. (1999) Linear coupling between cerebral blood flow and oxygen consumption in activated human cortex. Proc Natl Acad Sci, USA 96: 9403-9408.

13. Kim SG, Rostrup E, Larsson HBW, Ogawa S, Paulson OB (1999) Determination of relative CMRO2 from CBF and BOLD changes: significant increase of oxygen consumption rate during visual stimulation. Magn Reson Med 41: 1152-1161.

14. Kastrup A, Kruger G, Neumann-Haefelin T, Glover GH, Moseley ME (2002) Changes of cerebral blood flow, oxygenation, and oxidative metabolism during graded motor activation. Neuroimage 15: 74-82.

15. Stefanovic B, Warnking JM, Kobayashi E, Bagshaw AP, Hawco C, et al. (2005) Hemodynamic and metabolic responses to activation, deactivation and epileptic discharges. Neuroimage 28: 205-215.

16. Uludag K, Dubowitz DJ, Yoder EJ, Restom K, Liu TT, et al. (2004) Coupling of cerebral blood flow and oxygen consumption during physiological activation and deactivation measured with fMRI. Neuroimage 23: 148-155.

17. St Lawrence KS, Ye FQ, Lewis BK, Frank JA, McLaughlin AC (2003) Measuring the effects of indomethacin on changes in cerebral oxidative metabolism and cerebral blood flow during sensorimotor activation. Magn Reson Med 50: 99-106.

18. Chiarelli PA, Bulte DP, Gallichan D, Piechnik SK, Wise R, et al. (2007) Flow-metabolism coupling in human visual, motor, and supplementary motor areas assessed by magnetic resonance imaging. Magn Reson Med 57: 538-547.

19. Leontiev O, Buxton RB (2007) Reproducibility of BOLD, perfusion, and CMRO(2) measurements with calibrated-BOLD fMRI. Neuroimage 35: 175-184.

20. Pike GB (2012) Quantitative functional MRI: Concepts, issues and future challenges. Neuroimage 62: 1234-1240.

21. Blockley NP, Griffeth VEM, Simon AB, Buxton RB (in press) A review of calibrated BOLD methods for measuring task-induced changes in brain oxygen metabolism. NMR in Biomedicine.

22. Perthen JE, Lansing AE, Liau J, Liu TT, Buxton RB (2008) Caffeine-induced uncoupling of cerebral blood flow and oxygen metabolism: a calibrated BOLD fMRI study. Neuroimage 40: 237-247.

23. Jain V, Langham MC, Floyd TF, Jain G, Magland JF, et al. (2011) Rapid magnetic resonance measurement of global cerebral metabolic rate of oxygen consumption in humans during rest and hypercapnia. J Cereb Blood Flow Metab 31: 1504-1512.

24. Sicard KM, Duong TQ (2005) Effects of hypoxia, hyperoxia, and hypercapnia on baseline and stimulus-evoked BOLD, CBF, and CMRO2 in spontaneously breathing animals. Neuroimage 25: 850-858.

25. Kim T, Hendrich KS, Masamoto K, Kim SG (2007) Arterial versus total blood volume changes during neural activity-induced cerebral blood flow change: implication for BOLD fMRI. J Cereb Blood Flow Metab 27: 1235-1247.

26. Hillman EM, Devor A, Bouchard MB, Dunn AK, Krauss GW, et al. (2007) Depth-resolved optical imaging and microscopy of vascular compartment dynamics during somatosensory stimulation. Neuroimage 35: 89-104.

27. Liang CL, Ances BM, Perthen JE, Moradi F, Liau J, et al. (2013) Luminance contrast of a visual stimulus modulates the BOLD response more than the cerebral blood flow response in the human brain. Neuroimage 64: 104-111.

28. Severinghaus JW (1979) Simple, accurate equations for human blood O2 dissociation computations. J Appl Physiol 46: 599-602.

29. Chiarelli PA, Bulte DP, Wise R, Gallichan D, Jezzard P (2007) A calibration method for quantitative BOLD fMRI based on hyperoxia. Neuroimage 37: 808-820.

30. van der Zwaag W, Francis S, Head K, Peters A, Gowland P, et al. (2009) fMRI at 1.5, 3 and 7 T: characterising BOLD signal changes. Neuroimage 47: 1425-1434.

31. Silvennoinen MJ, Clingman CS, Golay X, Kauppinen RA, van Zijl PC (2003) Comparison of the dependence of blood R2 and R2* on oxygen saturation at 1.5 and 4.7 Tesla. Magn Reson Med 49: 47-60.

32. Blockley NP, Jiang L, Gardener AG, Ludman CN, Francis ST, et al. (2008) Field strength dependence of R1 and R2* relaxivities of human whole blood to ProHance, Vasovist, and deoxyhemoglobin. Magn Reson Med 60: 1313-1320.

33. Chen JJ, Pike GB (2009) BOLD-specific cerebral blood volume and blood flow changes during neuronal activation in humans. NMR Biomed 22: 1054-1062.

34. Chen JJ, Pike GB (2010) Global cerebral oxidative metabolism during hypercapnia and hypocapnia in humans: implications for BOLD fMRI. J Cereb Blood Flow Metab 30: 1094-1099.

35. Jones M, Berwick J, Hewson-Stoate N, Gias C, Mayhew J (2005) The effect of hypercapnia on the neural and hemodynamic responses to somatosensory stimulation. Neuroimage 27: 609-623.

36. Mark CI, Fisher JA, Pike GB (2011) Improved fMRI calibration: precisely controlled hyperoxic versus hypercapnic stimuli. Neuroimage 54: 1102-1111.

37. Boxerman JL, Hamberg LM, Rosen BR, Weisskoff RM (1995) MR contrast due to intravascular magnetic susceptibility perturbations. Magn Reson Med 34: 555-566.

38. Lin AL, Fox PT, Yang Y, Lu H, Tan LH, et al. (2008) Evaluation of MRI models in the measurement of CMRO2 and its relationship with CBF. Magn Reson Med 60: 380-389.

39. Moradi F, Buracas GT, Buxton RB (2012) Attention strongly increases oxygen metabolic response to stimulus in primary visual cortex. Neuroimage.

40. Stefanovic B, Warnking JM, Pike GB (2004) Hemodynamic and metabolic responses to neuronal inhibition. Neuroimage 22: 771-778.

41. Wong EC, Buxton RB, Frank LR (1998) Quantitative imaging of perfusion using a single subtraction (QUIPSS and QUIPSS II). Magn Reson Med 39: 702-708.

42. Gauthier CJ, Madjar C, Tancredi FB, Stefanovic B, Hoge RD (2011) Elimination of visually evoked BOLD responses during carbogen inhalation: implications for calibrated MRI. Neuroimage 54: 1001-1011.

43. Grubb RL, Raichle ME, Eichling JO, Ter-Pogossian MM (1974) The effects of changes in $PaCO_2$ on cerebral blood volume, blood flow, and vascular mean transit time. Stroke 5: 630 - 639.

44. Spees WM, Yablonskiy DA, Oswood MC, Ackerman JJ (2001) Water proton MR properties of human blood at 1.5 Tesla: magnetic susceptibility, T(1), T(2), T*(2), and non-Lorentzian signal behavior. Magn Reson Med 45: 533-542.

45. Uludag K, Muller-Bierl B, Ugurbil K (2009) An integrative model for neuronal activity-induced signal changes for gradient and spin echo functional imaging. Neuroimage 48: 150-165.

46. Stephan KE, Weiskopf N, Drysdale PM, Robinson PA, Friston KJ (2007) Comparing hemodynamic models with DCM. Neuroimage 38: 387-401.

47. Buxton RB, Wong EC, Frank LR (1998) Dynamics of blood flow and oxygenation changes during brain activation: the balloon model. Magn Reson Med 39: 855-864.

48. Simon AB, Griffeth VE, Wong EC, Buxton RB (2013) A novel method of combining blood oxygenation and blood flow sensitive magnetic resonance imaging techniques to measure the cerebral blood flow and oxygen metabolism responses to an unknown neural stimulus. PLoS One 8: e54816.

CHAPTER 3

Contents lists available at ScienceDirect

NeuroImage

journal homepage: www.elsevier.com/locate/ynimg

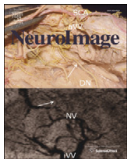

Prospects for quantitative fMRI: Investigating the effects of caffeine on baseline oxygen metabolism and the response to a visual stimulus in humans

Valerie E.M. Griffeth [a], Joanna E. Perthen [b], Richard B. Buxton [b,*]

[a] Department of Bioengineering, and Center for Functional Magnetic Resonance Imaging, University of California, San Diego, CA 92093, USA
[b] Department of Radiology, and Center for Functional Magnetic Resonance Imaging, University of California, San Diego, CA 92093, USA

ARTICLE INFO

Article history:
Received 4 February 2011
Revised 8 April 2011
Accepted 29 April 2011
Available online 7 May 2011

Keywords:
Blood oxygenation level dependent
Cerebral blood flow
Cerebral metabolic rate of oxygen
Caffeine
Functional MRI
Arterial spin labeling

ABSTRACT

Functional magnetic resonance imaging (fMRI) provides an indirect reflection of neural activity change in the working brain through detection of blood oxygenation level dependent (BOLD) signal changes. Although widely used to map patterns of brain activation, fMRI has not yet met its potential for clinical and pharmacological studies due to difficulties in quantitatively interpreting the BOLD signal. This difficulty is due to the BOLD response being strongly modulated by two physiological factors in addition to the level of neural activity: the amount of deoxyhemoglobin present in the baseline state and the coupling ratio, n, of evoked changes in blood flow and oxygen metabolism. In this study, we used a quantitative fMRI approach with dual measurement of blood flow and BOLD responses to overcome these limitations and show that these two sources of modulation work in opposite directions following caffeine administration in healthy human subjects. A strong 27% reduction in baseline blood flow and a 22% increase in baseline oxygen metabolism after caffeine consumption led to a decrease in baseline blood oxygenation and were expected to increase the subsequent BOLD response to the visual stimulus. Opposing this, caffeine reduced n through a strong 61% increase in the evoked oxygen metabolism response to the visual stimulus. The combined effect was that BOLD responses pre- and post-caffeine were similar despite large underlying physiological changes, indicating that the magnitude of the BOLD response alone should not be interpreted as a direct measure of underlying neurophysiological changes. Instead, a quantitative methodology based on dual-echo measurement of blood flow and BOLD responses is a promising tool for applying fMRI to disease and drug studies in which both baseline conditions and the coupling of blood flow and oxygen metabolism responses to a stimulus may be altered.

Introduction

Functional magnetic resonance imaging (fMRI) is a powerful tool to localize metabolic activity and blood flow changes resulting from brain activity. It is widely used for mapping spatial and temporal patterns of neural activity in fields as diverse as neuroscience, psychology, and economics, but fMRI has not lived up to its promise in the field of medicine. Although there are a number of potential clinical applications of fMRI, they have thus far been limited because of the complexity of the BOLD response. The BOLD signal results from changes in local deoxyhemoglobin content (Ogawa et al., 1993), which depends on the relative changes in cerebral blood flow (CBF) and the cerebral metabolic rate of oxygen ($CMRO_2$). The primary physiological phenomenon underlying the BOLD response is that CBF increases much more than $CMRO_2$ with neural stimulation, reducing the local deoxyhemoglobin content and increasing the MR signal.

The magnitude of the BOLD signal depends strongly on two additional factors: (1) the exact balance of the changes in CBF and $CMRO_2$, which have opposite effects on the change in blood oxygenation, and (2) how much deoxyhemoglobin is present in the baseline state (Buxton, 2010). This complexity of the signal leads to a fundamental problem in interpreting the magnitude of the BOLD response: for example, if the magnitude of the BOLD response in the hippocampus to a standard memory task is altered in disease or after administration of a drug, how should this be interpreted? Such a finding could mean that the neural response to the stimulus is altered, but it could also be due to disease- or drug-related chronic changes in the baseline state (Ances et al., 2009; Brown et al., 2003; Fleisher et al., 2009) or altered coupling of the CBF and $CMRO_2$ responses to the stimulus (Ances et al., 2008). The inability of BOLD-fMRI to disentangle these possible effects underlying changes in the BOLD response amplitude is the primary limitation to a broader application of fMRI as a quantitative probe of brain function.

Abbreviations: ASL, arterial spin labeling; BOLD, blood oxygenation level dependent; CBF, cerebral blood flow; $CMRO_2$, cerebral metabolic rate of oxygen; CBV, cerebral blood volume; fMRI, functional magnetic resonance imaging; R_2^*, signal decay rate; TE, echo time.

* Corresponding author at: University of California, San Diego, 9500 Gilman Dr. MC 0677, La Jolla, CA 92093-0677, USA. Fax: +1 858 822 0605.
E-mail address: rbuxton@ucsd.edu (R.B. Buxton).

1053-8119/$ – see front matter © 2011 Elsevier Inc. All rights reserved.
doi:10.1016/j.neuroimage.2011.04.064

Adding quantitative measurements of CBF based on arterial spin labeling (ASL) methods can help to untangle these confounding effects in three ways. First, ASL techniques provide information on CBF in the baseline state and on how CBF changes with activation. Second, the ASL measurement is more stable in the face of scanner drift, so that it is possible to measure changes in activity between two states widely separated in time (Borogovac et al., 2010; Wang et al., 2003). Third, while the complex sensitivity of the BOLD signal creates difficulty in interpretation, it also offers the possibility of calculating changes in $CMRO_2$ when BOLD and CBF measurements are combined. The calibrated-BOLD approach proposed by Davis et al. (1998) utilizes this additional measurement of CBF to estimate the $CMRO_2$ change during brain activation, and offers the potential to broaden fMRI from a mapping tool into a true probe of brain function in health and disease.

In this paper, we show how a quantitative fMRI approach can be used to more fully assess how a drug alters both baseline CBF and $CMRO_2$ and the CBF and $CMRO_2$ responses to a standard stimulus. A quantitative methodology requires simultaneous measurements of CBF and BOLD responses and improved temporal stability of the BOLD response. The dual-echo spiral ASL pulse sequence (Wong et al., 1998) addresses these requirements by providing both CBF and BOLD time series (Fig. 1). In addition, quantification and comparison of BOLD signals widely separated in time is made possible through measurement of the absolute transverse relaxation rate (R_2^*), which is the physical parameter underlying the BOLD effect. Using this methodology we examined the effect of caffeine as a model drug affecting both baseline neurophysiology and the neural response to a simple visual stimulus.

Caffeine, part of the methylxanthine family of chemicals, acts as a non-selective antagonist of adenosine receptors, especially types A_1, A_{2A}, and A_{2B} (Fredholm et al., 1999; Pelligrino et al., 2010). Typically adenosine acts to inhibit release of excitatory neurotransmitters at A_1 receptors. By blocking these receptors the inhibitory activity is lifted, thereby increasing neuronal firing rate (Dunwiddie and Masino, 2001; Fredholm et al., 1999). In addition, adenosine acts as a vasodilator through A_{2A} and A_{2B} receptors located on blood vessels, and by blocking these receptors caffeine decreases CBF (Kusano et al., 2010; Pelligrino et al., 2010). This dual action of caffeine on both neural activity and blood flow through different regulatory mechanisms leads to the physiological uncoupling of CBF and $CMRO_2$, which makes caffeine an ideal drug for studying how changes in both CBF and $CMRO_2$ affect the BOLD response.

Several studies have found that caffeine reduces baseline CBF (Cameron et al., 1990a; Field et al., 2003; Mathew and Wilson, 1985), while studies on how caffeine affects the BOLD response to a stimulus have yielded conflicting results (Laurienti et al., 2003; Liau et al., 2008; Mulderink et al., 2002). In comparison, there is relatively little information available on how caffeine affects $CMRO_2$. A recent study combining CBF and BOLD response measurements found that the coupling ratio of the CBF and $CMRO_2$ stimulus responses ($n = \delta CBF/\delta CMRO_2$) decreased after caffeine administration (Chen and Parrish, 2009b), and another study from the same group found different dose-dependent effects on the BOLD and CBF responses (Chen and Parrish, 2009a). Yet, we were unable to find a study specifically measuring the combined effect of caffeine on baseline $CMRO_2$ and the evoked $CMRO_2$ response to a stimulus. This would provide a greater understanding of how caffeine affects neural metabolism. One study in preterm infants using indirect calorimetry found that caffeine increased total body oxygen consumption (Bauer et al., 2001) while another study in preterm infants demonstrated reduced cerebral oxygenation after administration of caffeine (Tracy et al., 2010). How these studies translate to cerebral oxygen metabolism in adults is unknown.

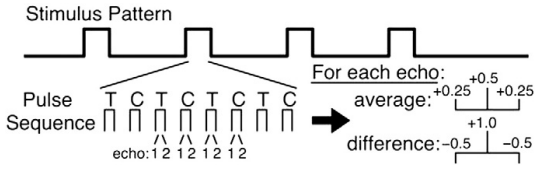

Fig. 1. Experimental design for acquisition of simultaneous BOLD and CBF data showing stimulus pattern with a 60 s baseline followed by 4 cycles of 20 s of stimulus/60 s of rest and a final 30 s of rest. Tag and control images are alternated each TR (2.5 s), during which two echoes are acquired ($TE_1 = 2.9$ ms and $TE_2 = 24$ ms). For each echo, the surround average and surround difference of the tag and control images are calculated as shown in order to produce average and difference time courses for each echo as shown in Supplementary Fig. S1.

For the current study, an analysis of the baseline effects of caffeine on CBF and $CMRO_2$ in these data was previously reported (Perthen et al., 2008), while here we present an integrated analysis of the modulations of both the baseline state and the evoked responses incorporating a new model for the BOLD response. Our primary findings were: 1) that caffeine produced a significant uncoupling in the baseline state, reducing CBF while increasing $CMRO_2$; and 2) that caffeine significantly increased the absolute $CMRO_2$ response to the visual stimulus. These effects are consistent with the inhibition of the dual action of adenosine, which lowers CBF while increasing neural excitability. This raises baseline $CMRO_2$ and increases the $CMRO_2$ response to the stimulus. However, despite these large physiological changes, the standard BOLD response to the stimulus was unaltered by caffeine, emphasizing the limitations of BOLD-fMRI alone to detect the underlying physiological changes.

Methods

The study was performed on ten healthy adults reporting moderate daily caffeine intake (100–250 mg) who had abstained from caffeine consumption for at least 12 h prior to study participation. The institutional review board at the University of California San Diego approved the study, and written informed consent was obtained from all participants. Two functional scans were performed in each of the pre- and post-caffeine states. The functional scans consisted of four blocks of a black and white checkerboard flashing at 8 Hz for 20 s alternating with 60 s of a small stationary white square on a gray background. After the pre-caffeine functional scans, two 7-min (3-min of CO_2) hypercapnia scans were performed for calibration of the $CMRO_2$ calculations (Table 1). Subjects were then removed from the scanner and given a 200 mg caffeine tablet. After 30 min, subjects were placed back into the scanner and the scan protocol was repeated without the hypercapnia scan.

Using a spiral dual-echo ASL PICORE QUIPSS II (Wong et al., 1998) pulse sequence, we simultaneously measured the CBF and BOLD responses to a strong visual stimulus before and after administration of caffeine. ASL was used to directly measure CBF by magnetically labeling arterial water with an applied RF pulse. The tagged water was allowed to flow into the slice of interest followed by tagged image (T) acquisition. A control image (C) was acquired by repeating this sequence without magnetically tagging the water. Signal acquisition occurred at two echo times (TE) every 2.5 s ($TE_1 = 2.9$ ms and $TE_2 = 24$ ms). Surround average and difference time courses were computed using the weighting shown in Fig. 1.

Statistical analysis of the functional data was performed using a general linear model (GLM) approach similar to the method used in Perthen et al. (2008). An active visual cortex ROI was defined as voxels exhibiting CBF activation in the first echo difference data of the concatenated functional scans. The desired ROI size was set to 250 ± 25 voxels for both the pre- and post-caffeine runs. The minimum acceptable correlation coefficient was decreased until this ROI size was established with the additional requirement that voxels were included in the ROI only if there were two neighboring voxels that

were also above the correlation coefficient cutoff. The intersection of the pre-caffeine ROI and post-caffeine ROI was taken for each subject resulting in variable size of the CBF ROI between 100 and 167. The minimum CBF correlation coefficient varied between subjects from 0.11 to 0.28. Analysis was limited to voxels exhibiting a minimum signal to noise ratio of 100 and minimum CBF signal of 30% of the mean baseline CBF to preferentially increase the likelihood of gray matter over white matter inclusion in the ROI. For summary statistics, the baseline was averaged over the 10 s prior to the start of the stimulus and the stimulus response was averaged over the last 10 s of the stimulus. To test whether our method of ROI determination biased our results, we also analyzed our data using a combined BOLD/CBF ROI.

The surround average signal (A) of the tag and control images was calculated for each subject at the two echo times and averaged across the ROI (Supplementary Fig. S1). This was then used to measure the change in the apparent R_2^* by modeling the average signal as $A(t) = A_0(t)e^{-TE \cdot R_2^*(t)}$. The source of the BOLD response is the dependence of R_2^* on blood oxygenation, but the problem that usually confounds the interpretation of slow modulations of the BOLD response is that A_0 is sensitive to scanner drifts. The direct calculation of R_2^* minimizes this source of error. For display and analysis, we calculated an equivalent BOLD response with A_0 removed as in Perthen et al. (2008) using the definition $\delta\text{BOLD}(t) = e^{-TE_2 \cdot R_2^*(t)} - 1$ where δBOLD is the percent change in the BOLD signal. Surround subtraction produces a net signal that is proportional to the arterial spins delivered to the voxel (Liu and Wong, 2005), and quantification of this signal in absolute CBF units was performed as described in Perthen et al. (Chalela et al., 2000; Perthen et al., 2008).

To calculate $CMRO_2$ from normalized CBF and BOLD data, the Davis model (Davis et al., 1998) was used: $\delta S = M\left[1 - f^{\alpha}\left(\frac{r}{f}\right)^{\beta}\right]$. This model describes the BOLD response as a function of the normalized (activation/baseline) values of CBF (f) and $CMRO_2$ (r). Hypercapnic calibration was performed as described in Perthen et al. (2008) to determine the scaling parameter, M, which is the maximum BOLD response associated with the calibrated BOLD Davis model equation (Davis et al., 1998). This scaling parameter was then used to determine normalized $CMRO_2$ from which we calculated $\delta CMRO_2$. The central assumption of this calculation is that mild hypercapnia does not alter $CMRO_2$, so that M can be calculated from the model using the measured CBF and BOLD responses to hypercapnia (Chen and Pike, 2010; Jones et al., 2005; Sicard and Duong, 2005). To test whether bias in M would affect our conclusions, we also analyzed our data with $M \pm 30\%$.

In addition to determining M, values for the parameters α and β must be assumed. The conventional values of these exponential parameters are $\alpha = 0.38$ and $\beta = 1.5$ based on the original development by Davis et al. (1998). However, we recently revisited the question of the accuracy of the Davis model with a more detailed four compartment model of the BOLD response that includes effects left out of the original derivation, including omission of the intravascular signal compartment and volume exchange effects as CBV changes, as well as the assumption that CBV changes are uniformly distributed across vascular compartments (Griffeth and Buxton, submitted for publication).

With this analysis we found that the mathematical form of the Davis model provides a good fit to the BOLD response predicted by the detailed model as a function of changes in CBF and $CMRO_2$ if α and β are allowed to vary from their conventional values. We found best-fit values of $\alpha = 0.14$ and $\beta = 0.91$ using non-linear parameter optimization of the Davis model to simulated data produced by the detailed BOLD model. These values of α and β may seem counterintuitive when viewed in the context of the original derivation of the Davis model, but one should keep in mind that these values represent the best fit to a more complex model of the BOLD response that includes effects the Davis model was not originally intended to describe. Therefore the original biophysical meaning of these parameters should not be imposed on the new optimized parameters. To test whether the assumption of these parameter values affects the results of the study, we also analyzed our data with $\alpha = 0.38$ and $\beta = 1.5$.

All the BOLD, CBF, and $CMRO_2$ responses were expressed as a percent change from the pre-caffeine baseline and are denoted as δBOLD, δCBF, and $\delta CMRO_2$. This allowed us to measure changes in the baseline state and also to compare in an absolute fashion the evoked responses pre- and post-caffeine. In addition, for comparison with previous studies where this was not possible we also expressed each response as a fraction of the immediately preceding baseline value.

Results

Table 1 shows the mean CBF, R_2^* and BOLD responses to 5% CO_2 inhalation along with the calculated M values for the two sets of Davis model parameters. The fractional BOLD and CBF time courses for hypercapnia are provided in the Supplementary data (Fig. S2).

Using the dual-echo ASL sequence, surround average and difference data were determined for each TE from the alternating tag and control images and averaged over the region of interest (ROI) as shown for one subject in Fig. 2. To show the applicability of this technique to single subjects, curves for absolute CBF and R_2^* are shown for one subject in Fig. 3. Group averages over the baseline and stimulus time points are included in Table 2. Using the CBF ROI, baseline CBF was reduced (pre = 82.6 ± 4.4 ml/100 ml/min versus post = 59.9 ± 3.5 ml/100 ml/min, $p < 0.001$) following caffeine administration. The absolute ΔCBF response to the visual stimulus was also reduced post-caffeine (pre = 42.0 ± 2.6 ml/100 ml/min versus post = 33.7 ± 2.2 ml/100 ml/min, $p = 0.033$). Baseline R_2^* was increased post-caffeine ($24.4 \pm 1.1\ s^{-1}$ versus $27.1 \pm 1.2\ s^{-1}$, $p < 0.001$) while R_2^* in response to the visual stimulus was not significantly affected by caffeine (Fig. 4b, pre = $-0.50 \pm 0.4\ s^{-1}$ versus post = $-0.51 \pm 0.03\ s^{-1}$, $p = 0.67$).

Fig. 4 shows the effect of caffeine on the stimulus-evoked response relative to the pre-caffeine baseline in the top row and relative to the baseline immediately preceding the stimulus in the bottom row. All results are shown as percent change from their respective baselines. All numerical values reported here for the $CMRO_2$ change are steady state values calculated from the average values of CBF and BOLD on the plateau of the baseline and the response using the optimized steady-state Davis model of the BOLD effect. Without the ability to directly measure changes in the baseline BOLD and CBF, the conventional analysis as displayed on the bottom row does not reveal the full extent of physiological modulation by caffeine (Figs. 4d–f). In fact with the conventional analysis, the effects of caffeine on the evoked responses to the stimulus were modest, with no change in the BOLD response, an insignificant change of 9.3% ($p = 0.38$) in the evoked CBF response, and a 34% ($p = 0.01$) increase in the $CMRO_2$ response (Table 3).

Table 1
Response to hypercapnia. Mean (one s.e.m.), *$p < 0.01$, **$p < 0.001$, measured in the pre-dose caffeine hypercapnia experiment and calculated M values. Note the M denoted as 'optimized' refers to use of the new values of α and β and 'classic' refers to use of the original values of α and β in the Davis model (Davis et al., 1998). All significance values indicate a significant difference from zero.

Response to hypercapnia (standard error)	
	CBF ROI
δCBF (%)	29.5 (8.3)* p = 0.006
ΔR_2^* (s^{-1})	−0.73 (0.14)**
δBOLD (%)	1.78 (0.33)**
M, optimized (%)	11.9 (1.7)**
M, classic (%)	8.47 (1.2)**

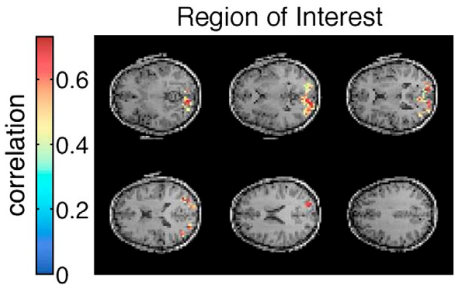

Fig. 2. CBF-based activation map for a single subject, showing correlation coefficients calculated using the general linear model. Regions of interest (ROIs) were determined by thresholding the activation maps as described in the text.

Table 2
Absolute CBF and R_2*. Mean (one s.e.m., *p<0.001), absolute values of CBF and R_2* measured in the pre- and post-caffeine experiments (10 subjects). 'Baseline' is averaged over the 10 s prior to the start of the stimulus during which a gray background with a white square in the middle was presented. The 'stimulus' response was averaged over the last 10 s of the stimulus and denotes the steady state response to the flashing checkerboard visual stimulus. Significance for the pre-caffeine stimulus response and the post-caffeine baseline shift were tested against the pre-caffeine baseline. Significance for the post-caffeine stimulus response was tested against the post-caffeine baseline.

Absolute CBF and R_2*		
	CBF ROI	
	CBF (ml/100 ml/min)	R_2* (s^{-1})
Pre-caffeine (baseline)	82.6 (4.4)	24.4 (1.1)
Pre-caffeine (stimulus)	124.6 (5.2)*	23.9 (1.1)*
Post-caffeine (baseline)	59.9 (3.5)*	27.1 (1.2)*
Post-caffeine (stimulus)	93.6 (4.8)*	26.6 (1.2)*

In contrast, the full quantitative analysis (Figs. 4a–c) showed four large effects of caffeine: a 27% ($p<0.001$) decrease in baseline CBF, a 22% ($p=0.030$) increase in baseline $CMRO_2$, a 61% ($p<0.001$) increase in the absolute magnitude of the $CMRO_2$ response to the stimulus, and a 20% ($p=0.036$) decrease in the absolute magnitude of the CBF response (Table 3). The time courses illustrated in Fig. 4 for $CMRO_2$ should be taken as approximate because they were calculated by assuming that the steady-state model can be applied dynamically, but this may not be accurate (Buxton et al., 2004).

The importance of the increase of the stimulus-evoked $CMRO_2$ response is that it was not matched by a corresponding increase of the CBF response. The coupling of CBF and $CMRO_2$ responses can be described by an empirical index n, defined as the dimensionless ratio of the fractional changes in CBF and $CMRO_2$. In this experiment, n significantly decreased with administration of caffeine ($pre=1.96\pm0.06$ versus $post=1.60\pm0.03$, $p<0.001$) in agreement with previous findings (Chen and Parrish, 2009b). Even though the changes in pre-caffeine and post-caffeine n appear small, they represent significant changes in underlying physiology. These decreases of n are evident even for individual subject data (Supplementary data, Fig. S3).

To test whether the choice of ROI biased our results, we also used an ROI determined from the intersection of voxels exhibiting CBF activation and BOLD activation (as determined from the second echo average data). This produced very similar results: a 27% ($p<0.001$) decrease in baseline CBF, a 10% ($p=0.23$) increase in baseline $CMRO_2$ that did not reach significance, a 52% ($p<0.001$) increase in the absolute magnitude of the $CMRO_2$ response to the stimulus, and a 23% ($p=0.042$) decrease in the absolute magnitude of the CBF response. In the combined BOLD/CBF ROI, the coupling parameters were systematically higher due to a systematically higher BOLD response and lower $CMRO_2$ response. However, caffeine ingestion still resulted in lower n ($pre=2.32\pm0.08$ versus $post=1.78\pm0.05$, $p<0.001$). Full results are given in the Supplementary data.

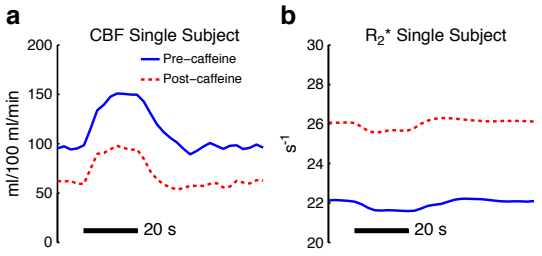

Fig. 3. Single cycle CBF and R_2*. Black bar shows stimulus period of 20 s. a, Absolute CBF was calculated from echo 1 and echo 2 difference data for a single subject. b, Absolute R_2* was calculated from average echo 1 and echo 2 data for a single subject.

We also examined whether the choice of α and β would affect the results by using the parameters from the original Davis model, $\alpha=0.38$ and $\beta=1.5$. This resulted in a systematic decrease in calculated $\delta CMRO_2$ but did not change our main conclusion that caffeine decreases n by increasing the $CMRO_2$ response (54%, $p<0.001$) and decreasing the CBF responses to the visual stimulus. Baseline $CMRO_2$ also increased with a trend toward significance ($13.3\pm6.4\%$, $p=0.067$) (Supplementary data, Table S4).

Since the assumption that hypercapnia does not change $CMRO_2$ has been challenged (Kliefoth et al., 1979; Xu et al., 2011; Zappe et al., 2008), we tested whether our conclusions depend on the exact value of M. We repeated the analysis assuming a fixed value for M of $\pm30\%$ of the average M from the hypercapnia experiment. This range brackets the results from a number of similar studies (Ances et al., 2008; Chiarelli et al., 2007; Hoge et al., 1999; Liau and Liu, 2009; Mark et al., 2011; Stefanovic et al., 2006) after adjusting for TE, α and β. Even with these large variations in M, we found that caffeine still decreased n by increasing the $CMRO_2$ response to the stimulus (Table S5). Baseline $CMRO_2$ also increased post-caffeine for different values of M with $M=8.3\%$ resulting in a strong 42% ($p=0.006$) increase in baseline $CMRO_2$ while $M=15.4\%$ resulted in a trend toward increased $CMRO_2$ (Table S5).

Discussion

Fluctuations in oxygen metabolism may in fact provide a much more accurate reflection of neural activity than changes in the BOLD signal alone since aerobic metabolism of glucose is the primary metabolic fuel for energy production in the human brain. Recent research has shown that changes in $CMRO_2$ are expected to reflect the underlying energy requirement of evoked neural activity (Lin et al., 2010), which is primarily the energy cost of pumping ions against their gradient at neuronal synapses (Attwell and Iadecola, 2002; Attwell and Laughlin, 2001). The importance of accurately and non-invasively measuring $CMRO_2$ is emphasized by the many common psychiatric and neurological diseases demonstrating changes in $CMRO_2$ such as schizophrenia (Gur et al., 1987; Hoyer and Oesterreich, 1975), depression (Videbech et al., 2001), bipolar disorder (Brooks et al., 2006; Yatham and Maj, 2010), Alzheimer's (Ishii et al., 1996), chronic traumatic encephalopathy (Zauner et al., 2002), and epilepsy (Greene et al., 2003). Therefore by improving our ability to non-invasively determine $CMRO_2$ dynamics, we will also unlock the ability to expand our knowledge of these diseases and, potentially, our ability to treat them. The current study demonstrates that a dual-echo calibrated-BOLD approach provides the capability of quantitatively assessing physiological changes in the

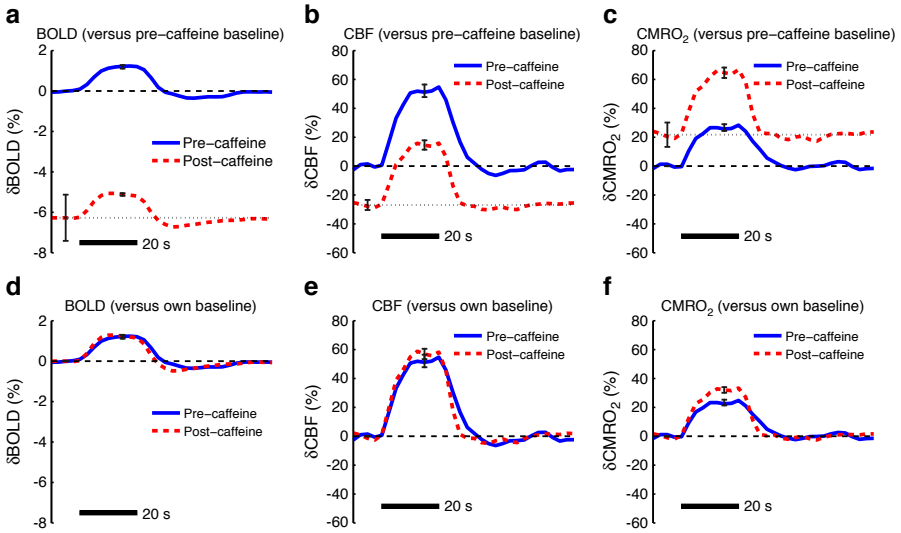

Fig. 4. Fractional changes in BOLD, CBF and $CMRO_2$ relative to either the pre-caffeine baseline (a–c) or relative to the baseline immediately preceding the stimulus (d–f). Blue time courses are pre-caffeine. Red time courses are post-caffeine. Black bars indicate the stimulus period of 20 s. Error bars indicate ± s.e.m. At baseline, error is considered relative to 0. Evoked response s.e.m. is considered relative to mean baseline shown. Percent changes from the pre-caffeine baseline: a, the BOLD baseline was shifted post-caffeine (change of −6.27 ± 1.1%, $p<0.001$), while the BOLD response to the visual stimulus was not significantly different (change of −3.64 ± 7.3%, $p=0.63$). b, There was a large overall decrease in the baseline CBF (−26.9 ± 3.5%, $p<0.001$) and in the fractional δCBF response post-caffeine (−20.3 ± 8.2%, $p=0.036$). c, In contrast to the baseline CBF decrease, there was a trend for increased baseline $CMRO_2$ (+21.8 ± 8.4%, $p=0.030$), and the δ$CMRO_2$ response to the visual stimulus was dramatically increased (60.7 ± 9.5%, $p<0.001$) post-caffeine. Conventional analysis showing percent changes relative to the baseline preceding the stimulus: d, baseline shifts are no longer apparent, and the BOLD response to the visual stimulus remained unchanged (pre = 1.20 ± 0.09 versus post = 1.23 ± 0.07, $p=0.67$). e, When considered relative to the baseline preceding the stimulus, the fractional δCBF response increased slightly relative to the pre-caffeine response (9.28 ± 10.2%, $p=0.38$). f, Similarly, the fractional δ$CMRO_2$ response also increased (34.0 ± 10.7%, $p=0.01$) but less so than when considered relative to the pre-caffeine baseline.

brain in response to a drug, including both baseline changes and alterations in the response to a standard stimulus.

While CBF is a physiological measurement of direct interest, R_2^* is primarily of interest as a means to estimate $CMRO_2$ changes using hypercapnic calibration and a mathematical model of the BOLD effect (Davis et al., 1998). Typically, $CMRO_2$ changes are calculated relative to the baseline immediately preceding the stimulus. After administration of a drug, this relative $CMRO_2$ response could change either with a shift in the baseline $CMRO_2$ or with modulation of the absolute evoked $CMRO_2$ response to the stimulus. A novel feature of our analysis is that we were able to refer all changes pre- and post-caffeine to the pre-caffeine baseline state, which is possible because CBF and R_2^* are both relatively robust absolute values that allow for increased inter-study reliability as they are not affected by slow signal changes due to scanner drift. In this way we were able to measure both changes in the baseline state and also the ratio of the absolute evoked $CMRO_2$ responses to the stimulus.

The primary new finding of this study was that the absolute evoked $CMRO_2$ response to the stimulus was ~61% larger post caffeine, while the absolute CBF response decreased by ~20%. This divergence of CBF and $CMRO_2$ responses to the stimulus was also evident in the baseline shifts due to caffeine. Baseline $CMRO_2$ increased by ~22% due to caffeine, consistent with previous studies in rats showing a 15% increase in cerebral glucose utilization after 10 mg/kg caffeine administration (Nehlig et al., 1984). Also consistent with previous studies, we found a significant reduction in baseline CBF by ~27% (Cameron et al., 1990b; Field et al., 2003; Laurienti et al., 2003; Mathew and Wilson, 1985). With the more conventional analysis, taking each response as a fractional change from its own preceding baseline condition, this combination of changes led to a

Table 3
Fractional percent changes in CBF, BOLD, and $CMRO_2$. Nomenclature for 'baseline' and 'stimulus' is explained in the caption for Table 2. All significance values indicate a significant difference from zero except the values of *n* for which the post-caffeine *n* was compared to the pre-caffeine *n*. 'Response percent change' refers to the percent change in the post-caffeine stimulus response compared to the pre-caffeine stimulus response ('a percent of a percent').

Fractional changes (standard error) (*$p<0.05$, **$p<0.001$)				
	δCBF (%)	δBOLD (%)	δ$CMRO_2$ (%)	*n*
Relative to pre-caffeine baseline (CBF ROI)				
Pre-caffeine (stimulus)	52.1 (4.4)**	1.20 (0.09)**	26.7 (2.3)**	1.96 (0.06)
Post-caffeine (baseline)	−26.9 (3.5)**	−6.27 (1.1)**	21.8 (8.4)*, $p=0.030$	
Post-caffeine (stimulus)	41.5 (3.2)**	1.15 (0.06)**	42.9 (3.6)**	
Response percent change	−20.3 (8.2)*, $p=0.036$	−3.64 (7.3), $p=0.63$	60.7 (9.5)**	
Conventional analysis relative to immediately preceding baseline (CBF ROI)				
Post-caffeine (stimulus)	57.0 (3.6)**	1.23 (0.07)**	35.8 (2.3)**	1.60 (0.03)**
Response percent change	9.28 (10.2), $p=0.38$	2.96 (6.7), $p=0.67$	34.0 (10.7)*, $p=0.01$	

reduction in the coupling ratio, n, of CBF and $CMRO_2$ responses to the visual stimulus, consistent with the finding of Chen and Parrish (2009b).

Of interest is that the large physiological changes found in this study in both the baseline state and in the response to the stimulus were not reflected in the BOLD response because they have opposing effects. The post-caffeine drop in baseline CBF with a corresponding increase in $CMRO_2$ required increased extraction of oxygen and consequently a higher level of deoxyhemoglobin in this baseline state, which acted to increase the magnitude of the evoked BOLD response post-caffeine. On the other hand, the $CMRO_2$ change evoked by the stimulus was much larger after caffeine administration while the CBF change was slightly smaller, and this reduced the magnitude of the BOLD response.

Previous results for the effect of caffeine on the evoked BOLD and CBF responses are mixed. For example, Chen and Parrish (2009a) found an increase in the fractional CBF response post-caffeine, and many groups have found the mean BOLD response to be increased (Behzadi and Liu, 2006; Chen and Parrish, 2009a; Morton et al., 2002; Mulderink et al., 2002) while others have found the peak BOLD response to be unchanged (Liu et al., 2004) or highly variable between subjects (Laurienti et al., 2003). Differences from the results of Chen and Parrish (2009a) are of particular interest due to the similarity of their approach. Both studies found that caffeine reduced the ratio of blood flow to oxygen metabolism changes in response to a visual stimulus, but the major difference in the current approach is use of the dual-echo acquisition, which allows for absolute quantification of R_2^* and CBF rather than only relative quantification. This is most apparent in Fig. 4: the relative approach only allows for production of panels d–f while the dual-echo technique allows production of panels a–c. The latter panels also show the baseline shifts and permit comparison of the magnitudes of the absolute BOLD, CBF and $CMRO_2$ responses. The importance of this is emphasized when comparing the CBF results in Figs. 4b and e. Examining Fig. 4e, there is a small although insignificant increase in the relative response of CBF to the stimulus post-caffeine ($9.3 \pm 10.2\%$, $p = 0.38$) similar to the results from Chen and Parrish (2009a). Yet when referred to the same baseline as in Fig. 4b, this insignificant increase becomes a significant decrease in the absolute CBF response.

Apparent inconsistencies in the literature regarding the effects of caffeine on the BOLD response might be explained by the current findings of opposing effects due to increased baseline deoxyhemoglobin combined with a decreased coupling ratio n post-caffeine. Depending on the particular set of subjects chosen and experimental conditions, it is easy to imagine this balance shifting to produce variable changes in the BOLD response. This potentially variable balance of opposing effects may also underlie the differential dose dependence of the CBF and BOLD responses for different levels of caffeine administration found by Chen and Parrish (2009a).

Our study involved subjects who were all moderate daily caffeine consumers who had not consumed any caffeine for at least 12 h before the study. For this reason, it is more accurate to view this group as recovering from caffeine withdrawal during imaging. The relatively high baseline CBF pre-caffeine in these subjects (Table 2) suggests that adenosine or adenosine receptor levels had adjusted to the subjects' regular levels of caffeine consumption. Abstaining from caffeine increased activation of the adenosine system in these subjects elevating baseline CBF and suppressing baseline $CMRO_2$. With typical daily caffeine restored, baseline CBF was reduced to a level consistent with non-caffeine consuming controls (Rack-Gomer et al., 2009) while $CMRO_2$ was increased, also presumably to a more typical level. A similar experiment to the current one with caffeine-naïve subjects could yield significantly different results, and is an important area for future work.

A potential limitation of the current work is that the derived estimates of $CMRO_2$ response depend on the accuracy of the Davis model (Davis et al., 1998) for the relationship between the BOLD response and changes in CBF, cerebral blood volume (CBV) and $CMRO_2$. Potential limitations include the following possibilities: that the model is oversimplified, leaving out potential contributions to the BOLD signal; that the model does not adequately capture the effects of CBV change, particularly if CBV changes are primarily arterial; and that the hypercapnia calibration experiment may decrease baseline $CMRO_2$, contrary to the assumption of the calibrated-BOLD method (Buxton, 2010). In a recent modeling study we considered each of these limitations in detail (Supplementary data, Table S4), and developed a detailed mathematical model of the BOLD signal against which we compared the Davis model (Griffeth and Buxton, submitted for publication). Our primary finding was that despite the limitations of the original Davis model the mathematical form works well as a description of how the BOLD response varies as CBF and $CMRO_2$ are changed. However, because this simple form now describes effects that were not included in the original derivation of the Davis model, such as intravascular signal changes, the parameters should be treated as simply fitting parameters without any specific physical meaning. We used these optimized parameters for the primary estimates of $CMRO_2$ change reported here. To test whether these assumptions strongly affected the conclusions, we reanalyzed the data with the conventional Davis model parameters and found similar results (Supplementary data, Table S4). It is notable that while the factors listed above modify the absolute values of the estimated $CMRO_2$ changes, the primary conclusion that caffeine increases the stimulus-evoked change in $CMRO_2$ is not changed. However due to the non-linear nature of the Davis model, the optimized parameters have a larger effect on calculations of $CMRO_2$ changes due to caffeine alone. While the classic Davis model parameters produce a trend for increased post-caffeine baseline $CMRO_2$, using the optimized parameters the increase was significant.

These small uncertainties in the exact values for $CMRO_2$ are less important than the broader implications that this study has for fMRI based on the BOLD effect. In this study, the BOLD response was insensitive to the physiological effects of an administered drug despite large changes in both the baseline state and the stimulus-evoked metabolic response. Combined with previous studies finding strong variation of the BOLD response with the baseline state (Brown et al., 2003) or with the CBF/$CMRO_2$ coupling ratio (Ances et al., 2008; Lin et al., 2008), these data support the general conclusion that the BOLD response should be interpreted with caution as a quantitative reflection of the underlying physiological changes. Our results also demonstrate that the quantitative approach used here, measuring both baseline and evoked response changes, can resolve many of the ambiguities of the BOLD response alone. The key element that makes this possible is the measurement of absolute CBF and R_2^* (Fig. 3 and Table 2). This approach will be useful for evaluating drug effects, and also for studies in disease populations where the baseline state may be altered due to the disease process itself or to medications.

Our results also have implications for our basic understanding of the connections between neural activity, blood flow and energy metabolism. The increase in the absolute magnitude of stimulus-evoked change in $CMRO_2$ suggests an increase in the overall evoked neural response, and yet this increase was not fully reflected in the CBF response. One possible explanation is that changes in CBF are not directly tied to $CMRO_2$ changes. Instead, CBF is driven in a feed-forward manner by agents released by neural activity (Attwell and Iadecola, 2002; Hamel, 2006) or through activation of astrocytes (Iadecola and Nedergaard, 2007; Koehler et al., 2009). In contrast, $CMRO_2$ adjusts as needed to meet the energy requirements of the evoked neural response.

This picture of CBF and $CMRO_2$ driven in parallel, potentially by different aspects of neural activity, opens the theoretical possibility that the balance of CBF and $CMRO_2$ changes may vary depending on specific aspects of the neural activity change (e.g. input activity vs. evoked

response, bottom-up vs. top-down modulation, etc.). Our current results provide an example of this variability in the coupling of CBF and $CMRO_2$ revealing that the $CMRO_2$ response to the visual stimulus is increased post-caffeine, which is consistent with caffeine increasing neuronal excitability. The failure of CBF to respond as strongly post-caffeine might be due to the inhibition of the vasodilatory effects of adenosine by caffeine. Another possibility is that CBF is more strongly driven by the initial input stage of the neural response rather than the full ongoing evoked response. This is also consistent with the idea of feed-forward neurovascular coupling. Further experiments will be needed to evaluate these possibilities.

Supplementary materials related to this article can be found online at doi:10.1016/j.neuroimage.2011.04.064.

Author contributions

J.E.P. and R.B.B. designed the experiments. J.E.P. conducted fMRI experiments. V.E.M.G. performed data analysis. V.E.M.G. and R.B.B. prepared the figures and wrote the paper. R.B.B. supervised all aspects of the work.

Acknowledgments

This work was supported by NIH grants NS-36722, NS-42069, and NS-51661. V.E.M.G. received support from HHMI-NIBIB Interfaces grant EB-9380-1, NRSA grant HL-7089-34, and NIGMS MSTP training grant GM-7198-33. We thank N. Blockley, F. Moradi, and A. Simon for assistance in fMRI data analysis.

References

Ances, B.M., Leontiev, O., Perthen, J.E., Liang, C., Lansing, A.E., Buxton, R.B., 2008. Regional differences in the coupling of cerebral blood flow and oxygen metabolism changes in response to activation: implications for BOLD-fMRI. Neuroimage 39, 1510–1521.

Ances, B.M., Liang, C.L., Leontiev, O., Perthen, J.E., Fleisher, A.S., Lansing, A.E., Buxton, R.B., 2009. Effects of aging on cerebral blood flow, oxygen metabolism, and blood oxygenation level dependent responses to visual stimulation. Hum. Brain Mapp. 30, 1120–1132.

Attwell, D., Iadecola, C., 2002. The neural basis of functional brain imaging signals. Trends Neurosci. 25, 621–625.

Attwell, D., Laughlin, S.B., 2001. An energy budget for signaling in the grey matter of the brain. J. Cereb. Blood Flow Metab. 21, 1133–1145.

Bauer, J., Maier, K., Linderkamp, O., Hentschel, R., 2001. Effect of caffeine on oxygen consumption and metabolic rate in very low birth weight infants with idiopathic apnea. Pediatrics 107, 660–663.

Behzadi, Y., Liu, T.T., 2006. Caffeine reduces the initial dip in the visual BOLD response at 3 T. Neuroimage 32, 9–15.

Borogovac, A., Habeck, C., Small, S.A., Asllani, I., 2010. Mapping brain function using a 30-day interval between baseline and activation: a novel arterial spin labeling fMRI approach. J. Cereb. Blood Flow Metab. 30, 1721–1733.

Brooks III, J.O., Wang, P.W., Strong, C., Sachs, N., Hoblyn, J.C., Fenn, R., Ketter, T.A., 2006. Preliminary evidence of differential relations between prefrontal cortex metabolism and sustained attention in depressed adults with bipolar disorder and healthy controls. Bipolar Disord. 8, 248–254.

Brown, G.G., Eyler Zorrilla, L.T., Georgy, B., Kindermann, S.S., Wong, E.C., Buxton, R.B., 2003. BOLD and perfusion response to finger–thumb apposition after acetazolamide administration: differential relationship to global perfusion. J. Cereb. Blood Flow Metab. 23, 829–837.

Buxton, R.B., 2010. Interpreting oxygenation-based neuroimaging signals: the importance and the challenge of understanding brain oxygen metabolism. Front. Neuroenerg. 2, 8.

Buxton, R.B., Uludag, K., Dubowitz, D.J., Liu, T.T., 2004. Modeling the hemodynamic response to brain activation. Neuroimage 23 (Suppl. 1), S220–S233.

Cameron, O.G., Modell, J.G., Hariharan, M., 1990a. Caffeine and human cerebral blood flow: a positron emission tomography study. Life Sci. 47, 1141–1146.

Cameron, O.G., Modell, J.G., Hichwa, R.D., Agranoff, B.W., Koeppe, R.A., 1990b. Changes in sensory–cognitive input: effects on cerebral blood flow. J. Cereb. Blood Flow Metab. 10, 38–42.

Chalela, J.A., Alsop, D.C., Gonzalez-Atavales, J.B., Maldjian, J.A., Kasner, S.E., Detre, J.A., 2000. Magnetic resonance perfusion imaging in acute ischemic stroke using continuous arterial spin labeling. Stroke 31, 680–687.

Chen, Y., Parrish, T.B., 2009a. Caffeine dose effect on activation-induced BOLD and CBF responses. Neuroimage 46, 577–583.

Chen, Y., Parrish, T.B., 2009b. Caffeine's effects on cerebrovascular reactivity and coupling between cerebral blood flow and oxygen metabolism. Neuroimage 44, 647–652.

Chen, J.J., Pike, G.B., 2010. MRI measurement of the BOLD-specific flow–volume relationship during hypercapnia and hypocapnia in humans. Neuroimage 53, 383–391.

Chiarelli, P.A., Bulte, D.P., Wise, R., Gallichan, D., Jezzard, P., 2007. A calibration method for quantitative BOLD fMRI based on hyperoxia. Neuroimage 37, 808–820.

Davis, T.L., Kwong, K.K., Weisskoff, R.M., Rosen, B.R., 1998. Calibrated functional MRI: mapping the dynamics of oxidative metabolism. Proc. Natl. Acad. Sci. USA 95, 1834–1839.

Dunwiddie, T.V., Masino, S.A., 2001. The role and regulation of adenosine in the central nervous system. Annu. Rev. Neurosci. 24, 31–55.

Field, A.S., Laurienti, P.J., Yen, Y.F., Burdette, J.H., Moody, D.M., 2003. Dietary caffeine consumption and withdrawal: confounding variables in quantitative cerebral perfusion studies? Radiology 227, 129–135.

Fleisher, A.S., Podraza, K.M., Bangen, K.J., Taylor, C., Sherzai, A., Sidhar, K., Liu, T.T., Dale, A.M., Buxton, R.B., 2009. Cerebral perfusion and oxygenation differences in Alzheimer's disease risk. Neurobiol. Aging 30, 1737–1748.

Fredholm, B.B., Battig, K., Holmen, J., Nehlig, A., Zvartau, E.E., 1999. Actions of caffeine in the brain with special reference to factors that contribute to it widespread use. Pharmacol. Rev. 51, 83–133.

Greene, A.E., Todorova, M.T., Seyfried, T.N., 2003. Perspectives on the metabolic management of epilepsy through dietary reduction of glucose and elevation of ketone bodies. J. Neurochem. 86, 529–537.

Griffeth, V.E.M., Buxton, R.B., submitted for publication. A theoretical framework for the calibrated BOLD method to estimate CMRO2: modeling the effects of blood volume distribution, hematocrit, oxygen extraction fraction, and tissue signal properties on the BOLD signal.

Gur, R.E., Resnick, S.M., Alavi, A., Gur, R.C., Caroff, S., Dann, R., Silver, F.L., Saykin, A.J., Chawluk, J.B., Kushner, M., et al., 1987. Regional brain function in schizophrenia. I. A positron emission tomography study. Arch. Gen. Psychiatry 44, 119–125.

Hamel, E., 2006. Perivascular nerves and the regulation of cerebrovascular tone. J. Appl. Physiol. 100, 1059–1064.

Hoge, R.D., Atkinson, J., Gill, B., Crelier, G.R., Marrett, S., Pike, G.B., 1999. Investigation of BOLD signal dependence on cerebral blood flow and oxygen consumption: the deoxyhemoglobin dilution model. Magn. Reson. Med. 42, 849–863.

Hoyer, S., Oesterreich, K., 1975. Blood flow and oxidative metabolism of the brain in patients with schizophrenia. Psychiatr. Clin. (Basel) 8, 304–313.

Iadecola, C., Nedergaard, M., 2007. Glial regulation of the cerebral microvasculature. Nat. Neurosci. 10, 1369–1376.

Ishii, K., Kitagaki, H., Kono, M., Mori, E., 1996. Decreased medial temporal oxygen metabolism in Alzheimer's disease shown by PET. J. Nucl. Med. 37, 1159–1165.

Jones, M., Berwick, J., Hewson-Stoate, N., Gias, C., Mayhew, J., 2005. The effect of hypercapnia on the neural and hemodynamic responses to somatosensory stimulation. Neuroimage 27, 609–623.

Kliefoth, A.B., Grubb Jr., R.L., Raichle, M.E., 1979. Depression of cerebral oxygen utilization by hypercapnia in the rhesus monkey. J. Neurochem. 32, 661–663.

Koehler, R.C., Roman, R.J., Harder, D.R., 2009. Astrocytes and the regulation of cerebral blood flow. Trends Neurosci. 32, 160–169.

Kusano, Y., Echeverry, G., Miekisiak, G., Kulik, T.B., Aronhime, S.N., Chen, J.F., Winn, H.R., 2010. Role of adenosine A2 receptors in regulation of cerebral blood flow during induced hypotension. J. Cereb. Blood Flow Metab. 30, 808–815.

Laurienti, P.J., Field, A.S., Burdette, J.H., Maldjian, J.A., Yen, Y.F., Moody, D.M., 2003. Relationship between caffeine-induced changes in resting cerebral perfusion and blood oxygenation level-dependent signal. AJNR. Am. J. Neuroradiol. 24, 1607–1611.

Liau, J., Liu, T.T., 2009. Inter-subject variability in hypercapnic normalization of the BOLD fMRI response. Neuroimage 45, 420–430.

Liau, J., Perthen, J.E., Liu, T.T., 2008. Caffeine reduces the activation extent and contrast-to-noise ratio of the functional cerebral blood flow response but not the BOLD response. Neuroimage 42, 296–305.

Lin, A.L., Fox, P.T., Yang, Y., Lu, H., Tan, L.H., Gao, J.H., 2008. Evaluation of MRI models in the measurement of CMRO2 and its relationship with CBF. Magn. Reson. Med. 60, 380–389.

Lin, A.L., Fox, P.T., Hardies, J., Duong, T.Q., Gao, J.H., 2010. Nonlinear coupling between cerebral blood flow, oxygen consumption, and ATP production in human visual cortex. Proc. Natl. Acad. Sci. USA 107, 8446–8451.

Liu, T.T., Wong, E.C., 2005. A signal processing model for arterial spin labeling functional MRI. Neuroimage 24, 207–215.

Liu, T.T., Behzadi, Y., Restom, K., Uludag, K., Lu, K., Buracas, G.T., Dubowitz, D.J., Buxton, R.B., 2004. Caffeine alters the temporal dynamics of the visual BOLD response. Neuroimage 23, 1402–1413.

Mark, C.I., Fisher, J.A., Pike, G.B., 2011. Improved fMRI calibration: precisely controlled hyperoxic versus hypercapnic stimuli. Neuroimage 54, 1102–1111.

Mathew, R.J., Wilson, W.H., 1985. Caffeine induced changes in cerebral circulation. Stroke 16, 814–817.

Morton, D.W., Maravilla, K.R., Meno, J.R., Winn, H.R., 2002. Systemic theophylline augments the blood oxygen level-dependent response to forepaw stimulation in rats. AJNR. Am. J. Neuroradiol. 23, 588–593.

Mulderink, T.A., Gitelman, D.R., Mesulam, M.M., Parrish, T.B., 2002. On the use of caffeine as a contrast booster for BOLD fMRI studies. Neuroimage 15, 37–44.

Nehlig, A., Lucignani, G., Kadekaro, M., Porrino, L.J., Sokoloff, L., 1984. Effects of acute administration of caffeine on local cerebral glucose utilization in the rat. Eur. J. Pharmacol. 101, 91–100.

Ogawa, S., Menon, R.S., Tank, D.W., Kim, S.-G., Merkle, H., Ellerman, J.M., Ugurbil, K., 1993. Functional brain mapping by blood oxygenation level-dependent contrast magnetic resonance imaging: a comparison of signal characteristics with a biophysical model. Biophys. J. 64, 803–812.

Pelligrino, D.A., Xu, H.L., Vetri, F., 2010. Caffeine and the control of cerebral hemodynamics. J. Alzheimers Dis. 20 (Suppl. 1), S51–S62.

Perthen, J.E., Lansing, A.E., Liau, J., Liu, T.T., Buxton, R.B., 2008. Caffeine-induced uncoupling of cerebral blood flow and oxygen metabolism: a calibrated BOLD fMRI study. Neuroimage 40, 237–247.

Rack-Gomer, A.L., Liau, J., Liu, T.T., 2009. Caffeine reduces resting-state BOLD functional connectivity in the motor cortex. Neuroimage 46, 56–63.
Sicard, K.M., Duong, T.Q., 2005. Effects of hypoxia, hyperoxia, and hypercapnia on baseline and stimulus-evoked BOLD, CBF, and CMRO2 in spontaneously breathing animals. Neuroimage 25, 850–858.
Stefanovic, B., Warnking, J.M., Rylander, K.M., Pike, G.B., 2006. The effect of global cerebral vasodilation on focal activation hemodynamics. Neuroimage 30, 726–734.
Tracy, M.B., Klimek, J., Hinder, M., Ponnampalam, G., Tracy, S.K., 2010. Does caffeine impair cerebral oxygenation and blood flow velocity in preterm infants? Acta Paediatr. 99, 1319–1323.
Videbech, P., Ravnkilde, B., Pedersen, A.R., Egander, A., Landbo, B., Rasmussen, N.A., Andersen, F., Stodkilde-Jorgensen, H., Gjedde, A., Rosenberg, R., 2001. The Danish PET/depression project: PET findings in patients with major depression. Psychol. Med. 31, 1147–1158.
Wang, J., Aguirre, G.K., Kimberg, D.Y., Roc, A.C., Li, L., Detre, J.A., 2003. Arterial spin labeling perfusion fMRI with very low task frequency. Magn. Reson. Med. 49, 796–802.
Wong, E.C., Buxton, R.B., Frank, L.R., 1998. Quantitative imaging of perfusion using a single subtraction (QUIPSS and QUIPSS II). Magn. Reson. Med. 39, 702–708.
Xu, F., Uh, J., Brier, M.R., Hart Jr., J., Yezhuvath, U.S., Gu, H., Yang, Y., Lu, H., 2011. The influence of carbon dioxide on brain activity and metabolism in conscious humans. J. Cereb. Blood Flow Metab. 31, 58–67.
Yatham, L.N., Maj, M., 2010. Bipolar Disorder: Clinical and Neurobiological Foundations. Wiley, Chichester, UK.
Zappe, A.C., Uludag, K., Logothetis, N.K., 2008. Direct measurement of oxygen extraction with fMRI using 6% CO_2 inhalation. Magn. Reson. Imaging 26, 961–967.
Zauner, A., Daugherty, W.P., Bullock, M.R., Warner, D.S., 2002. Brain oxygenation and energy metabolism: part I—biological function and pathophysiology. Neurosurgery 51, 289–301 discussion 302.

Supplementary Information

Data from a single subject averaged across the ROI is shown as the surround average (A) and surround subtraction (D) of echoes one and two (Fig. S1). This shows the reliability of this method for individual subjects and demonstrates the first step in the process of converting raw MRI signal data into CBF and R_2^*. Time courses of the fractional BOLD and CBF time courses during hypercapnia are also shown (Fig. S2). Data from the two minutes prior to hypercapnia stimulation was averaged for the baseline and from the last two minutes of stimulation for the hypercapnia response. This resulted in the average values listed in Table 1 and allowed for calculation of *M*.

In developing BOLD fMRI into a clinical tool, two concerns are reliability and reproducibility. To address the concern of inter-subject variability and reproducibility, we examined the effects of caffeine on individual subjects, and found that for nine out of ten subjects the coupling ratio of evoked changes in blood flow and oxygen metabolism was decreased suggesting very good reproducibility even for individual subjects (Fig. S3).

There are three major issues involving the reliability of the calibrated-BOLD method for calculating $CMRO_2$ using the Davis model. These criticisms are that the model is oversimplified, leaving out potential contributions to the BOLD signal such as intravascular signal changes [1] and volume exchange effects [2-4]; that the model does not adequately capture the effects of CBV change, particularly if CBV changes are primarily arterial as more recent studies suggest [5-8]; and that the hypercapnia calibration experiment may decrease baseline $CMRO_2$, contrary to the assumption of the calibrated-BOLD method, thereby overestimating *M* [9]. Addressing the last criticism, we determined how deviations in *M* from our calculated mean value of 11.9±1.7% using the optimized parameters (Table 1) would affect our $CMRO_2$ calculations by allowing *M* to vary ±30%. Table S4 shows the results for the visual

stimulus response both pre- and post-caffeine, the effect on the coupling parameter, *n*, and how caffeine affects baseline $CMRO_2$ alone. Even with these large variations in *M*, the post-caffeine $\delta CMRO_2$ response increased with caffeine administration, and *n* decreased.

In order to address the inaccuracies of the Davis model [10], we developed a detailed model of the BOLD response [11]. This model includes effects of intravascular and extravascular signal changes, hematocrit (*Hct*), oxygen extraction fraction (*OEF*), and blood volume distribution. We used this detailed model to test and improve the accuracy of the Davis model [10] used for the estimation of $CMRO_2$ with a calibrated-BOLD methodology. The original Davis model is widely used, but it assumes CBV changes are uniformly distributed across vascular compartments, and neglects intravascular signal changes and volume exchange effects as CBV changes. More recent studies suggest that venous CBV changes are smaller than arterial changes [5,12], and that intravascular signal changes and CBV exchange effects can bias estimated $CMRO_2$ [1,3]. The scaling factor, *M*, measured during hypercapnic calibration, absorbs many of the variable factors that affect the BOLD response, and the essential question for the calibrated BOLD experiment is whether these factors also affect the basic mathematical form of the model.

We tested this by developing a much more complete BOLD model similar to Uludag et al. [13] to simulate hypercapnia and activation BOLD data for many combinations of CBF and $CMRO_2$ responses. We then tested the accuracy of $\delta CMRO_2$ estimates by analyzing the simulated BOLD data with the Davis model. Using reasonable estimates for the input parameters (*Hct*=0.44, baseline *OEF*=0.4 [14], O_2 *saturation*=0.99, baseline *CBV* fraction=0.047 [15], distribution of 20-40-40% arterial-capillary-venous of vascular volumes [16], and Grubb parameter α_v=0.2 [5] for venous volume changes), the variation of the BOLD signal with changes in CBF and $CMRO_2$ was captured by the Davis model by allowing α and β to vary independently. The best fit of the simulated data was found with α=0.14 and β=0.91.

Using the classic Davis model parameters for comparison, we calculated changes in the $CMRO_2$ response pre- and post-caffeine with results presented in Table S4 under "Classic Davis Model." These results show an increase in the evoked $CMRO_2$ response to the visual stimulus post-caffeine when using either model, i.e. the classic Davis model or the optimized model the includes the effects of intravascular signal changes, volume exchange effects and arterial CBV changes. Note that both the optimized parameters and a lower *M* value (consistent with a $CMRO_2$ decrease during hypercapnia) give larger relative changes in $CMRO_2$ then suggested by the classic parameters. Additionally although the classic parameters do not reveal a significant shift in $CMRO_2$ due to caffeine alone, the optimized parameters do reveal an increase. This large effect of using the optimized parameters for the effect of caffeine alone is due to the non-linearity of the BOLD model in the area of the caffeine effect (decreased CBF and increased $CMRO_2$).

We also examined the effects of selecting ROI based on the intersection of BOLD and CBF ROIs selected as described in the main text. BOLD activation was defined as voxels exhibiting activation in the second echo average data of the concatenated functional scans. Size of the combined BOLD-CBF ROI varied between 60 and 152. The minimum CBF correlation coefficient for these voxels varied between 0.09 and 0.19; the minimum BOLD correlation coefficients varied between 0.19 and 0.56. Results from this analysis are presented for the hypercapnia calibration in Table S1 and for the activation experiment in Tables S2 and S3. These tables are analogous to Tables 1-3 in the main text.

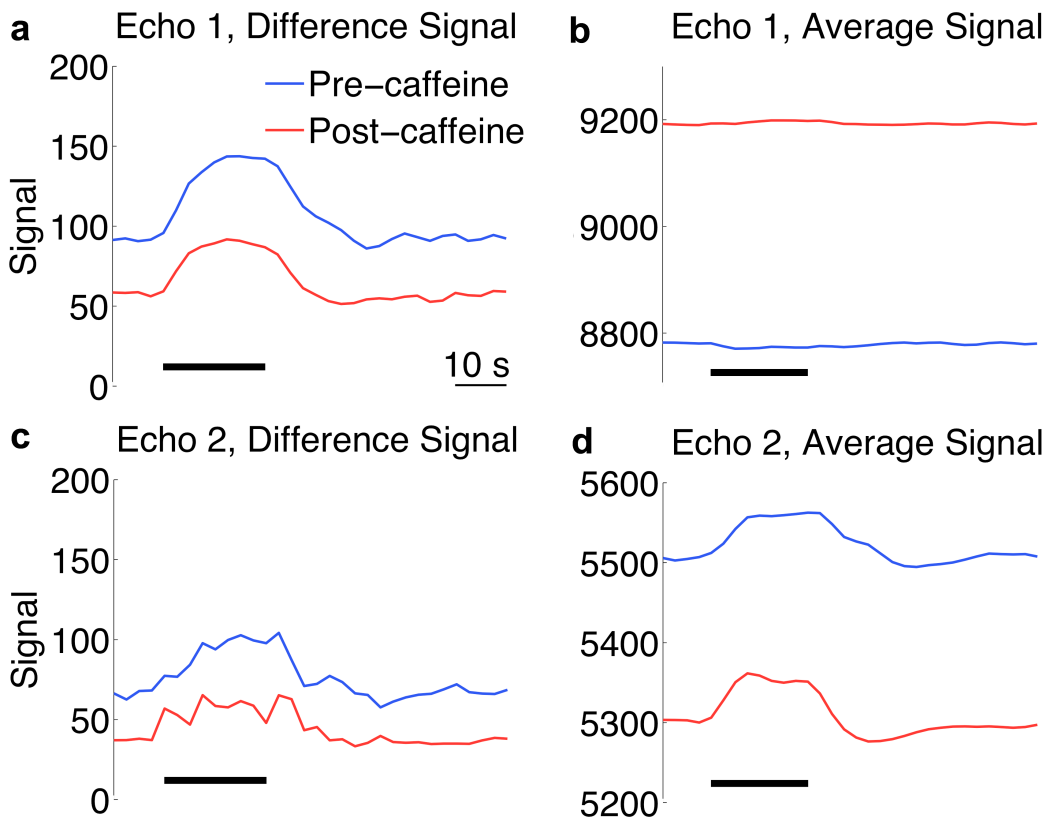

Supplementary Figure S1.3.5. Dual echo, single subject surround average and surround difference time courses of one subject averaged across all cycles averaged and across the ROI.

Thick black bars show stimulus period of 20 s. **a**, Echo 1 surround difference signal reflects the typical signal used to determine CBF. **b**, Echo 1 surround average signal varies minimally. **c**, Echo 2 surround difference signal demonstrates that the signal at this echo is biased by CBF. **d**, Echo 2 surround average signal is the typical BOLD signal and reflects a response to the visual stimulus.

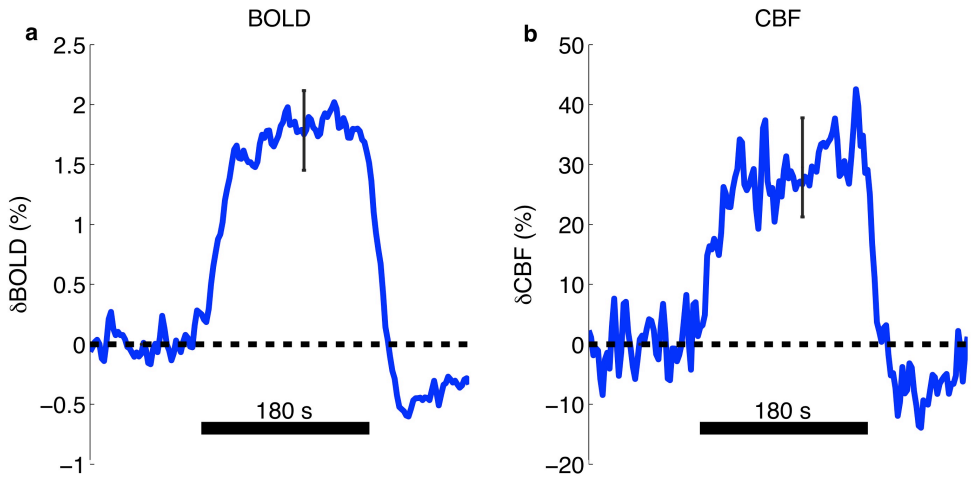

Supplementary Figure S2.3.6. Fractional changes in (a) BOLD and (b) CBF in response to hypercapnia.

Black bars indicate hypercapnia period of 180 s. Error bars for evoked response indicate ± s.e.m. Mean baseline was determined from the first 110 s of recorded data. Mean responses were determined over the second and third minutes of hypercapnia.

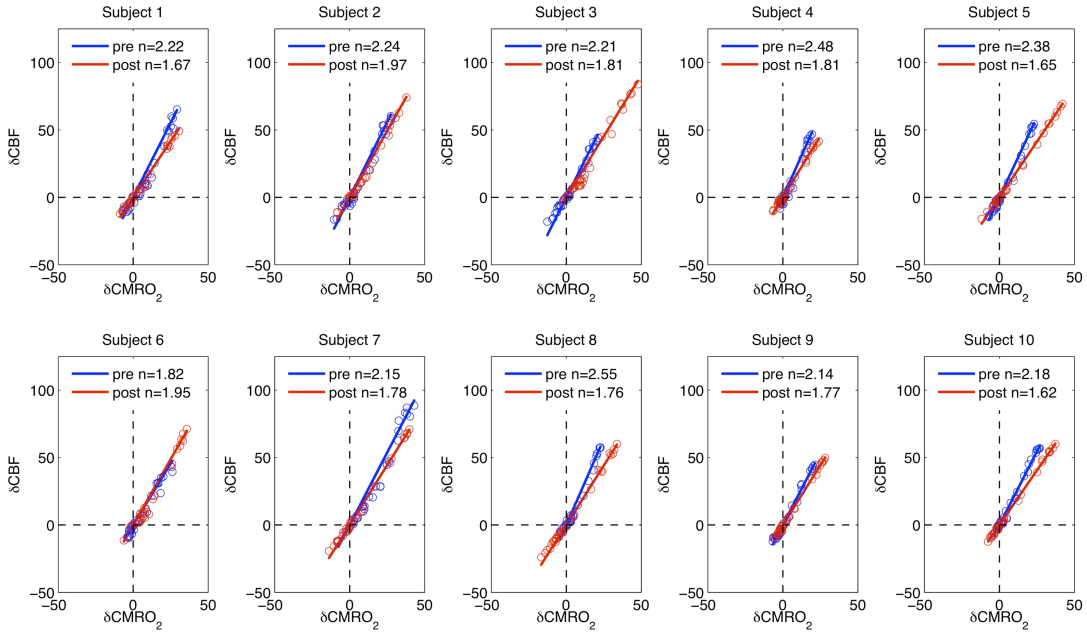

Supplementary Figure S3.3.7. Individual CBF/CMRO$_2$ coupling parameter values (*n*).

Scatter plots of dCBF versus δCMRO$_2$ for single cycle data showing decrease in *n* with caffeine administration is consistent even for individual subjects. One subject showed an increase in *n*, which is possibly due to a difference between the 200 mg caffeine tablet administered and normal daily caffeine consumption for this subject.

Supplementary Table S1.3.4. Response to hypercapnia in the combined BOLD/CBF ROI.

Mean (one s.e.m., *p<0.01, **p<0.001), measured in the pre-dose caffeine hypercapnia experiment and calculated *M* values. Note the *M* denoted as 'optimized' refers to use of the new values of a and b and 'classic' refers to use of the original values of a and b in the Davis model [10].

	BOLD/CBF ROI
δCBF (%)	28.0 (7.7)*
ΔR_2^* (s^{-1})	-0.83 (0.13)**
δBOLD (%)	2.02 (0.33)**
M, optimized (%)	13.4 (1.2)**
M, classic (%)	9.6 (0.82)**

Supplementary Table S2.3.5. Absolute CBF and R_2* in the combined BOLD/CBF ROI.

Mean (one s.e.m., *p<0.001), absolute values of CBF and R_2* measured in the pre- and post-caffeine experiments (10 subjects). Nomenclature for 'baseline' and 'stimulus' are explained in the caption for Table 2. Significance for the pre-caffeine stimulus response and the post-caffeine baseline were tested against the pre-caffeine baseline. Significance for the post-caffeine stimulus response was testing against the post-caffeine baseline.

	BOLD/CBF ROI	
	CBF (ml/100 ml/min)	ΔR_2* (s^{-1})
Pre-caffeine (baseline)	82.8 (4.4)	23.2 (0.88)
Pre-caffeine (stimulus)	122.9 (4.7)*	22.5 (1.0)*
Post-caffeine (baseline)	60.5 (2.9)*	25.4 (0.83), p=0.002
Post-caffeine (stimulus)	91.9 (4.3)*	24.7 (0.82)*

Supplementary Table S3.3.6. Fractional percent changes in CBF, BOLD, and $CMRO_2$ in the combined BOLD/CBF ROI.

Nomenclature for 'baseline' and 'stimulus' are explained in the caption for Table 2. All significance values were tested against zero. "Difference in the response" refers to the percent change in the post-caffeine stimulus response compared to the pre-caffeine stimulus response (a percent of a percent).

Relative to pre-caffeine baseline (BOLD/CBF ROI):				
	δCBF (%)	δBOLD (%)	$\delta CMRO_2$ (%)	*n*
Pre-caffeine (stimulus)	49.9 (4.4)**	1.64 (0.10)**	21.9 (2.3)**	2.32 (0.08)
Post-caffeine (baseline)	-26.1 (3.5)**	-5.20 (1.1)*, p=0.001	10.1 (6.7), p=0.17	
Post-caffeine (stimulus)	38.7 (3.2)**	1.52 (0.10)**	32.4 (2.8)**	
Difference in response	-22.5 (9.0)*, p=0.035	-7.29 (5.1), p=0.18	48.0 (11.9)*, p=0.003	
Conventional analysis relative to immediately preceding baseline (CBF ROI):				
	δCBF (%)	δBOLD (%)	$\delta CMRO_2$ (%)	*n*
Post-caffeine (stimulus)	52.4 (3.4)**	1.60 (0.11)**	29.6 (2.0)**	1.78 (0.05)**
Difference in response	4.99 (10.8), p=0.65	-1.96 (5.0), p=0.71	35.3 (13.3)*, p=0.026	

* $p<0.05$, ** $p<0.001$

Supplementary Table S4.3.7. Alternate analyses effects on δCMRO$_2$ (%).

Effect of using the classic Davis model parameters to evaluate the dCMRO$_2$ response in percent change (mean ± one s.e.m., *p<0.05, **p<0.001). All significance values were tested against zero except for the coupling parameter, *n*, for which the post-caffeine *n* was compared to the pre-caffeine *n*. "Response percent change" refers to the percent change in the post-caffeine stimulus response compared to the pre-caffeine stimulus response ("a percent of a percent"). Note our conclusion regarding the increase in CMRO$_2$ evoked response with caffeine to the visual stimulus is not changed. even with large changes in *M* as the "Response percent change" is always significantly increased.

	Optimized Davis Model	Classic Davis Model
Pre-caffeine (stimulus)	26.7 (2.3)**	23.4 (2.0)**
Post-caffeine (baseline)	21.8 (8.4)*, p=0.030	13.3 (6.4), p=0.067
Post-caffeine (stimulus)	42.9 (3.6)**	35.9 (2.6)**
Response percent change:	60.7 (9.5)**	53.7 (7.6)**
Pre-caffeine *n*	1.96 (0.06)	2.24 (0.06)
Post-caffeine *n*	1.60 (0.03)**	1.78 (0.04)**

Supplementary Table S5.3.8. Alternate analyses effects on $\delta CMRO_2$ (%).

Effect of varying *M* on calculations of the $\delta CMRO_2$ response in percent change (mean ± one s.e.m., *p<0.05, **p<0.001). All significance values were tested against zero except for the coupling parameter, *n*, for which the post-caffeine *n* was compared to the pre-caffeine *n*. Note our conclusion regarding the increase in $CMRO_2$ evoked response with caffeine to the visual stimulus is not changed even with large changes in *M* as the "Response percent change" is always significantly increased.

	Optimized Davis Model	*M*=8.3%	*M*=15.4%
Pre-caffeine (stimulus)	26.7 (2.3)**	20.0 (2.0)**	30.3 (2.6)**
Post-caffeine (baseline)	21.8 (8.4)*, p=0.030	41.7 (11.8)* p=0.006	11.2 (6.8), p=0.13
Post-caffeine (stimulus)	42.9 (3.6)**	46.1 (4.9)**	41.2 (3.1)**
Response percent change:	60.7 (9.5)**	131.3 (20.6)**	35.7 (6.6)**
Pre-caffeine *n*	1.96 (0.06)	2.67 (0.15)	1.72 (0.03)
Post-caffeine *n*	1.60 (0.03)**	1.75 (0.06)**	1.52 (0.02)*, p=0.001

Acknowledgements

Chapter 3, in full, is a reprint of the material as it appears in Neuroimage 2011. Griffeth, VEM and Buxton, RB (2011). Prospects for quantitative fMRI: investigating the effects of caffeine on baseline oxygen metabolism and the response to a visual stimulus in humans. Neuroimage 57: 809-816. The dissertation author was the primary investigator and author of this paper.

References (Supplementary)

1. Boxerman JL, Bandettini PA, Kwong KK, Baker JR, Davis TL, et al. (1995) The intravascular contribution to fMRI signal change: Monte Carlo modeling and diffusion-weighted studies in vivo. Magn Reson Med 34: 4-10.

2. Buxton RB, Uludag K, Dubowitz DJ, Liu TT (2004) Modeling the hemodynamic response to brain activation. Neuroimage 23 Suppl 1: S220-233.

3. Obata T, Liu TT, Miller KL, Luh WM, Wong EC, et al. (2004) Discrepancies between BOLD and flow dynamics in primary and supplementary motor areas: application of the balloon model to the interpretation of BOLD transients. Neuroimage 21: 144-153.

4. Leontiev O, Buxton RB (2007) Reproducibility of BOLD, perfusion, and CMRO(2) measurements with calibrated-BOLD fMRI. Neuroimage 35: 175-184.

5. Chen JJ, Pike GB (2009) BOLD-specific cerebral blood volume and blood flow changes during neuronal activation in humans. NMR Biomed 22: 1054-1062.

6. Hillman EM, Devor A, Bouchard MB, Dunn AK, Krauss GW, et al. (2007) Depth-resolved optical imaging and microscopy of vascular compartment dynamics during somatosensory stimulation. Neuroimage 35: 89-104.

7. Kim T, Hendrich KS, Masamoto K, Kim SG (2007) Arterial versus total blood volume changes during neural activity-induced cerebral blood flow change: implication for BOLD fMRI. J Cereb Blood Flow Metab 27: 1235-1247.

8. Kim T, Kim SG (2006) Quantification of cerebral arterial blood volume using arterial spin labeling with intravoxel incoherent motion-sensitive gradients. Magn Reson Med 55: 1047-1057.

9. Zappe AC, Uludag K, Oeltermann A, Ugurbil K, Logothetis NK (2008) The influence of moderate hypercapnia on neural activity in the anesthetized nonhuman primate. Cereb Cortex 18: 2666-2673.

10. Davis TL, Kwong KK, Weisskoff RM, Rosen BR (1998) Calibrated functional MRI: mapping the dynamics of oxidative metabolism. Proc Natl Acad Sci USA 95: 1834-1839.

11. Griffeth VEM, Buxton RB. Modeling the effects of changes in hematocrit, O2 extraction fraction, and blood volume distribution on the BOLD signal and estimates of CMRO2 change with a calibrated BOLD model; 2010.

12. Kim T, Kim SG (2010) Cortical layer-dependent arterial blood volume changes: improved spatial specificity relative to BOLD fMRI. Neuroimage 49: 1340-1349.

13. Uludag K, Muller-Bierl B, Ugurbil K (2009) An integrative model for neuronal activity-induced signal changes for gradient and spin echo functional imaging. Neuroimage 48: 150-165.

14. Marchal G, Rioux P, Petit-Taboue M-C, Sette G, Travere J-M, et al. (1992) Regional cerebral oxygen consumption, blood flow, and blood volume in healthy human aging. Arch Neurol 49: 1013-1020.

15. Roland PE, Eriksson L, Stone-Elander S, Widen L (1987) Does mental activity change the oxidative metabolism of the brain? J Neuroc 7: 2373-2389.

16. Weber B, Keller AL, Reichold J, Logothetis NK (2008) The microvascular system of the striate and extrastriate visual cortex of the macaque. Cereb Cortex 18: 2318-2330.

CHAPTER 4

Effect of watching a complex movie on blood flow and oxygen metabolism coupling

Abstract

Direct attentional modulation evokes a blood flow response with a relatively large oxygen metabolism response in comparison to an unattended stimulus, which evokes a much smaller metabolic response. However the effect of a naturalistic stimulus in comparison to a simple repetitive stimulus on blood flow and oxygen metabolism coupling is less clear. Combined blood flow and oxygenation measurements provide the best tool for investigating modulations of the flow-metabolism relationship. We measured the human visual cortex response to two contrast levels of a radial flickering checkerboard in comparison to the response to free viewing of brief movie clips. We found no difference in the coupling between the movie stimulus and the flickering checkerboards employing two different methods: a standard analysis using the Davis model and a new analysis using a heuristic model dependent only on measureable quantities. This finding suggests that the attentional modulation with this study design was not sufficient to provoke a change in the coupling or that the design disrupted the cognitive processes underlying response to a more natural stimulus.

Introduction

A fascinating characteristic of neural activity is the divergent physiological responses of cerebral blood flow (CBF) and the cerebral metabolic rate of oxygen ($CMRO_2$). The brain's typical response to a stimulus involves a much greater CBF response than $CMRO_2$ response, and this is an essential component underlying the blood oxygen level dependent (BOLD) functional MRI (fMRI) signal. The ratio of the CBF and $CMRO_2$ responses is known as the coupling parameter, $n=\%\Delta CBF/\%\Delta CMRO_2$. The fact that CBF increase so much more than $CMRO_2$, by some measures as much as five to six times [1,2], suggests that these responses while in parallel are actually driven by separate mechanisms. For instance, neural activity may increase CBF in a feed forward mechanism while $CMRO_2$ is simply a measure of the evoked neural response reflecting increased metabolism and energy requirement. If this is the case, changes in the type of neural activity or changes in the driving force behind the neural response could lead to changes in the coupling ratio. In order to examine this hypothesis, we tested whether an engaging naturalistic stimulus would affect the neurophysiological response and the coupling parameter differently than a typical flickering checkerboard stimulus.

There is extensive literature examining the neurophysiologic response to flickering checkerboards at different frequencies, luminance and with different colors [2-5], but the literature is sparser on how flow and metabolism in the visual cortex change in response to a more natural and complex stimulus. One study using a James Bond movie as a stimulus found that functional segregation of the brain is preserved even when many features must be processed simultaneously [6]. Other studies have found a significant level of voxel-by-voxel synchronization between individuals while watching a movie [7,8] suggesting that these patterns of regional brain activation are preserved between subjects. Yet another study measured CBF with continuous arterial spin labeling (CASL) and concurrent BOLD imaging to

measure responses as subjects were freely watching a cartoon movie [9]. In this study, they found that CBF changes dominant BOLD changes in multiple areas of the brain including the visual cortex. However, they did not examine changes in the coupling of flow and oxygen metabolism, instead focusing the advantages of ASL over BOLD imaging for detecting slow variations in brain function over long time periods.

In this experiment, we focused on determining how CBF and $CMRO_2$ respond to free viewing of brief movie clips in comparison to fixation on a flickering checkerboard. Previous research has show variation in *n* to different stimuli. For example, *n* increases with increasing stimulus intensity [10] and decreases with increased attention to the stimulus [11]. Additionally, different coupling ratios have been found to exist in different areas of the brain. For example, lower *n* has been found in the visual cortex in comparison to the lentiform nuclei [12], the somatosensory cortex [13], and the supplementary motor area [14]. Differences in *n* have also been found between the motor and visual cortices, although results in these areas are conflicting [14,15].

In this study, we compared the brain's response to free viewing of a complex and engaging movie stimulus versus fixation on two contrast levels of a simple flickering checkerboard (10% and 40%) in order to test if the differences in these stimuli would create a difference in the coupling parameter. It was our hypothesis that the more complex movie stimulus would lead to recruitment of additional higher brain regions that would produce positive feedback on the visual cortex, increasing neural activity and $CMRO_2$. In turn, this would lead to a reduction in the coupling parameter. We did not find this to be the case as there was no significant difference in the coupling of blood flow and oxygen metabolism between the movie and the flickering checkerboards.

Methods

The study was performed on 15 healthy adults who had abstained from caffeine for at least 12 hours prior to study participation. The institutional review board at the University of California, San Diego approved the study, and written informed consent was obtained from all participants. Two scan sessions including three functional runs and one functional localizer were performed on each subject. The functional runs consisted of four 20 s blocks of activation with 55 s periods of baseline. Activation periods cycled between movie clips from Earth: The Biography (BBC Video) along with 10% and 40% black-white contrast 8 Hz flickering radial checkerboards such that each stimulus type had a total of four blocks of activation. Baseline consisted of a gray background with luminance normalized to that of the flickering checkerboards. Subjects were asked to fixate on a black cross in the middle of the screen during the baseline and flickering checkerboard tasks. The functional localizer consisted of alternating 20 s blocks of activation with 20 s periods of baseline. Activation periods alternated between clips from Earth: The Biography and 100% black-white contrast 8 Hz flickering radial checkerboards.

Using a spiral dual-echo ASL PICORE QUIPSS II [16] pulse sequence, we simultaneously measured the CBF and BOLD responses to these stimuli. ASL was used to directly measure CBF by magnetically labeling arterial water with an applied RF pulse. The tagged water was allowed to flow into the slice of interest followed by tagged image (T) acquisition. A control image (C) was acquired by repeating this sequence without magnetically tagging the water. Signal acquisition occurred at two echo times (TE) every 2.5 s (TE_1=9.1 ms

and TE_2=30 ms). Surround average and difference time courses were computed for each TE as in Griffeth et al. [17].

Statistical analysis of the functional data was performed using a general linear model (GLM) approach. An active visual cortex region of interest (ROI) was defined as voxels exhibiting CBF activation in the first echo difference data of the functional localizer run. The desired ROI size was set to 100±10 voxels and was achieved by decreasing the acceptable per-voxel P-value from 0.01 until the ROI passed this threshold. Voxels were also required to be in clusters of a size consistent with the whole cluster passing a significance threshold of $\alpha \leq 0.05$ determined using AFNI AlphaSim [18]. Four scan sessions from three subjects were eliminated as the number of voxels did not reach this threshold. Five addition scan sessions in three subjects were eliminated due to poor BOLD correlation scores in the functional runs despite good correlations in the localizer run. Analysis was limited to voxels exhibiting a minimum signal to noise ratio of 200 and a minimum CBF signal of 40% of the mean baseline CBF to preferentially increase the likelihood of gray matter over white matter inclusion in the ROI. For summary statistics, the baseline was averaged over the 10 s prior to the start of the stimulus and the stimulus response was averaged over the last 10 s of the stimulus. To test whether our method of ROI determination biased our results, we also analyzed our data using a combined BOLD/CBF ROI, which produced no differences in the significant results.

The change in the apparent rate of signal decay, R_2^*, was calculated from the surround average signal (A) of the tag and control images by modeling the average signal as $A(t) = A_0(t)e^{-TE \cdot R_2^*(t)}$. The source of the BOLD response is changes in blood oxygenation, which results in changes in R_2^*, but the problem that usually confounds the interpretation of slow modulations of the BOLD response is that A_0 is sensitive to scanner drifts. To minimize

this source of error, we directly calculated R_2^*. For display and analysis, we calculated an equivalent BOLD response with A_0 removed as in Perthen et al. [19] using the definition $\%\Delta\mathrm{BOLD}(t) = e^{-TE_2 \cdot \Delta R_2^*(t)} - 1$ where %ΔBOLD is the percent change in the BOLD signal due to the stimulus. Surround subtraction produces a net signal that is proportional to the arterial spins delivered to the voxel [20], and quantification of this signal in absolute CBF units was performed as described previously [19,21].

To calculate $CMRO_2$ from normalized CBF and BOLD data, the Davis model [22] was used: $\%\Delta BOLD = M\left[1 - f^{\alpha}\left(\frac{r}{f}\right)^{\beta}\right]$. This model describes the BOLD response as a function of the normalized (activation/baseline) values of CBF (*f*) and $CMRO_2$ (*r*). Values for the parameters α=0.14 and β=0.91 were taken from a more detailed four compartment model of the BOLD response that includes effects left out of the original derivation including intravascular signal changes, volume exchange effects due to variation in blood volume, and unequal distribution of blood volume changes between vascular compartments [23]. The scaling parameter, *M*, was assumed to be 11.9% as calculated from hypercapnia calibration using similar subjects in Griffeth et al. [17]. To test whether bias in the parameters α, β or *M* would affect our conclusions, we also analyzed our data with *M*±30% and the original Davis model parameters of α=0.38 and β=1.5 (using *M*=8.5%). All BOLD, CBF, and $CMRO_2$ responses were expressed as a percent change from the pre-stimulus baseline and are denoted %ΔBOLD, %ΔCBF, and $\%\Delta CMRO_2$.

To more directly examine the effects of different stimuli on the coupling of CBF and $CMRO_2$, we used a heuristic model that was recently published [24]. This model maintains the non-linear dependence of the BOLD signal on flow, reduces the number of parameters from

three to two, and directly incorporates the coupling parameter, *n*. This simple model was inspired by work with the much more detailed model [23], which appeared to produce a very smooth BOLD surface suggesting that the parameters α and β of the Davis model may be over-fitting the data. This new equation is: $\%\Delta BOLD = A\left(1-1/f\right)\left(1-1/n\right)$ where f is the normalized CBF change. The power of this new model is that the coupling of CBF and $CMRO_2$ expressed as *n* can be directly compared without knowing the scaling parameter *A*. Instead, by creating a null hypothesis that *n* is the same for two stimulus types, the ratio of the two BOLD signals becomes:

$$\frac{\%\Delta BOLD}{\%\Delta BOLD_{ref}} = \frac{\left(1-1/f\right)}{\left(1-1/f_{ref}\right)}$$

By performing a two-tailed paired t-test comparing the left and right sides of this equation, this hypothesis can be tested. If these ratios are significantly different, then the coupling parameter between the two stimulus types is different.

Results

We measured the BOLD and CBF responses to short movie clips and flickering checkerboards at both 10% and 40% contrast (Fig. 1). The BOLD response to the 10% contrast (0.86±0.1%) was lower than the responses to both the 40% contrast (1.3±0.1%, $p<0.001$) and the movie stimulus (1.2±0.1%, $p<0.001$). Although the BOLD response was slightly lower from 40% contrast to the movie stimulus, the difference was not significant ($p=0.076$). The CBF response was also significantly increased from 10% contrast (23.4±3.3%) to both the movie

stimulus (31.3±1.8%, p=0.02) and to 40% contrast (36.7±2.3%, p=0.001). Additionally, the increase in the flow response from the movie stimulus to 40% contrast was significant (p=0.05).

Using the optimized Davis model, we also calculated the $CMRO_2$ responses to the three stimulus types (Fig. 2). We found a significant increase in the $CMRO_2$ response from 10% contrast (9.5±2.0%) to 40% contrast (13.9±1.7%, p=0.03), although there was not a significant difference in comparison to the movie stimulus (11.6±1.1%, p=0.26). The difference between the movie stimulus and 40% contrast was also not significant (p=0.14). Varying the scaling parameter M±30% resulted in large changes in $CMRO_2$, but this did not affect the relationship of $CMRO_2$ between the states with the exception that for a much lower M=8.3% the statistical significance of the increase in $\%\Delta CMRO_2$ from 10% to 40% contrast disappears. Using the original Davis model, the values of $\%\Delta CMRO_2$ are similar: 10% contrast=8.5±1.8%, 40% contrast=12.3±1.5%, and movie clips=10.3±1.0%. The only statistical difference is between the two levels of contrast (p=0.03).

To examine the difference in 40% contrast checkerboard and the movie stimulus more closely, we plotted $1/n$ ($\%\Delta CMRO_2/\%\Delta CBF$) for the movie stimulus versus $1/n$ for 40% contrast for each full scan acquired. $1/n$ has less variability than n as $\%\Delta CMRO_2$ is sometimes a small number. All points fall close to the equality line suggesting there is no difference between the two stimulus types (Fig. 3). We confirmed this using a two-tailed paired t-test (p=0.97). There is also no statistical difference in $1/n$ between the 10% contrast checkerboard and the other two stimuli.

We also tested whether there may be a difference in the flow-metabolism coupling using the simplified model introduced above. We created a null hypothesis that there is no difference in the coupling parameter between the movie stimulus and the 40% contrast. We

tested this hypothesis by taking the ratio of the BOLD signals and CBF signals as the scaling parameter *A* and also the *n* term cancel under this assumption. Again, we found no difference in these ratios that fell close to the equality line (p=0.77, Fig. 4).

Discussion

We found there is no difference in the flow-metabolism coupling for brief movie clips compared to a 40% contrast flickering checkerboard. Additionally, these two stimuli produced comparable levels of flow response. Figure 1 comparing the BOLD and CBF response between these stimulus types shows that they appear to follow similar coupling parameter lines as determined by the optimized Davis model (with *M*=11.9%). We demonstrated this more conclusively with two different methods comparing flow-metabolism coupling: Figure 3 compares values of 1/*n* calculated using the Davis model and Figure 4 examines the variations in the BOLD and flow signal between the two states using a new simplified model. These results do not support our hypothesis that increased attention to the movie stimulus would result in top-down modulation of neural activity producing stronger modulation of CBF and $CMRO_2$ than BOLD. Comparison of the 10% contrast to the 40% contrast also showed no significant difference in the coupling, although there is a trend for a higher 1/n with the 40% checkerboard consistent with previous studies examining effects of varying contrast levels on neurophysiology [10].

Previous research on attentional modulation of BOLD, CBF and $CMRO_2$ informed our hypothesis that free viewing of movie clips would alter the coupling of CBF and $CMRO_2$ in comparison to fixation on a 40% contrast checkerboard. As the movie is a more engaging task, we hypothesized that an increased level of attention to the movie would result in increased

neural activity and larger modulation of $CMRO_2$ in comparison to CBF thereby altering flow-metabolism coupling. Previous research has shown that neurons increases their firing rate in response to a stimulus when it is attended [25-27], yet in fMRI studies there is only a moderate attentional modulation of the BOLD signal [28-32]. Interpretation of these results is difficult, because of the intrinsic complexity of the BOLD signal. Increased CBF drives out deoxyhemoglobin thereby increase the BOLD signal while increased $CMRO_2$ produces deoxyhemoglobin and decreases the BOLD signal.

In a previous experiment also comparing concurrent measurements of CBF and BOLD, it was found that the CBF response was much greater than the BOLD response in the visual cortex during free viewing of a movie stimulus [9]. However, this study used a movie clip of 6.5 minutes. For a stimulation this long in duration, it has been noted that there is lower sensitivity of BOLD contrast compared to CBF contrast [33] making it difficult then to determine $CMRO_2$ response. In contrast, the current experiment optimized the sensitivity of the BOLD response using a block design and optimal scan parameters (dual-echo acquisition). The draw back of this experimental design is that it could potentially disrupt the cognitive process that occurs in response to a natural situation, yet another reason we may not have measured a difference in the flow-metabolism coupling.

It is also possible that the indirect attentional modulation due to the greater inherent interest of the movie clips was not enough to alter the coupling. In comparison another experiment by our group that directly and purposefully altered attention found that attention resulted in increased modulation of $CMRO_2$ and decreased the coupling ratio n [34]. In the current experiment, subjects were told to freely watch the movie while during the flickering checkerboard they were told to fixate on a cross in the middle of the screen. In may be that this

required fixation commanded a similar level of attention as the movie stimulus even if the movie clips were of greater interest.

Conclusions

Contrary to our hypothesis, there is no difference in the coupling in the visual cortex between free viewing of brief movie clips and fixation on a flickering checkerboard. It is possible that the attentional modulation was not sufficient to provoke such a modulation or that the study design disrupted the cognitive processes underlying response to a more natural stimulus.

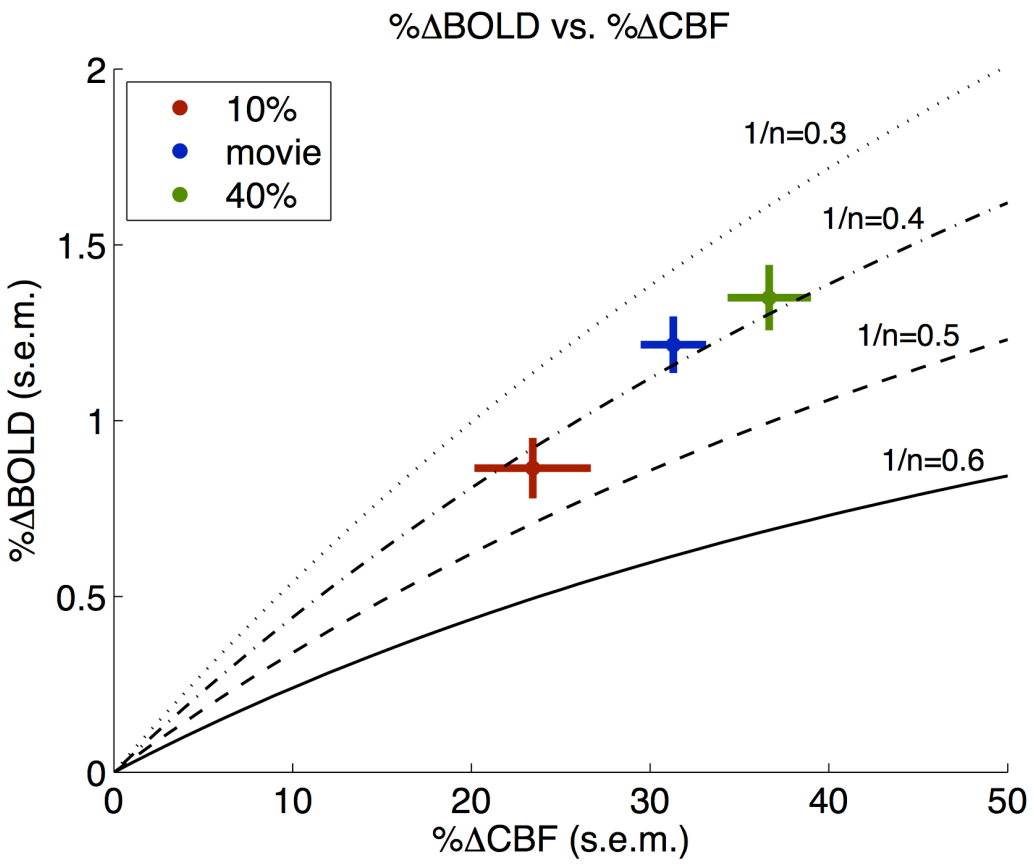

Figure 4.1. BOLD plotted against CBF for the three stimulus types.

Crossbars represent standard error of the mean for CBF (horizontal) and BOLD (vertical). Lines for 1/*n* plotted using the Davis model with *M*=11.9%. The three stimulus types bracket the line corresponding to *n*=2.5.

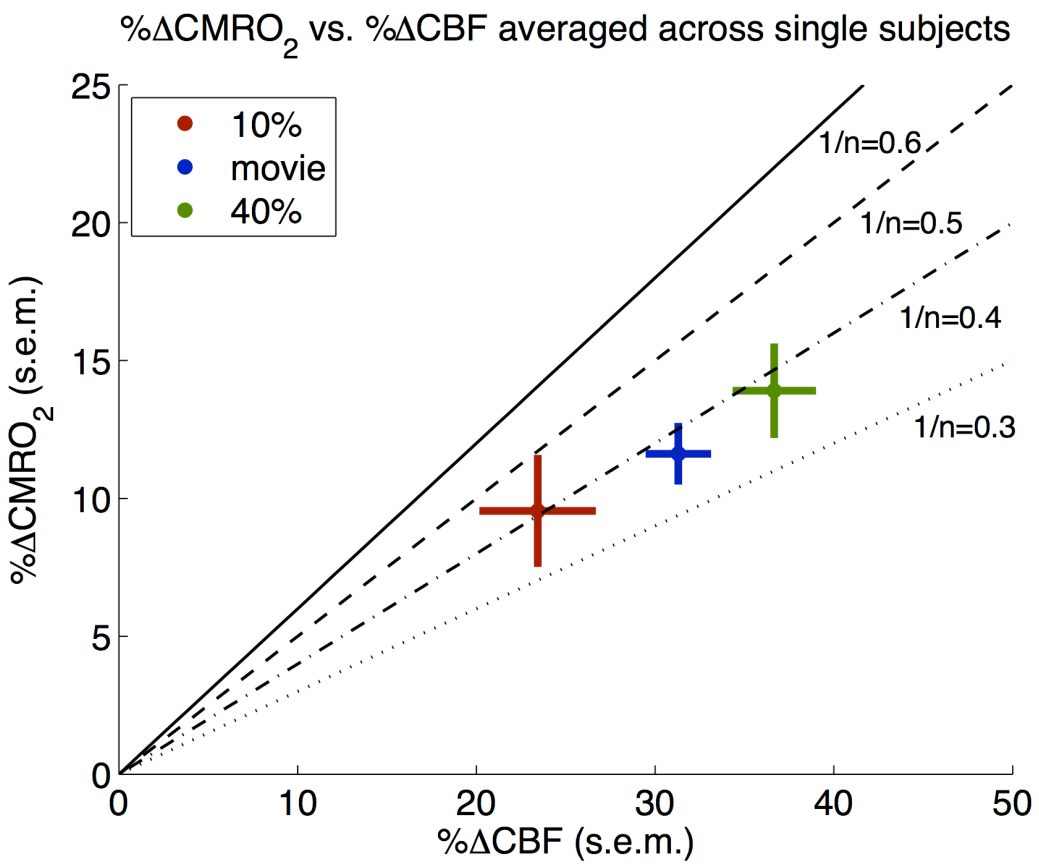

Figure 4.2. $CMRO_2$ plotted against CBF for the three stimulus types.

Crossbars represent standard error of the mean for CBF (horizontal) and $CMRO_2$ (vertical). Lines for $1/n$ plotted using the Davis model with M=11.9%. The three stimulus types bracket the line corresponding to n=2.5.

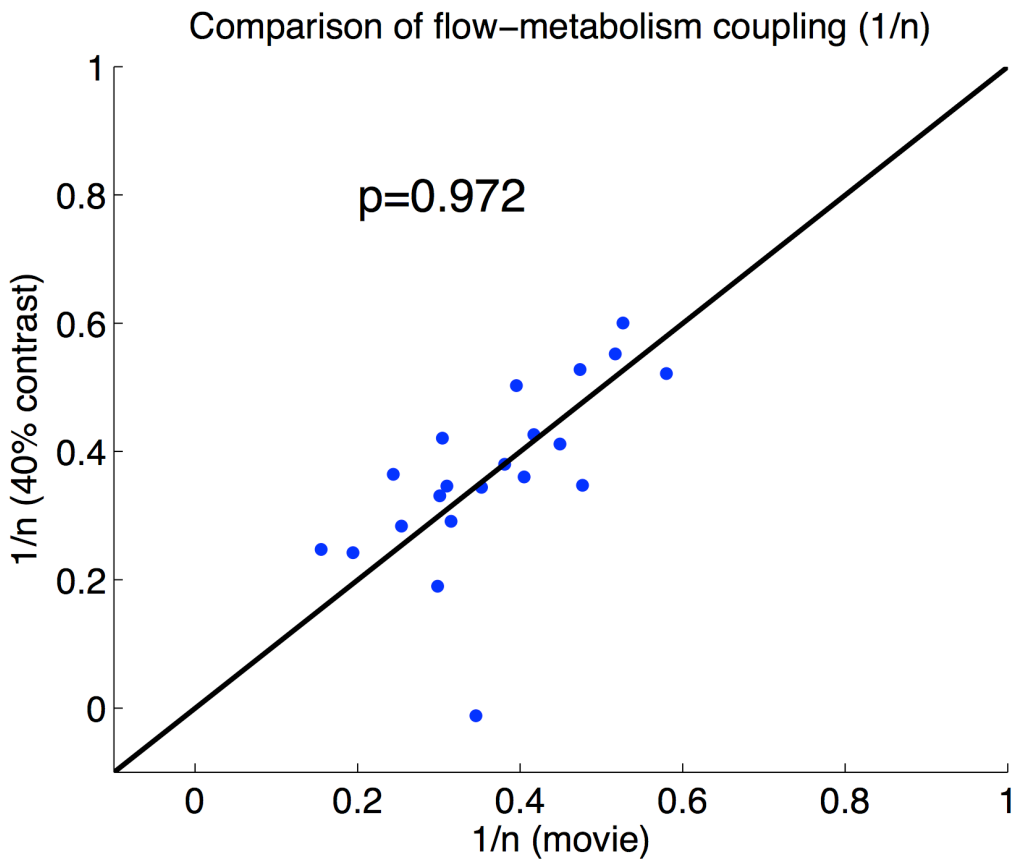

Figure 4.3. Comparison of $CMRO_2$-CBF coupling between 40% contrast flickering checkerboard and free viewing of movie clips for each scan session using 1/*n* calculated from the Davis model.

The solid black line denotes equality. Note the data parallels the equality line demonstrating that there is no statistical difference in the flow-metabolism coupling between the two states.

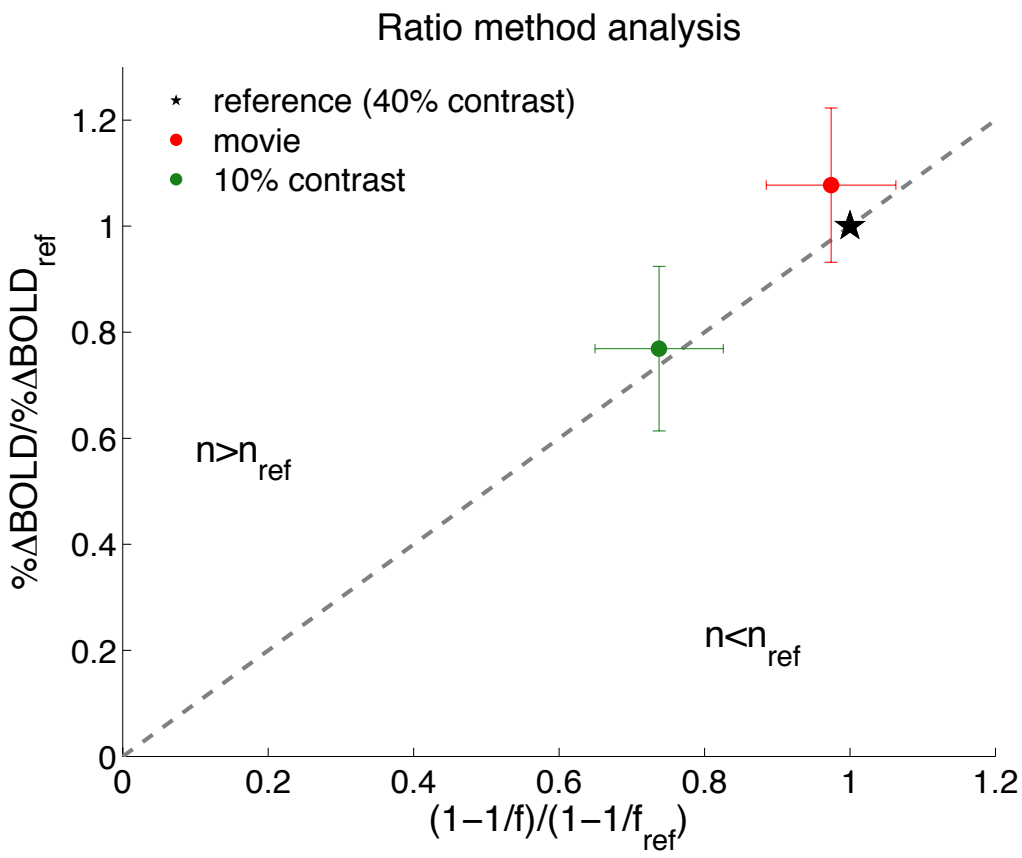

Figure 4.4. Comparison of $CMRO_2$-CBF coupling between 40% contrast flickering checkerboard and free viewing of movie clips for each scan session using the ratio method.

The solid black equality line represents the null hypothesis that *n* is the same between the two states. Note the data parallels this line demonstrating that there is no statistical difference in the flow-metabolism coupling between the two states. Error bars represent the standard error of the mean.

Acknowledgements

Chapter 4, in part, is currently being prepared for submission for publication of the material. Griffeth VEM, Simon AB, Buxton RB. Effect of watching a complex movie on blood flow and oxygen metabolism coupling as well as fMRI signal variability in the human visual cortex. The dissertation author is the primary investigator and author of this material.

References

1. Fox PT, Raichle ME (1986) Focal physiological uncoupling of cerebral blood flow and oxidative metabolism during somatosensory stimulation in human subjects. Proc Natl Acad Sci USA 83: 1140-1144.

2. Lin AL, Fox PT, Yang Y, Lu H, Tan LH, et al. (2008) Evaluation of MRI models in the measurement of CMRO2 and its relationship with CBF. Magn Reson Med 60: 380-389.

3. Hoge RD, Atkinson J, Gill B, Crelier GR, Marrett S, et al. (1999) Stimulus-dependent BOLD and perfusion dynamics in human V1. Neuroimage 9: 573-585.

4. Mohamed FB, Pinus AB, Faro SH, Patel D, Tracy JI (2002) BOLD fMRI of the visual cortex: quantitative responses measured with a graded stimulus at 1.5 Tesla. J Magn Reson Imaging 16: 128-136.

5. Vafaee MS, Gjedde A (2000) Model of blood-brain transfer of oxygen explains nonlinear flow-metabolism coupling during stimulation of visual cortex. J Cereb Blood Flow Metab 20: 747-754.

6. Bartels A, Zeki S (2004) Functional brain mapping during free viewing of natural scenes. Hum Brain Mapp 21: 75-85.

7. Hasson U, Nir Y, Levy I, Fuhrmann G, Malach R (2004) Intersubject synchronization of cortical activity during natural vision. Science 303: 1634-1640.

8. Jaaskelainen IP, Koskentalo K, Balk MH, Autti T, Kauramaki J, et al. (2008) Inter-subject synchronization of prefrontal cortex hemodynamic activity during natural viewing. Open Neuroimag J 2: 14-19.

9. Rao H, Wang J, Tang K, Pan W, Detre JA (2007) Imaging brain activity during natural vision using CASL perfusion fMRI. Hum Brain Mapp 28: 593-601.

10. Liang CL, Ances BM, Perthen JE, Moradi F, Liau J, et al. (2013) Luminance contrast of a visual stimulus modulates the BOLD response more than the cerebral blood flow response in the human brain. Neuroimage 64: 104-111.

11. Moradi F, Buracas GT, Buxton RB (2011) Attention strongly increases oxygen metabolic response to stimulus in primary visual cortex. Neuroimage.

12. Ances BM, Leontiev O, Perthen JE, Liang C, Lansing AE, et al. (2008) Regional differences in the coupling of cerebral blood flow and oxygen metabolism changes in response to activation: Implications for BOLD-fMRI. Neuroimage 39: 1510-1521.

13. Mark CI, Pike GB. Hyperoxic versus hypercapnic BOLD calibration under precise end-tidal control to improve the estimation of oxygen consumption; 2011; Montreal, Canada.

14. Chiarelli PA, Bulte DP, Gallichan D, Piechnik SK, Wise R, et al. (2007) Flow-metabolism coupling in human visual, motor, and supplementary motor areas assessed by magnetic resonance imaging. Magn Reson Med 57: 538-547.

15. Stefanovic B, Warnking JM, Rylander KM, Pike GB (2006) The effect of global cerebral vasodilation on focal activation hemodynamics. Neuroimage 30: 726-734.

16. Wong EC, Buxton RB, Frank LR (1998) Quantitative imaging of perfusion using a single subtraction (QUIPSS and QUIPSS II). Magn Reson Med 39: 702-708.

17. Griffeth VE, Perthen JE, Buxton RB (2011) Prospects for quantitative fMRI: Investigating the effects of caffeine on baseline oxygen metabolism and the response to a visual stimulus in humans. Neuroimage 57: 809-816.

18. Cox RW (1996) AFNI: software for analysis and visualization of functional magnetic resonance neuroimages. Comput Biomed Res 29: 162-173.

19. Perthen JE, Lansing AE, Liau J, Liu TT, Buxton RB (2008) Caffeine-induced uncoupling of cerebral blood flow and oxygen metabolism: a calibrated BOLD fMRI study. Neuroimage 40: 237-247.

20. Liu TT, Wong EC (2005) A signal processing model for arterial spin labeling functional MRI. Neuroimage 24: 207-215.

21. Chalela JA, Alsop DC, Gonzalez-Atavales JB, Maldjian JA, Kasner SE, et al. (2000) Magnetic resonance perfusion imaging in acute ischemic stroke using continuous arterial spin labeling. Stroke 31: 680-687.

22. Davis TL, Kwong KK, Weisskoff RM, Rosen BR (1998) Calibrated functional MRI: mapping the dynamics of oxidative metabolism. Proc Natl Acad Sci USA 95: 1834-1839.

23. Griffeth VE, Buxton RB (2011) A theoretical framework for estimating cerebral oxygen metabolism changes using the calibrated-BOLD method: modeling the effects of blood volume distribution, hematocrit, oxygen extraction fraction, and tissue signal properties on the BOLD signal. Neuroimage 58: 198-212.

24. Griffeth VE, Blockley NP, Simon AB, Buxton RB (2013) A simplified model for the blood oxygenation level dependent (BOLD) effect for estimating brain oxygen metabolism changes. PLoS One.

25. Ito M, Gilbert CD (1999) Attention modulates contextual influences in the primary visual cortex of alert monkeys. Neuron 22: 593-604.

26. McAdams CJ, Reid RC (2005) Attention modulates the responses of simple cells in monkey primary visual cortex. J Neurosci 25: 11023-11033.

27. Motter BC (1993) Focal attention produces spatially selective processing in visual cortical areas V1, V2, and V4 in the presence of competing stimuli. J Neurophysiol 70: 909-919.

28. Brefczynski JA, DeYoe EA (1999) A physiological correlate of the 'spotlight' of visual attention. Nat Neurosci 2: 370-374.

29. Buracas GT, Boynton GM (2007) The effect of spatial attention on contrast response functions in human visual cortex. J Neurosci 27: 93-97.

30. Gandhi SP, Heeger DJ, Boynton GM (1999) Spatial attention affects brain activity in human primary visual cortex. Proc Natl Acad Sci U S A 96: 3314-3319.

31. Somers DC, Dale AM, Seiffert AE, Tootell RB (1999) Functional MRI reveals spatially specific attentional modulation in human primary visual cortex. Proc Natl Acad Sci U S A 96: 1663-1668.

32. Tootell RB, Hadjikhani N, Hall EK, Marrett S, Vanduffel W, et al. (1998) The retinotopy of visual spatial attention. Neuron 21: 1409-1422.

33. Wang J, Aguirre GK, Kimberg DY, Roc AC, Li L, et al. (2003) Arterial spin labeling perfusion fMRI with very low task frequency. Magn Reson Med 49: 796-802.

34. Moradi F, Buracas GT, Buxton RB (2012) Attention strongly increases oxygen metabolic response to stimulus in primary visual cortex. Neuroimage 59: 601-607.

CHAPTER 5

Applications of the detailed BOLD model: testing the utility of gas-inhalation and optimizing the signal-to-noise ratio of the cerebral blood flow measurement

Special issue review article

NMR IN BIOMEDICINE

Received: 23 March 2012, Revised: 17 July 2012, Accepted: 2 August 2012, Published online in Wiley Online Library: 2012

(wileyonlinelibrary.com) DOI: 10.1002/nbm.2847

A review of calibrated blood oxygenation level-dependent (BOLD) methods for the measurement of task-induced changes in brain oxygen metabolism

Nicholas P. Blockley[a]*, Valerie E. M. Griffeth[b], Aaron B. Simon[b] and Richard B. Buxton[a,c]

The dynamics of the blood oxygenation level-dependent (BOLD) response are dependent on changes in cerebral blood flow, cerebral blood volume and the cerebral metabolic rate of oxygen consumption. Furthermore, the amplitude of the response is dependent on the baseline physiological state, defined by the haematocrit, oxygen extraction fraction and cerebral blood volume. As a result of this complex dependence, the accurate interpretation of BOLD data and robust intersubject comparisons when the baseline physiology is varied are difficult. The calibrated BOLD technique was developed to address these issues. However, the methodology is complex and its full promise has not yet been realised. In this review, the theoretical underpinnings of calibrated BOLD, and issues regarding this theory that are still to be resolved, are discussed. Important aspects of practical implementation are reviewed and reported applications of this methodology are presented. Copyright © 2012 John Wiley & Sons, Ltd.

Keywords: review; calibrated BOLD; oxygen metabolism; respiratory challenge

INTRODUCTION

The introduction of blood oxygenation level-dependent (BOLD) contrast in the early 1990s heralded a revolution in functional neuroimaging (1–4) that led to the widespread application of functional MRI (fMRI) to map patterns of activation in the human brain. However, the BOLD response to task-related activation is a complex function of underlying changes in cerebral blood flow (CBF) and cerebral metabolic rate of oxygen consumption ($CMRO_2$). This is characterised by a disproportionate increase in CBF relative to the accompanying increase in $CMRO_2$ generated by increased neuronal activity (5). It is important to note, however, that the relative changes in CBF and $CMRO_2$ alone do not determine the amplitude of the BOLD response. The scaling of the BOLD response is also determined by the baseline physiological state of the individual under examination. This baseline is determined by the total amount of deoxyhaemoglobin present in the voxel, which is a function of the subject's haematocrit (Hct), baseline oxygen extraction fraction (OEF) and baseline cerebral blood volume (CBV). As these physiological variables are typically unknown in an fMRI experiment, it is not possible to interpret the BOLD signal in a quantitative manner.

Combining a BOLD response measurement with an additional measurement of CBF, acquired with an arterial spin labelling (ASL) experiment, provides a more quantitative insight into the underlying physiological changes. However, this still does not provide sufficient information to estimate $CMRO_2$, because of the unknown baseline state variables. The calibrated BOLD approach seeks to measure this baseline condition through a calibration experiment (6). When combined with measurements of CBF and BOLD acquired during a stimulation experiment, the percentage change in $CMRO_2$ during the stimulation can be measured. The development and evolution of calibrated BOLD methods have been reviewed recently by Pike (7).

Although BOLD fMRI alone is essentially a qualitative index of brain activity, the calibrated BOLD method offers the potential

* *Correspondence to: N. Blockley, FMRIB Centre, Nuffield Department of Clinical Neurosciences, University of Oxford, John Radcliffe Hospital, Headington, Oxford, OX3 9DU, UK.*
E-mail: nicholas.blockley@ndcn.ox.ac.uk

a *N. P. Blockley, R. B. Buxton*
Center for Functional Magnetic Resonance Imaging, Department of Radiology, University of California San Diego, La Jolla, CA, USA

b *V. E. M. Griffeth, A. B. Simon*
Department of Bioengineering and Medical Scientist Training Program, University of California San Diego, La Jolla, CA, USA

c *R. B. Buxton*
Kavli Institute for Brain and Mind, University of California San Diego, La Jolla, CA, USA

Abbreviations used: *ASE, asymmetric spin echo; ASL, arterial spin labelling; BOLD, blood oxygenation level dependent; CASL, continuous ASL; CBF, cerebral blood flow; CBV, cerebral blood volume; CBV_v, venous CBV; $CMRO_2$, cerebral metabolic rate of oxygen consumption; [dHb], deoxyhaemoglobin concentration; fMRI, functional MRI; GCM, generalised calibration model; GESSE, gradient echo sampling of spin echo; [Hb], haemoglobin concentration; Hct, haematocrit; M, BOLD scaling parameter; MEG, magnetoencephelography; n, $CBF/CMRO_2$ coupling ratio; OEF, oxygen extraction fraction; P_aO_2, arterial partial pressure of oxygen; PASL, pulsed ASL; PCASL, pseudo-continuous ASL; PET, positron emission tomography; $P_{ET}O_2/CO_2$, end-tidal partial pressure of oxygen/carbon dioxide; P_vO_2, venous partial pressure of oxygen; S_aO_2, arterial haemoglobin saturation; TRUST, T_2 relaxation under spin tagging; VASO, vascular space occupancy; VERVE, venous refocusing for volume estimation.*

to make fMRI into a quantitative probe of brain physiology with the promise of an expanded clinical role. The methodology is complex, however, and this promise has not yet been realised. In this review, we discuss the theoretical underpinnings of calibrated BOLD, and issues regarding this theory that still need to be resolved. We also review aspects of practical implementation and reported applications of this methodology.

THEORETICAL UNDERPINNINGS

Physiology of the BOLD response

The interpretation of the relative changes in the BOLD signal in terms of metabolic activity is much more difficult than merely mapping its location, because the BOLD signal depends on CBF, CBV and $CMRO_2$ in a complex manner (Fig. 1). Together, these parameters determine the amount of deoxyhaemoglobin present in the imaging voxel. This is important as haemoglobin exists in two forms: paramagnetic deoxyhaemoglobin and diamagnetic oxyhaemoglobin (8). The deoxyhaemoglobin concentration within the blood is therefore the major determinant of its magnetic susceptibility, in turn altering the MR signal both within the vessel and around it (1). At rest, arterial blood is nearly fully oxygenated with approximately 40% of the oxygen extracted during its transit across the capillary bed (9,10). This creates a significant amount of deoxyhaemoglobin in the venous and capillary vessels. If, during neural activation, OEF remained constant, the deoxyhaemoglobin concentration would be unchanged, and only small changes in the MR signal would occur as a result of volume exchange effects (11). Fortunately for the neuroimaging community, neural activation is accompanied by a much larger increase in CBF than in $CMRO_2$ (5), resulting in a disproportionate increase in blood oxygenation. As the deoxyhaemoglobin concentration of the blood is decreased, the MR signal is increased, giving rise to the classic positive BOLD response (12). Changes in CBV add to this complexity by altering the total amount of deoxyhaemoglobin in the voxel and also through volume exchange effects, whereby the intravascular *blood* volume replaces extravascular *tissue* volume. The establishment of a firm understanding of the relationship between the BOLD signal and the underlying neurophysiology, including CBF, CBV and $CMRO_2$, remains a challenging yet vital task for the accurate interpretation of fMRI studies.

Modelling the BOLD response

A key component of the calibrated BOLD method is an accurate mathematical model describing how the BOLD signal depends on the underlying physiological changes. We first describe the standard model that typically has been used for the calibrated BOLD method, together with the calibration methods that have been proposed, and then consider some of the potential issues.

The Davis model was originally derived as a basic biophysical model of the dependence of the BOLD signal on changes in deoxyhaemoglobin content (6). The paramagnetic nature of deoxyhaemoglobin results in a large susceptibility difference between deoxygenated blood vessels and the diamagnetic tissue surrounding them. This difference in susceptibility results in microscopic magnetic field gradients outside of the vessels, which enhance the rate of decay of tissue protons that experience them. Theoretical and Monte Carlo numerical analyses of the extravascular change in R_2^* resulting from this effect (δR_2^*) have shown that it is a function of venous CBV (CBV_v, V_0) and the blood concentration of deoxyhaemoglobin ($[dHb]_0$) (13–15). This latter parameter is proportional to the product of Hct and the resting OEF (E_0). The effect of δR_2^* can be intuitively described as the signal difference between the normal resting deoxyhaemoglobin content and the case in which all of the deoxyhaemoglobin has been removed:

$$\delta R_2^* = \kappa V_0 [\mathrm{dHb}]_0^{\beta}, \text{ where } [\mathrm{dHb}]_0 \propto E_0 \mathrm{Hct} \qquad [1]$$

The constant κ incorporates several properties of brain tissue, including vessel geometry, magnetic field strength and the

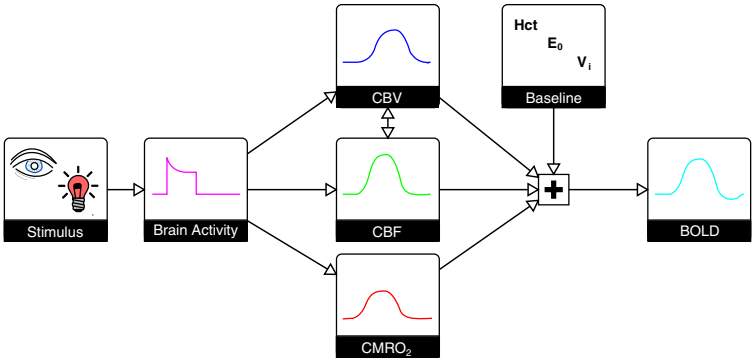

Figure 1. The blood oxygenation level-dependent (BOLD) response is a complex signal. Basic sensory stimuli elicit an increase in neural activity, resulting in an increase in the cerebral blood flow (CBF) and cerebral metabolic rate of oxygen consumption ($CMRO_2$). CBF increases to a larger degree than $CMRO_2$, and also leads to a local increase in the cerebral blood volume (CBV). The amplitude of the resulting BOLD response is not only dependent on these changes, but also on the baseline physiological state. This baseline is determined by the blood haematocrit (Hct), resting oxygen extraction fraction (OEF) and CBV. An increase in CBF causes an increase in the BOLD signal, whereas increases in venous CBV (CBV_v) and $CMRO_2$ cause a decrease. Typically, the CBF effect is dominant, creating a positive BOLD response. The maximum BOLD signal change is determined by the baseline physiological state and increases with increasing Hct, OEF and CBV.

susceptibility difference between blood and tissue. The value of β is described as being dependent on the diameter of the blood vessels involved as a result of diffusion effects around the smallest vessels, with $\beta = 1$ for larger vessels (venules and larger draining veins) and $\beta = 2$ for capillaries (13). Davis *et al.* (6) performed Monte Carlo simulations to determine an average value of β given the distribution of vessel sizes in the brain, and suggested a value of 1.5 for experiments at 1.5 T.

The BOLD signal change can be expressed in terms of the change in R_2^* between activated and rest states (ΔR_2^*), where V and [dHb] are CBV_v and the deoxyhaemoglobin concentration in the activated state, respectively:

$$\Delta R_2^* = \kappa V[\mathrm{dHb}]^\beta - \kappa V_0[\mathrm{dHb}]_0^\beta \quad [2]$$

For small changes in ΔR_2^*, this can be linearised (16):

$$\frac{\Delta S}{S_0} = \mathrm{e}^{-\mathrm{TE}\Delta R_2^*} - 1 \approx -\mathrm{TE}\Delta R_2^* \quad [3]$$

Substituting for ΔR_2^* in Equation [3] leads to:

$$\frac{\Delta S}{S_0} = \mathrm{TE}\kappa V_0[\mathrm{dHb}]_0^\beta\left[1 - \frac{V}{V_0}\left(\frac{[\mathrm{dHb}]}{[\mathrm{dHb}]_0}\right)^\beta\right] \quad [4]$$

This equation describes the basic extravascular physiological changes underlying the BOLD response, including the effect of baseline deoxyhaemoglobin content. This baseline effect is incorporated in a constant $M = \mathrm{TE}\kappa V_0[\mathrm{dHb}]_0^\beta$, representing the maximum signal change, sometimes known as the *ceiling* effect (17).

Traditionally, the measurement of CBV has proved difficult; therefore, in calibrated BOLD, this is generally inferred from measurements of CBF. This assumes a power law relationship $\mathrm{CBV} = k{\cdot}\mathrm{CBF}^\alpha$, where $\alpha = 0.38$ is the classic value assumed from the early work of Grubb *et al.* (18). Following Fick's principle ($\mathrm{CMRO_2} = C_\alpha{\cdot}\mathrm{CBF}{\cdot}E$), Equation [4] can be rewritten in terms of CBF and $\mathrm{CMRO_2}$:

$$\frac{\Delta S}{S_0} = M\left[1 - \left(\frac{\mathrm{CBF}}{\mathrm{CBF}_0}\right)^{\alpha-\beta}\left(\frac{\mathrm{CMRO_2}}{\mathrm{CMRO_{2,0}}}\right)^\beta\right] \quad [5]$$

This is more commonly written in terms of CBF and $\mathrm{CMRO_2}$ normalised to baseline values: f and r, respectively. Here, the fractional change in the BOLD signal ($\Delta S/S_0$) is given the symbol δs:

$$\delta s = M\left[1 - f^{\alpha-\beta}r^\beta\right] \quad [6]$$

This classic Davis model demonstrates the basic dependence of the BOLD response on CBF, the physiological maximum BOLD signal change M and changes in $\mathrm{CMRO_2}$.

Although the parameter α in the Davis model has a relatively straightforward interpretation in terms of venous volume change, the parameter β is more complicated and has led to some confusion. In the original derivation, the physical motivation for $\beta > 1$ was the physics of how localised magnetic susceptibility differences create R_2^* depending on whether diffusion is important ($\beta = 2$, capillaries) or unimportant ($\beta = 1$, veins) (13). However, the Davis model only takes into account extravascular signal changes and, as such, ignores contributions from the intravascular signal change. This contribution could be significant as R_2^* of blood increases quadratically with increasing deoxygenation of haemoglobin (19–21). At magnetic field strengths below 3.0 T, the intravascular signal from the veins represents an important fraction of the BOLD signal and is estimated to be approximately 57% at 1.5 T and approximately 36% at 3.0 T (11). At 7.0 T, the venous signal is negligible in extravascular BOLD-weighted images. However, the effect of deoxygenated capillary blood becomes increasingly important at this field strength and contributes to the increased specificity of spin echo fMRI (22). Fortunately, the Davis model can be adapted to correct for the intravascular signal. Taking $\beta > 1$ provides a mathematical form that captures the basic effect produced by intravascular signal changes because it means that the BOLD response does not depend only on total deoxyhaemoglobin (i.e. V[dHb]). As a simple example of the expected effect of intravascular signal changes, let us suppose that activation induces an increase in blood oxygenation (decreased [dHb]) with an increase in CBV_v (V) which perfectly balances to create no change in total deoxyhaemoglobin: will there be a BOLD signal change? We might expect the extravascular BOLD effect to be minimal because total deoxyhaemoglobin does not change, but we would expect an intravascular BOLD effect because the intrinsic blood concentration of deoxyhaemoglobin is reduced. Because $\beta > 1$, the Davis model predicts a BOLD response for this scenario. Simulations with a much more detailed model of the BOLD response, including mixed effects of both small and large vessels, have found that the Davis model is reasonably accurate despite the limitations of the original derivation. It has also been shown that, if the parameters α and β are treated simply as fitting parameters, the predictions of the detailed model can be approximated more closely with reduced values of α and β. Nevertheless, the original values are reasonably accurate (23). It is important to note, however, that the parameter β captures multiple effects, and should not be interpreted in the way in which it was originally introduced. Other models have sought to directly incorporate intravascular signal changes (24) and measurements of CBV (25), but these methods still rely on the basic Davis model. The quantitative BOLD method developed by Yablonskiy and colleagues (26,27) uses a similar contrast mechanism to calibrated BOLD, but does not rely on the Davis model. In the quantitative BOLD model, the extravascular BOLD signal is effectively modelled by $\beta = 1$. However, $\beta > 1$ is not required to model the intravascular signal as this is an explicit part of the quantitative BOLD model.

The calibrated BOLD method is motivated by the mathematical form of Equation [6], which illustrates the fundamental complexity of the BOLD signal. Even if the values of α and β are assumed to be constant across subjects, there still remains uncertainty in the value of M. Because this parameter captures a number of aspects of the baseline physiological state, which are variable and unknown in most studies, it must be determined individually for a quantitative determination of the $\mathrm{CMRO_2}$ change. It should be noted that, if M is known, a combined measurement of BOLD and CBF signals in response to a stimulus makes it possible to measure the fractional $\mathrm{CMRO_2}$ change from Equation [6]. The goal of the calibration part of the experiment is to measure M.

Hypercapnia calibration

The administration of a hypercapnic gas mixture to the subject is used to elicit a CBF response and concomitant BOLD signal

change with the assumption that only CBF is changed, with $CMRO_2$ unaffected (6). This gas mixture typically consists of 5% carbon dioxide, 21% oxygen and 74% nitrogen (6). Simultaneous measurements of CBF and BOLD during such a challenge are then combined with the Davis model Equation [6] to estimate the calibration parameter *M*:

$$M_{hc} = \frac{\delta s}{1 - f^{\alpha-\beta} r^{\beta}} \quad [7]$$

Subscript 'hc' is used to differentiate this formulation from that of the other calibrations described below. Constants α and β represent flow/volume coupling (18) and the relationship between blood oxygenation and the BOLD signal (13), respectively. Modern practice sets the value of α as 0.2 based on measurements of CBV_v change, the vascular compartment that underlies the BOLD response (28). Similarly, β is chosen to be 1.3 for experiments at 3.0 T (29). The usual assumption that $CMRO_2$ is not altered by hypercapnia corresponds to $r = 1$.

As an alternative to gas administration, hypercapnia calibration has also been performed by means of a breath-hold. Similar changes in the arterial partial pressure of CO_2 (PCO_2) have been reported, but also result in a reduced arterial PO_2 (30). Whether such a stimulus has an effect on resting $CMRO_2$ is an unknown and complex issue. For a realistic breath-hold duration, only mild hypoxia is experienced, which may be at least partially compensated by increases in PCO_2 (31). Reasonable values for M_{hc} have been measured (30,32), with breath-holds of greater than 15 s duration also having been shown to be very reproducible (33). However, an altered arterial PO_2 may confound these estimates by producing an additional arterial signal weighting not present in artificially induced hypercapnia.

Hyperoxia calibration

With the hypercapnia approach to calibration, the idea is to measure the BOLD signal when CBF is varied by a known amount, but $CMRO_2$ is constant. In the hyperoxia approach, the goal is to measure the BOLD signal when venous oxygenation is changed by a known amount, but both CBF and $CMRO_2$ remain constant. In hyperoxia calibration, air with an enhanced oxygen level is administered to the subject (34). Hyperoxic gas mixtures containing between 25% (29) and 100% (34) oxygen have been reported in the literature. Because arterial haemoglobin is nearly fully saturated in normoxia, the extra inhaled O_2 is carried as dissolved gas in plasma. Because of this extra O_2 delivered to tissue, the venous haemoglobin oxygen saturation will increase slightly, producing a BOLD signal change. In the ideal experiment, CBF does not change during the inhalation of the hyperoxic gas mixture, meaning that measurements of CBF are not required to calculate *M*. Here, we use subscript 'ho' to differentiate the hyperoxic calibration parameter. For constant *V*, Equation [4] leads to Equation [8]:

$$M_{ho} = \frac{\delta s}{1 - \left(1 + \frac{\Delta[dHb]}{[dHb]_0}\right)^{\beta}} \quad [8]$$

The value of β takes the same definition as for hypercapnia calibration, leaving only the fractional change in deoxyhaemoglobin concentration ($\Delta[dHb]/[dHb]_0$) to be determined. This is achieved using a model of the oxygen-carrying capacity of the blood and measurements of the end-tidal oxygen partial pressure ($P_{ET}O_2$). These measurements are used to infer the arterial partial pressure of oxygen (P_aO_2) after taking into account the alveolar–arterial oxygen gradient and assuming that arterial blood is well equilibrated with gas in the alveoli (34). [For details on how to perform such calculations, see Xu *et al*. (35).] This latter assumption relies on healthy lung function for its validity. At normoxia, oxygen is mostly carried bound to haemoglobin, with only a small amount dissolved in plasma. The amount of oxygen carried by arterial blood is determined by P_aO_2, which is linearly related for plasma (εP_aO_2) and nonlinearly related by the oxygen dissociation curve for haemoglobin saturation (S_aO_2). This latter component can be approximated by the following relation (36):

$$S_aO_2 = \frac{1}{\frac{23400}{(P_aO_2)^3 + 150 P_aO_2} + 1} \quad [9]$$

As a result of the sigmoidal form of Equation [9], an increase in P_aO_2 caused by hyperoxia causes only a slight increase in S_aO_2. However, an increase in P_aO_2 results in a much larger increase in the amount of oxygen carried by the plasma, such that, during hyperoxia, the plasma contributes to a greater degree to the total delivery of oxygen than during normoxia. As blood passes through the capillary bed, the extraction of the excess oxygen in plasma offsets the extraction of oxygen bound to haemoglobin, so that, overall, the venous haemoglobin saturation increases. Regardless of the increase in oxygen carried by arterial plasma, the amount of oxygen carried by venous plasma remains small, as the venous partial pressure (P_vO_2) is low. Therefore, the assumption that P_vO_2 is negligible should not result in a large error, allowing $\Delta[dHb]/[dHb]_0$ to be estimated as:

$$\frac{\Delta[dHb]}{[dHb]_0} = \frac{\phi[Hb]\Delta S_aO_2 + \varepsilon \Delta P_aO_2}{\phi[Hb](1 - S_aO_2(1 - E_0)) - \varepsilon P_aO_2(1 - E_0)} \quad [10]$$

where ϕ is the oxygen-carrying capacity of haemoglobin (1.34 mL O_2/g Hb), ε is the solubility coefficient of oxygen in plasma (0.0031 mL O_2/dL/mmHg) and ΔS_aO_2 and ΔP_aO_2 are the changes in these parameters as a result of hyperoxia relative to normoxia. For the calculation of M_{ho}, the haemoglobin concentration ([Hb]) is assumed to be 15 g Hb/dL (29,34) and the resting OEF (E_0) is assumed to be 0.3 (29). Essentially, these assumed values amount to a strong assumption that the venous deoxyhaemoglobin concentration in the baseline state is the same for all brain regions and all subjects. However, as [Hb] is related to Hct (Hct $\approx 0.03 \times$ [Hb]), which is known to vary amongst subjects, this may be a source of error. In addition, this value of OEF is lower than the value of 0.4 generally reported (10), and OEF may well vary across the brain, particularly in disease. Unfortunately, CBF has been observed to decrease during hyperoxia (37). In this case, an additional measurement of CBF can be used to perform a correction for this effect (34):

$$M_{ho} = \frac{\delta s}{1 - f^{\alpha}\left(\frac{\Delta[dHb]}{[dHb]_0} + \frac{r}{f}\right)^{\beta}} \quad [11]$$

Here, $\Delta[dHb]/[dHb]_0$ reflects changes in the venous deoxyhaemoglobin concentration resulting from an increase in P_aO_2, and r/f accounts for changes that result from an alteration of $CMRO_2$ or CBF. It is assumed that $CMRO_2$ does not change during

hyperoxia ($r = 1$). Although there is still debate about the validity of this assumption, the change in $CMRO_2$ is generally thought to be small (34,38).

R_2' calibration

Although calibration can be performed without the administration of gases by asking the subject to hold his or her breath, it is also possible to calibrate the BOLD response without performing any respiratory manipulation at all, thereby avoiding physiological confounders, such as changes in CBF and $CMRO_2$. One way to achieve this is by estimating the baseline deoxyhaemoglobin content through a measurement of the relaxation properties of brain tissue (39,40). More specifically, the sensitivity of different aspects of transverse relaxation to deoxygenated blood vessels within brain tissue is exploited to make this possible. Transverse relaxation can be separated into processes that may be refocused by a spin echo and those that cannot, where R_2 is the irreversible relaxation and R_2^* is the sum of the reversible and irreversible decay. The difference between these quantities is R_2' (reversible relaxation alone). This parameter is sensitive to magnetic field inhomogeneity from several sources that act at different length scales. The macroscopic scale represents distances that are greater than the voxel dimension and result from differences in susceptibility at boundaries, e.g. the air–tissue interface. At the opposing extreme, the microscopic scale represents processes that occur at the atomic and molecular level. The space between these scales is defined as the mesoscopic scale. Importantly, at this scale, deoxygenated blood vessels cause local magnetic field inhomogeneities in the tissue. The magnitude of these fields, and hence their effect on the MR signal, is proportional to the deoxyhaemoglobin content of the voxel.

As a motivation for the use of R_2' to estimate M, we note that *if* all of the effects underlying the BOLD response were reversible with a spin echo, then δR_2^* in Equation [1] (the change in R_2^* caused by the presence of deoxyhaemoglobin) would be R_2'. From this, it follows that M is simply TE multiplied by R_2' in the baseline state:

$$M_{R'_2} = \mathrm{TE}\kappa V_0[\mathrm{dHb}]_0^{\beta} = \mathrm{TE}R'_2 \qquad [12]$$

Again, the subscript 'R_2'' is used to differentiate this definition of M from the two previous definitions. It is interesting to note that, in this definition, a value of β is not required as it is inherent in the measurement of R_2'. As an additional benefit, this method does not alter resting $CMRO_2$ or CBF, as may be the case with hypercapnia or hyperoxia. The central problem with this general argument, however, is that the effects leading to ΔR_2^* are not all reversible. The diffusion-dependent simulations of Ogawa (13) suggest that both reversible and irreversible components exist, and perhaps, more importantly, intravascular signal changes at long refocusing intervals are expected to be largely irreversible. Nevertheless, simulations with a detailed model of the BOLD response suggest that these other effects approximately scale with R_2' in the baseline state (40). However, R_2' is also sensitive to the macroscopic field inhomogeneity caused by air–tissue susceptibility gradients in the head. To be a viable calibration method, the effects of this large-scale field inhomogeneity must be removed from the measurement of R_2' in order to accurately estimate the baseline physiological state.

PRACTICAL IMPLEMENTATION

Multimodal imaging: combining measurements of BOLD and CBF

Calibrated BOLD relies on an inherently multimodal approach to imaging. Although the complexity of the BOLD response creates difficulties for the interpretation of the experimental results, when combined with measurements of CBF (and/or CBV) this complexity becomes an advantage. This combination allows changes in $CMRO_2$ to be investigated given a suitable mathematical framework (6,17,25). Measurements of CBF can be made using a range of ASL techniques. The specific details of the ASL method will not be covered here, as they are covered elsewhere in this special issue, but issues relevant to calibrated BOLD are discussed.

Although, initially, ASL and BOLD data were acquired in separate experiments (6), it is now far more common to acquire both within the same experiment. This is achieved in one of two ways: interleaved or single shot. In the interleaved method, the ASL and BOLD data are acquired from separate excitations, e.g. ASL tag image, BOLD image, ASL control image, BOLD image (16,30,34). The benefit of this approach is that images can be acquired at the optimal TE for each of the modalities. For ASL, the shortest attainable TE should be used (41), whereas it has been shown that the BOLD response is maximised when $\mathrm{TE} = T_2^*$ (42). However, as this is a combination of two experiments, the ultimate temporal resolution is reduced, with a minimum around 4.5 s (30). The single shot method enables a higher temporal resolution by acquiring both ASL and BOLD from the same excitation (29,43–47). ASL and BOLD signals are disentangled by performing a surround subtraction or addition, respectively (48–50). In the simplest implementation of this method, a single echo is used with a TE selected as a trade-off between the optimal ASL or BOLD TE (29,45,47). However, a dual echo approach is recommended, giving more accurate CBF and BOLD measurements, as well as a greater degree of independence between datasets (43,44,51).

The term 'arterial spin labelling' applies to a collection of techniques developed to isolate and quantify the component of the MR signal that is derived from inflowing arterial blood delivered to capillary beds within the image voxel. The modelling of this signal can be performed to quantify local perfusion, more commonly referred to as 'CBF' (41). Many different perfusion-sensitive techniques have been created since the development of the first ASL method in 1992 (52), and each possesses a unique set of features designed to address one or more challenges associated with the measurement of CBF. These techniques can be broken down into two categories: pulsed ASL (PASL) (53) and continuous ASL (CASL) (52). Currently, the PASL technique is most commonly used in calibrated BOLD experiments, although CASL methods are seeing a resurgence with pseudo-continuous ASL (PCASL) methods (54). In the context of calibrated BOLD, it is important to consider several systematic errors that must be accounted for if accurate measurements of CBF are to be made. Of particular importance are the tagging efficiency, alterations to the T_1 of blood and accounting for transit delays. These sources of error have different implications for PASL and CASL techniques. In the latter case, we only consider PCASL, as CASL is rarely used in practice.

The tagging efficiency describes the effectiveness of a tagging pulse (or pulse train) at producing a bolus of blood with fully inverted magnetisation. This is an assumed value within the

model used to quantify perfusion, required for the accurate measurement of CBF in physiological units (41). However, for calibrated BOLD, a measurement of absolute CBF is not necessary, as fractional changes are the only requirement of the Davis model Equation [6]. Therefore, as long as the tagging efficiency is constant throughout the experiment, its precise value is no longer important. A decreased tagging efficiency will, however, result in reduced signal-to-noise ratio in the acquired data. This assumption is valid for PASL techniques, but may be problematic for PCASL, which relies on a flow-driven inversion and is therefore dependent on the velocity of blood in the arterial blood vessels at the tagging location (55). Under most experimental conditions, this velocity will remain fairly constant; however, under hypercapnia, a large increase in blood velocity within the internal carotid and vertebral arteries has been observed (55). It has been suggested that this will result in a reduced tagging efficiency, which will lead to a reduced fractional change in CBF.

The T_1 of arterial blood is similarly important in the quantification of CBF, and is assumed to be constant (41). Again, in general, this is a fair assumption, except under hyperoxia, where T_1 is known to be shortened by the presence of paramagnetic oxygen within the plasma (56,57). If this reduction in T_1 is not accounted for in the analysis, the expected flow reduction will be overestimated (37). This problem will affect both PASL- and PCASL-based techniques.

Finally, a key requirement of any ASL sequence is to produce a bolus of tagged blood with a well-defined temporal width and to ensure that the timing of the sequence allows for all of the tagged blood to be delivered to the tissue by the time images are acquired (48). An important problem in meeting this latter requirement is the variability of the transit delay time of arterial blood: the time required for blood to move from the tagging plane to the capillaries of the imaging voxel. The goal in an ASL experiment is to create a well-defined bolus of tagged blood and to wait a sufficiently long time for that bolus to clear from the large arteries and be delivered to the microvasculature within the image voxel. If the time between tagging and imaging is too short (i.e. an insufficiently long inversion time), regional CBF will be inaccurately measured. This will lead to an overestimation of CBF if tagged blood remains in the arterial macrovasculature. However, if the large vessel blood signal is suppressed, most commonly by the application of diffusion weighting, CBF will be underestimated, as not all of the tagged bolus has been delivered to the tissue at the time of imaging. In addition, the transit delay is not uniform across the brain, requiring that this variability must be accounted for in multislice imaging (58,59). This effect has the potential to affect both PASL and PCASL techniques.

Multimodal imaging: incorporating measurements of CBV

The incorporation of a measurement of CBV removes the assumptions about CBF/CBV coupling, but is complicated by the need to measure the volume change within the vascular compartment that underlies the BOLD response, primarily CBV_v. Techniques to measure CBV (60) predate both BOLD (1) and ASL (52) techniques. However, typically, they are sensitive to the total blood volume, i.e. the sum of arterial, capillary and venous volumes. In humans, these methods include gadolinium-based contrast agent techniques (61,62), as well as endogenous contrasts, such as vascular space occupancy (VASO) (63). Unfortunately, it has been shown that, during the active condition, arterial volume changes are proportionately larger than venous changes (64–66), and hence these techniques have the potential to overestimate the contribution of CBV_v to the BOLD response.

Formerly, it was assumed that the majority of blood volume change occurs in venous vessels (12,67). This motivated some researchers to incorporate a measurement of CBV into their calibrated protocol using the VASO technique (25,68). This provides a very elegant protocol, as it is possible to measure CBF, CBV and BOLD in a single experiment using a combined pulse sequence (69). However, the data of Lin *et al.* (25) suggest that $\alpha = 0.62$, given a 68% increase in CBF and a 38% increase in CBV. This is consistent with positron emission tomography (PET) measurements of CBF/CBV coupling, where $\alpha = 0.64$ was measured for total CBV in cortical grey matter (70). A larger value of α is consistent with a larger increase in CBV relative to CBF, which we would expect to be the case if arterial blood volume changes dominate.

To address this issue, new methods have been developed to specifically measure CBV_v. The venous refocusing for volume estimation (VERVE) method has been used to measure CBF/CBV_v coupling during neuronal activation (28) and in response to a hypercapnia challenge (71). However, this method is not easily incorporated into an ASL–BOLD pulse sequence and hence cannot be acquired simultaneously. CBV_v has also been measured using hyperoxia as a contrast agent (72,73), and has recently been incorporated into a calibrated BOLD measurement (74). Similar to VERVE, this method cannot be simultaneously acquired alongside ASL and BOLD data, as it requires BOLD-weighted data acquired at normoxia and hyperoxia. Finally, a new technique based on the principles of the VASO method has been developed to selectively image arterial CBV, known as inflow-based VASO (75). In combination with conventional VASO, this technique allows CBV_v to be estimated, but is critically dependent on accurate quantification in both methods.

Respiratory challenges

Hypercapnia and hyperoxia calibrations require the administration of gases to the subject, breath-holding excepted. There are many ways in which respiratory challenges can be performed, but they can largely be placed into two categories: those that present a gas with a fixed composition and those that target a specific end-tidal partial pressure of carbon dioxide ($P_{ET}CO_2$) or oxygen ($P_{ET}O_2$). The former methods benefit from experimental simplicity, whereas the latter provide greater repeatability across sessions and between subjects. A brief summary of both approaches is now presented.

The fixed inspired hypercapnia challenge is typified by the use of a non-rebreathing mask connected to a large gas reservoir (Fig. 2a). A non-rebreathing mask ensures that the subject breathes in the prescribed CO_2 concentration. However, such a system does not control for the large difference in ventilatory response observed across the population (76). This can lead to large differences in $P_{ET}CO_2$ across subjects. Periods of normocapnia are interleaved with periods of hypercapnia in a block design by switching between room air and a premixed gas mixture. As noted above, hypercapnia calibration typically utilises a 5% CO_2–21% O_2–74% N_2 mixture (6), but other variations have also been employed. A lower 4% CO_2–21% O_2–75% N_2 mixture is used by some to mitigate the effects of any accompanying $CMRO_2$ reduction (30), whereas much higher 10% CO_2–90% O_2 carbogen mixtures have also been used to provide a more direct

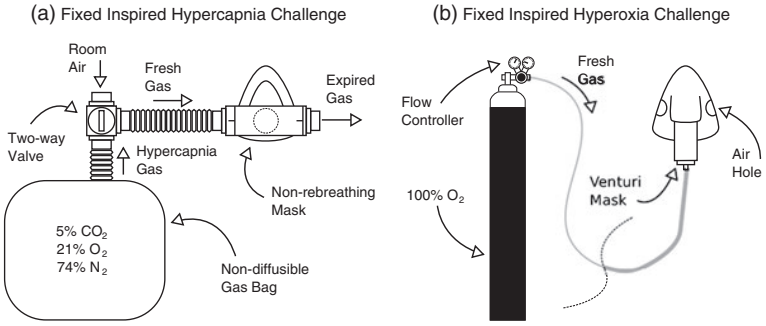

Figure 2. Schematic diagrams of the apparatus typically used to generate a fixed inspired hypercapnia challenge (a) and a fixed inspired hyperoxia challenge (b). In (a), a manually actuated valve enables the inspired gas to be switched between room air and a 5% CO_2–air mixture, whereas, in (b), during baseline subjects breathe room air through holes in the mask and hyperoxia is induced by allowing 100% O_2 to flow into the mask. Mixing with entrained room air reduces the inspired fraction of oxygen to approximately 50%.

measurement of M by attempting to increase CBF to such a degree that deoxyhaemoglobin is completely washed out in order to produce the maximum possible BOLD signal (51).

With a fixed inspired hyperoxia challenge, a non-rebreathing mask is normally replaced with a standard venturi mask, or a nasal cannula (Fig. 2b). In both cases, 100% O_2 from a pressurised source is delivered to the mask/cannula, where it mixes with air entrained from the room, resulting in an O_2 concentration of approximately 50%. Interleaved blocks of normoxia and hyperoxia are achieved by switching off the oxygen source during normoxia, causing the subject to breathe room air through holes in the mask, and re-establishing flowing oxygen during hyperoxic periods. In a similar manner to the fixed inspired hypercapnia challenge, the final $P_{ET}O_2$ is dependent on each individual's ventilatory response to the hyperoxic gas mixture.

There are two end-tidal targeting methods currently in use with MRI that rely on either feedback (77,78) or feedforward (79) algorithms coupled to a computer-controlled gas mixer. Basically, the feedback method works by analysing the gas composition of the preceding breath of a subject and adjusting the composition of the inflowing fresh gas to force the end-tidal value towards the targeted value in the following breath. Hence, this method is often referred to as 'dynamic end-tidal forcing'. This method requires fast gas analysers, and gas mixing must be performed close to the subject in order for rapid changes in composition to be made (Fig. 3a). The feedforward method relies on a model of alveolar gas exchange and the principles of sequential gas delivery. The inspired gas composition required to reach the targeted end-tidal value is determined prior to the start of the experiment. Gases are mixed outside of the magnet room and conveyed over gas lines to a sequential gas delivery mask worn by the subject (Hi-Ox[80], VIASYS Healthcare, Yorba Linda, CA, USA) (Fig. 3b). However, this method requires values for each subject's metabolic rates of CO_2 production and O_2 consumption. These can be estimated from a look up chart, and are often refined by performing several test runs. For hypercapnia, calibration changes in $P_{ET}CO_2$ between 3 and 9 mmHg have been performed, whereas, for hyperoxia, changes in $P_{ET}O_2$ between 140 and 340 mmHg have been used (29). The advantage of using an end-tidal targeting method is that this targeted $P_{ET}CO_2/O_2$ level is independent of each subject's ventilatory response, unlike fixed inspired challenges, giving rise to reduced intersession and intersubject variability (80,81).

Relaxometry

There are two main ways to measure R_2'. Both methods exploit an asymmetric spin echo (ASE), but differ in how the images are acquired. We refer to these methods as single shot ASE (82) and gradient echo sampling of spin echo (GESSE) (26). The ASE experiment is a modification of the spin echo experiment, in which a 180° refocusing pulse is applied at TE/2 and the signal is acquired at TE. In the ASE experiment, the signal is still acquired at TE, but the 180° pulse is shifted in time by $\tau/2$. This results in a spin echo being formed at TE – τ, and hence the signal is acquired with additional R_2' weighting. However, it will also include additional signal decay as a result of the macroscopic magnetic field inhomogeneity, leading to the attenuation factor F, which is similarly a function of τ:

$$S_{ASE} = S_0 e^{-TER_2} e^{-\tau R'_2} F(\tau) \quad [13]$$

For a linear through-plane gradient under the assumption of a square slice profile, this attenuation factor can be described by a sinc function (26):

$$F(\tau) = \frac{\sin(\tau\Delta\omega/2)}{\tau\Delta\omega/2} \quad [14]$$

where $\Delta\omega$ is the frequency difference across the voxel. This is a function of the gradient (G_z) and the slice thickness (Δz), where γ is the gyromagnetic ratio for hydrogen.

$$\Delta\omega = \gamma G_z \Delta z \quad [15]$$

Therefore, care must be taken to account for the macroscopic field inhomogeneity. This is typically achieved by acquiring a high-resolution field map, calculating the derivative in the slice direction and correcting the intensity data using Equations [13]–[15] (26,27,83).

For single shot ASE, images are acquired using echo planar (82) or spiral (84) imaging techniques (Fig. 4a). Multiple

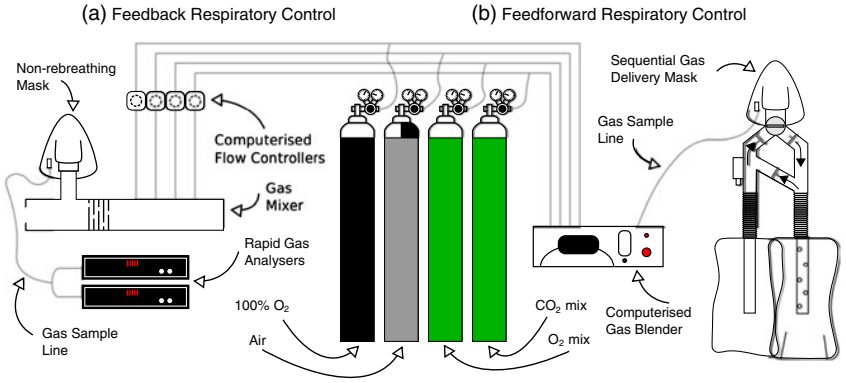

Figure 3. Schematic diagrams of the automated respiratory challenge apparatus currently in use with feedback (a) and feedforward (b) algorithms. The feedback algorithm works by analysing the gas composition of the preceding breath and adjusting the composition of the inflowing fresh gas to force the subject's end-tidal values towards the targeted values in the following breath. The feedforward algorithm works by calculating the required gas composition to reach the given target end-tidal values using a model of alveolar gas exchange prior to the start of the experiment.

experiments are performed with different values of τ, whilst keeping TE constant. As a constant TE leads to constant R_2 weighting Equation [13], R_2' is easily measured by plotting S_{ASE} *versus* τ. However, correction for the magnetic field inhomogeneity can only be performed by acquiring a field map in a separate imaging experiment.

At first glance, the image acquisition for the GESSE technique may seem to be remarkably similar. The switched gradient of the echo planar imaging sequence is retained, but rather than playing a blipped phase encode prior to each *k*-space line traversal, phase encoding is applied before the switched gradient and is incremented with each repetition of the whole sequence. Multiple shots are therefore required to cover the whole of *k* space. In this way, it is akin to a multi-echo spin warp sequence with the addition of spin echo refocusing (85). Lines of *k* space with the same effective TE are grouped together and reconstructed to form many images with a short interecho spacing. Unlike single shot ASE, both TE and τ are varied simultaneously, requiring that both R_2 and R_2' be fitted. There are two ways of achieving this: simultaneous fitting of R_2 and R_2' using Equation [13] (26) or fitting for R_2 first, then R_2' (86). In the latter method, pairs of echoes either side of the spin echo are divided to remove R_2' weighting and plotted *versus* 2τ to measure R_2. On removing the R_2 effect from the original data, R_2' can be measured. Despite a more complicated fitting procedure, the data generated by the GESSE experiment can also be used to produce a field map without increasing the acquisition time (83,87). This can then be used to correct for the magnetic field inhomogeneity.

Finally, the temporal characteristics of the signal decay must also be considered when measuring R_2'. It has been shown that, for small values of τ, i.e. at points close to the spin echo, the signal decay is quadratically exponential, whereas, at longer τ, it reverts to the more usual monoexponential decay (14). This behaviour is a result of the susceptibility difference between deoxygenated blood within blood vessels and the surrounding tissue. This results in magnetic field gradients in tissue causing additional signal decay of tissue protons, and is the origin of the extravascular BOLD signal. This regime can be avoided by choosing values of $\tau \geq 1.5\ t_c$, where t_c is dependent on the geometry of the vessels (4/3), the gyromagnetic ratio of hydrogen (γ), the magnetic field strength (B_0), the susceptibility difference between purely deoxygenated blood and tissue ($\Delta\omega$) and the venous blood oxygen saturation (Y):

$$t_c = \frac{1}{\frac{4}{3}\pi\gamma B_0 \Delta\chi(1-Y)} \quad [16]$$

Typical values predict t_c to be of the order of 20 ms at 1.5 T and 10 ms at 3.0 T (14). Hence, at 3.0 T, only data with $\tau > 15$ ms should be used for the calculation of R_2'.

POTENTIAL SOURCES OF ERROR

Hypercapnia calibration

Hypercapnia calibration relies on the assumption that hypercapnia is an isometabolic stimulus, i.e. it does not alter $CMRO_2$. Hence, in Equation [7], r is assumed to be unity. However, recently, it was observed that the inhalation of a 5% CO_2 mixture causes an appreciable reduction in resting metabolism (88). Using a combination of the T_2 relaxation under spin tagging (TRUST) method and phase contrast flow measurements, a 13.4% drop in $CMRO_2$ was measured. This is consistent with intracortical recordings that show a reduction in spontaneous neuronal activity during hypercapnia (89). In this case, inhalation of a 6% CO_2 mixture resulted in an approximately 15% reduction in multiunit activity. It must be noted, however, that the blood CO_2 levels reached in these artificially ventilated animal experiments will be higher than those expected in free-breathing humans, as humans are able to increase their ventilation rate and lower their PCO_2. Conversely, measurements using a susceptometry-based oximetry method did not observe any change in $CMRO_2$ in response to a 5% CO_2 challenge (90). A recent study with magnetoencephalography (MEG) found a fractional decrease in MEG power in the gamma band of 11% with the inhalation of 5% CO_2 in humans (91). Assuming that this translates to an equal fractional reduction in $CMRO_2$, the authors

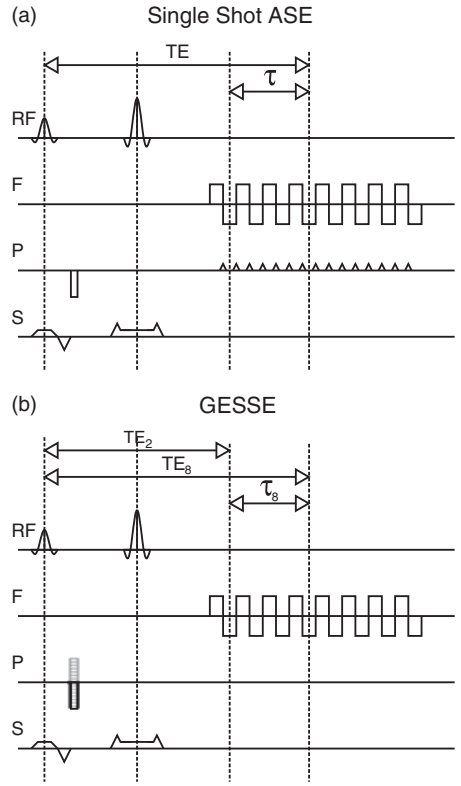

Figure 4. Pulse sequence diagrams for the most common asymmetric spin echo (ASE) methods: (a) single shot ASE; (b) gradient echo sampling of spin echo (GESSE). The methods look very similar, but differ in the way in which phase encoding is applied. For the single shot approach, phase encoding is incremented between *k*-space traversals in the frequency encode direction using a phase encoding *blip*. The GESSE method takes a multi-shot approach in which phase encoding is applied prior to the switched frequency encoding gradient. Each lobe of this gradient produces multiple echoes with the same phase encoding. This phase encoding is then incremented across repetitions to fully sample *k* space.

estimated the degree to which the assumption of isometabolism with CO_2 inhalation affects the estimates of $CMRO_2$ change.

The question of the degree of $CMRO_2$ reduction with mild hypercapnia requires further study, but this is an important concern for the accuracy of the hypercapnia calibration. Reduced resting $CMRO_2$ would lead to an overestimated M_{hc} value and, in turn, an overestimated stimulus-evoked $CMRO_2$ change. To estimate the magnitude of this error, we can substitute standard literature values into Equation [7], assuming $r = 1$ (no $CMRO_2$ change) or $r = 0.87$ (13% reduction in $CMRO_2$). With a true M_{hc} of 6.4%, a flow change caused by hypercapnia of 44% [cf. ref. (29)] and α/β = 0.2/1.3, the value of M_{hc} is predicted to be 35% overestimated. Given a 1.2% stimulus-evoked BOLD response and accompanying 48% flow change, this results in an approximately 5% overestimation of the stimulus-evoked $CMRO_2$ change. As a result of the nonlinear form of the Davis model, this error could vary considerably for different conditions, i.e. different BOLD/CBF changes, values of α and β, etc.

Hyperoxia calibration

It has also been observed that hyperoxia may alter resting $CMRO_2$ (38). In this work, a 10% reduction in $CMRO_2$ was observed in response to a 50% O_2 mixture. However, stimulus-evoked $CMRO_2$ changes have been shown to be unaltered by the inhalation of 100% O_2 (92), and PET data acquired in patients with traumatic brain injury showed no change in resting $CMRO_2$ (93).

Assuming, for the sake of argument, that $CMRO_2$ is reduced during hyperoxia, then M_{ho} will be overestimated in the calibration experiment. In turn, this will cause the stimulus-evoked $CMRO_2$ change to be overestimated. The same approach as for hypercapnia calibration can be used to estimate this error with a hyperoxic $r = 0.9$. Following the data analysis approach of Mark *et al.* (29) and using their measured M_{ho} value of 5.2% as truth, we found that M_{ho} was overestimated by 53%. This results in an 8% overestimate of the change in $CMRO_2$. These estimates include the same caveats as mentioned for hypercapnia.

In addition to the assumption of isometabolism, hyperoxia-calibrated BOLD requires strong assumptions about the baseline physiology of the subject. In order to calculate the change in deoxyhaemoglobin concentration ($\Delta[dHb]/[dHb]_0$) using Equation [10], values for the total haemoglobin concentration ([Hb], approximately equivalent to Hct/0.03) and OEF (E_0) are required. The former is standardly assumed to be 15 g Hb/dL (Hct $\approx$ 0.45) (29,34), whereas the latter is assumed to be 0.3 (29). This value of OEF is lower than generally reported values of 0.4 in the PET literature (10). Recent simulations have shown that these assumed values do not enable hyperoxia calibration to account for differences in physiological baseline across the population (40). Figure 5 propagates these errors through to the measurement of the stimulus-evoked $CMRO_2$ change for three different levels: 10%, 20% or 30% increase in $CMRO_2$. Random combinations of the variables Hct, E_0 and V_i (total CBV) were selected from the following ranges: Hct = 0.37–0.50, $E_0 = 0.3$–0.55 and $V_i = 0.01$–0.10. Each point in Fig. 5 represents one of these combinations, with corresponding BOLD responses and *M* values calculated for each combination [see ref. (40) for further details]. The effect of this variability on the standard hyperoxia calibration approach can be seen in Fig. 5a. It is not possible to distinguish different lines of $CMRO_2$ change, apart from very low CBF changes. In contrast, when the values of Hct and OEF are known, and can be substituted into Equation [10], this variability is drastically reduced (Fig. 5b). For comparison, Fig. 5c displays the simulation for hypercapnia calibration in which assumptions about baseline physiology are not required. Unfortunately, information about local OEF is not easy to obtain, even though the systemic Hct is easily measured from a sample of the subject's blood. Whole brain measurements of OEF can be made using the TRUST technique by measuring the oxygen saturation of blood in the sagittal sinus (94). Local information regarding vessel geometry and CBV_v can then be retained by substituting this information into Equation [10], although spatial information will inevitably be lost because of the use of a global value of OEF.

Finally, as noted above, the presence of paramagnetic oxygen in plasma causes a reduction in blood T_1 that confounds the estimation of CBF using ASL. This effect has additional implications for BOLD measurements using rapid gradient echo

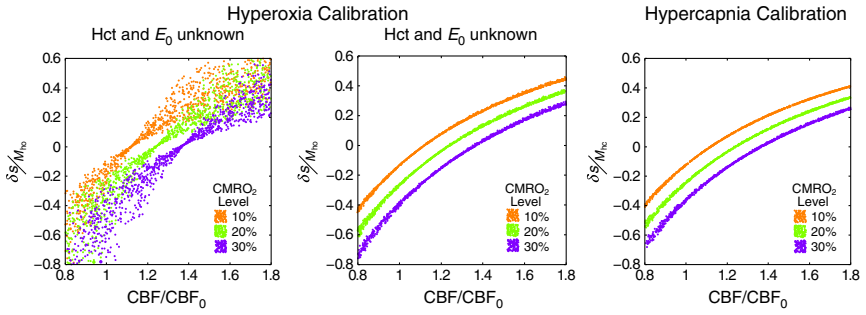

Figure 5. Simulation of the effect of baseline physiological variability on two calibration methods. (a) Using the standard approach to hyperoxia calibration results in a high degree of uncertainty in the resultant measurement of the cerebral metabolic rate of oxygen consumption ($CMRO_2$) because of the use of an assumed haematocrit (Hct) and resting oxygen extraction fraction (OEF). The blood oxygenation level-dependent (BOLD) signal change normalised by the BOLD scaling parameter (δ S/M) is plotted against the change in cerebral blood flow (CBF) normalised to baseline (CBF_0). (b) If these values are known on an individual subject basis, this uncertainty is markedly reduced. (c) For comparison, the standard approach to hypercapnia does not suffer from the same uncertainty as it does not require assumptions about baseline physiology.

imaging. However, typically, the repetition time of ASL/BOLD acquisitions is greater than 2.4 s, where such T_1 effects will be insignificant.

R_2' calibration

Although R_2' calibration does not require assumptions of isometabolism or physiological baseline, it is sensitive to macroscopic field inhomogeneity. This residual field distortion is caused by susceptibility differences within the head, i.e. at the nasal sinuses, where tissue and air have very different susceptibilities. The resulting ASE signal Equation [13] therefore suffers an additional attenuation (F) which is dependent on the magnitude of the magnetic field gradient across the slice and the value of τ. This is evidently a potential source of error in R_2' calibration and could lead to an overestimation of $M_{R_2'}$ and the stimulus-evoked $CMRO_2$ change. Assuming $M_{R_2'}$ = 6.4% [i.e. equivalent to M_{hc} in ref. (29)] would require an R_2' value of 2.14 s^{-1} given the standard BOLD-weighted TE of 30 ms Equation [12]. Taking a typical frequency difference across a voxel of 20 s^{-1} (40), this would increase R_2' to 2.64 s^{-1}. Consequently, $M_{R_2'}$ is overestimated by 24% and the stimulus-evoked $CMRO_2$ change by 3%. This estimation is based on the same BOLD and CBF changes as used for the other calibrations, and is subject to the same provisos.

As a consequence of acquiring $M_{R_2'}$ in the resting condition, it is likely that it will be underestimated with respect to M_{hc}. This is a result of the use of a 180° radiofrequency pulse and its efficiency at refocusing the dephasing of protons surrounding vessels of different scales. This effect is characterised by two regimes: static dephasing and motional narrowing. In the former regime, protons are considered to be static with respect to deoxygenated blood vessels. Under this condition, the amount of phase accrued before and after the refocusing pulse is equal but opposite in sign, enabling the signal to be refocused. In practice, to satisfy this condition, the proton must only diffuse a small distance relative to the diameter of the blood vessel to retain its spin history. However, in the motional narrowing regime, the diffusion length of the proton is large compared with the vessel diameter and, as such, will sample a large number of different field gradients. In this case, the spin history of the proton is lost and the signal cannot be recovered. Equation [1] models this effect through the parameter β, with $\beta = 1$ for static dephasing and $\beta = 2$ for motional narrowing. The transition between these regimes occurs around a diameter of approximately 7 μm, with capillaries below this threshold and venules and larger draining veins above it. In addition, the motional narrowing regime is at play within the vessels in which proton diffusion lengths are greater than the diameter of the deoxyhaemoglobin-containing red blood cells. Therefore, we expect to be missing extravascular signal contributions from capillaries and intravascular signals from blood. Following the simulation methodology of Blockley *et al.* (40), we can calculate this underestimate for a reasonable range of physiological variability: Hct = 0.37–0.50, E_0 = 0.3–0.55 and V_i = 0.01–0.10. Figure 6 plots

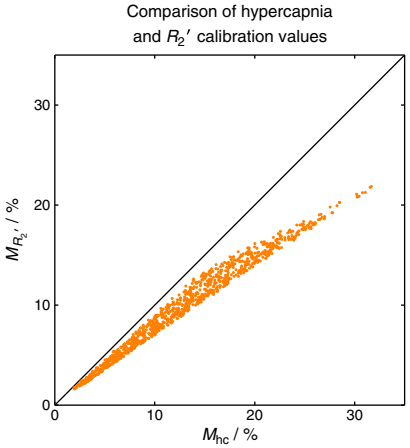

Figure 6. Simulation of blood oxygenation level-dependent (BOLD) scaling parameter M for the hypercapnia and R_2' calibration methods. As a result of the effect of diffusion around capillaries, the spin echo refocusing pulse is unable to recover signal lost to dephasing around these vessels. Therefore, R_2' calibration will give a value of M that is lower than that measured using hypercapnia. Further simulations suggest that the required scaling between these methods is relatively stable across different physiological baseline conditions.

the results of the generation of M values for each random combination of physiological parameters. Although $M_{R_2'}$ tracks linearly with M_{hc}, it is not directly proportional. Fitting to this data reveals that the value of $M_{R_2'}$ is only approximately 75% of M_{hc}. However, simulations to assess the variability of this scaling with variations in physiology have shown this value to be relatively stable (40).

Finally, R_2' calibration assumes that deoxyhaemoglobin is the dominant source of paramagnetism in the brain (95). However, the presence of another source of paramagnetism is not sufficient to confound the use of R_2' as a calibration. The geometry of the inclusion determines its effect on R_2', with maximal effect when the length scale of the deposit is in the static dephasing regime. This dimension is approximately equivalent to a cylinder with a radius of 7 μm, but falls away rapidly with reduced radius (15). There are two main conditions in which an elevated R_2' has been measured as a result of paramagnetic deposits: Parkinson's disease and brain haemorrhage. Parkinson's disease is known to result in increased deposition of iron in the substantia nigra, consisting of neuromelanin granules and iron-filled Lewi bodies (96). This has been shown to result in elevated R_2' measurements (97). Brain haemorrhage causes bleeding into the extravascular space and the production of haemosiderin, leading to an increase in R_2' (98). Care must be taken when performing R_2' calibration in individuals with these conditions. Other brain iron sources, such as ferritin and transferrin, have sufficiently small dimensions such that they do not exhibit an R_2' effect as a result of motional narrowing. For example, changes in R_2 are measured in Alzheimer's disease, but changes in R_2' have not been reported, suggesting that iron inclusions in this disease are in the motional narrowing regime. Further work is required to examine other diseases in which iron is thought to be deposited for their effect on R_2', such as multiple sclerosis, Huntington's disease, neuroferritinopathy and Friedrich's ataxia.

CBF/CBV coupling

In general, changes in CBV are inferred from measurements of CBF in the calibrated BOLD experiment (6). This is achieved by assuming a power law relationship between CBF and CBV based on the animal work performed by Grubb *et al.* (18); hence, the exponent is often referred to as the Grubb constant α:

$$\upsilon = f^{\alpha} \qquad [17]$$

Here v and f are the normalised changes in CBV and CBF. Grubb *et al.* measured α to be 0.38. Recently, work based on measurements of CBV_v, the vascular compartment that underlies the BOLD response, have caused this value to be revised to between 0.18 and 0.23 (28,71). However, these values only represent the mean coupling ratio and, in practice, there could be substantial variation across subjects. A recent simulation study examined the sensitivity of the Davis model to the value of α, alongside other physiological parameters (23). Although α was not the largest driver of variation in M, it was shown to cause the largest error in the estimate of the change in $CMRO_2$. Further simulations showed that this error was not as large for hypercapnia calibration as for hyperoxia and R_2' calibrations (40). This is presumably a result of the inclusion of α in both the calibration Equation [7] and $CMRO_2$ estimation Equation [6] steps of hypercapnia calibration, leading to some compensation for inaccuracies in the value of α.

APPLICATIONS

Coupling of CBF and $CMRO_2$

A number of studies have investigated the variability in the coupling of CBF and $CMRO_2$. This is often characterised by the parameter n, the ratio of the fractional changes in CBF and $CMRO_2$:

$$n = \frac{f-1}{r-1} \qquad [18]$$

One study investigating the reproducibility of calibrated BOLD studies found that the value of n was more reproducible than the values of the CBF and BOLD responses themselves, consistent with the idea that a subject's response to the same stimulus could vary day to day, but the CBF/$CMRO_2$ coupling ratio is more stable (99). In comparing different reported values of n, it is important to keep in mind the potential biases in these measurements related to the estimate of M (43,100): for given CBF and BOLD responses to a stimulus, if M is overestimated, n will be underestimated.

Studies measuring n in motor and visual areas have found values in the range 2–4, with perhaps a trend for higher values in motor areas (6,16,43,99,101–103). Two studies in subcortical regions both found $n < 2$ (104,105). These studies also emphasise that the BOLD response is sensitive to the value of n when $n \sim 2$. For example, n was found to be reduced in basal ganglia structures when compared with visual cortex (105). Although the basal ganglia BOLD response to a complex finger-tapping task was about seven times weaker than the visual cortex BOLD response to a visual task, the ratio of the $CMRO_2$ response was only around two-fold weaker. This effect was not caused by differences in M, but rather to a modest change in n, from approximately 1.7 in the basal ganglia to approximately 2.3 in the visual cortex. This illustrates that the relative magnitudes of the BOLD responses are a poor quantitative guide to the magnitudes of the underlying physiological changes. To date, there have been a few studies of CBF/$CMRO_2$ coupling in deactivations (102,106,107), but this remains an area that requires further exploration.

More recently, the effect of stimulus strength was investigated by varying the contrast of a simple visual stimulus; it was found that, within the same region of visual cortex, n increased with increasing stimulus contrast (108). Similarly, a change in n with the frequency of the visual stimulus has been reported based on PET measurements (109) and, more recently, using calibrated BOLD (110). In another recent study looking at the effects of attention, it was found that n was substantially larger when a stimulus was attended compared with when it was unattended (111). Finally, a few promising studies have begun to look at CBF/$CMRO_2$ coupling during resting state spontaneous activity (112,113), and this is another area of future growth.

In short, the interesting idea suggested by calibrated BOLD studies is that the coupling ratio n is not fixed, and can vary depending on the neural activity evoked. This basic uncoupling is consistent with current ideas about the drivers of CBF and $CMRO_2$ changes in response to neural activity. Although the $CMRO_2$ response may simply reflect the energy cost of the evoked neural activity, the fast CBF response associated with fMRI signals is thought to be driven directly by neural signalling itself (114), with the astrocytes as intermediaries (115,116),

and not by the energy metabolism change. This may be a feed-forward response, increasing CBF in anticipation of a need for increased $CMRO_2$ in order to prevent a decrease in tissue oxygen (17,117). The important bottom line, however, is that the variation of n, even in the healthy brain, has a substantial effect on the BOLD response, justifying more routine application of the calibrated BOLD methodology.

Prior to the introduction of calibrated BOLD methods, PET methods were used to measure the $CBF/CMRO_2$ coupling ratio under different stimulus conditions. However, the early results measured by both techniques revealed a discrepancy. For example, the seminal PET study of Fox and Raichle (5) with somatosensory stimulation found $n \sim 5$, whereas the pioneering calibrated BOLD studies of Davis *et al.* (6) and Hoge *et al.* (16) found $n \sim 2$–3 in visual cortex. However, subsequent PET studies have found a broader range of n [including $n \sim 2$ in visual cortex (118)]. At this point, it is unclear whether there is a systematic difference between the methodologies (17,25) and, in part, the variability may reflect the true variability across the brain and with different stimuli, as discussed below.

Pharmacological confounders of the BOLD response

The potential effect of drugs on the BOLD response is one of the most important confounding effects that must be addressed when performing fMRI studies in disease populations. Any drug that alters baseline CBF, $CMRO_2$ or, plausibly, even Hct could alter M. In an early study of the effect of acetazolamide, a carbonic anhydrase inhibitor, a modest increase in baseline CBF (~20%) was observed and an associated larger decrease in the BOLD response (~35%) to a simple finger-tapping task (119). This strong effect on the BOLD response is consistent with the expected reduction in M caused by a 20% increase in baseline CBF with no change in baseline $CMRO_2$. Similarly, the effect of indomethacin on CBF and $CMRO_2$ has been investigated using calibrated BOLD (120). Indomethacin is a nonsteroidal anti-inflammatory drug commonly used to reduce fever, pain and stiffness. Baseline CBF was observed to decrease following indomethacin administration, and the CBF and BOLD responses to a finger-tapping task were reduced (46% and 22%, respectively) when compared with the pre-drug responses. The $CMRO_2$ response, as calculated using the Davis model (6), did not change between the pre- and post-drug states, which was interpreted as evidence that indomethacin has a purely vasoactive effect on the brain. However, in this analysis, changes in CBF and BOLD were calculated with respect to the resting condition of the respective pre- or post-drug trials. It was shown later that, when these changes were calculated with respect to the resting condition of pre-drug trials, baseline $CMRO_2$ and the $CMRO_2$ response to stimulus were also reduced by indomethacin (121). This led to the alternative interpretation that indomethacin could have a primary effect on $CMRO_2$, with an associated coupled change in CBF.

Caffeine provides a useful pharmacological test of the calibrated BOLD methodology (44,45,122). It is a vasoconstrictor within the brain (123) and acts as an antagonist of adenosine receptors (124). Adenosine is an inhibitor of excitatory neural activity; therefore, the blocking of adenosine receptors by substances such as caffeine should result in the disinhibition of affected neurons. Experiments examining the effect of caffeine on the BOLD response have yielded conflicting results (123,125,126), with a number of studies reporting a reduction in baseline CBF (127–129). Calibrated BOLD, therefore, offers a way to disentangle the multiple effects that give rise to these results. Initial experiments confirmed a reduced baseline CBF (44,45) and an increased M value following caffeine administration (45). This latter finding is consistent with increased oxygen extraction at rest as a result of a decrease in CBF. However, both of these studies measured BOLD and CBF relative to their pre-stimulus baselines. This approach does not take into account the baseline shifts in absolute $CMRO_2$ and CBF, and led to the belief that CBF was more strongly affected than $CMRO_2$ by caffeine (44). More recently, the data of Perthen *et al.* (44) were revisited with a view to accounting for changes in baseline (122). This was achieved by quantifying the ASL data in physiological units and calculating R_2^* from dual-echo BOLD-weighted data. Both measures are relatively robust absolute values, enabling pre- and post-caffeine data to be referred to the pre-caffeine baseline. This analysis showed a reduced CBF baseline, as before, and a smaller CBF response to stimulus. In addition, a trend towards increased baseline $CMRO_2$ was observed and a significant increase in the absolute $CMRO_2$ response to stimulus was found. These results offer a possible explanation for previous inconsistencies in the literature. The observed changes in CBF and $CMRO_2$ have opposing effects on the BOLD response, and it is easy to imagine the balance between them shifting to produce variable changes in the BOLD response.

Effects of ageing on the BOLD response

The use of calibrated BOLD in studies of ageing can help to disentangle the multiple effects at play. In one study, the effect of ageing on the stimulus-evoked response in the visual cortex was investigated (130). Hypercapnia calibration combined with a visual stimulus experiment was performed in two groups: younger (age, 21–35 years) and older (age, 45–60 years). Older subjects were observed to have lower baseline CBF in the visual cortex, but decreased values of M. This is somewhat paradoxical, as we would expect that reduced baseline CBF should increase oxygen extraction, leading to a larger value of M. However, a reduced M value could occur if $CMRO_2$ were also to decrease with CBF. During neural activation, the BOLD response was observed to decrease with age, but CBF and $CMRO_2$ were unaffected. This corresponds to a constant $CBF/CMRO_2$ coupling with age.

A further study of ageing used hyperoxia calibration with the aim of improving subject comfort and tolerance (47). In contrast with the previous study, this work examined the effect of ageing using a cognitive task rather than a basic visual stimulus. Unlike the study using a visual stimulus, the BOLD response was observed to increase with age in cognitive areas, but the CBF response did not. As the task was cognitive, performance accuracy data enabled the older subject group to be split into low- and high-performing groups. This further subdivision of the group revealed that the difference in BOLD, CBF and $CMRO_2$ responses to stimulus were not significant between young and old high-performing groups. However, the BOLD and $CMRO_2$ responses of young *versus* old low-performing groups were significantly different. These results suggest that the $CBF/CMRO_2$ coupling ratio (n) of the older high-performing group is not that different from that of the young group, but that the older low-performing subjects have an increased value of n. Further work is evidently required in the field of ageing to account for baseline

changes in $CMRO_2$, and to confirm the reduction hypothesised by Ances *et al.* (130).

Measurement of resting $CMRO_2$ using calibrated BOLD

The next step in the development of calibrated BOLD has led researchers to consider its use for the measurement of the absolute resting $CMRO_2$ (131,132). It has always been clear that M contains information about baseline $CMRO_2$ because of its dependence on the resting OEF, but a means to disentangle its contribution to M has not existed until recently. Two methods have been proposed and both hinge on the idea of estimating M by two independent methods: hypercapnia and hyperoxia. Both also rely on the sensitivity of the hyperoxia method to Hct and baseline oxygen extraction (see section on Potential sources of error). However, they differ in the way in which OEF is estimated from the data. When this measurement of oxygen extraction is combined with CBF data, baseline $CMRO_2$ can be estimated via Fick's law.

The method of Bulte *et al.* (132) uses Equation [7] to calculate M_{hc}, substitutes this value into Equation [8] and then rearranges for $\Delta[dHb]/[dHb]_0$. For the ideal hyperoxia experiment, this gives:

$$\frac{\Delta[\mathrm{dHb}]}{[\mathrm{dhb}]_0} = \left[1 - \frac{\delta s}{M_{\mathrm{hc}}}\right]^{\frac{1}{\beta}} - 1 \qquad [19]$$

where δs is the signal change caused by hyperoxia challenge. Given a measurement of Hct, Equation [10] can be rearranged to provide a measurement of OEF. The method proposed by Gauthier *et al.* (131) takes a subtly different approach. They previously proposed a generalised calibration model (GCM) suitable for calibration experiments with any combination of hypercapnia and/or hyperoxia (51). A single equation, based on Equation [4], can then be used to estimate M for a respiratory challenge with any combination of CO_2 and/or O_2:

$$\delta s = M\left[1 - f^{\alpha}\left(\frac{[\mathrm{dHb}]}{[\mathrm{dHb}]_0}\right)^{\beta}\right] \qquad [20]$$

The GCM enables $[dHb]/[dHb]_0$ to be calculated:

$$\frac{[\mathrm{dHb}]}{[\mathrm{dHb}]_0} = \underbrace{\left(\frac{\frac{C_aO_2|_0 E_0}{\phi[\mathrm{Hb}]}}{1 - \frac{C_aO_2|_0}{\phi[\mathrm{Hb}]}(1 - E_0)}\right)}_{A}\frac{1}{f} + \underbrace{\left(\frac{1 - \frac{C_aO_2}{\phi[\mathrm{Hb}]}}{1 - \frac{C_aO_2|_0}{\phi[\mathrm{Hb}]}(1 - E_0)}\right)}_{B} \qquad [21]$$

where C_aO_2 is the amount of oxygen carried by arterial blood during the respiratory challenge and at baseline (subscript 0). All other parameters are as defined in the section on Theoretical underpinnings. Part A of Equation [21] deals with changes in oxygenation caused by a change in flow, whereas part B models changes caused by a change in P_aO_2. This equation enables M to be determined as a function of OEF (E_0). Gauthier *et al.* (131) plot the hypercapnic and hyperoxic M values for the full range of OEF. The intercept of these lines then defines the local OEF of the subject under examination. It is interesting to note that hypercapnia calibration only requires part A of Equation [21] and, for plausible values of OEF, can be reduced to $1/f$. In this case, the methods of Gauthier *et al.* (131) and Bulte *et al.* (132) are mathematically equivalent. However, the use of GCM enables alternative calibration gases to be used, such as carbogen (5% CO_2, 95% O_2) (131).

There is one caveat related to this novel application of combined hypercapnia and hyperoxia calibrations that deserves comment. In deriving the modelling equations, we followed the historical development of the Davis model, which led to an expression for M as the particular lumped set of parameters in Equation [4]. However, we know that this form was derived by considering only extravascular signal changes, and more recent modelling indicates that intravascular signal changes and volume exchange effects play a significant role. For this reason, Equation [4] does not capture all of the effects that contribute to M. Nevertheless, this is not a problem in applying the Davis model for standard calibrated BOLD with hypercapnia calibration, as long as these other effects basically track with the extravascular effects, and more detailed modelling supports this (23). Put another way, the exact form of M in terms of the underlying physiological variables is never used in the hypercapnia-calibrated method; the scaling parameter M is simply measured. However, the combined hyperoxia and hypercapnia methods appear to require that Equation [4] is accurate, which is problematic given current modelling studies. This is an issue that requires further investigation.

SUMMARY AND FUTURE DIRECTIONS

The calibrated BOLD approach is beginning to mature as it has been adopted by a growing number of investigators. The technique has enormous potential to make fMRI quantitative, and to significantly improve the study of disease populations and the measurement of drug effects. In comparing responses in these applications, BOLD fMRI alone cannot distinguish between variations in the CBF response, $CBF/CMRO_2$ coupling (n) or the baseline state (M) (133). Calibrated BOLD offers the promise to resolve these ambiguities and to provide quantitative measurements of basic physiological variables. Nevertheless, there are still questions that need to be resolved and which deserve further investigation.

How large and how reproducible are the $CMRO_2$ changes with moderate hypercapnia?

The literature is variable on this question, and more experiments are needed to quantify this effect, particularly with regard to regional variation in the brain. If a given level of $CMRO_2$ reduction can be assumed, the hypercapnia calibration can be improved with an assumed value of r in Equation [7].

Is hyperoxia reliable for calibration?

The theoretical analysis suggests that the calibration is very sensitive to the assumed value of OEF. Although OEF at rest is relatively uniform in the healthy brain (134), this assumption could be problematic in studies of disease or drug effects.

Can the R_2' method yield robust measurements?

This depends in part on the technical issue of correcting for the effects of large-scale field gradients on R_2'. In addition, R_2' does not capture all of the effects associated with the BOLD signal change, as described above. For this reason, the derived estimate of M needs to be scaled up. Theoretical calculations

suggest that this scaling is relatively stable in the face of variable physiology (40), but direct experimental comparisons between the calibration methods are needed.

How much does CBV_v change with activation?

This remains one of the most important confounding effects in the calibrated BOLD method. An advantage of the hypercapnia method is that it is less sensitive to the assumed change, because it is involved in the calibration experiment as well [although it is still important to consider whether the CBV change is different for hypercapnia and neural activation (135)]. The other two methods, however, do not involve CBV changes in the calibration, and it is thus critical to determine whether the assumed CBV change during neural stimulation is accurate. Further experimental work to determine the CBV_v change is needed.

Can we apply steady-state models to dynamic changes?

One of the most exciting possibilities of the calibrated BOLD method is to provide a way to measure, for the first time, the dynamics of $CMRO_2$ (136). A central question for future investigations is how our models need to be modified to make them accurate for dynamic changes.

Acknowledgements

NPB would like to thank Alex Gardener, Michael Kelly, Tom Okell and Daniel Bulte for useful discussions during the preparation of this manuscript.

REFERENCES

1. Ogawa S, Lee TM, Kay AR, Tank DW. Brain magnetic resonance imaging with contrast dependent on blood oxygenation. Proc. Natl. Acad. Sci. USA 1990; 87: 9868–9872.
2. Ogawa S, Tank DW, Menon RS, Ellermann JM, Kim SG, Merkle H, Ugurbil K. Intrinsic signal changes accompanying sensory stimulation: functional brain mapping with magnetic resonance imaging. Proc. Natl. Acad. Sci. USA 1992; 89: 5951–5955.
3. Kwong KK, Belliveau JW, Chesler DA, Goldberg IE, Weisskoff RM, Poncelet BP, Kennedy DN, Hoppel BE, Cohen MS, Turner R. Dynamic magnetic resonance imaging of human brain activity during primary sensory stimulation. Proc. Natl. Acad. Sci. USA 1992; 89: 5675–5679.
4. Bandettini PA, Wong EC, Hinks RS, Tikofsky RS, Hyde JS. Time course EPI of human brain function during task activation. Magn. Reson. Med. 1992; 25: 390–397.
5. Fox PT, Raichle ME. Focal physiological uncoupling of cerebral blood flow and oxidative metabolism during somatosensory stimulation in human subjects. Proc. Natl. Acad. Sci. USA 1986; 83: 1140–1144.
6. Davis TL, Kwong KK, Weisskoff RM, Rosen BR. Calibrated functional MRI: mapping the dynamics of oxidative metabolism. Proc. Natl. Acad. Sci. USA 1998; 95: 1834–1839.
7. Pike GB. Quantitative functional MRI: concepts, issues and future challenges. Neuroimage 2012; 62: 1234–1240.
8. Pauling L, Coryell CD. The magnetic properties and structure of the hemochromogens and related substances. Proc. Natl. Acad. Sci. USA 1936; 22: 159–163.
9. Marchal G, Rioux P, Petit-Taboué MC, Sette G, Travère JM, Le Poec C, Courtheoux P, Derlon JM, Baron JC. Regional cerebral oxygen consumption, blood flow, and blood volume in healthy human aging. Arch. Neurol. 1992; 49: 1013–1020.
10. Perlmutter JS, Powers WJ, Herscovitch P, Fox PT, Raichle ME. Regional asymmetries of cerebral blood flow, blood volume, and oxygen utilization and extraction in normal subjects. J. Cereb. Blood Flow Metab. 1987; 7: 64–67.
11. Uludağ K, Müller-Bierl B, Uğurbil K. An integrative model for neuronal activity-induced signal changes for gradient and spin echo functional imaging. Neuroimage 2009; 48: 150–165.
12. Buxton RB, Wong EC, Frank LR. Dynamics of blood flow and oxygenation changes during brain activation: the balloon model. Magn. Reson. Med. 1998; 39: 855–864.
13. Ogawa S, Menon RS, Tank DW, Kim SG, Merkle H, Ellermann JM, Ugurbil K. Functional brain mapping by blood oxygenation level-dependent contrast magnetic resonance imaging. A comparison of signal characteristics with a biophysical model. Biophys. J. 1993; 64: 803–812.
14. Yablonskiy DA, Haacke EM. Theory of NMR signal behavior in magnetically inhomogeneous tissues: the static dephasing regime. Magn. Reson. Med. 1994; 32: 749–763.
15. Boxerman JL, Hamberg LM, Rosen BR, Weisskoff RM. MR contrast due to intravascular magnetic susceptibility perturbations. Magn. Reson. Med. 1995; 34: 555–566.
16. Hoge RD, Atkinson J, Gill B, Crelier GR, Marrett S, Pike GB. Investigation of BOLD signal dependence on cerebral blood flow and oxygen consumption: the deoxyhemoglobin dilution model. Magn. Reson. Med. 1999; 42: 849–863.
17. Buxton RB. Interpreting oxygenation-based neuroimaging signals: the importance and the challenge of understanding brain oxygen metabolism. Front Neuroenerg. 2010; 2: article 8.
18. Grubb RL, Raichle ME, Eichling JO, Ter-Pogossian MM. The effects of changes in $PaCO_2$ on cerebral blood volume, blood flow, and vascular mean transit time. Stroke 1974; 5: 630–639.
19. Silvennoinen MJ, Clingman CS, Golay X, Kauppinen RA, van Zijl PCM. Comparison of the dependence of blood R_2 and R_2^* on oxygen saturation at 1.5 and 4.7 Tesla. Magn. Reson. Med. 2002; 49: 47–60.
20. Zhao JM, Clingman CS, Närväinen MJ, Kauppinen RA, van Zijl PCM. Oxygenation and hematocrit dependence of transverse relaxation rates of blood at 3T. Magn. Reson. Med. 2007; 58: 592–597.
21. Blockley N, Jiang L, Gardener AG, Ludman CN, Francis ST, Gowland PA. Field strength dependence of R_1 and R_2* relaxivities of human whole blood to prohance, vasovist, and deoxyhemoglobin. Magn. Reson. Med. 2008; 60: 1313–1320.
22. Yacoub E, Duong TQ, Van De Moortele PF, Lindquist M, Adriany G, Kim SG, Urbil KM, Hu X. Spin-echo fMRI in humans using high spatial resolutions and high magnetic fields. Magn. Reson. Med. 2003; 49: 655–664.
23. Griffeth VEM, Buxton RB. A theoretical framework for estimating cerebral oxygen metabolism changes using the calibrated-BOLD method: modeling the effects of blood volume distribution, hematocrit, oxygen extraction fraction, and tissue signal properties on the BOLD signal. Neuroimage 2011; 58: 198–212.
24. Obata T, Liu TT, Miller KL, Luh WM, Wong EC, Frank LR, Buxton RB. Discrepancies between BOLD and flow dynamics in primary and supplementary motor areas: application of the balloon model to the interpretation of BOLD transients. Neuroimage 2004; 21: 144–153.
25. Lin AL, Fox PT, Yang Y, Lu H, Tan LH, Gao JH. Evaluation of MRI models in the measurement of $CMRO_2$ and its relationship with CBF. Magn. Reson. Med. 2008; 60: 380–389.
26. Yablonskiy DA. Quantitation of intrinsic magnetic susceptibility-related effects in a tissue matrix. Phantom study. Magn. Reson. Med. 1998; 39: 417–428.
27. He X, Yablonskiy DA. Quantitative BOLD: mapping of human cerebral deoxygenated blood volume and oxygen extraction fraction: default state. Magn. Reson. Med. 2007; 57: 115–126.
28. Chen JJ, Pike GB. BOLD-specific cerebral blood volume and blood flow changes during neuronal activation in humans. NMR Biomed. 2009; 22: 1054–1062.
29. Mark CI, Fisher JA, Pike GB. Improved fMRI calibration: precisely controlled hyperoxic versus hypercapnic stimuli. Neuroimage, 2011; 54:1102–1111.
30. Bulte DP, Drescher K, Jezzard P. Comparison of hypercapnia-based calibration techniques for measurement of cerebral oxygen metabolism with MRI. Magn. Reson. Med. 2009; 61: 391–398.
31. Siesjö BK. *Brain energy metabolism*. Wiley & Sons, Chichester, UK, 1978, format: xii, p. 607: ill.; 24 cm.
32. Kastrup A, Krüger G, Glover GH, Moseley ME. Assessment of cerebral oxidative metabolism with breath holding and fMRI. Magn. Reson. Med. 1999; 42: 608–611.
33. Magon S, Basso G, Farace P, Ricciardi GK, Beltramello A, Sbarbati A. Reproducibility of BOLD signal change induced by breath holding. Neuroimage 2009; 45: 702–712.
34. Chiarelli PA, Bulte DP, Wise R, Gallichan D, Jezzard P. A calibration method for quantitative BOLD fMRI based on hyperoxia. Neuroimage, 2007; 37: 808–820.

35. Xu F, Liu P, Pascual JM, Xiao G, Lu H. Effect of hypoxia and hyperoxia on cerebral blood flow, blood oxygenation, and oxidative metabolism. J. Cereb. Blood Flow Metab. 2012; doi: 10.1038/jcbfm.2012.93
36. Severinghaus JW. Simple, accurate equations for human blood O_2 dissociation computations. J. Appl. Physiol. 1979; 46: 599–602.
37. Bulte DP, Chiarelli PA, Wise RG, Jezzard P. Cerebral perfusion response to hyperoxia. J. Cereb. Blood Flow Metab. 2007; 27: 69–75.
38. Xu F, Liu P, Lu H. Effect of graded O_2 challenge on vascular and metabolic parameters. Proc. Int. Soc. Magn. Reson. Med. 2011; 19: 765.
39. Fujita N, Matsumoto K, Tanaka H, Watanabe Y, Murase K. Quantitative study of changes in oxidative metabolism during visual stimulation using absolute relaxation rates. NMR Biomed. 2006; 19: 60–68.
40. Blockley N, Griffeth VEM, Buxton RB. A general analysis of calibrated BOLD methodology for measuring $CMRO_2$ responses: comparison of a new approach with existing methods. Neuroimage, 2011; 60: 279–289.
41. Buxton RB, Frank LR, Wong EC, Siewert B, Warach S, Edelman RR. A general kinetic model for quantitative perfusion imaging with arterial spin labeling. Magn. Reson. Med. 1998; 40: 383–396.
42. Posse S, Wiese S, Gembris D, Mathiak K, Kessler C, Grosse-Ruyken ML, Elghahwagi B, Richards T, Dager SR, Kiselev VG. Enhancement of BOLD-contrast sensitivity by single-shot multi-echo functional MR imaging. Magn. Reson. Med. 1999; 42: 87–97.
43. Leontiev O, Dubowitz DJ, Buxton RB. CBF/$CMRO_2$ coupling measured with calibrated BOLD fMRI: sources of bias. Neuroimage, 2007; 36: 1110–1122.
44. Perthen JE, Lansing AE, Liau J, Liu TT, Buxton RB. Caffeine-induced uncoupling of cerebral blood flow and oxygen metabolism: a calibrated BOLD fMRI study. Neuroimage, 2008; 40: 237–247.
45. Chen Y, Parrish TB. Caffeine's effects on cerebrovascular reactivity and coupling between cerebral blood flow and oxygen metabolism. Neuroimage, 2009; 44: 647–652.
46. Ances BM, Vaida F, Ellis R, Buxton RB. Test–retest stability of calibrated BOLD-fMRI in HIV − and HIV + subjects. Neuroimage, 2011; 54: 2156–2162.
47. Mohtasib RS, Lumley G, Goodwin JA, Emsley HCA, Sluming V, Parkes LM. Calibrated fMRI during a cognitive Stroop task reveals reduced metabolic response with increasing age. Neuroimage 2012; 59: 1143–1151.
48. Wong EC, Buxton RB, Frank LR. Implementation of quantitative perfusion imaging techniques for functional brain mapping using pulsed arterial spin labeling. NMR Biomed. 1997; 10: 237–249.
49. Liu TT, Wong EC. A signal processing model for arterial spin labeling functional MRI. Neuroimage 2005; 24: 207–215.
50. Lu H, Donahue MJ, van Zijl PCM. Detrimental effects of BOLD signal in arterial spin labeling fMRI at high field strength. Magn. Reson. Med. 2006; 56: 546–552.
51. Gauthier CJ, Madjar C, Tancredi FB, Stefanovic B, Hoge RD. Elimination of visually evoked BOLD responses during carbogen inhalation: implications for calibrated MRI. Neuroimage 2011; 54: 1001–1011.
52. Detre JA, Leigh JS, Williams DS, Koretsky AP. Perfusion imaging. Magn. Reson. Med. 1992; 23: 37–45.
53. Kim SG. Quantification of relative cerebral blood flow change by flow-sensitive alternating inversion recovery (FAIR) technique: application to functional mapping. Magn. Reson. Med. 1995; 34: 293–301.
54. Dai W, Garcia D, de Bazelaire C, Alsop DC. Continuous flow-driven inversion for arterial spin labeling using pulsed radio frequency and gradient fields. Magn. Reson. Med. 2008; 60: 1488–1497.
55. Aslan S, Xu F, Wang PL, Uh J, Yezhuvath US, van Osch M, Lu H. Estimation of labeling efficiency in pseudocontinuous arterial spin labeling. Magn. Reson. Med. 2010; 63: 765–771.
56. Tadamura E, Hatabu H, Li W, Prasad PV, Edelman RR. Effect of oxygen inhalation on relaxation times in various tissues. J. Magn. Reson. Imaging 1997; 7: 220–225.
57. Silvennoinen MJ, Kettunen MI, Kauppinen RA. Effects of hematocrit and oxygen saturation level on blood spin–lattice relaxation. Magn. Reson. Med. 2003; 49: 568–571.
58. Wong EC, Buxton RB, Frank LR. Quantitative imaging of perfusion using a single subtraction (QUIPSS and QUIPSS II). Magn. Reson. Med. 1998; 39: 702–708.
59. Luh WM, Wong EC, Bandettini PA, Hyde JS. QUIPSS II with thin-slice TI_1 periodic saturation: a method for improving accuracy of quantitative perfusion imaging using pulsed arterial spin labeling. Magn. Reson. Med. 1999; 41: 1246–1254.
60. Villringer A, Rosen BR, Belliveau JW, Ackerman JL, Lauffer RB, Buxton RB, Chao YS, Wedeen VJ, Brady TJ. Dynamic imaging with lanthanide chelates in normal brain: contrast due to magnetic susceptibility effects. Magn. Reson. Med. 1988; 6: 164–174.
61. Belliveau JW, Kennedy DN, McKinstry RC, Buchbinder BR, Weisskoff RM, Cohen MS, Vevea JM, Brady TJ, Rosen BR. Functional mapping of the human visual cortex by magnetic resonance imaging. Science, 1991; 254: 716–719.
62. Pears JA, Francis ST, Butterworth SE, Bowtell RW, Gowland PA. Investigating the BOLD effect during infusion of Gd-DTPA using rapid T_2* mapping. Magn. Reson. Med. 2003; 49: 61–70.
63. Lu H, Golay X, Pekar JJ, van Zijl PCM. Functional magnetic resonance imaging based on changes in vascular space occupancy. Magn. Reson. Med. 2003; 50: 263–274.
64. Lee SP, Duong TQ, Yang G, Iadecola C, Kim SG. Relative changes of cerebral arterial and venous blood volumes during increased cerebral blood flow: implications for BOLD fMRI. Magn. Reson. Med. 2001; 45: 791–800.
65. Hillman EMC, Devor A, Bouchard MB, Dunn AK, Krauss GW, Skoch J, Bacskai BJ, Dale AM, Boas DA. Depth-resolved optical imaging and microscopy of vascular compartment dynamics during somatosensory stimulation. Neuroimage, 2007; 35: 89–104.
66. Kim T, Hendrich KS, Masamoto K, Kim SG. Arterial versus total blood volume changes during neural activity-induced cerebral blood flow change: implication for BOLD fMRI. J. Cereb. Blood Flow Metab. 2007; 27: 1235–1247.
67. Mandeville JB, Marota JJ, Kosofsky BE, Keltner JR, Weissleder R, Rosen BR, Weisskoff RM. Dynamic functional imaging of relative cerebral blood volume during rat forepaw stimulation. Magn. Reson. Med. 1998; 39: 615–624.
68. Donahue MJ, Blicher JU, Østergaard L, Feinberg DA, MacIntosh BJ, Miller KL, Günther M, Jezzard P. Cerebral blood flow, blood volume, and oxygen metabolism dynamics in human visual and motor cortex as measured by whole-brain multi-modal magnetic resonance imaging. J. Cereb. Blood Flow Metab. 2009; 29: 1856–1866.
69. Yang Y, Gu H, Stein EA. Simultaneous MRI acquisition of blood volume, blood flow, and blood oxygenation information during brain activation. Magn. Reson. Med. 2004; 52: 1407–1417.
70. Rostrup E, Knudsen GM, Law I, Holm S, Larsson HBW, Paulson OB. The relationship between cerebral blood flow and volume in humans. Neuroimage, 2005; 24: 1–11.
71. Chen JJ, Pike GB. MRI measurement of the BOLD-specific flow–volume relationship during hypercapnia and hypocapnia in humans. Neuroimage, 2010; 53: 383–391.
72. Bulte DP, Chiarelli PA, Wise R, Jezzard P. Measurement of cerebral blood volume in humans using hyperoxic MRI contrast. J. Magn. Reson. Imaging, 2007; 26: 894–899.
73. Blockley N, Driver ID, Fisher JA, Francis ST, Gowland PA. Measuring venous blood volume changes during activation using hyperoxia. Neuroimage, 2012; 59: 3266–3274.
74. Driver ID, Hall E, Pritchard S, Francis ST, Gowland PA. A new approach for venous blood oxygenation and calibrated BOLD using hyperoxia. Proc. Int. Soc. Magn. Reson. Med. 2011; 19: 3597.
75. Hua J, Qin Q, Donahue MJ, Zhou J, Pekar JJ, van Zijl PCM. Inflow-based vascular-space-occupancy (iVASO) MRI. Magn. Reson. Med. 2011; 66: 40–56.
76. Lansing RW, Gracely RH, Banzett RB. The multiple dimensions of dyspnea: review and hypotheses. Respir. Physiol. Neurobiol. 2009; 167: 53–60.
77. Robbins PA, Swanson GD, Howson MG. A prediction-correction scheme for forcing alveolar gases along certain time courses. J. Appl. Physiol. 1982; 52: 1353–1357.
78. Robbins PA, Swanson GD, Micco AJ, Schubert WP. A fast gas-mixing system for breath-to-breath respiratory control studies. J. Appl. Physiol. 1982; 52: 1358–1362.
79. Slessarev M, Han J, Mardimae A, Prisman E, Preiss D, Volgyesi G, Ansel C, Duffin J, Fisher JA. Prospective targeting and control of end-tidal CO_2 and O_2 concentrations. J. Physiol. 2007; 581: 1207–1219.
80. Wise RG, Pattinson KTS, Bulte DP, Chiarelli PA, Mayhew SD, Balanos GM, O'Connor DF, Pragnell TR, Robbins PA, Tracey I, Jezzard P. Dynamic forcing of end-tidal carbon dioxide and oxygen applied to functional magnetic resonance imaging. J. Cereb. Blood Flow Metab. 2007; 27: 1521–1532.
81. Mark CI, Slessarev M, Ito S, Han J, Fisher JA, Pike GB. Precise control of end-tidal carbon dioxide and oxygen improves BOLD and ASL cerebrovascular reactivity measures. Magn. Reson. Med. 2010; 64: 749–756.

82. An H, Lin W. Impact of intravascular signal on quantitative measures of cerebral oxygen extraction and blood volume under normo- and hypercapnic conditions using an asymmetric spin echo approach. Magn. Reson. Med. 2003; 50: 708–716.
83. Dickson JD, Ash TWJ, Williams GB, Harding SG, Carpenter TA, Menon DK, Ansorge RE. Quantitative BOLD: the effect of diffusion. J. Magn. Reson. Imaging, 2010; 32: 953–961.
84. Brewer KD, Rioux JA, D'Arcy RCN, Bowen CV, Beyea SD. Asymmetric spin-echo (ASE) spiral improves BOLD fMRI in inhomogeneous regions. NMR Biomed. 2009; 22: 654–662.
85. Edelstein WA, Hutchison JM, Johnson G, Redpath T. Spin warp NMR imaging and applications to human whole-body imaging. Phys. Med. Biol. 1980; 25: 751–756.
86. An H, Lin W. Quantitative measurements of cerebral blood oxygen saturation using magnetic resonance imaging. J. Cereb. Blood Flow Metab. 2000; 20: 1225–1236.
87. Dahnke H, Schaeffter T. Limits of detection of SPIO at 3.0 T using T_2* relaxometry. Magn. Reson. Med. 2005; 53: 1202–1206.
88. Xu F, Uh J, Brier MR, Hart J, Yezhuvath US, Gu H, Yang Y, Lu H. The influence of carbon dioxide on brain activity and metabolism in conscious humans. J. Cereb. Blood Flow Metab. 2010; 31: 58–67.
89. Zappe AC, Uludag K, Oeltermann A, Ugurbil K, Logothetis NK. The influence of moderate hypercapnia on neural activity in the anesthetized nonhuman primate. Cereb. Cortex, 2008; 18: 2666–2673.
90. Jain V, Langham MC, Floyd TF, Jain G, Magland JF, Wehrli FW. Rapid magnetic resonance measurement of global cerebral metabolic rate of oxygen consumption in humans during rest and hypercapnia. J. Cereb. Blood Flow Metab. 2011; 31: 1504–1512.
91. Thesen T, Leontiev O, Song T, Dehghani N, Hagler DJ, Huang M, Buxton RB, Halgren E. Depression of cortical activity in humans by mild hypercapnia. Hum. Brain Mapp. 2012; 33: 715–726.
92. Sicard KM, Duong TQ. Effects of hypoxia, hyperoxia, and hypercapnia on baseline and stimulus-evoked BOLD, CBF, and $CMRO_2$ in spontaneously breathing animals. Neuroimage 2005; 25: 850–858.
93. Diringer MN, Aiyagari V, Zazulia AR, Videen TO, Powers WJ. Effect of hyperoxia on cerebral metabolic rate for oxygen measured using positron emission tomography in patients with acute severe head injury. J. Neurosurg. 2007; 106: 526–529.
94. Lu H, Ge Y. Quantitative evaluation of oxygenation in venous vessels using T2-relaxation-under-spin-tagging MRI. Magn. Reson. Med. 2008; 60: 357–363.
95. Stankiewicz J, Panter SS, Neema M, Arora A, Batt CE, Bakshi R. Iron in chronic brain disorders: imaging and neurotherapeutic implications. Neurotherapeutics, 2007; 4: 371–386.
96. Castellani RJ, Siedlak SL, Perry G, Smith MA. Sequestration of iron by Lewy bodies in Parkinson's disease. Acta Neuropathol. 2000; 100: 111–114.
97. Ordidge RJ, Gorell JM, Deniau JC, Knight RA, Helpern JA. Assessment of relative brain iron concentrations using T_2-weighted and T_2*-weighted MRI at 3 Tesla. Magn. Reson. Med. 1994; 32: 335–341.
98. Wismer GL, Buxton RB, Rosen BR, Fisel CR, Oot RF, Brady TJ, Davis KR. Susceptibility induced MR line broadening: applications to brain iron mapping. J. Comput. Assist. Tomogr. 1988; 12: 259–265.
99. Leontiev O, Buxton RB. Reproducibility of BOLD, perfusion, and $CMRO_2$ measurements with calibrated-BOLD fMRI. Neuroimage 2007; 35: 175–184.
100. Chiarelli PA, Bulte DP, Piechnik S, Jezzard P. Sources of systematic bias in hypercapnia-calibrated functional MRI estimation of oxygen metabolism. Neuroimage 2007; 34: 35–43.
101. Kastrup A, Krüger G, Neumann-Haefelin T, Glover GH, Moseley ME. Changes of cerebral blood flow, oxygenation, and oxidative metabolism during graded motor activation. Neuroimage 2002; 15: 74–82.
102. Stefanovic B, Warnking JM, Pike GB. Hemodynamic and metabolic responses to neuronal inhibition. Neuroimage 2004; 22: 771–778.
103. Chiarelli PA, Bulte DP, Gallichan D, Piechnik SK, Wise R, Jezzard P. Flow-metabolism coupling in human visual, motor, and supplementary motor areas assessed by magnetic resonance imaging. Magn. Reson. Med. 2007; 57: 538–547.
104. Restom K, Perthen JE, Liu TT. Calibrated fMRI in the medial temporal lobe during a memory-encoding task. Neuroimage 2008; 40: 1495–1502.
105. Ances BM, Leontiev O, Perthen J, Liang C. Regional differences in the coupling of cerebral blood flow and oxygen metabolism changes in response to activation: implications for BOLD-fMRI. Neuroimage 2008; 54: 2156–2162.
106. Uludağ K, Dubowitz DJ, Yoder EJ, Restom K, Liu TT, Buxton RB. Coupling of cerebral blood flow and oxygen consumption during physiological activation and deactivation measured with fMRI. Neuroimage 2004; 23: 148–155.
107. Pasley BN, Inglis BA, Freeman RD. Analysis of oxygen metabolism implies a neural origin for the negative BOLD response in human visual cortex. Neuroimage 2007; 36: 269–276.
108. Liang C, Ances BM, Perthen J, Liau J, Buracas G, Hopkins S, Buxton RB. The ratio of CBF to $CMRO_2$ change with brain activation increases with increasing stimulus amplitude in human visual cortex. Proc. Int. Soc. Magn. Reson. Med. 2009; 17: 1630.
109. Vafaee MS, Meyer E, Marrett S, Paus T, Evans AC, Gjedde A. Frequency-dependent changes in cerebral metabolic rate of oxygen during activation of human visual cortex. J. Cereb. Blood Flow Metab. 1999; 19: 272–277.
110. Lin AL, Fox PT, Yang Y, Lu H, Tan LH, Gao JH. Time-dependent correlation of cerebral blood flow with oxygen metabolism in activated human visual cortex as measured by fMRI. Neuroimage 2009; 44: 16–22.
111. Moradi F, Buračas GT, Buxton RB. Attention strongly increases oxygen metabolic response to stimulus in primary visual cortex. Neuroimage 2012; 59: 601–607.
112. Fukunaga M, Horovitz SG, de Zwart JA, van Gelderen P, Balkin TJ, Braun AR, Duyn JH. Metabolic origin of BOLD signal fluctuations in the absence of stimuli. J. Cereb. Blood Flow Metab. 2008; 28: 1377–1387.
113. Wu CW, Gu H, Lu H, Stein EA, Chen JH, Yang Y. Mapping functional connectivity based on synchronized $CMRO_2$ fluctuations during the resting state. Neuroimage 2009; 45: 694–701.
114. Attwell D, Iadecola C. The neural basis of functional brain imaging signals. Trends Neurosci. 2002; 25: 621–625.
115. Iadecola C, Nedergaard M. Glial regulation of the cerebral microvasculature. Nat. Neurosci. 2007; 10: 1369–1376.
116. Koehler RC, Roman RJ, Harder DR. Astrocytes and the regulation of cerebral blood flow. Trends Neurosci. 2009; 32: 160–169.
117. Devor A, Sakadzic S, Saisan PA, Yaseen MA, Roussakis E, Srinivasan VJ, Vinogradov SA, Rosen BR, Buxton RB, Dale AM, Boas DA. "Overshoot" of O_2 is required to maintain baseline tissue oxygenation at locations distal to blood vessels. J. Neurosci. 2011; 31: 13 676–13 681.
118. Vafaee MS, Gjedde A. Model of blood–brain transfer of oxygen explains nonlinear flow–metabolism coupling during stimulation of visual cortex. J. Cereb. Blood Flow Metab. 2000; 20: 747–754.
119. Brown GG, Eyler Zorrilla LT, Georgy B, Kindermann SS, Wong EC, Buxton RB. BOLD and perfusion response to finger–thumb apposition after acetazolamide administration: differential relationship to global perfusion. J. Cereb. Blood Flow Metab. 2003; 23: 829–837.
120. Lawrence KS, Ye FQ, Lewis BK, Frank JA, McLaughlin AC. Measuring the effects of indomethacin on changes in cerebral oxidative metabolism and cerebral blood flow during sensorimotor activation. Magn. Reson. Med. 2003; 50: 99–106.
121. Uludağ K, Buxton RB. Measuring the effects of indomethacin on changes in cerebral oxidative metabolism and cerebral blood flow during sensorimotor activation. Magn. Reson. Med. 2004; 51: 1088–9; author reply 1090.
122. Griffeth VEM, Perthen JE, Buxton RB. Prospects for quantitative fMRI: investigating the effects of caffeine on baseline oxygen metabolism and the response to a visual stimulus in humans. Neuroimage 2011; 57: 809–816.
123. Mulderink TA, Gitelman DR, Mesulam MM, Parrish TB. On the use of caffeine as a contrast booster for BOLD fMRI studies. Neuroimage 2002; 15: 37–44.
124. Nehlig A, Daval JL, Debry G. Caffeine and the central nervous system: mechanisms of action, biochemical, metabolic and psychostimulant effects. Brain Res. Brain Res. Rev. 1992; 17: 139–170.
125. Laurienti PJ, Field AS, Burdette JH, Maldjian JA, Yen YF, Moody DM. Relationship between caffeine-induced changes in resting cerebral perfusion and blood oxygenation level-dependent signal. Am. J. Neuroradiol. 2003; 24: 1607–1611.
126. Liau J, Perthen JE, Liu TT. Caffeine reduces the activation extent and contrast-to-noise ratio of the functional cerebral blood flow response but not the BOLD response. Neuroimage 2008; 42: 296–305.
127. Mathew RJ, Wilson WH. Caffeine induced changes in cerebral circulation. Stroke, 1985; 16: 814–817.

128. Cameron OG, Modell JG, Hariharan M. Caffeine and human cerebral blood flow: a positron emission tomography study. Life Sci. 1990; 47: 1141–1146.
129. Field AS, Laurienti PJ, Yen YF, Burdette JH, Moody DM. Dietary caffeine consumption and withdrawal: confounding variables in quantitative cerebral perfusion studies? Radiology 2003; 227: 129–135.
130. Ances BM, Liang CL, Leontiev O, Perthen JE, Fleisher AS, Lansing AE, Buxton RB. Effects of aging on cerebral blood flow, oxygen metabolism, and blood oxygenation level dependent responses to visual stimulation. Hum. Brain Mapp. 2009; 30: 1120–1132.
131. Gauthier CJ, Hoge RD. Magnetic resonance imaging of resting OEF and $CMRO_2$ using a generalized calibration model for hypercapnia and hyperoxia. Neuroimage 2012; 60: 1212–1225.
132. Bulte DP, Kelly M, Germuska M, Xie J, Chappell MA, Okell TW, Bright MG, Jezzard P. Quantitative measurement of cerebral physiology using respiratory-calibrated MRI. Neuroimage 2011; 60: 582–591.
133. Small SA, Schobel SA, Buxton RB, Witter MP, Barnes CA. A pathophysiological framework of hippocampal dysfunction in ageing and disease. Nat. Rev. Neurosci. 2011; 12: 585–601.
134. Gusnard DA, Raichle ME, Raichle ME. Searching for a baseline: functional imaging and the resting human brain. Nat. Rev. Neurosci. 2001; 2: 685–694.
135. Hua J, Stevens RD, Huang AJ, Pekar JJ, van Zijl PCM. Physiological origin for the BOLD poststimulus undershoot in human brain: vascular compliance versus oxygen metabolism. J. Cereb. Blood Flow Metab. 2011; 31: 1599–1611.
136. Hyder F, Sanganahalli BG, Herman P, Coman D, Maandag NJG, Behar KL, Blumenfeld H, Rothman DL. Neurovascular and neurometabolic couplings in dynamic calibrated fMRI: transient oxidative neuroenergetics for block-design and event-related paradigms. Front Neuroenerg. 2010; 2: article 18.

Section B: An analysis of calibrated BOLD

Contents lists available at SciVerse ScienceDirect

NeuroImage

journal homepage: www.elsevier.com/locate/ynimg

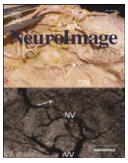

A general analysis of calibrated BOLD methodology for measuring $CMRO_2$ responses: Comparison of a new approach with existing methods

Nicholas P. Blockley [a,*], Valerie E.M. Griffeth [b], Richard B. Buxton [a,c]

[a] Center for Functional Magnetic Resonance Imaging, Department of Radiology, University of California San Diego, La Jolla, CA, USA
[b] Department of Bioengineering and Medical Scientist Training Program, University of California San Diego, La Jolla, CA, USA
[c] Kalvi Institute for Brain and Mind, University of California San Diego, La Jolla, CA, USA

ARTICLE INFO

Article history:
Received 19 August 2011
Revised 21 October 2011
Accepted 25 November 2011
Available online 6 December 2011

Keywords:
Calibrated BOLD
Cerebral metabolic rate of oxygen
Functional MRI
Hypercapnia
Hyperoxia

ABSTRACT

The amplitude of the BOLD response to a stimulus is not only determined by changes in cerebral blood flow (CBF) and oxygen metabolism ($CMRO_2$), but also by baseline physiological parameters such as haematocrit, oxygen extraction fraction (OEF) and blood volume. The calibrated BOLD approach aims to account for this physiological variation by performing an additional calibration scan. This calibration typically consists of a hypercapnia or hyperoxia respiratory challenge, although we propose that a measurement of the reversible transverse relaxation rate, R_2', might also be used. A detailed model of the BOLD effect was used to simulate each of the calibration experiments, as well as the activation experiment, whilst varying a number of physiological parameters associated with the baseline state and response to activation. The effectiveness of the different calibration methods was considered by testing whether the BOLD response to activation scaled by the calibration parameter combined with the measured CBF provides sufficient information to reliably distinguish different levels of $CMRO_2$ response despite underlying physiological variability. In addition the effect of inaccuracies in the underlying assumptions of each technique were tested, e.g. isometabolism during hypercapnia.

The three primary findings of the study were: 1) The new calibration method based on R_2' worked reasonably well, although not as well as the ideal hypercapnia method; 2) The hyperoxia calibration method was significantly worse because baseline haematocrit and OEF must be assumed, and these physiological parameters have a significant effect on the measurements; and 3) the venous blood volume change with activation is an important confounding variable for all of the methods, with the hypercapnia method being the most robust when this is uncertain.

Introduction

The BOLD signal is dependent on changes in cerebral blood flow (CBF) and oxidative metabolism ($CMRO_2$). However, changes in CBF and $CMRO_2$ alone do not determine the amplitude of the BOLD response to neural activity. It is therefore possible to measure BOLD responses with different amplitudes that result from the same underlying changes in CBF and $CMRO_2$. The scale of the BOLD response is determined by the baseline physiological state of the tissue contained within the imaging voxel. This baseline is characterised by the total amount of deoxyhaemoglobin present, which is dependent on the haematocrit, baseline oxygen extraction fraction (OEF), and baseline blood volume.

The calibrated BOLD approach (Davis et al., 1998) was proposed to measure changes in $CMRO_2$ using measurements of CBF and BOLD. This is achieved by characterising differences in baseline physiology using a calibration experiment. Traditionally this experiment consists of simultaneous measurements of CBF and BOLD acquired during interleaved periods of normocapnia and hypercapnia (Davis et al., 1998; Hoge et al., 1999). Hypercapnia is induced by presenting the participant with carbon dioxide rich gas mixture (typically 5% CO_2, 21% O_2, 74% N_2) and results in an increase in CBF and the BOLD signal. A model of the BOLD signal is then used to convert these changes into a measure of the baseline physiological state (Davis et al., 1998), under the assumption that baseline $CMRO_2$ is not altered by hypercapnia (Jain et al., 2011; Sicard and Duong, 2005).

More recently an alternative respiratory challenge was presented whereby hypercapnia was replaced with hyperoxia (Chiarelli et al., 2007). Experiments have been performed with oxygen content ranging from 25% (Mark et al., 2011) to 100% (Chiarelli et al., 2007; Goodwin et al., 2009). Hyperoxia does not substantially increase arterial blood oxygen saturation, but does increase the oxygen carried by arterial blood through an increased plasma oxygen concentration.

* Corresponding author at: University of California San Diego, Radiology - Center for Functional MRI, 9500 Gilman Drive #0677, La Jolla, CA 92093-0677, USA. Fax: +1 858 822 0605.
E-mail address: nblockley@ucsd.edu (N.P. Blockley).

1053-8119/$ – see front matter © 2011 Elsevier Inc. All rights reserved.
doi:10.1016/j.neuroimage.2011.11.081

This results in an increase in venous blood oxygen saturation and hence an increase in BOLD signal. A modification of the BOLD signal model used for hypercapnia calibration can then be used to characterise the baseline state (Chiarelli et al., 2007).

However, respiratory challenges are time consuming to set up, uncomfortable and may be contraindicated for some subjects, for example in Chronic Obstructive Pulmonary Disease (COPD) (Moore et al., 2009). Therefore, it would be useful to be able to calibrate without administering gases. It has long been known that the reversible transverse relaxation rate, R_2', is sensitive to venous cerebral blood volume (CBVv) and the concentration of deoxyhaemoglobin ([*dHb*]) (Yablonskiy and Haacke, 1994). This sensitivity is exploited by the qBOLD approach to make absolute measurements of resting CBVv and OEF (He and Yablonskiy, 2006). However, this method has poor temporal resolution and is not suitable for measuring $CMRO_2$ changes on short timescales. Nevertheless, R_2' is dependent on haematocrit, OEF and blood volume and as such captures most of the characteristics of the baseline physiological state that are important for determining the scaling of the BOLD response, particularly total deoxyhaemoglobin content. Can we therefore use this information to calibrate the BOLD response? In this study we investigate whether R_2' can be used to calibrate the BOLD response through detailed simulation. In addition, we compare this new calibration method with the existing respiratory challenge calibrations, hypercapnia and hyperoxia. The simplifying assumptions of each of these methods are investigated and the uncertainty they introduce into the calibration process assessed.

Theory

A general model for calibrated BOLD

The aim of calibrated BOLD is to take measurements of BOLD signal and CBF and combine them with information about the baseline state to estimate $CMRO_2$ changes. This baseline information is gathered from a calibration experiment. In the classic approach introduced by Davis and colleagues, the BOLD response is modeled as:

$$\delta s = M\left[1 - f^{\alpha}\left(\frac{r}{f}\right)^{\beta}\right] \tag{1}$$

where δs is the percentage BOLD signal change, f is the CBF ratio and r is the $CMRO_2$ ratio (activation/baseline), and α and β are model parameters. The calibration parameter M that scales the BOLD signal is calculated from the measured BOLD and CBF responses to hypercapnia, with the assumption of no change in $CMRO_2$ ($r = 1$). Physically, the calibration parameter M depends on a number of physiological variables that affect the local deoxyhaemoglobin concentration in the baseline state, and so represents an important source of variation across subjects and across brain regions. It also depends on image acquisition parameters, so that M is not simply a property of the brain, and comparing M values across different studies requires some care.

In the current study our goal is take a more general approach to the process of calibration, as a way of accounting for variations in the baseline state, without assuming the simple form of the Davis model. More generally the calibrated BOLD experiment can be stated in the following way,

$$\delta s = B\, h(f, r) \tag{2}$$

where B is the calibration parameter and $h(f,r)$ is a function that describes the effect of normalised changes in CBF and $CMRO_2$, on the change in BOLD signal. To model h we use a recently described detailed model for the BOLD response that includes a number of physiological variables that were not included in the original Davis model (Griffeth and Buxton, 2011). The model includes three blood compartments (arterial, capillary and venous) as well as the extravascular compartment, and models BOLD signal contributions from all compartments as well as effects of volume exchange as a blood compartment expands. The model also allows the baseline blood volume fractions to be varied, as well as the volume changes of these vascular compartments with activation. Baseline oxygen extraction fraction and blood haematocrit also can be varied. Although this model does not provide a simple closed form for $h(f,r)$ like Eq. (1), it provides a flexible way to simulate the BOLD response for a wide range of physiological baseline states. The model is described in more detail in Appendix A.

The detailed model allows us to test any proposed method for calibration in the following way. The calibration experiment itself is simulated with the detailed BOLD model for a given set of baseline physiological parameters, and the value of B is calculated for the prescribed calibration method from the simulated BOLD and CBF responses. The activation experiment is then simulated for particular values of f and r with the same baseline physiological parameters, and the BOLD response normalized to the calibration parameter ($\delta s/B$) is then plotted as a function of f. This plot represents a simulation of the measured results of a calibrated BOLD study. This procedure is then repeated for many variations of the baseline physiological parameters and the CBF change f, but for the same $CMRO_2$ change r, with each simulation plotted as one point in the $\delta s/B$ vs. f plot. If the calibration is perfect, these points for a constant r should fall on a single curve, and when the simulations are repeated for a different value of r the points should fall on a distinctly different curve. In this way the calibration completely captures the variability due to the baseline state and the measurements of $\delta s/B$ and f uniquely define r. Note that the shape of the curve for a particular value of r, which effectively is determined by h, is not what we are after here. Instead, the central question is whether a calibration method produces a clean separation of the points for different values of r.

As an initial demonstration of the importance of calibration, Fig. 1 omits calibration and plots δs versus f. Three different levels of $CMRO_2$ change are displayed; 10%, 20% and 30% increases. When baseline haematocrit, *Hct*, oxygen extraction fraction, E_0, and blood volume, V, are randomly varied across the physiological range, all three $CMRO_2$ levels overlap and cannot be clearly separated. A calibration experiment is therefore required to determine B and to reduce the uncertainty in r. This commonly takes the form of a hypercapnia or hyperoxia respiratory challenge, although here we also consider an alternative technique based on measurements of R_2'.

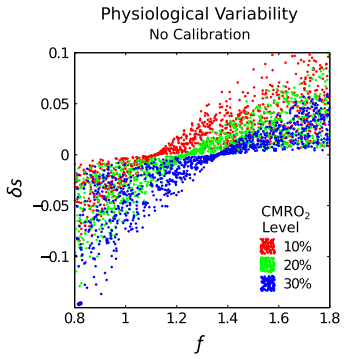

Fig. 1. The effect of physiological variability in haematocrit, baseline oxygen extraction fraction and baseline blood volume on the relationship between the BOLD response (δs) and CBF (f). These simulations show that the effect of physiological variability on δs does not allow 10% step changes in $CMRO_2$ to be clearly separated, confirming that this information is insufficient to accurately measure $CMRO_2$.

Hypercapnia calibration

Hypercapnia calibration is performed by presenting a hypercapnic gas mixture to the participant whilst measurements of BOLD signal and CBF are made (Davis et al., 1998). These measurements are combined with the Davis model to estimate the calibration parameter B with Eq. (3). Typically this is known as M, with subscript hc added here to distinguish hypercapnia from hyperoxia.

$$B \equiv M_{hc} = \frac{\delta s}{1 - f^{\alpha-\beta} r^{\beta}} \tag{3}$$

Here, the constants α and β represent flow-volume coupling (Grubb et al., 1974) and the relationship between blood oxygenation and the BOLD signal (Ogawa et al., 1993), respectively. Current practice sets the value of α as 0.2 based on measurements of CBVv, the vascular compartment that underlies the BOLD response (Chen and Pike, 2009). Similarly β is chosen to be 1.3 for experiments performed at 3.0 T (Mark et al., 2011). In the ideal calibration experiment it is assumed that $CMRO_2$ is not altered by hypercapnia ($r = 1$) and this was initially assumed in these simulations.

Hyperoxia calibration

Hyperoxia calibration is performed in a similar manner to hypercapnia calibration, by presenting a hyperoxic gas mixture to the participant whilst recording measurements of BOLD and CBF (Chiarelli et al., 2007). The BOLD scaling parameter is termed M_{ho} and is equivalent to B in Eq. (2). In the ideal experiment it is assumed that CBF does not change during hyperoxia, in which case measurements of CBF are not necessary during calibration. Hence,

$$B \equiv M_{ho} = \frac{\delta s}{1 - \left(\frac{[dHb]}{[dHb]_0}\right)^{\beta}} \tag{4}$$

where β takes the same definition as for hypercapnia calibration and $[dHb]/[dHb]_0$ is the change in deoxyhaemoglobin concentration due to breathing the hyperoxic gas mixture, relative to normoxia (Chiarelli et al., 2007). To calculate M_{ho} using Eq. (4) $[dHb]/[dHb]_0$ must be estimated. This is achieved using a model of the oxygen carrying capacity of the blood that is a function of the arterial partial pressure of oxygen (PaO_2). In practice this is inferred from the end-tidal pressure of oxygen ($P_{ET}O_2$) expired by the participant, taking into account alveolar–arterial oxygen gradient and assuming that the arterial blood is well equilibrated with the gas in the alveoli. This latter assumption relies upon healthy lung function for validity. Oxygen is mostly carried bound to haemoglobin within the blood, however a small amount is carried by the plasma. The PaO_2 of the blood determines how much is carried by both of these compartments. The oxygen carried by the plasma is a linear function of PaO_2 (εPaO_2) and for bound oxygen the haemoglobin saturation of arterial blood (SaO_2) can be calculated from an approximation for the oxygen dissociation curve (Severinghaus, 1979):

$$SaO_2 = \frac{1}{\frac{23400}{(PaO_2)^3 + 150 PaO_2} + 1} \tag{5}$$

During hyperoxia the amount of oxygen carried bound to haemoglobin in the arteries increases slightly, alongside a larger increase in the amount carried as dissolved gas in plasma. Therefore, under hyperoxia the amount of oxygen carried by plasma contributes to a greater degree to the overall delivery of oxygen than during normoxia due to the asymptotic nature of Eq. (5). During passage through the capillary bed the extraction of the excess oxygen in plasma offsets the extraction of oxygen bound to haemoglobin, so that venous haemoglobin saturation increases. However, in the venous blood the partial pressure of oxygen (PvO_2) remains low and represents less than 1% of total amount of oxygen carried by venous blood. Therefore, assuming that PvO_2 is negligible should not result in a large error and allows $[dHb]/[dHb]_0$ to be estimated as:

$$\frac{[dHb]}{[dHb]_0} = 1 + \frac{\Delta[dHb]}{[dHb]_0} = 1 - \frac{\phi[Hb]\Delta SaO_2 + \varepsilon \Delta PaO_2}{\phi[Hb](1 - SaO_2(1 - E_0)) + \varepsilon PaO_2(1 - E_0)} \tag{6}$$

where ϕ is the oxygen carrying capacity of haemoglobin ($1.34\ \mathrm{ml O_2\, g_{Hb}^{-1}}$), ε is the solubility coefficient of oxygen in blood ($0.0031\ \mathrm{ml O_2\, dl^{-1}\, mmHg^{-1}}$), and ΔSaO_2 and ΔPaO_2 are the change in these parameters due to hyperoxia relative to the normoxic state. Haemoglobin concentration, $[Hb]$, is assumed to be $15\ \mathrm{g_{Hb}\, dl^{-1}}$ (Chiarelli et al., 2007; Mark et al., 2011) and the oxygen extraction fraction, E_0, is assumed to be 0.3 (Mark et al., 2011). This value of E_0 is lower than the generally reported values of approximately 0.4 (Perlmutter et al., 1987), however we retain this value to reflect current practice in the papers describing the hyperoxia calibration method. Haemoglobin concentration can be converted to haematocrit using a simple approximation, $Hct \approx 0.03 \times [Hb]$. In summary, the hyperoxia calibration method requires assumed values for several variables. Oxygen carrying capacity and solubility are standard physical parameters that should not vary across subjects. However, haematocrit may well vary across subjects, and baseline O_2 extraction fraction could also vary across brain regions within the same subject.

R_2' calibration

Analytical results (Yablonskiy and Haacke, 1994) and Monte Carlo (Ogawa et al., 1993) simulations have shown that R_2' is a function of blood volume, haematocrit and OEF.

$$R_2' = \kappa V\ (Hct\ E_0)^{\beta} \tag{7}$$

The constant κ subsumes various properties of brain tissue including vessel geometry, magnetic field strength and the susceptibility difference between blood and tissue, and β follows the same definition as in hypercapnia and hyperoxia calibration. If we consider the BOLD signal to be a largely extravascular effect then changes in R_2' determine changes in the BOLD signal. Hence the maximum BOLD signal change during activation is determined by R_2' in the baseline state. Assuming monoexponential decay, the gradient echo (GE) and spin echo (SE) signal at the BOLD echo time, TE, can be described by the following equations, where $R_2^* = R_2 + R_2'$.

$$S_{GE}(TE) = S(0) e^{-TE(R_2 + R_2')} \tag{8a}$$

$$S_{SE}(TE) = S(0) e^{-TE\ R_2} \tag{8b}$$

We propose to use the ratio of these signals to define the calibration parameter B.

$$B \equiv \ln \frac{S_{SE}(TE)}{S_{GE}(TE)} = TE\, R_2' \tag{9}$$

The echo time, TE, is included to account for the echo time dependence of the magnitude of the BOLD response. This approach assumes that intravascular signal contributions are negligible and that diffusional narrowing does not dominate. These assumptions were tested using an extension of the detailed BOLD signal model (Griffeth and Buxton, 2011). This was achieved by considering the signal contributions from each of the compartments of the detailed signal model under GE and SE pulse sequences during a resting baseline and is described in detail in Appendix A. It must be noted that the measured

value of R_2' is dependent on the way in which it is measured. It is generally assumed that the transverse signal decay of a homogenous voxel is monoexponential. However, for time points close to the excitation pulse in a GE sequence, and close to the refocusing pulse for a SE sequence, this decay has been shown to be quadratically exponential in nature (Yablonskiy and Haacke, 1994). In the case of Eq. (9) the SE signal will be acquired in this short echo time regime whilst the GE signal will be acquired in the long echo time regime. Models for the SE signal compartments were chosen to be consistent with the short echo time regime (Uludağ et al., 2009; Zhao et al., 2007).

Methods

Simulations

The detailed signal model was used to simulate calibration using hypercapnia, hyperoxia and R_2' using Eqs. (3), (4) and (9), respectively, as prescriptions for taking specific measured signals and calculating *B*. Note that the first two methods explicitly depend on the parameter β, which functions as a way to approximate multiple factors affecting the BOLD response. This parameter does not appear in the detailed BOLD model because these different mechanisms are individually modeled. Similarly, the parameter α is related to CBVv change, and in the detailed model the changes in different vascular compartments are simulated.

All simulations were performed in MATLAB (Mathworks, Natick, MA). The main aim of these simulations was to determine how variability in physiology affects the uncertainty in a measurement of $CMRO_2$. For variations in a single parameter simulations are performed by propagating linearly spaced values of this parameter through the detailed signal model. However, for variations in baseline physiology we expect multiple parameters to vary simultaneously and the compound effect of these variations isn't clear. Simple linear ranges for multiple parameters would be slow and produce multidimensional data that is difficult to visualise. Here we take an alternative approach by drawing random combinations of these parameters from predefined ranges. Multiple repeats of this process enable a 'cloud' of data to be generated that can be visualised in two dimensions, as shown in Fig. 1.

In order to investigate the sensitivity of each of the calibration methods to baseline physiological variability and the assumptions of each method, the change in BOLD signal was divided by the calibration scaling factor. In the following figures this quantity, $\delta s/B$, is plotted against *f*. These simulations are performed for two different scenarios; fixed $CMRO_2$ level or fixed CBF-$CMRO_2$ coupling value, *n*, defined as,

$$n = \frac{f-1}{r-1.} \tag{10}$$

Fixed $CMRO_2$ changes enables us to visualise how well different $CMRO_2$ levels can be separated, whilst fixed CBF-$CMRO_2$ coupling shows the uncertainty in these measurements for more physiologically plausible combinations of CBF and $CMRO_2$. Fixed $CMRO_2$ levels of 10%, 20% and 30% increases and CBF-$CMRO_2$ coupling values of $n = 1.3$, 2 and 3 were simulated. An *n* value of 1.3 represents a special case where the increase in blood oxygenation due to increased CBF is approximately balanced by increased oxygen extraction due to metabolism, resulting in a net zero BOLD signal change. The exact value of *n* required to achieve this condition is CBF dependent and can be estimated from the Davis model (Eq. (1)) for specific values of α and β. Therefore, $n = 1.3$ is an approximate BOLD-nulling value for the CBF values simulated.

Each of the calibration parameter values was calculated as described in the Theory section. In summary, the hypercapnia calibration scaling factor, M_{hc}, is calculated using Eq. (3) under the assumption that $CMRO_2$ does not change ($r = 1$) and a 47% increase in CBF due to hypercapnia ($f = 1.47$). In all simulations α in Eq. (3) was chosen to be 0.2. The hyperoxia calibration, M_{ho}, is calculated using Eq. (4), relying on Eq. (6) to determine $[dHb]/[dHb]_0$, following the method of Mark et al., and $[Hb]$ and E_0 in this equation have fixed values of 15 $g_{Hb}\,dl^{-1}$ and 0.3, respectively (Mark et al., 2011). Hyperoxia calibration was simulated as an ideal experiment where CBF is not altered by hyperoxia. In both traditional methods β was chosen to be 1.3. In R_2' calibration the scaling factor is the product of *TE* and R_2', and is calculated using Eq. (9). No assumptions about isometabolism or the value of α and β are required.

Baseline physiological variation

The parameters that determine the baseline state are haematocrit, baseline OEF and baseline blood volume. Haematocrit is known to vary between males and females with typical ranges of 0.42–0.50 and 0.37–0.47, respectively (McPhee and Hammer, 2009). However, there is a great deal of overlap and typically calibration methods do not take account of sex during data processing, therefore a range of 0.37–0.50 was tested. Ranges for baseline OEF are similarly wide at 0.35–0.55 (Marchal et al., 1992). This range was extended at the low end to encompass the assumed OEF value of 0.3 used in the hyperoxia calibration method. The baseline total blood volume fraction is typically measured to be 0.05 in grey matter (Roland et al., 1987). However, to account for the partial volume effect at the low end of the range and for incorporation of large vessels at the high end of the range a total blood volume fraction between 0.01 and 0.1 was tested. Relative volume fractions for arteries, capillaries and veins were fixed at 0.2, 0.4 and 0.4, respectively. This resulted in simulated venous volume fractions in the range 0.004 to 0.04. Finally, the activation induced change in CBF was simulated across a large range (0.8 to 1.8) to encompass all physiologically plausible eventualities. Values for the remaining model parameters are listed in Table 1.

Randomly generated combinations of these parameters were selected from their respective ranges, including activation induced CBF change, using a uniform random number generator. A uniform random distribution was chosen as the mean and standard deviation of each of the physiological parameters is not generally known. For each simulation 1,000 repeats of the random parameter generation process were completed. These values were propagated through the detailed signal model to generate a stimulus induced BOLD signal change, δs, and a calibration parameter, *B*, for each calibration method. To simplify the simulation process CBF was included as an additional randomly generated value providing the third experimental variable of the calibrated BOLD approach.

Flow-volume coupling assumption

A general assumption of all calibrated BOLD methods is that changes in CBVv can be inferred from measurements of CBF through a power law relationship defined by α. An inaccurate value of α would be a source of systematic error. Here we aim to determine the sensitivity of each of the calibration methods to the value of α. Traditionally α was defined as 0.4 based on measurements of total CBV (Grubb et al., 1974), but has more recently been superseded by a value of 0.2 using measurements of venous CBV change (Chen and Pike, 2009). These values were used to test the extremes of the range for flow-volume coupling given our current knowledge. When calculating M_{hc}, α in Eq. (3) was fixed at 0.2 regardless of the value of the underlying flow-volume coupling. This reflects the way that hypercapnia calibration is performed, whereby a value of α must be assumed that may not reflect the true underlying changes in volume.

Table 1
Constants required for the detailed signal model (Griffeth and Buxton, 2011) and extension to simulate R_2'.

Constant	Value	Description
TE	32 ms	Imaging echo time.
ε_A	1.30	Ratio of baseline intravascular arterial to extravascular signal (Griffeth and Buxton, 2011).
ε_C	1.02	Ratio of baseline intravascular capillary to extravascular signal (Griffeth and Buxton, 2011).
ε_V	0.50	Ratio of baseline intravascular venous to extravascular signal (Griffeth and Buxton, 2011).
a^*_L	4.3	Coefficient describing extravascular signal resulting from vessels in the range 16–200 μm diameter under a gradient echo (Ogawa et al., 1993).
a^*_S	0.04 s	Coefficient describing extravascular signal resulting from 5 μm diameter vessels under a gradient echo (Ogawa et al., 1993).
$a_{L,5}$	-1.92×10^{-11} s^4	Coefficients describing extravascular signal resulting from 16 μm diameter vessels under a spin echo (Uludağ et al., 2009).
$a_{L,4}$	-1.26×10^{-8} s^3	
$a_{L,3}$	-2.89×10^{-6} s^2	
$a_{L,2}$	2.51×10^{-4} s	
$a_{L,1}$	0.0067	
$a_{L,0}$	-0.0382 s^{-1}	
$a_{S,5}$	-1.13×10^{-11} s^4	Coefficients describing extravascular signal resulting from 5 μm diameter vessels under a spin echo (Uludağ et al., 2009).
$a_{S,4}$	0.96×10^{-8} s^3	
$a_{S,3}$	-3.22×10^{-6} s^2	
$a_{S,2}$	4.90×10^{-4} s	
$a_{S,1}$	-3.58×10^{-6}	
$a_{S,0}$	0.0175 s^{-1}	
$\Delta\chi$	2.64×10^{-7}	Susceptibility of fully deoxygenated blood (Spees et al., 2001).
Y_{off}	0.95	Blood saturation for equal tissue–blood susceptibility (Spees et al., 2001).
$R_{2,0}$	25.1 s^{-1}	Intrinsic transverse relaxation rate for extravascular tissue (Perthen et al., 2008).

Effect of errors in assumptions

Assumptions that would lead to the largest sources of error in each method were identified and the effect of systematic error in these assumptions was tested. Baseline physiological variability was not included in these simulations, unless otherwise stated, and standard values for these parameters were assumed ($Hct = 0.45$, $E_0 = 0.4$, $V_{l,0} = 0.05$).

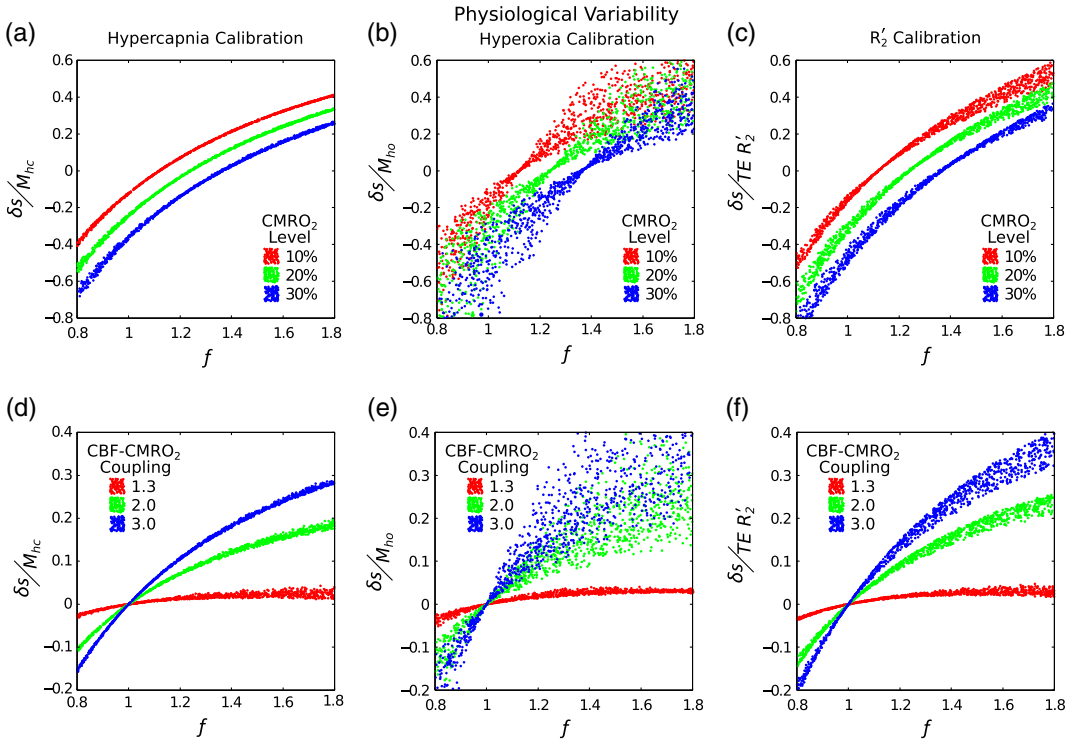

Fig. 2. Three different calibration techniques were investigated to account for physiological variability; hypercapnia, hyperoxia, and R_2' calibration (columns left-right). By simultaneously varying haematocrit (0.37–0.50), oxygen extraction fraction (0.30–0.55) and blood volume (0.01–0.10) we are able to assess how well each method copes with this physiological variability. Simulations were performed for both fixed increases in $CMRO_2$ (top row) and for fixed coupling of CBF and $CMRO_2$ (Eq. (10)) (bottom row). For a perfect calibration each of the simulated points should fall on a single curve, which should be distinctly different for each $CMRO_2$ level or CBF-$CMRO_2$ coupling value.

It has been shown by a number of experiments that hypercapnia may cause a reduction in baseline $CMRO_2$ (Xu et al., 2010). It is normally assumed that there is no change in $CMRO_2$ due to hypercapnia, ($r=1$). In order to consider the effect of reduced $CMRO_2$ the value of $r=0.85$ was also simulated to reflect a 15% reduction in $CMRO_2$ during the hypercapnia challenge.

For hyperoxia the estimation of M_{ho} is dependent on the calculation of $[dHb]/[dHb]_0$ from the change in $PETO_2$ measured during hyperoxia. To simplify this calculation values for $[Hb]$ and E_0 are assumed (Mark et al., 2011). Simulations were performed to determine whether more accurate values of one or both parameters would enable variations in baseline physiology to be better accounted for. Since the accuracy of these assumptions is dependent on physiological variability, the same approach of generating random combinations of baseline parameters as used for baseline physiological variation alone was used.

Measurements of R_2' are not only sensitive to mesoscopic sources of magnetic field inhomogeneity around blood vessels but also to large scale magnetic field inhomogeneity that are not removed during shimming. The sensitivity of R_2' calibration to large scale magnetic field inhomogeneity was tested by simulating (Eq. (A8)) a frequency difference across the voxel, $\Delta\omega$, of 20 Hz (An and Lin, 2003).

Results

Baseline physiological variability

Fig. 2 displays the effect of normalising the BOLD signal change using a calibration measurement. All three calibration methods drastically reduce the variability in the relationship between BOLD and CBF (cf. Fig. 1). The width of the lines for each $CMRO_2$ level (Figs. 2a–c), or CBF-$CMRO_2$ coupling value (Figs. 2d–e), are proportional to the error in the final measurement of $CMRO_2$. In an ideal calibration experiment there would be no deviation from the mean and the width of the line would be zero.

For hypercapnia calibration the line width appears to be constant with increasing CBF and independent of the $CMRO_2$ level (Fig. 2a) or CBF-$CMRO_2$ coupling value (Fig. 2d). Hyperoxia calibration shows an increase in the line width with increasing CBF (Figs. 2b,e). The line width is minimised when CBF and $CMRO_2$ balance to give a zero BOLD signal change equivalent to $n=1.3$ in the plot of CBF-$CMRO_2$ coupling (Fig. 2e). R_2' calibration shows a similar trend to hyperoxia calibration, but with a reduced line width (Figs. 2c,f).

Flow-volume coupling assumption

The effect of assuming that the coupling between CBF and CBVv is accurately known is displayed in Fig. 3. Solid lines are used to represent the case where $\alpha=0.2$ and dashed lines for when $\alpha=0.4$. Here we are examining the effect of assuming an incorrect value for α. Therefore, a calibration method with low sensitivity to this parameter should show only a minor shift between these lines, ultimately minimising the error in the measurement of $CMRO_2$.

Hypercapnia shows the smallest shift, representing the lowest sensitivity to an inaccurately assumed value of α (Figs. 3a,d). The magnitude of this shift appears to increase with increasing change in the $CMRO_2$ level (Fig. 3a). Hyperoxia and R_2' calibration both

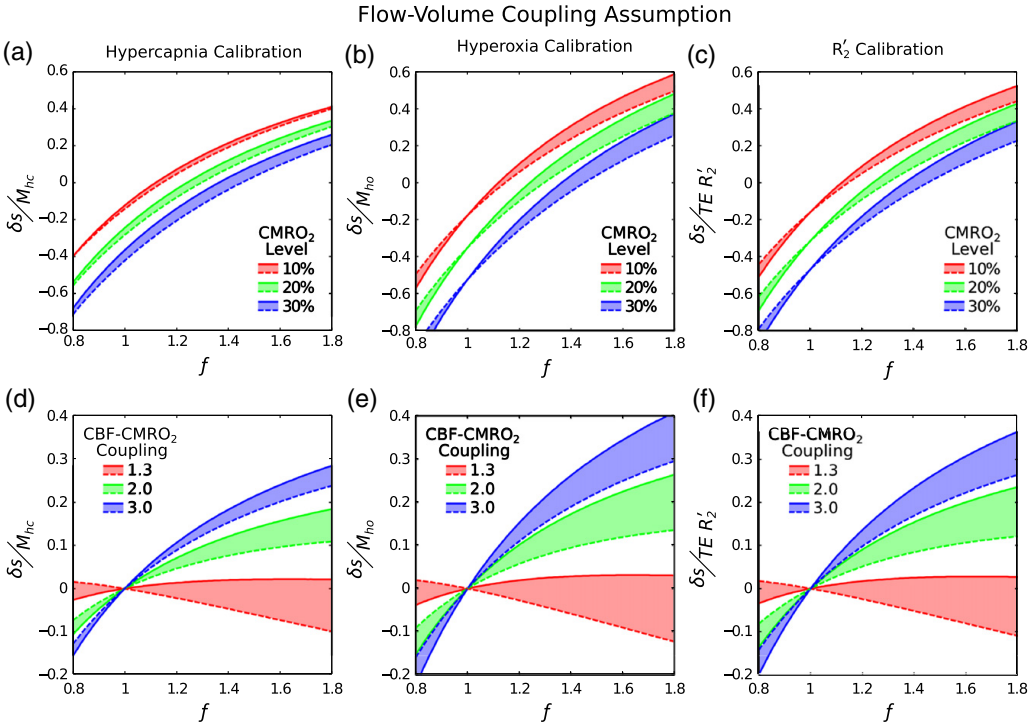

Fig. 3. An inaccurate assumption of the flow-volume coupling constant α would result in a systematic error. Here the effect of different underlying physiological values of this coupling were investigated where a solid line represents $\alpha=0.2$ and the dashed line $\alpha=0.4$. A minimal shift in the dashed line with respect to the solid line would reflect lower sensitivity to the assumed value of α. Physiological variability is not included in these simulations and haematocrit, oxygen extraction fraction and blood volume were assumed to be 0.45, 0.4, 0.05, respectively.

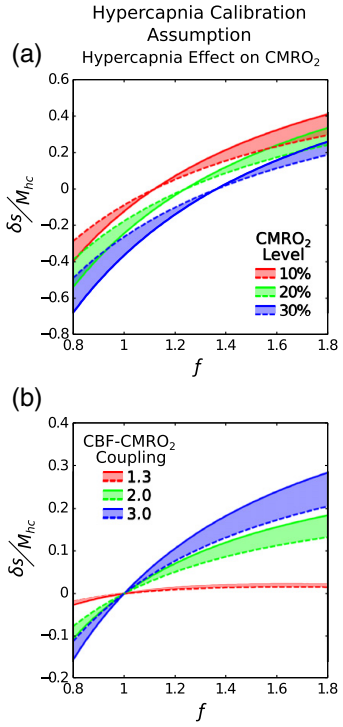

Fig. 4. It has been observed that hypercapnia may cause a reduction in baseline $CMRO_2$. Here we consider what effect this would have on hypercapnia calibration when $CMRO_2$ is reduced by 15% ($r=0.85$ in Eq. (3)). Physiological variability was not included for clarity. Isometabolism ($r=1$) is plotted as a solid line whilst reduced $CMRO_2$ is plotted as a dashed line. Shifting of the dashed line with respect to the solid line suggests that reduced baseline $CMRO_2$ would have a marked effect on the accuracy of hypercapnia calibration.

show a larger shift than hypercapnia calibration (Figs. 3b,e; Figs. 3c,f). In all cases the effect of assuming an inaccurate value of α causes the greatest effect for $n=1.3$ in plots of CBF-$CMRO_2$ coupling.

Hypercapnia calibration assumption

Fig. 4 considers the effect of a change in baseline $CMRO_2$ during hypercapnia. Solid lines represent $r=1$ during hypercapnia and dashed lines $r=0.85$. The shift between these lines appears to increase with $CMRO_2$ level (Fig. 4a) and CBF-$CMRO_2$ coupling (Fig. 4b). Unlike flow-volume coupling, changes in $CMRO_2$ during hypercapnia have little to no effect when $n=1.3$.

Hyperoxia calibration assumptions

Investigation of the origin of the increased variability in hyperoxia calibration is displayed in Fig. 5. Including more accurate information about either haematocrit (Figs. 5a,d) or baseline oxygenation (Figs. 5b, e) reduces this variability. Information about both of these parameters (Figs. 5c,f) reduces variability to similar levels as hypercapnia calibration (Figs. 2a,d).

R_2' calibration assumption

Fig. 6 considers the effect of large scale magnetic field inhomogeneity on R_2' calibration. Solid lines represent a perfectly homogenous field ($\Delta\omega=0$) and dashed lines represent $\Delta\omega=20$ Hz. The shift between these lines is of a similar order to that seen for $CMRO_2$ change during hypercapnia (Fig. 4).

Discussion

Use of the calibrated BOLD approach has improved the interpretation of fMRI by accounting for physiological variability. Without this calibration procedure measurements of BOLD signal and CBF cannot be used to determine the change in $CMRO_2$ (Fig. 1). However, the extent to which this physiological variability can be characterised by existing methods is not easily accessible in an experimental setting. The simulations performed in this study enable us to investigate these methods and the assumptions that underpin them. Key to this approach was the use of a detailed model of the BOLD effect that allowed us to vary a number of physiological parameters associated with the baseline state and the response to activation. This allowed us to model effects that were not included in the simpler Davis model standardly used for calibrated BOLD experiments. The effectiveness of the different calibration methods was tested by simulating the calibration experiment as well as the activation experiment, and testing whether the measured BOLD response to activation scaled by the calibration parameter combined with the measured CBF response provides sufficient information to reliably distinguish different levels of $CMRO_2$ response despite underlying physiological variability. We evaluated the original hypercapnia method (Davis et al., 1998), the more recently proposed hyperoxia method (Chiarelli et al., 2007) and a novel method based on R_2'. The simulation methodology used here has previously been used to optimise hypercapnia calibrated BOLD (Griffeth and Buxton, 2011), the results of which have been applied experimentally (Griffeth et al., 2011). Extensions to the detailed signal model allowed us to simulate R_2' in the baseline state, in order to assess its use as an alternative calibration method.

There were three primary findings of this study: 1) The new calibration method based on R_2' worked reasonably well, although not as well as the ideal hypercapnia method; 2) The hyperoxia calibration method was significantly worse because baseline haematocrit and OEF must be assumed, and variability of these physiological parameters has a significant effect on the measurements; and 3) the venous blood volume change with activation is an important confounding variable for all of the methods, with the hypercapnia method being the most robust when this is uncertain. The results for each of the calibration methods tested are discussed in more detail below.

Hypercapnia calibration

Simulation of hypercapnia calibration revealed that this method provides an accurate calibration for baseline physiological variability (Figs. 2a,d). The broadening of the line due to physiological variability shows only very weak dependence on the change in CBF. Uncertainty in the value of α causes additional deviation of the lines of $CMRO_2$ that appears to increase with increasing $CMRO_2$ change (Figs. 3a,d). We also tested the resulting errors if the assumption of no $CMRO_2$ change with hypercapnia is wrong. When a reduction in $CMRO_2$ during hypercapnia was simulated a shift in the lines of $CMRO_2$ was observed (Fig. 4). This could result in an inaccurate measurement of $CMRO_2$, for example when $f=1.6$ a 10% $CMRO_2$ change when $r=0.85$ would appear similar to a 20% change when $r=1$.

Hyperoxia calibration

Simulations of hyperoxia calibration, when values for baseline [*Hb*] and E_0 are assumed, predict poor performance of this method for normalising the BOLD signal change (Figs. 2b,e). Further investigation revealed that when more information is known, such as [*Hb*] (Figs. 5a,d) or E_0 (Figs. 5b,e), then uncertainty is reduced. When

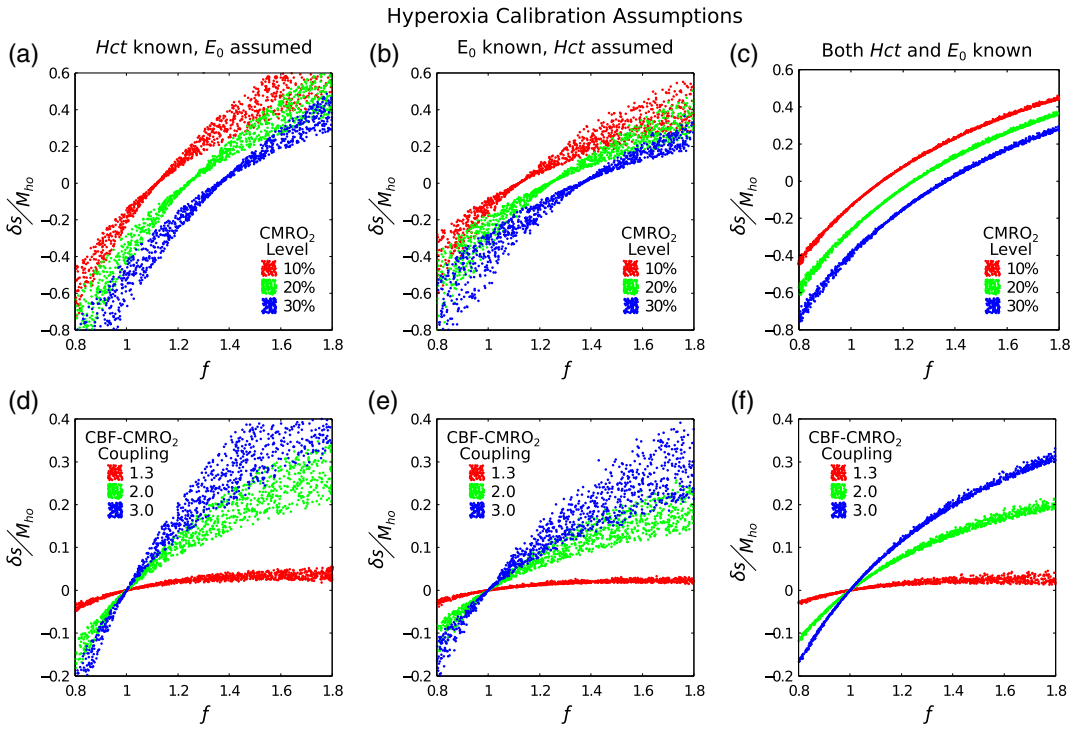

Fig. 5. Further investigation of hyperoxia calibration was undertaken to better understand the large observed variability. This was achieved by increasing the amount of information used to estimate the calibration scaling factor M_{ho}; haematocrit known, oxygen extraction fraction known and both known (columns left-right). Physiological variability was included as it is the origin of the observed variability in Figs. 2b,e. More information about the baseline physiology reduces the variability in hyperoxia calibration.

both variables are known then uncertainty is reduced to the same level as hypercapnia calibration (Figs. 5c,f). This uncertainty is minimised when the combination of CBF and $CMRO_2$ changes result in a net zero BOLD signal (as is also the case for R_2' calibration). This effectively means that the venous oxygen saturation is unchanged between the rest and activated states and hence the physiological variability does not have any effect.

The origin of the observed poor performance of hyperoxia calibrated BOLD can be determined by considering Eq. (6). The change in deoxyhaemoglobin concentration due to hyperoxia ($[dHb]/[dHb]_0$) is determined by the decrease in concentration $\Delta[dHb]$ and the baseline concentration $[dHb]_0$. The former is determined by $[Hb]$, as this adjusts the balance of oxygen carried by haemoglobin and plasma, and is independent of E_0, whereas the latter is a function of E_0 at normoxia and $[Hb]$. Accurate values of $[Hb]$ and E_0 are therefore required as $[dHb]/[dHb]_0$ is used to convert measurements of the BOLD signal change during hyperoxia to M_{ho} (Eq. (4)). This conversion is provided by the denominator of Eq. (4) producing a scaling of the BOLD signal change equivalent to one over the denominator. For the extremes of the $[Hb]$ and E_0 ranges tested here, and a fixed ΔPaO_2 of 310 mm Hg, this scaling value is in the range 5.9 to 15.6 (assuming $\beta = 1.3$). In contrast, the approach taken by Mark et al. (2011) will always scale the hyperoxic BOLD signal change by 7.9 for the same fixed ΔPaO_2. Whilst the extremes of the $[Hb]$ and E_0 ranges are unlikely to simultaneously exist this analysis illustrates the sensitivity of hyperoxia calibration to assumed values for these parameters, and explains the reduced variability encountered when both are known (Figs. 5c,f). Therefore, hyperoxia calibration may be improved by acquiring more accurate information about baseline physiology. This could be achieved by making direct MR measurements of deoxyhaemoglobin concentration in the sagittal sinus as an approximation for E_0 (Jain et al., 2011; Lu et al., 2012) or by measuring the haematocrit from a venous blood sample.

It is unclear whether this expected variability has been observed in the literature, largely due to the limited number of studies having undertaken this calibration. A large spread in the calibration parameter M_{ho} has been observed (Goodwin et al., 2009), which would result from the variability we see, but it is unclear whether the uncontrolled manual hyperoxia challenge employed in this study may have contributed to this effect. Studies using controlled hyperoxic challenges have suggested that the variability in measurements of $CMRO_2$ is lower for hyperoxia calibration when compared with hypercapnia calibration (Mark et al., 2011). The results of our simulations conflict with this observation.

Hyperoxia calibration also shows greater sensitivity to flow-volume coupling than hypercapnia calibration (Figs. 3b,e). The resulting shift in the lines of $CMRO_2$ could result in a large error in the magnitude of the $CMRO_2$ change if the assumed flow-volume coupling does not match the physiological relationship.

R_2' calibration

The concept of using R_2' to calibrate the BOLD response is based on this parameter's well known dependence on haematocrit, OEF and blood volume (Yablonskiy and Haacke, 1994). Currently this effect is exploited by the qBOLD method to measure baseline blood oxygenation and volume (He and Yablonskiy, 2006). However, to date it has not been used within a calibrated BOLD framework to measure

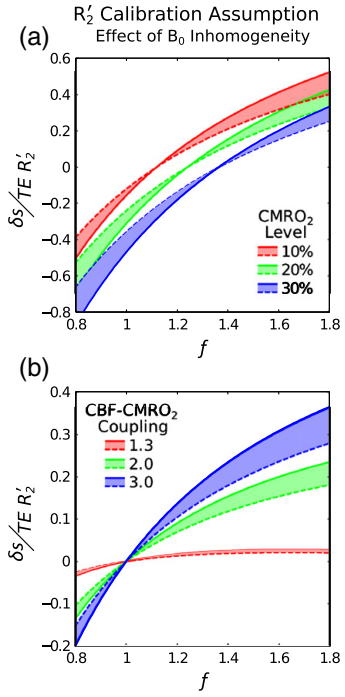

Fig. 6. It is well known that R_2' is sensitive to both mesoscopic and macroscopic sources of magnetic field inhomogeneity. The former represents the effect of blood vessels, which underlies the BOLD response, and the latter is caused by disturbance of the magnetic field by the head. Here we compare perfect field homogeneity ($\Delta\omega = 0$), plotted as a solid line, with a through slice gradient $\Delta\omega = 20$ Hz, plotted as a dashed line. Shifting of the dashed line with respect to the solid line emphasises that macroscopic field inhomogeneity effects must be minimised.

changes in $CMRO_2$ during activation. At first glance it appears that R_2' would be a poor choice for calibration because the BOLD response depends in part on signal changes that would not be captured by R_2'. In a gradient echo-based BOLD experiment the signal change is due largely to changes in the transverse relaxation rate R_2^*, which is taken to be a sum of processes that cannot be reversed by a spin echo (R_2) and processes that can be reversed (R_2'). Motional narrowing due to diffusion of spins around sources of magnetic field heterogeneity means that a good part of the intravascular signal changes and part of the extravascular signal change around the smallest vessels cannot be fully refocused by a spin echo, and so should not contribute to R_2'. In addition, volume exchange effects as blood vessels expand also contribute to the BOLD effect, but are not directly related to R_2'. Nevertheless, our simulations indicate that R_2' in the baseline state captures much of the physiological variability of the baseline state that does affect the BOLD response. The reason it works as well as it does is probably that R_2' essentially reflects the amount of deoxyhaemoglobin in the baseline state, and the other factors affecting the BOLD response for the most part tend to scale with total deoxyhaemoglobin.

The main weakness of this calibration method is its sensitivity to magnetic field inhomogeneity. Investigation of a 20 Hz frequency difference across a voxel in one dimension showed that this causes a shift in the lines of $CMRO_2$ that increases with changes in CBF (Fig. 6). The magnitude of this shift is very similar to that caused by $CMRO_2$ changes during hypercapnia calibration. For example, a 10% $CMRO_2$ change when $\Delta\omega = 20$ Hz leads to the same R_2' as a 20% change when $\Delta\omega = 0$ ($f = 1.6$).

This magnitude of magnetic field inhomogeneity is likely for regions of the brain that are not close to air-tissue interfaces. For regions of the brain closer to the surface, where $\Delta\omega$ is larger, measurements of R_2' will need to be corrected for residual field gradients (Yablonskiy, 1998) or their effect minimised by the acquisition technique (Christen et al., 2010). Experiments using the qBOLD technique have shown that this effect can be corrected enabling R_2' calibrated BOLD to become a practical alternative to hypercapnia or hyperoxia (He and Yablonskiy, 2006). The major benefit of this alternative method is a reduction in the complexity of the experimental protocol. Equipment to perform a respiratory challenge is not required, saving time and permitting the calibration scan to be based purely on endogenous contrast.

For this approach to yield an accurate calibration factor it is assumed that deoxyhaemoglobin is the dominant source of paramagnetism in the brain. Other possible sources of iron in the brain include ferritin, transferrin, neuromelanin and haemosiderin (Stankiewicz et al., 2007). However, the sensitivity of R_2' to these sources is also dependent on the geometry of the iron deposition. This effect is maximised in the static dephasing regime where the diffusion length of protons around the susceptibility inclusion is much shorter than the dimension of the inclusion itself. This dimension is approximately equivalent to a cylinder with a radius of 7 μm, but this R_2' contrast falls away rapidly with radius. (Boxerman et al., 1995). Very small scale inclusions, such as ferritin and transferrin, do not produce R_2' contrast and appear as a pure R_2 effect. There are two main conditions in which elevated values of R_2' are measured in the brain; Parkinson's disease and brain haemorrhage. In Parkinson's disease deposits of iron in the substantia nigra, consisting of neuromelanin granules and iron filled Lewy bodies (Castellani et al., 2000), have been shown to result in elevated R_2' measurements (Ordidge et al., 1994). Lewy bodies have a diameter of approximately 8 μm and are likely to exhibit an R_2' effect. Brain haemorrhage causes bleeding into the tissues of the brain and production of haemosiderin, and has also been shown to increase R_2' (Wismer et al., 1988). If R_2' calibration is to be performed in patients with either of these conditions then care must be taken to avoid affected areas of the brain.

Estimating $CMRO_2$ changes

A measurement of $CMRO_2$ change is the ultimate aim of calibrated BOLD, converting information contained in δs, B and f into a measure of r. In the traditional approach the Davis model plays a dual role, first as a way to convert measured hypercapnia responses into a calibration factor, and second as a way to use that factor in combination with measured responses to activation to estimate the $CMRO_2$ change. In the current analysis we have essentially broken the link between the two steps. With this approach we can consider any potential method for calibrating the BOLD signal, and determine an appropriate form of $h(f,r)$ in Eq. (2) through simulations of both the calibration experiment and the activation experiment with the detailed BOLD model. That is, $h(f,r)$ is given implicitly through the detailed model by the curves in the $\delta s/B$ versus f plane (e.g., Figs. 2a and c for the hypercapnia and R_2' methods, respectively). An appropriate lookup table, or parameterization of the curves in the figures, would allow calculation of r for a given set of measurements, effectively defining $h(f,r)$. That is, although the Davis model was used to define the calibration experiment for hypercapnia, this was simply used as a particular recipe for calculating a value of B, and the detailed model was used to simulate that recipe and provide curves of how the measured signals vary with different $CMRO_2$ changes. In this way the detailed model provides a form for $h(f,r)$ that is appropriate for the defined method of calculating B. If that method changed (e.g., if the hypercapnia responses were used to calculate M with different values of α and β), then the detailed simulations would provide a

shifted set of curves defining a new form of $h(f,r)$ appropriate for the new definition of the method for calculating B.

Conclusion

The simulations performed in this study enable the potential strengths and weaknesses of BOLD calibration methods to be investigated. In addition, a new calibration method is proposed that does not require a respiratory challenge. Hypercapnia calibration is shown to be robust even when isometabolism during hypercapnia is not assumed and the flow-volume coupling is altered. Simulations of hyperoxia calibration reveal hitherto unexplored weaknesses due to the assumptions that must be made in the model of oxygen transport used to estimate the change in venous blood oxygenation due to hyperoxia. This suggests further experimental validation of this method is required before it may be used routinely. Examination of R_2' as a new calibration method show that such a technique is promising. Whilst the uncertainty in the measurement of $CMRO_2$ may be increased when compared with hypercapnia, this method is more generally applicable to the population at large as it does not require gases to be administered. However, further work is needed to develop robust acquisition methods that allow correction for large scale field inhomogeneity effects.

Additionally, in the absence of measurements of CBF, a measurement of R_2' may also be useful as a normalisation procedure to reduce intersubject variability in the BOLD response. These approaches compare the stimulus evoked BOLD response with measurements of the BOLD response to a hypercapnia challenge (Biswal et al., 2007), or with a single aspect of baseline physiology such as CBF (Liau and Liu, 2009) or baseline blood oxygenation (Lu et al., 2008). A measurement of R_2', however, is sensitive to multiple sources of physiological variability through its sensitivity to blood volume, blood oxygenation and haematocrit and may account for a greater degree of intersubject variability than traditional methods.

Acknowledgments

We would like to thank Aaron Simon, Farshad Moradi and David Dubowitz for helpful discussions regarding this work. This work was supported by funding from NIH/NINDS grant NS-036722.

Appendix A

Simulations of the effect of changes in CBF, $CMRO_2$ and baseline physiology were performed using a previously reported detailed BOLD signal model (Griffeth and Buxton, 2011). Constants required for this model are detailed in Table 1. This model was further extended to enable R_2' in the baseline resting state to be simulated. Taking Eq. (8) as a starting point, we can expand these relations to include multiple signal compartments for both gradient echo (GE) and spin echo (SE) pulse sequences.

$$S_{GE}(TE) = \left\{\left(1-V_{I,0}\right)S_{E,0}(0)e^{-TE\left(R_{2,0}+R^*_{2E}\right)} + V_{A,0}S_{A,0}(0)e^{-TE\ R'_{2A}} + V_{C,0}\,S_{C,0}(0)e^{-TE\ R'_{2C}} + V_{V,0}\,S_{V,0}(0)e^{-TE\ R'_{2V}}\right\} F(TE) \quad \text{(A1a)}$$

$$S_{SE}(TE) = \left(1-V_{I,0}\right)S_{E,0}(0)e^{-TE\left(R_{2,0}+R_{2E}\right)} + V_{A,0}\,S_{A,0}(0)e^{-TE\ R_{2A}} + V_{C,0}\,S_{C,0}(0)e^{-TE\ R_{2C}} + V_{V,0}\,S_{V,0}(0)e^{-TE\ R_{2V}} \quad \text{(A1b)}$$

Here V, $S(0)$, R_2^* and R_2 are the volume fraction, proton density and transverse relaxation rates for their respective compartments indicated by subscripts; intravascular (I), extravascular (E), arterial (A), capillary (C) and venous (V). Parameters with subscript 0 reflect the baseline resting value. Monoexponential decay of each compartment is assumed with echo time TE. The extravascular transverse relaxation rate for both GE and SE signals is modelled as a baseline rate ($R_{2,0}$) plus an additive term (R^*_{2E} or R_{2E}). This term reflects dephasing of the signal due to mesoscopic magnetic field inhomogeneity for GE and incomplete refocussing of this dephasing due to diffusional narrowing in the case of the SE. To complete the model, expressions for intra- and extravascular R_2 and R_2^* are required along with the definition of $F(TE)$, the signal attenuation due to magnetic field inhomogeneity. Intravascular signal was modelled using measurements of the dependency of R_2^* on haematocrit and blood oxygenation saturation (Y) (Zhao et al., 2007).

$$R^*_{2I} = A^* + C^*(1-Y)^2 \quad \text{(A2)}$$

In order to further generalise the detailed signal model, the dependency of A^* and C^* on haematocrit (Hct) was approximated by linearly fitting to data acquired at 3.0 T (Griffeth and Buxton, 2011; Zhao et al., 2007).

$$A^* = 14.9\,Hct + 14.7 \quad \text{(A3a)}$$

$$C^* = 302.1\,Hct + 41.8 \quad \text{(A3b)}$$

Similarly R_2 was modelled based on measurements of the dependency of blood R_2 on oxygenation and haematocrit (Zhao et al., 2007).

$$R_{21} = A + C(1-Y)^2 \quad \text{(A4)}$$

$$A = 16.4\,Hct + 4.5 \quad \text{(A5a)}$$

$$C = 165.2\,Hct + 55.7 \quad \text{(A5b)}$$

These measurements were acquired using a single spin echo pulse sequence, stepped through a range of echo time values, and hence are consistent with the short time regime of transverse signal decay (Yablonskiy and Haacke, 1994). Extravascular R_2^* was modelled using the results of Monte Carlo simulations (Ogawa et al., 1993),

$$\Delta R^*_{2E} = a^*_L \Delta_\chi\, Hct\, \omega_0 \left[V\left|Y_{off}-Y\right| - V_0\left|Y_{off}-Y_0\right|\right] \text{ for large vessels} \quad \text{(A6a)}$$

$$\Delta R^*_{2E} = a^*_S \Delta_\chi\, Hct\, \omega_0 \left[V\left|Y_{off}-Y\right|^2 - V_0\left|Y_{off}-Y_0\right|^2\right] \text{ for small vessels} \quad \text{(A6b)}$$

where the constants a^*_L and a^*_S scale R^*_{2E} for large and small vessels, respectively, and ω_0 is the proton Larmor frequency. Vessels are categorised as being large with diameters in the range 16–200 μm (arterioles and venules) or small (capillaries) with a diameter of 5 μm (Ogawa et al., 1993). Fully oxygenated blood and tissue do not have the same susceptibility and this is reflected by the blood oxygen saturation offset Y_{off}, i.e. the point at which fully oxygenated blood and tissue have the same susceptibility (Spees et al., 2001). The results of Monte Carlo simulations for a single spin echo pulse sequence were used to simulate the extravascular R_2 (Uludağ et al., 2009). These simulations are consistent with the blood R_2 measurements of Zhao et al. and with acquisition in the short echo time regime (Yablonskiy and Haacke, 1994). The large vessel relation was derived from simulations of 16 μm diameter vessels (arterioles and venules) and the small vessel relation from vessels (capillaries) of 5 μm diameter.

$$R_{2E} = V_0 \sum_n a_{L,n} \left[\Delta_\chi\, Hct\, \omega_0 \left|Y_{off}-Y_0\right|\right]^n \text{ for large vessels} \quad \text{(A7a)}$$

$$R_{2E} = V_0 \sum_n a_{S,n} \left[\Delta_\chi\, Hct\, \omega_0 \left|Y_{off}-Y_0\right|\right]^n \text{ for small vessels} \quad \text{(A7b)}$$

Finally, the signal attenuation of the gradient echo data due to large scale magnetic field inhomogeneity can also be modeled (Yablonskiy, 1998),

$$F(TE) = \frac{\sin(\Delta\omega TE/2)}{(\Delta\omega TE/2)} \quad \text{(A8)}$$

where $\Delta\omega$ is the frequency difference across the voxel. The constants detailed in these equations are listed in Table 1.

References

An, H., Lin, W., 2003. Impact of intravascular signal on quantitative measures of cerebral oxygen extraction and blood volume under normo- and hypercapnic conditions using an asymmetric spin echo approach. Magn. Reson. Med. 50, 708–716.

Biswal, B.B., Kannurpatti, S.S., Rypma, B., 2007. Hemodynamic scaling of fMRI-BOLD signal: validation of low-frequency spectral amplitude as a scalability factor. Magn. Reson. Imaging 25, 1358–1369.

Boxerman, J.L., Hamberg, L.M., Rosen, B.R., Weisskoff, R.M., 1995. MR contrast due to intravascular magnetic susceptibility perturbations. Magn. Reson. Med. 34, 555–566.

Castellani, R.J., Siedlak, S.L., Perry, G., Smith, M.A., 2000. Sequestration of iron by Lewy bodies in Parkinson's disease. Acta Neuropathol. 100, 111–114.

Chen, J.J., Pike, G.B., 2009. BOLD-specific cerebral blood volume and blood flow changes during neuronal activation in humans. NMR Biomed. 22, 1054–1062.

Chiarelli, P.A., Bulte, D.P., Wise, R., Gallichan, D., Jezzard, P., 2007. A calibration method for quantitative BOLD fMRI based on hyperoxia. NeuroImage 37, 808–820.

Christen, T., Lemasson, B., Pannetier, N., Farion, R., Segebarth, C., Rémy, C., Barbier, E.L., 2010. Evaluation of a quantitative blood oxygenation level-dependent (qBOLD) approach to map local blood oxygen saturation. NMR Biomed. 24, 393–403.

Davis, T.L., Kwong, K.K., Weisskoff, R.M., Rosen, B.R., 1998. Calibrated functional MRI: mapping the dynamics of oxidative metabolism. Proc. Natl. Acad. Sci. U. S. A. 95, 1834–1839.

Goodwin, J.A., Vidyasagar, R., Balanos, G.M., Bulte, D., Parkes, L.M., 2009. Quantitative fMRI using hyperoxia calibration: reproducibility during a cognitive Stroop task. NeuroImage 47, 573–580.

Griffeth, V.E.M., Buxton, R.B., 2011. A theoretical framework for estimating cerebral oxygen metabolism changes using the calibrated-BOLD method: modeling the effects of blood volume distribution, hematocrit, oxygen extraction fraction, and tissue signal properties on the BOLD signal. NeuroImage 58, 198–212.

Griffeth, V.E.M., Perthen, J.E., Buxton, R.B., 2011. Prospects for quantitative fMRI: investigating the effects of caffeine on baseline oxygen metabolism and the response to a visual stimulus in humans. NeuroImage 57, 809–816.

Grubb, R.L., Raichle, M.E., Eichling, J.O., Ter-Pogossian, M.M., 1974. The effects of changes in PaCO2 on cerebral blood volume, blood flow, and vascular mean transit time. Stroke 5, 630–639.

He, X., Yablonskiy, D.A., 2006. Quantitative BOLD: mapping of human cerebral deoxygenated blood volume and oxygen extraction fraction: default state. Magn. Reson. Med. 57, 115–126.

Hoge, R.D., Atkinson, J., Gill, B., Crelier, G.R., Marrett, S., Pike, G.B., 1999. Investigation of BOLD signal dependence on cerebral blood flow and oxygen consumption: the deoxyhemoglobin dilution model. Magn. Reson. Med. 42, 849–863.

Jain, V., Langham, M.C., Floyd, T.F., Jain, G., Magland, J.F., Wehrli, F.W., 2011. Rapid magnetic resonance measurement of global cerebral metabolic rate of oxygen consumption in humans during rest and hypercapnia. J. Cereb. Blood Flow Metab. 31, 1504–1512.

Liau, J., Liu, T.T., 2009. Inter-subject variability in hypercapnic normalization of the BOLD fMRI response. NeuroImage 45, 420–430.

Lu, H., Zhao, C., Ge, Y., Lewis-Amezcua, K., 2008. Baseline blood oxygenation modulates response amplitude: physiologic basis for intersubject variations in functional MRI signals. Magn. Reson. Med. 60, 364–372.

Lu, H., Xu, F., Grgac, K., Liu, P., Qin, Q., van Zijl, P., 2012. Calibration and validation of TRUST MRI for the estimation of cerebral blood oxygenation. Magn. Reson. Med. 67, 42–49.

Marchal, G., Rioux, P., Petit-Taboué, M.C., Sette, G., Travère, J.M., Le Poec, C., Courtheoux, P., Derlon, J.M., Baron, J.C., 1992. Regional cerebral oxygen consumption, blood flow, and blood volume in healthy human aging. Arch. Neurol. 49, 1013–1020.

Mark, C.I., Fisher, J.A., Pike, G.B., 2011. Improved fMRI calibration: precisely controlled hyperoxic versus hypercapnic stimuli. NeuroImage 54, 1102–1111.

McPhee, S.J., Hammer, G.D., 2009. Pathophysiology of Disease An Introduction to Clinical Medicine, Sixth Edition. (Lange Medical Books).

Moore, R., Berlowitz, D., Pretto, J., Brazzale, D., Denehy, L., Jackson, B., McDonald, C., 2009. Acute effects of hyperoxia on resting pattern of ventilation and dyspnoea in COPD. Respirology 14, 545–550.

Ogawa, S., Menon, R.S., Tank, D.W., Kim, S.-G., Merkle, H., Ellermann, J.M., Ugurbil, K., 1993. Functional brain mapping by blood oxygenation level-dependent contrast magnetic resonance imaging. A comparison of signal characteristics with a biophysical model. Biophys. J. 64, 803–812.

Ordidge, R.J., Gorell, J.M., Deniau, J.C., Knight, R.A., Helpern, J.A., 1994. Assessment of relative brain iron concentrations using T_2-weighted and T_2^*-weighted MRI at 3 Tesla. Magn. Reson. Med. 32, 335–341.

Perlmutter, J.S., Powers, W.J., Herscovitch, P., Fox, P.T., Raichle, M.E., 1987. Regional asymmetries of cerebral blood flow, blood volume, and oxygen utilization and extraction in normal subjects. J. Cereb. Blood Flow Metab. 7, 64–67.

Perthen, J.E., Lansing, A.E., Liau, J., Liu, T.T., Buxton, R.B., 2008. Caffeine-induced uncoupling of cerebral blood flow and oxygen metabolism: a calibrated BOLD fMRI study. NeuroImage 40, 237–247.

Roland, P.E., Eriksson, L., Stone-Elander, S., Widen, L., 1987. Does mental activity change the oxidative metabolism of the brain? J. Neurosci. 7, 2373–2389.

Severinghaus, J.W., 1979. Simple, accurate equations for human blood O2 dissociation computations. J. Appl. Physiol. 46, 599–602.

Sicard, K.M., Duong, T.Q., 2005. Effects of hypoxia, hyperoxia, and hypercapnia on baseline and stimulus-evoked BOLD, CBF, and CMRO2 in spontaneously breathing animals. NeuroImage 25, 850–858.

Spees, W.M., Yablonskiy, D.A., Oswood, M.C., Ackerman, J.J., 2001. Water proton MR properties of human blood at 1.5 Tesla: magnetic susceptibility, T_1, T_2, T_2^*, and non-Lorentzian signal behavior. Magn. Reson. Med. 45, 533–542.

Stankiewicz, J., Panter, S.S., Neema, M., Arora, A., Batt, C.E., Bakshi, R., 2007. Iron in chronic brain disorders: imaging and neurotherapeutic implications. Neurotherapeutics 4, 371–386.

Uludağ, K., Müller-Bierl, B., Uğurbil, K., 2009. An integrative model for neuronal activity-induced signal changes for gradient and spin echo functional imaging. NeuroImage 48, 150–165.

Wismer, G.L., Buxton, R.B., Rosen, B.R., Fisel, C.R., Oot, R.F., Brady, T.J., Davis, K.R., 1988. Susceptibility induced MR line broadening: applications to brain iron mapping. J. Comput. Assist. Tomogr. 12, 259–265.

Xu, F., Uh, J., Brier, M.R., Hart, J., Yezhuvath, U.S., Gu, H., Yang, Y., Lu, H., 2010. The influence of carbon dioxide on brain activity and metabolism in conscious humans. J. Cereb. Blood Flow Metab. 31, 58–67.

Yablonskiy, D.A., 1998. Quantitation of intrinsic magnetic susceptibility-related effects in a tissue matrix. Phantom study. Magn. Reson. Med. 39, 417–428.

Yablonskiy, D.A., Haacke, E.M., 1994. Theory of NMR signal behavior in magnetically inhomogeneous tissues: the static dephasing regime. Magn. Reson. Med. 32, 749–763.

Zhao, J.M., Clingman, C.S., Närväinen, M.J., Kauppinen, R.A., van Zijl, P.C.M., 2007. Oxygenation and hematocrit dependence of transverse relaxation rates of blood at 3T. Magn. Reson. Med. 58, 592–597.

Section C: Using Hyperoxia to measure venous CBV

Contents lists available at SciVerse ScienceDirect

NeuroImage

journal homepage: www.elsevier.com/locate/ynimg

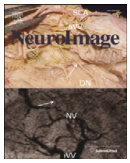

An analysis of the use of hyperoxia for measuring venous cerebral blood volume: Comparison of the existing method with a new analysis approach

Nicholas P. Blockley [a,b,*], Valerie E.M. Griffeth [c], Michael A. Germuska [b], Daniel P. Bulte [b], Richard B. Buxton [a,d]

[a] Center for Functional Magnetic Resonance Imaging, Department of Radiology, University of California San Diego, La Jolla, CA, USA
[b] FMRIB Centre, Nuffield Department of Clinical Neurosciences, University of Oxford, Oxford, UK
[c] Department of Bioengineering and Medical Scientist Training Program, University of California San Diego, La Jolla, CA, USA
[d] Kavli Institute for Brain and Mind, University of California San Diego, La Jolla, CA, USA

ARTICLE INFO

Article history:
Accepted 13 January 2013
Available online 28 January 2013

Keywords:
Venous cerebral blood volume
Hyperoxia
Oxygen
BOLD
fMRI

ABSTRACT

Hyperoxia is known to cause an increase in the blood oxygenation level dependent (BOLD) signal that is primarily localised to the venous vasculature. This contrast mechanism has been proposed as a way to measure venous cerebral blood volume (CBVv) without the need for more invasive contrast media. In the existing method the analysis modelled the data as a dynamic contrast agent experiment, with the assumption that the BOLD signal of tissue was dominated by intravascular signal. The effects on the accuracy of the method due to extravascular BOLD signal changes, as well as signal modulation by intersubject differences in baseline physiology, such as haematocrit and oxygen extraction fraction, have so far been unexplored. In this study the effect of extravascular signal and intersubject physiological variability was investigated by simulating the hyperoxia CBVv experiment using a detailed BOLD signal model. This analysis revealed substantial uncertainty in the measurement of CBVv using the existing analysis based on dynamic contrast agent experiments. Instead, the modelling showed a simple and direct relationship between the BOLD signal change and CBVv, and an alternative analysis method with much reduced uncertainty was proposed based on this finding. Both methods were tested experimentally, with the new method producing results that are consistent with the limited literature in this area.

Introduction

Hyperoxia has previously been proposed as a tracer for measuring venous cerebral blood volume (CBVv) (Bulte et al., 2007a, 2007b). The subject is asked to breathe a hyperoxic gas mixture interleaved with periods of air breathing. Breathing a hyperoxic gas mixture produces an increase in venous haemoglobin saturation resulting in an increase in the blood oxygenation level dependent (BOLD) signal. In analogy with T_1-based contrast agent studies for measuring total cerebral blood volume (CBV), the measured BOLD signal from tissue is normalised by the signal from a 100% CBV voxel located in a large vein (Newman et al., 2003; Rempp et al., 1994). This analysis approach assumes that the signals measured in both cases are dominated by intravascular signal change. However, the tissue signal has a significant extravascular component that makes up around 70% of the total signal at 3.0 T (Uludağ et al., 2009). The magnitude of the BOLD response is also dependent on physiological differences between subjects (Blockley et al., 2012) potentially confounding the measurement of CBVv. However, quantitative measurements of CBVv have a number of potential uses. For example, the acquisition of normative data in the healthy brain would allow for a comparison with the diseased state. In addition, the dynamic range of the BOLD response is strongly influenced by CBVv (Blockley et al., 2012). Therefore measurements of CBVv may be useful when controlling for differences in the magnitude of the BOLD response across subjects and in disease.

In this work we performed simulations of the existing method of measuring CBVv using a detailed model of the BOLD signal and its response to a hyperoxic stimulus. These simulations enable the physiological confounds of this method to be considered in a way that experiments alone could not achieve. Specifically the effect of intersubject variations in baseline physiology and alterations in cerebral blood flow (CBF) and oxygen metabolism ($CMRO_2$) due to hyperoxia were considered. Following on from these simulations an alternative analysis method is proposed that has lower sensitivity to baseline physiological variability.

* Corresponding author at: FMRIB Centre, Nuffield Department of Clinical Neurosciences, University of Oxford, John Radcliffe Hospital, Headington, Oxford, OX3 9DU, UK. Fax: +44 1865 222717.
E-mail address: nicholas.blockley@ndcn.ox.ac.uk (N.P. Blockley).

1053-8119/$ – see front matter © 2013 Elsevier Inc. All rights reserved.
http://dx.doi.org/10.1016/j.neuroimage.2013.01.039

Experiments were performed to establish the plausibility of the measurements produced by both methods with reference to literature values.

Theory and simulations

Extravascular BOLD signal

Firstly we consider the effect of an increase in venous haemoglobin saturation on the BOLD signal when the brain is under baseline resting conditions. At 3.0 T the majority of the BOLD signal originates in the extravascular compartment and is caused by an enhancement of the tissue transverse relaxation rate, R_2^*, by magnetic field gradients surrounding deoxygenated blood vessels. Theoretical and Monte Carlo numerical analyses have shown that the enhancement of extravascular R_2^* (δR_2^*) is a function of CBVv (V_v) and venous deoxyhaemoglobin concentration ($[dHb]_v$, $g_{dHb} dl_{blood}^{-1}$) (Ogawa et al., 1993; Yablonskiy and Haacke, 1994).

$$\delta R_2^* = \kappa V_v [dHb]_v^{\beta} \tag{1}$$

Here κ reflects properties of the experiment including vessel geometry, field strength and the susceptibility of deoxyhaemoglobin. The exponent β is dependent on the blood vessel scale under examination due to diffusion of water protons around these vessels, with $\beta = 1$ being used for larger vessels, such as venules and larger, and $\beta = 2$ being used for capillaries. The aim of this study was to target CBVv and hence $\beta = 1$ is most appropriate, leading to the following relation for the change in extravascular R_2^* (ΔR_2^*). Since the aim of these experiments was to measure resting baseline CBVv it is assumed to be unchanged in this simple model.

$$\Delta R_2^* = \kappa V_v \Delta [dHb]_v \tag{2}$$

Hyperoxia results in only small changes in ΔR_2^* suggesting that a linear approximation is appropriate to describe the fractional change in BOLD signal (δS_{tiss}).

$$\delta S_{tiss} \approx TE \kappa V_v \Delta [dHb]_v \tag{3}$$

Therefore, for venous vessels the resting CBVv is a function of the BOLD signal change that results from the change in deoxyhaemoglobin concentration ($\Delta[dHb]_v$) caused by a hyperoxic stimulus. This enables CBVv to be measured as long as $\Delta[dHb]_v$ can be accurately estimated. However, it is clear that this would not be the case for capillaries. In addition this model does not take account of intravascular signal change, which still represents a significant fraction of the total signal at 3.0 T. Therefore, detailed modelling of the BOLD signal, incorporating all of these effects, is required to test whether CBVv can be measured in this way.

Oxygen transport modelling

We now consider the underlying physiology that results in an increase in venous haemoglobin saturation during the administration of a hyperoxic stimulus. Oxygen is carried by the blood in two ways, bound to haemoglobin or dissolved in plasma. If we first consider the arterial blood, its saturation (SaO_2) is dependent on the oxygen partial pressure of the blood (PaO_2) in units of mm Hg. This can be approximated by the following relation (Severinghaus, 1979).

$$SaO_2 = \frac{1}{\frac{23400}{(PaO_2)^3 + 150 PaO_2} + 1} \tag{4}$$

The total oxygen content of the blood (CaO_2) is the sum of the haemoglobin (ϕ [*Hb*] SaO_2) and plasma (ε PaO_2) contributions.

$$CaO_2 = \phi [Hb] SaO_2 + \varepsilon PaO_2 \tag{5}$$

The constants ϕ, [*Hb*] and ε are the oxygen carrying capacity of haemoglobin ($\phi = 1.34\ ml O_2 g_{Hb}^{-1}$), the blood haemoglobin concentration ($[Hb] = 15\ g_{Hb} dl_{blood}^{-1}$, equivalent to a haematocrit of 0.45) and the solubility coefficient of oxygen in blood ($\varepsilon = 0.0031\ ml O_2 dl_{blood}^{-1}$ mm Hg^{-1}), respectively (Chiarelli et al., 2007). This relation holds for venous blood, but the total oxygen content of venous blood (CvO_2) can also be defined in terms of CaO_2, where $CmetO_2$ is the oxygen extracted to serve oxidative metabolism.

$$CvO_2 = CaO_2 - CmetO_2 \tag{6}$$

Rearranging, the venous haemoglobin saturation (SvO_2) can be written in the following way, where PvO_2 is the oxygen partial pressure of venous blood.

$$SvO_2 = \frac{CaO_2 - CmetO_2 - \varepsilon PvO_2}{\phi [Hb]} \tag{7}$$

Hence the resting $[dHb]_v$ level can be evaluated given the following relation.

$$[dHb]_v = [Hb](1 - SvO_2) \tag{8}$$

It is fair to assume that PvO_2 is negligibly small as the oxygen in the venous plasma is in equilibrium with that bound to haemoglobin. Since the change in haemoglobin saturation due to hyperoxia is relatively small the change in PvO_2 will be even smaller, i.e. $\Delta PvO_2 \approx 3$ mm Hg. For now, we will consider that $CmetO_2$ is not altered by hyperoxia. With these assumptions the change in venous deoxyhaemoglobin concentration, $\Delta[dHb]_v$, can then be described by,

$$\Delta [dHb]_v = \frac{\phi [Hb] \Delta SaO_2 + \varepsilon \Delta PaO_2}{\phi}. \tag{9}$$

Here ΔSaO_2 and ΔPaO_2 are the changes in SaO_2 and PaO_2 in response to hyperoxia, respectively. Unlike PvO_2, PaO_2 contributes significantly to $\Delta[dHb]_v$ as it can be easily three orders of magnitude greater than the venous effect, i.e. $\Delta PaO_2 \approx 200$ mm Hg. Eq. (9) predicts that changes in venous blood oxygen saturation will dominate during a hyperoxic stimulus. For example, when $\Delta PaO_2 = 200$ mm Hg and $[Hb] = 15\ g_{Hb} dl_{blood}^{-1}$, the change in arterial deoxyhaemoglobin content, $\Delta[dHb]_a$, is approximately $-0.24\ g_{dHb} dl_{blood}^{-1}$, whilst $\Delta[dHb]_v$ is approximately $-0.70\ g_{dHb} dl_{blood}^{-1}$. This equates to a ~3 times larger change in [*dHb*] in venous vessels. Hence changes in the BOLD signal will be strongly weighted towards the venous vasculature. However, Eq. (9) assumes isometabolism and therefore detailed modelling of the BOLD signal is required to examine the results when this is not true.

Simulations

Simulations were performed to test the underlying principle of using hyperoxia to measure resting baseline CBVv and the sensitivity of this method to intersubject variations in physiology. Oxygen transport and the BOLD signal are dependent on properties of the blood, with the haematocrit and venous haemoglobin saturation being the most important. However, the value of these parameters does have substantial variation within the population. The PET literature defines a relatively broad range of OEF values from 0.35 to 0.55 (Marchal et al., 1992). Similarly haematocrit varies in the ranges of 0.42–0.50 for males and 0.37–0.47 for females (McPhee and Hammer, 2009). These parameters, along with CBVv, determine the maximum BOLD signal amplitude. A detailed BOLD signal model (Griffeth and Buxton,

2011) was used to simulate the BOLD response to hyperoxia to investigate the effect of variability in baseline physiology. A summary of the salient features of the model and analysis approach will now be presented; see Griffeth and Buxton (2011) and Blockley et al. (2012) for further detail. The detailed BOLD signal model includes intra- and extravascular signal contributions from three vascular compartments; arteries, capillaries and veins. Extravascular signals were modelled using the results of numerical simulations for two vessel scales to reflect the different signal characteristics of capillaries ($\beta = 2$) compared with arteries and veins ($\beta = 1$) (Ogawa et al., 1993). Intravascular signals were described using empirical measurements of blood R_2^* as a function of oxygenation and haematocrit (Griffeth and Buxton, 2011; Zhao et al., 2007). Capillary blood haemoglobin saturation was described by a weighted average of the arterial and venous values (Griffeth and Buxton, 2011). Distribution of blood to the three compartments was achieved by assigning a value of total CBV and partitioning this volume into relative volume fractions, Ω, for each of the compartments (subscripts a, c, v for the arterial, capillary and venous compartments, respectively). Relative volume fractions were initially set as $\Omega_a = 0.2$, $\Omega_c = 0.4$ and $\Omega_v = 0.4$. The effect of physiological variation was simulated by randomly selecting pairs of haematocrit and OEF values to sample the expected distribution of the population (Blockley et al., 2012). Values were selected in the ranges of 0.37–0.50 and 0.35–0.55 for haematocrit and OEF, respectively. The baseline total CBV fraction was added as an additional randomly selected value meaning that each data point was defined by three parameters. Total CBV fraction was allowed to vary in the range of 0 to 0.1 to bracket the experimentally observed value of 0.05 (Roland et al., 1987).

The following steps were followed to simulate the CBVv experiment. The BOLD signal change ($\delta S = \Delta S / S_0$) resulting from breathing a hyperoxic gas mixture was simulated for tissue (tiss) and vein (vein) using the detailed BOLD signal model. One thousand values of δS_{tiss} and δS_{vein} were produced using a uniform random number generator to select values for haematocrit, OEF and CBVv in the ranges described above. The uncertainty introduced by this physiological variability was assessed by plotting the measured signals against the true CBVv to assess the scatter in this relationship. For the existing method the measured quantity is the tissue signal normalised by the signal from a vein measured at steady state, per Eq. (10) (Bulte et al., 2007b). This equation is re-written in terms of percentage CBVv rather than ml g^{-1} of tissue as in the original reference.

$$\mathrm{CBVv} = h \frac{\ln(\delta S_{tiss} + 1)}{\ln(\delta S_{vein} + 1)} \tag{10}$$

Scaling of the measured signals in terms of CBVv is provided by the constant $h = (1 - \mathrm{Hct}) / (1 - \mathrm{r\,Hct})$, where Hct is the haematocrit and r = 0.85 corrects for differences between small and large vessel haematocrit. However, this scaling was neglected at this stage in order to test the fundamental relationship between the measured quantity and CBVv. Figs. 1a–c plot the effect of intersubject physiological variation on this relationship for three different levels of hyperoxia: $\Delta PaO_2 = 200$ mm Hg, 300 mm Hg and 400 mm Hg. The effect of haematocrit and OEF alone, and in combination, reveals that OEF causes substantial variability in this relationship. Such variability will increase the uncertainty on the measurement of CBVv.

This result led us to consider an alternative analysis approach that does not require a measurement of the venous BOLD signal change (δS_{vein}). Figs. 1d–f plot the unnormalised tissue BOLD signal, δS_{tiss}, against CBVv for the same hyperoxic levels to investigate the effect of haematocrit and OEF alone and in combination. A much tighter and approximately linear relationship is revealed that shows lower sensitivity to OEF. However, the slope of this relationship is dependent on the specific ΔPaO_2 experienced by the subject. Due to the linearity of the relationship between δS_{tiss} and CBVv a method for scaling the former in units of the latter is required. Figs. 1d–f show that variations in haematocrit and OEF result in much less uncertainty in this relationship than was the case for the existing method. However this effect is relatively small, leading to a ±5% variation in the value of $\Delta[dHb]_v$ with respect to the

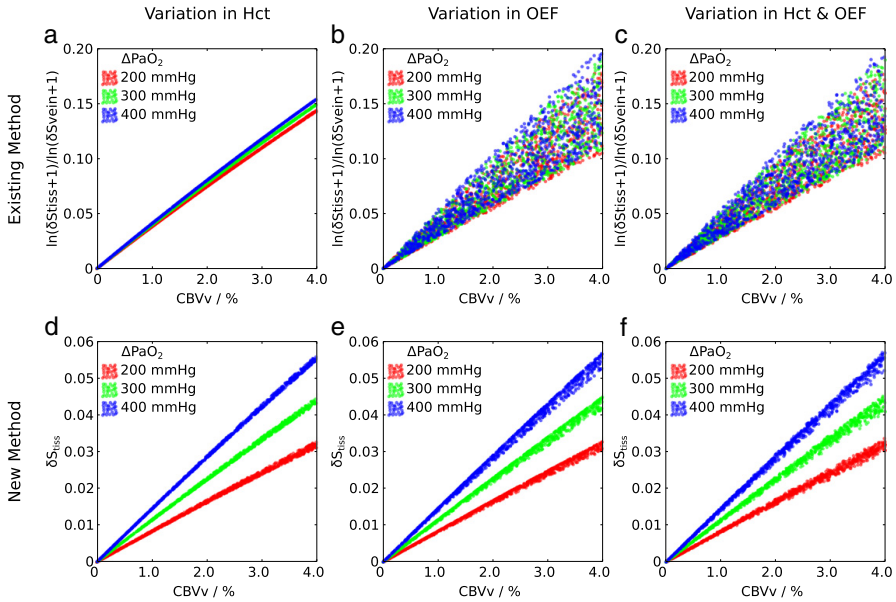

Fig. 1. Simulation of the relationship between the measured signal and true CBVv for the existing (Eq. (10)) and new methods (Eq. (11)). Three different hyperoxia levels were simulated described by the change in arterial PO_2 (ΔPaO_2). The effect of variations in haematocrit (a,d) and OEF (b,e) alone, and in combination (c,f), is considered. A large amount of uncertainty is observed for the existing method suggesting that it cannot accurately account for physiological variability. By plotting the unnormalised tissue BOLD signal response a much tighter and approximately linear response is revealed.

mean value for $\Delta PaO_2 = 200$ mm Hg (typical of the experiments below) given the range of haematocrit expected in the population. This variation is similarly small for the OEF. Therefore, an empirical model, inspired by the form of Eq. (3), is proposed to calculate an appropriate scaling factor as a function of echo time (TE) and ΔPaO_2 alone. The error caused by not including the effects of variation in haematocrit and OEF is likely to be smaller than the typical precision of this experiment. This also results in a more practical method as further measurements of haematocrit and OEF are not required.

$$CBVv = \left(\frac{A}{TE} + B\right)\left(\frac{C}{\Delta PaO_2} + D\right)\delta S_{tiss} \quad (11)$$

Further simulations were performed (not shown) varying TE and ΔPaO_2 to estimate A, B, C and D yielding the following values: A = 27.0 ms, B = 0.2, C = 245.1 mm Hg, D = 0.1.

Three potential confounds of this new method were identified. Firstly, the relative volume fractions (Ω) of the vascular compartments determine the proportion of the signal derived from the different extravascular regimes (static dephasing versus motional narrowing) with the potential to increase the uncertainty in the CBVv measurement. This effect was examined by setting the arterial volume fraction as $\Omega_a = 0.2$ and varying the venous fraction Ω_v between 0.4 and 0.6, whilst keeping the sum of Ω_v and, the capillary fraction, Ω_c constant. Fig. 2a shows that this has only a weak effect on the relationship between δS_{tiss} and CBVv. Secondly, it has been observed that CBF decreases during hyperoxia, through the direct effect of oxygen (Bulte et al., 2007a) and through an associated reduction in blood carbon dioxide (CO_2) levels (Iscoe and Fisher, 2005). This effect was investigated by simulating the effect of a 5% flow reduction during hyperoxia. The concomitant change in CBV was modelled as previously described (Griffeth and Buxton, 2011). Briefly, the change in total CBV at steady state was defined using Grubb's relation: $CBV = CBF^{\alpha}$ where $\alpha = 0.38$. This change was then distributed across the vascular compartments using similar power law relations. For the venous compartment α was set to 0.2 (Chen and Pike, 2009) and for the capillary compartment a value $\alpha = 0.1$ was used, with the arterial compartment contributing the remainder of the volume change. Since these experiments were performed at steady state, the slow recovery of CBVv due to balloon effects was not considered. Fig. 2b shows that this causes the relationship between δS_{tiss} and CBVv to shift and broaden. Finally, the effect of a change in $CMRO_2$ during hyperoxia was considered. However, it isn't clear from the literature whether $CMRO_2$ increases (Rockswold et al., 2010), remains the same (Diringer et al., 2007) or decreases (Richards et al., 2007; Xu et al., 2012) during hyperoxia. Therefore, $CMRO_2$ changes of $\pm 10\%$ were simulated. Fig. 2c shows that this causes the relationship between δS_{tiss} and CBVv to shift and broaden in a similar manner to Fig. 2b, but to a larger degree.

Experimental methods and results

Imaging

This study was approved by the National Research Ethics Service, Oxfordshire REC A. Informed consent was obtained from nine healthy subjects (6 male, mean age 28 ± 4 years). Subjects were scanned at 3.0 T on Siemens Trio (n = 7) and Verio (n = 2) scanners (Siemens Medical Solutions, Erlangen, Germany). Both systems were equipped with a transmit body coil and multi-channel head receive coils (Trio—12 channel, Verio—32 channel). Foam inserts were placed around the subject's head to minimise motion. Gradient-echo echo planar images (EPI) were acquired with BOLD-weighting (TE = 30 ms). Images were acquired with $3 \times 3 \times 3$ mm^3 spatial resolution using a 64×64 matrix over 53/44 (Trio/Verio) slices with a temporal resolution of 3.0/2.4 s. A high resolution structural MPRAGE scan (Mugler and Brookeman, 1990) was acquired to enable grey and white matter masks to be generated (TR/TE = 2040/4.7 ms, flip = 8°, 1 mm isotropic resolution).

The hyperoxic condition was achieved by presenting 100% oxygen to the subject via a two tube nasal cannula at 7 lpm, whilst simultaneously sampling inspired and expired gases. Due to mixing with room air, the inspired oxygen fraction was approximately 50%. Two 2 minute periods of hyperoxia were interleaved with 2 min of room air. End-tidal PO_2 ($P_{ET}O_2$) and PCO_2 ($P_{ET}CO_2$) were recorded throughout the experiment using a Biopac MP150 (Biopac Systems, Inc. Goleta, CA, USA) with oxygen and carbon dioxide gas analyser units (O2100C and CO2100C), at a sampling rate of 25 Hz. PCO_2 data were not analysed further due to a calibration error in some data sets.

Analysis

Two subjects were excluded from the analysis due to a $\Delta P_{ET}O_2$ less than 100 mm Hg. Images were pre-processed using FSL software tools for motion correction (Jenkinson et al., 2002) and brain extraction (Smith, 2002). High pass temporal filtering with a cut-off of 240 s and spatial smoothing with a Gaussian kernel with a full width half maximum of 5 mm were applied to the data. The BOLD signal response due to hyperoxia was analysed by fitting a general linear model of the expected time-course using FEAT (Woolrich et al., 2001). This model function was generated by convolving a 2 minute box-car with a Gamma-variate function (phase 0 s, standard deviation 30 s, mean lag 60 s) (Bulte et al., 2012). The $P_{ET}O_2$ time-course was not used as a regressor as this would require accurate synchronisation with the scanner, precise selection of the end-tidal PO_2 in the respiratory cycle and would lead to the inclusion of additional noise. The resulting parameter estimate for the hyperoxia challenge was converted to

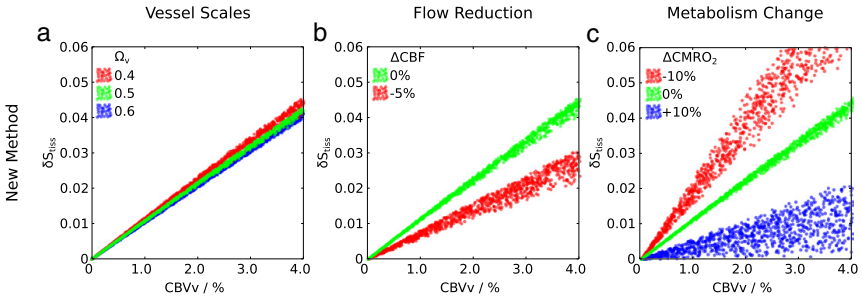

Fig. 2. Simulation of the relationship between the measured signal and true CBVv for the new method (Eq. (11)). (a) The effect caused by the distribution of vessel scales was examined by altering the fraction of the total CBV occupied by venous vessels (Ω_v), whilst keeping the combined capillary and venous fraction constant. (b) Hyperoxia has been shown to cause a reduction in CBF (ΔCBF), hence the effect of a 5% flow reduction was examined. (c) It has also been suggested that hyperoxia may alter resting $CMRO_2$. $CMRO_2$ changes of $\pm 10\%$ ($\Delta CMRO_2$) were considered.

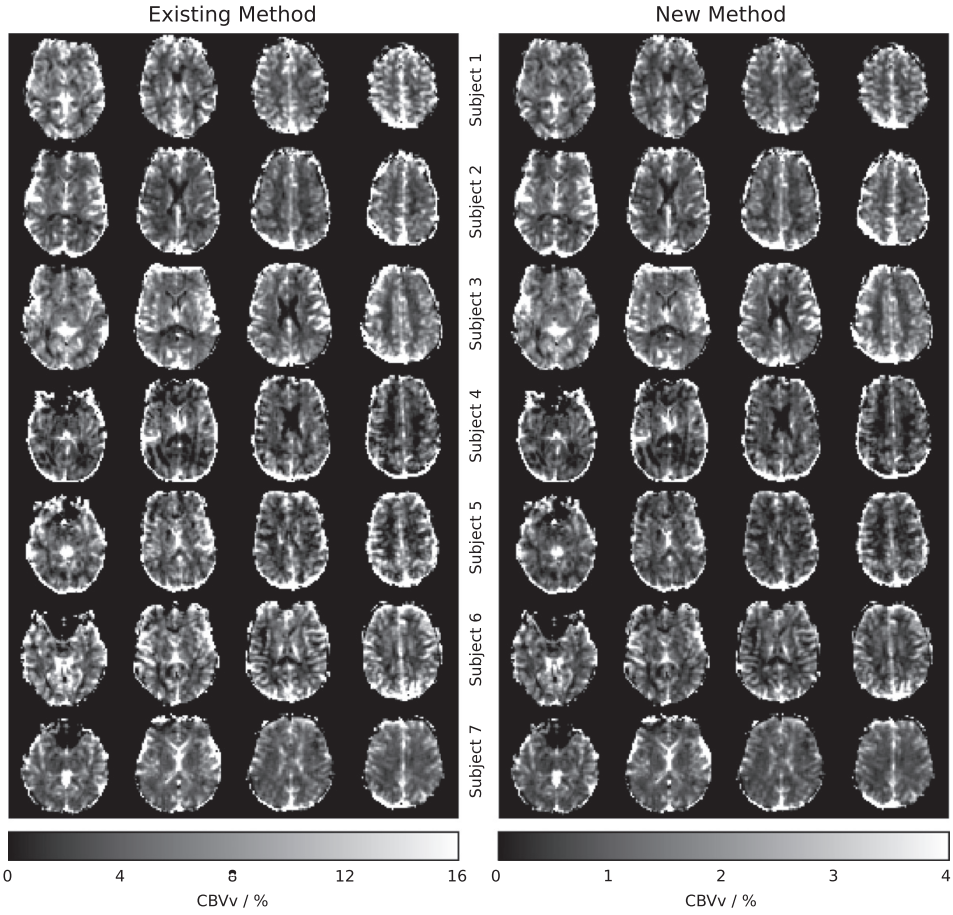

Fig. 3. Maps of CBVv for the existing and new methods, calculated using Eqs. (10) and (11) respectively, as a percentage of the total voxel volume. Note the difference in scaling between each of the methods; 0–16% versus 0–4%.

percent BOLD signal change by dividing by the mean signal intensity over time and multiplying by 100. Maps of percent BOLD signal change were then used to calculate CBVv in percent using Eq. (10) (existing method) and Eq. (11) (new method).

For the existing method, voxels within the sagittal sinus were selected in the following way. Firstly, the centre of the sagittal sinus was manually defined on 5 slices and a 3 dimensional spline fitted to these points. An 8×8 voxel region of interest was then placed at the vessel centre defined by the spline on a slice-by-slice basis to produce the final mask. The percent BOLD signal change map was then masked before thresholding at the 99th percentile. Finally, the mean of the remaining voxels was used to define δS_{vein} in Eq. (10). The new method (Eq. (11)) requires a measurement of the change in PaO_2 between the normoxic and hyperoxic states (ΔPaO_2). We infer this from measurements of $P_{ET}O_2$ under the assumption that the arterial blood is well equilibrated with the gas in the alveoli and that the alveolar-arterial oxygen gradient is not altered by hyperoxia. The hyperoxic $P_{ET}O_2$ was measured from the last 30 s of each 2 minute hyperoxia challenge, whilst the normoxic value was taken from a 1 minute window preceding the first hyperoxic block.

Functional data were also registered to the subject's own structural image (Jenkinson et al., 2002). Automated segmentation of the structural image was performed using FAST to produce grey matter, white matter and CSF regions of interest (ROI) (Zhang et al., 2001). Grey and white matter ROIs were then transformed back into functional space and subsequently used to calculate the mean and standard deviation of CBVv for these tissue types. Fig. 3 shows five example slices taken from approximately the same region of the brain in each of the subjects. Table 1 gives mean grey and white matter CBVv values.

Discussion

Measuring the BOLD response to a hyperoxia challenge has the potential to provide the most sensitive measurement available of CBVv. The existing analysis approach essentially treated hyperoxia as a contrast agent that simply alters the venous blood signal, so that normalising the BOLD signal change in a tissue voxel to the signal change measured inside a large vein gives the fractional venous CBV in that voxel. Here we used a detailed model of the BOLD effect to show that a different physical picture of the effect of hyperoxia can provide a better foundation for

Table 1
Mean grey and white matter percent CBVv for both methods. Regions of interest created by segmentation of a high resolution structural image.

Subject	Existing method				New method				
	Grey matter CBVv/%		White matter CBVv/%		Grey matter CBVv/%		White matter CBVv/%		$\Delta P_{ET}O_2$/mm Hg
	Mean	S.D.	Mean	S.D.	Mean	S.D.	Mean	S.D.	
1	9.77	9.53	6.69	5.07	2.38	2.70	1.64	1.33	198.4
2	8.16	9.20	4.21	2.91	2.68	3.31	1.37	0.97	201.6
3	9.14	8.04	5.41	2.94	2.75	2.79	1.60	0.88	161.5
4	6.53	7.31	3.90	3.26	1.76	2.19	1.06	0.98	147.3
5	8.68	8.61	4.64	4.41	2.03	2.15	1.08	1.08	149.1
6	8.42	7.81	4.74	3.38	1.88	2.29	1.11	0.83	197.0
7	7.01	6.35	4.62	2.79	1.81	2.04	1.24	0.80	222.9
Mean[a]	8.24	1.14	4.89	0.92	2.18	0.41	1.30	0.24	182.5

[a] Intersubject mean and standard deviation calculated from individual subject mean values.

determining CBVv. Specifically, we found that the BOLD signal change itself, without normalisation, has a simple and direct relationship with CBVv. The basic physical picture is that a given level of hyperoxia, in the absence of flow or metabolism changes, produces the same change in venous deoxyhaemoglobin concentration $\Delta[dHb]_v$ in all venous vessels, regardless of the baseline oxygen extraction fraction. Because the BOLD signal change is primarily driven by a change in total deoxyhaemoglobin (the product of CBVv and $\Delta[dHb]_v$), CBVv can be determined directly from the BOLD signal change provided that $\Delta[dHb]_v$ is accurately estimated. Experimental data was analysed based on using both the new approach and the existing approach. The results differed by about a factor of four, with the results of the new approach in good agreement with literature values.

In addition, we examined the confounding effects of subject variability of haematocrit and baseline oxygen extraction fraction on the estimate of CBVv. If there is no accompanying change in CBF or $CMRO_2$ with hyperoxia, the new method is insensitive to variations in baseline OEF. However, if CBF or $CMRO_2$ changes with hyperoxia, this conclusion changes, and the sensitivity to baseline OEF grows. For this reason, maintaining constant CBF and minimising the potential for $CMRO_2$ change are important goals for these experiments. We also examined the effect of variability in haematocrit, which affects the estimation of the deoxyhaemoglobin change $\Delta[dHb]_v$. Whilst this effect is small, accuracy can be improved by directly measuring haematocrit in each subject and including its effect in a model of the scaling factor. Knowledge of the subject's OEF could also improve the accuracy of the new method and could be incorporated into the model, but is unlikely to be available in practice.

Simulations

An ideal method for measuring CBVv should produce a tight one-to-one relationship between the measured quantities and CBVv, regardless of differences in haematocrit and OEF across subjects. If these unknown variables broaden the distribution of possible measurement outcomes for a given CBVv increase, the uncertainty of the CBVv estimate grows. Figs. 1a–c show that the existing measurement technique (Eq. (10)) gives a large uncertainty in CBVv. However, by plotting δS_{tiss} alone (Figs. 1d–f) a much lower uncertainty in the value of CBVv can be achieved. This perhaps paradoxical result can be explained by considering two elements of the signal change. Firstly, the change in BOLD signal due to hyperoxia is proportional to CBVv and $\Delta[dHb]_v$, as suggested by the simplistic model described by Eq. (3). Secondly, oxygen transport modelling reveals that when $CMRO_2$ is constant during hyperoxia $\Delta[dHb]_v$ is independent of OEF and only weakly dependent on haematocrit (Figs. 1d–f). Hence changes in tissue signal with hyperoxia should be proportional to CBVv. However, during an uncontrolled hyperoxic respiratory challenge it is likely that CBF may be reduced (Bulte et al., 2007a), resulting in an altered relationship between δS_{tiss} and CBVv, and increased uncertainty (Fig. 2b). A reduction in CBF causes an increase in the OEF. Importantly the resultant decrease in venous oxygen saturation is dependent on baseline OEF, unlike isometabolic hyperoxia. Correction for this effect requires an unconfounded estimate of the change in CBF (see discussion below). There is still much debate as to whether $CMRO_2$ is altered during hyperoxia (Diringer et al., 2007; Richards et al., 2007; Rockswold et al., 2010; Xu et al., 2012). However, it is clear from Fig. 2c that, if changes in this parameter were present, they would cause a large degree of uncertainty in measurements made with the new method. In a similar manner to changes in CBF, changes in $CMRO_2$ introduce a dependency on the baseline OEF. Likewise a measurement of OEF is required for correction, which is not easily obtainable.

The weak dependence of this method on haematocrit was predicted to produce a $\pm 5\%$ variation in $\Delta[dHb]_v$. Since the change in R_2^* due to hyperoxia is proportional to the product of CBVv and $\Delta[dHb]_v$, this results in a $\pm 5\%$ error in the estimation of CBVv. This error can be minimised by measuring haematocrit in each subject and including it in the model used to calculate the scaling factor (Eq. (11)). Alternatively this error can be reduced by increasing ΔPaO_2, resulting in an increased fraction of the total oxygen content to be carried by the plasma. Since the plasma content is independent of haematocrit the mean $\Delta[dHb]_v$ is increased, but the variability due to haematocrit is unchanged, diluting the effect of physiological variability. It must be noted that the parameters that define Eq. (11) are magnetic field dependent and hence the values presented here are only valid at 3.0 T. Similar simulations would be required to define these parameters at different magnetic field strengths.

The underlying cause of the uncertainty seen with the existing method can be explained by the differing relaxivity characteristics of the intravascular and extravascular signals. Fig. 2a suggests that the extravascular signal is dominated by larger venous vessels, since altering the volume fraction occupied by small vessels (capillaries) has only a weak effect on the resulting BOLD signal. We might therefore consider the extravascular compartment to have linear relaxivity (Eq. (2)) (Ogawa et al., 1993; Yablonskiy and Haacke, 1994). However, the relaxivity of blood has been shown by theory and experiment to be quadratic (Gardener et al., 2010; Jensen and Chandra, 2000; Silvennoinen et al., 2002; Thulborn et al., 1982) meaning that the change in intravascular signal is dependent on the normoxic haemoglobin saturation of the blood. This introduces a dependency on OEF, that does not exist for the extravascular signal, resulting in the observed uncertainty.

It is also important to note that the interpretation of the hyperoxia BOLD signal presented here is incompatible with using hyperoxia to calibrate the BOLD response (Chiarelli et al., 2007). In hyperoxia calibrated BOLD a hyperoxic respiratory challenge is used to measure the BOLD scaling parameter M, which encompasses properties of the baseline physiological state including CBVv and $[dHb]_0$ (Chiarelli et al., 2007). However, we have recently shown that this approach is only valid when the correct values for haematocrit and OEF are assumed in the calculation of M (Blockley et al., 2012). Therefore suggesting that the hyperoxia BOLD signal is predominantly modulated by CBVv.

Experiments

Experimental measurements of CBVv using both methods produced very different mean values; 8.24% and 2.18% for grey matter for the existing and new methods respectively. There are currently few studies in the literature that quantitatively measure CBVv. Variants of the qBOLD sequence have been used in several studies with whole brain average CBVv estimates in the range of 2.68% to 3.68% (An and Lin, 2002a, 2002b). One study presented grey and white matter specific CBVv values of 1.75% and 0.58% (He and Yablonskiy, 2007). The fact that the results of the new method are comparable with those derived from the qBOLD method lends credibility to the assumption that CBF and $CMRO_2$ changes are small or non-existent at the hyperoxic levels achieved in this study. However, confirmation of this assumption is still required and is the subject of ongoing work.

The consistency of the results of the new method with those from qBOLD is also not surprising, as measurements of CBVv made using hyperoxia and qBOLD share a common theoretical background. The qBOLD technique relies on the different characteristics of the extravascular transverse signal decay during short and long timescales following excitation or refocussing. In the short timescale the signal decay is quadratically exponential, but reverts to monoexponential in the long timescale. Each of these timescales is differently sensitive to CBVv and $[dHb]_v$ enabling these parameters to be disentangled when data are acquired in both conditions. The hyperoxia CBVv method only acquires data in the long timescale, relying on the effects of hyperoxia to separate the CBVv effect from $[dHb]_v$, i.e. by modulating $[dHb]_v$ whilst keeping CBVv constant.

Effects of hyperoxia

Changes in CBF during hyperoxia can theoretically be corrected by measuring this change using arterial spin labelling (ASL). However, oxygen is paramagnetic and is known to alter the T_1 of arterial blood (Silvennoinen et al., 2003). Accurate quantification of ASL data requires knowledge of the arterial blood T_1, confounding the estimation of CBF when the oxygen level changes during an experiment (Buxton et al., 1998). Recently this limitation has been overcome by measuring the T_1 of arterial blood in each experiment (Pilkinton et al., 2012). However, this technique is time consuming and has not yet been performed in humans.

Alternatively changes in CBF and $CMRO_2$ can be minimised by carefully controlling the respiratory stimulus. The major driver of changes in CBF during hyperoxia is the associated hypocapnic effect (Iscoe and Fisher, 2005). Similarly the effect of oxygen on $CMRO_2$ is proportional to the degree of hyperoxia induced (Xu et al., 2012). In the experiments performed in this study an uncontrolled hyperoxia challenge was employed. However, greater control can be achieved using automated respiratory control methods (Prisman et al., 2008; Wise et al., 2007). Such methods could be used to maintain isocapnia, whilst maintaining an oxygen level that minimises changes in $CMRO_2$. The ability to target specific changes in PaO_2 using these methods opens up a further interesting possibility. When $TE = 30$ ms and $\Delta PaO_2 = 306$ mm Hg the scaling factor between CBVv and δS_{tiss} is 1. Therefore, the percentage BOLD signal change in response to hyperoxia is numerically equivalent to the percentage CBVv.

Conclusion

It was shown by simulation that the existing method for measuring CBVv using hyperoxic contrast has substantial sensitivity to variations in baseline physiology. This sensitivity is caused by the normalisation of the mostly extravascular tissue signal by intravascular blood signal. This knowledge enabled an alternative analysis with reduced sensitivity to be proposed. Experimental application of this new method produced results that were consistent with the limited results available in the literature.

Acknowledgments

NPB, VEMG and RBB were supported by funding from NIH/NINDS grant NS-036722. NPB was also supported by funding from the Stroke Association and the Dunhill Medical Trust. VEMG was additionally supported by funding from NIH/NIMH grant MH095298. MAG and DPB were funded by the EPSRC.

References

An, H., Lin, W., 2002a. Cerebral oxygen extraction fraction and cerebral venous blood volume measurements using MRI: effects of magnetic field variation. Magn. Reson. Med. 47, 958–966.
An, H., Lin, W., 2002b. Cerebral venous and arterial blood volumes can be estimated separately in humans using magnetic resonance imaging. Magn. Reson. Med. 48, 583–588.
Blockley, N., Griffeth, V.E.M., Buxton, R.B., 2012. A general analysis of calibrated BOLD methodology for measuring $CMRO_2$ responses: comparison of a new approach with existing methods. NeuroImage 60, 279–289.
Bulte, D.P., Chiarelli, P.A., Wise, R.G., Jezzard, P., 2007a. Cerebral perfusion response to hyperoxia. J. Cereb. Blood Flow Metab. 27, 69–75.
Bulte, D.P., Chiarelli, P.A., Wise, R., Jezzard, P., 2007b. Measurement of cerebral blood volume in humans using hyperoxic MRI contrast. J. Magn. Reson. Imaging 26, 894–899.
Bulte, D.P., Kelly, M., Germuska, M., Xie, J., Chappell, M.A., Okell, T.W., Bright, M.G., Jezzard, P., 2012. Quantitative measurement of cerebral physiology using respiratory-calibrated MRI. NeuroImage 60, 582–591.
Buxton, R.B., Frank, L.R., Wong, E.C., Siewert, B., Warach, S., Edelman, R.R., 1998. A general kinetic model for quantitative perfusion imaging with arterial spin labeling. Magn. Reson. Med. 40, 383–396.
Chen, J.J., Pike, G.B., 2009. BOLD-specific cerebral blood volume and blood flow changes during neuronal activation in humans. NMR Biomed. 22, 1054–1062.
Chiarelli, P.A., Bulte, D.P., Wise, R., Gallichan, D., Jezzard, P., 2007. A calibration method for quantitative BOLD fMRI based on hyperoxia. NeuroImage 37, 808–820.
Diringer, M.N., Aiyagari, V., Zazulia, A.R., Videen, T.O., Powers, W.J., 2007. Effect of hyperoxia on cerebral metabolic rate for oxygen measured using positron emission tomography in patients with acute severe head injury. J. Neurosurg. 106, 526–529.
Gardener, A.G., Francis, S.T., Prior, M., Peters, A., Gowland, P.A., 2010. Dependence of blood R2 relaxivity on CPMG echo-spacing at 2.35 and 7 T. Magn. Reson. Med. 64, 967–974.
Griffeth, V.E.M., Buxton, R.B., 2011. A theoretical framework for estimating cerebral oxygen metabolism changes using the calibrated-BOLD method: modeling the effects of blood volume distribution, hematocrit, oxygen extraction fraction, and tissue signal properties on the BOLD signal. NeuroImage 58, 198–212.
He, X., Yablonskiy, D.A., 2007. Quantitative BOLD: mapping of human cerebral deoxygenated blood volume and oxygen extraction fraction: default state. Magn. Reson. Med. 57, 115–126.
Iscoe, S., Fisher, J.A., 2005. Hyperoxia-induced hypocapnia: an underappreciated risk. Chest 128, 430–433.
Jenkinson, M., Bannister, P., Brady, M., Smith, S., 2002. Improved optimization for the robust and accurate linear registration and motion correction of brain images. NeuroImage 17, 825–841.
Jensen, J.H., Chandra, R., 2000. NMR relaxation in tissues with weak magnetic inhomogeneities. Magn. Reson. Med. 44, 144–156.
Marchal, G., Rioux, P., Petit-Taboué, M.C., Sette, G., Travère, J.M., Le Poec, C., Courtheoux, P., Derlon, J.M., Baron, J.C., 1992. Regional cerebral oxygen consumption, blood flow, and blood volume in healthy human aging. Arch. Neurol. 49, 1013–1020.
McPhee, S.J., Hammer, G.D., 2009. Pathophysiology of Disease: An Introduction to Clinical Medicine, Sixth ed. Lange Medical Books.
Mugler, J.P., Brookeman, J.R., 1990. Three-dimensional magnetization-prepared rapid gradient-echo imaging (3D MP RAGE). Magn. Reson. Med. 15, 152–157.
Newman, G.C., Delucia-Deranja, E., Tudorica, A., Hospod, F.E., Patlak, C.S., 2003. Cerebral blood volume measurements by T*2-weighted MRI and contrast infusion. Magn. Reson. Med. 844–855.
Ogawa, S., Menon, R.S., Tank, D.W., Kim, S.-G., Merkle, H., Ellermann, J.M., Ugurbil, K., 1993. Functional brain mapping by blood oxygenation level-dependent contrast magnetic resonance imaging. A comparison of signal characteristics with a biophysical model. Biophys. J. 64, 803–812.
Pilkinton, D.T., Hiraki, T., Detre, J.A., Greenberg, J.H., Reddy, R., 2012. Absolute cerebral blood flow quantification with pulsed arterial spin labeling during hyperoxia corrected with the simultaneous measurement of the longitudinal relaxation time of arterial blood. Magn. Reson. Med. 67, 1556–1565.
Prisman, E., Slessarev, M., Han, J., Poublanc, J., Mardimae, A., Crawley, A.P., Fisher, J.A., Mikulis, D., 2008. Comparison of the effects of independently-controlled end-tidal PCO(2) and PO(2) on blood oxygen level-dependent (BOLD) MRI. J. Magn. Reson. Imaging 27, 185–191.
Rempp, K.A., Brix, G., Wenz, F., Becker, C.R., Gückel, F., Lorenz, W.J., 1994. Quantification of regional cerebral blood flow and volume with dynamic susceptibility contrast-enhanced MR imaging. Radiology 193, 637–641.

Richards, E.M., Fiskum, G., Rosenthal, R.E., Hopkins, I., McKenna, M.C., 2007. Hyperoxic reperfusion after global ischemia decreases hippocampal energy metabolism. Stroke 38, 1578–1584.
Rockswold, S.B., Rockswold, G.L., Zaun, D.A., Zhang, X., Cerra, C.E., Bergman, T.A., Liu, J., 2010. A prospective, randomized clinical trial to compare the effect of hyperbaric to normobaric hyperoxia on cerebral metabolism, intracranial pressure, and oxygen toxicity in severe traumatic brain injury. J. Neurosurg. 112, 1080–1094.
Roland, P.E., Eriksson, L., Stone-Elander, S., Widen, L., 1987. Does mental activity change the oxidative metabolism of the brain? J. Neurosci. 7, 2373–2389.
Severinghaus, J.W., 1979. Simple, accurate equations for human blood O2 dissociation computations. J. Appl. Physiol. 46, 599–602.
Silvennoinen, M.J., Clingman, C.S., Golay, X., Kauppinen, R.A., van Zijl, P.C.M., 2002. Comparison of the dependence of blood R_2 and R_2^* on oxygen saturation at 1.5 and 4.7 Tesla. Magn. Reson. Med. 49, 47–60.
Silvennoinen, M.J., Kettunen, M.I., Kauppinen, R.A., 2003. Effects of hematocrit and oxygen saturation level on blood spin-lattice relaxation. Magn. Reson. Med. 49, 568–571.
Smith, S.M., 2002. Fast robust automated brain extraction. Hum. Brain Mapp. 17, 143–155.
Thulborn, K.R., Waterton, J.C., Matthews, P.M., Radda, G.K., 1982. Oxygenation dependence of the transverse relaxation time of water protons in whole blood at high field. Biochim. Biophys. Acta 714, 265–270.
Uludağ, K., Müller-Bierl, B., Uğurbil, K., 2009. An integrative model for neuronal activity-induced signal changes for gradient and spin echo functional imaging. NeuroImage 48, 150–165.
Wise, R.G., Pattinson, K.T.S., Bulte, D.P., Chiarelli, P.A., Mayhew, S.D., Balanos, G.M., O'Connor, D.F., Pragnell, T.R., Robbins, P.A., Tracey, I., Jezzard, P., 2007. Dynamic forcing of end-tidal carbon dioxide and oxygen applied to functional magnetic resonance imaging. J. Cereb. Blood Flow Metab. 27, 1521–1532.
Woolrich, M.W., Ripley, B.D., Brady, M., Smith, S.M., 2001. Temporal autocorrelation in univariate linear modeling of FMRI data. NeuroImage 14, 1370–1386.
Xu, F., Liu, P., Pascual, J.M., Xiao, G., Lu, H., 2012. Effect of hypoxia and hyperoxia on cerebral blood flow, blood oxygenation, and oxidative metabolism. J. Cereb. Blood Flow Metab.
Yablonskiy, D.A., Haacke, E.M., 1994. Theory of NMR signal behavior in magnetically inhomogeneous tissues: the static dephasing regime. Magn. Reson. Med. 32, 749–763.
Zhang, Y., Brady, M., Smith, S., 2001. Segmentation of brain MR images through a hidden Markov random field model and the expectation-maximization algorithm. IEEE Trans. Med. Imaging 20, 45–57.
Zhao, J.M., Clingman, C.S., Närväinen, M.J., Kauppinen, R.A., van Zijl, P.C.M., 2007. Oxygenation and hematocrit dependence of transverse relaxation rates of blood at 3 T. Magn. Reson. Med. 58, 592–597.

OPEN ACCESS Freely available online

PLOS ONE

A Novel Method of Combining Blood Oxygenation and Blood Flow Sensitive Magnetic Resonance Imaging Techniques to Measure the Cerebral Blood Flow and Oxygen Metabolism Responses to an Unknown Neural Stimulus

Aaron B. Simon[1], Valerie E. M. Griffeth[1], Eric C. Wong[2], Richard B. Buxton[2,3]*

1 Department of Bioengineering and Medical Scientist Training Program, University of California San Diego, La Jolla, California, United States of America, **2** Center for Functional Magnetic Resonance Imaging, Department of Radiology, University of California San Diego, La Jolla, California, United States of America, **3** Kavli Institute for Brain and Mind, University of California San Diego, La Jolla, California, United States of America

Abstract

Simultaneous implementation of magnetic resonance imaging methods for Arterial Spin Labeling (ASL) and Blood Oxygenation Level Dependent (BOLD) imaging makes it possible to quantitatively measure the changes in cerebral blood flow (CBF) and cerebral oxygen metabolism ($CMRO_2$) that occur in response to neural stimuli. To date, however, the range of neural stimuli amenable to quantitative analysis is limited to those that may be presented in a simple block or event related design such that measurements may be repeated and averaged to improve precision. Here we examined the feasibility of using the relationship between cerebral blood flow and the BOLD signal to improve dynamic estimates of blood flow fluctuations as well as to estimate metabolic-hemodynamic coupling under conditions where a stimulus pattern is unknown. We found that by combining the information contained in simultaneously acquired BOLD and ASL signals through a method we term BOLD Constrained Perfusion (BCP) estimation, we could significantly improve the precision of our estimates of the hemodynamic response to a visual stimulus and, under the conditions of a calibrated BOLD experiment, accurately determine the ratio of the oxygen metabolic response to the hemodynamic response. Importantly we were able to accomplish this without utilizing *a priori* knowledge of the temporal nature of the neural stimulus, suggesting that BOLD Constrained Perfusion estimation may make it feasible to quantitatively study the cerebral metabolic and hemodynamic responses to more natural stimuli that cannot be easily repeated or averaged.

Citation: Simon AB, Griffeth VEM, Wong EC, Buxton RB (2013) A Novel Method of Combining Blood Oxygenation and Blood Flow Sensitive Magnetic Resonance Imaging Techniques to Measure the Cerebral Blood Flow and Oxygen Metabolism Responses to an Unknown Neural Stimulus. PLoS ONE 8(1): e54816. doi:10.1371/journal.pone.0054816

Editor: Allan Siegel, University of Medicine & Dentistry of NJ - New Jersey Medical School, United States of America

Received August 22, 2012; **Accepted** December 17, 2012; **Published** January 31, 2013

Funding: This work was supported by National Institutes of Health grant NS-36722 and Grant A-44 20114049 from GE healthcare. The funders had no role in study design, data collection and analysis, decision to publish, or preparation of the manuscript.

Competing Interests: The authors have read the journal's policy and have the following conflicts: 1) Research grant from GE healthcare; 2) Patent Application (Invention Disclosure filed). This does not alter the authors' adherence to all the PLOS ONE policies on sharing data and materials.

* E-mail: rbuxton@ucsd.edu

Introduction

Functional hyperemia is a phenomenon by which blood flow to a volume of brain tissue increases rapidly and dramatically in response to a local increase in neural activity. Though still poorly understood, functional hyperemia is thought to play an important role in the maintenance of homeostasis in the brain, and its dysfunction has been postulated to play a role in the etiologies of several cerebral vascular and neurodegenerative diseases [1].

Functional Magnetic Resonance Imaging (fMRI) has become a popular method of studying functional hyperemia in humans, both because it is non-invasive and because it is capable of imaging large volumes of tissue with good spatial and temporal resolution. The most commonly used fMRI technique today is blood oxygenation level dependent (BOLD) imaging. Contrast in BOLD imaging is derived from the paramagnetic properties of deoxygenated hemoglobin, which increases the transverse relaxation rate of the MR signal [2]. In general, functional hyperemia leads to a local decrease in the fraction of oxygen extracted from capillaries, increasing the oxygenation of hemoglobin in downstream venules [3] and producing a robust increase in the BOLD signal. BOLD imaging is highly sensitive to fluctuations in blood oxygenation and is thus often used to localize regions of the brain where blood oxygen saturation changes in response to neural activity. However, BOLD imaging is limited in two ways. First, it cannot be interpreted in a quantitative physiological sense, as both the rate of delivery and rate of consumption of oxygen affect the magnitude of the BOLD signal and cannot be disentangled by BOLD imaging alone [4]. Second, the BOLD signal is a change between two acutely defined states, and so is not directly sensitive to chronic physiological changes that would affect the baseline state.

Arterial spin labeling (ASL), an MR imaging technique that creates contrast by magnetically labeling arterial blood as it enters

the cerebrovasculature, is a more direct method of imaging functional hyperemia and in principle overcomes the two limitations of BOLD imaging noted above [5,6]. Like BOLD imaging, ASL is non-invasive and sensitive to the fluctuations in local blood flow that accompany neural activity. However, unlike BOLD imaging, ASL can provide quantitative information about the local perfusion in absolute physiological units, including both the baseline and activated states, making it a potentially highly useful tool for understanding brain function and cerebrovascular physiology in health and disease [6,7]. In addition, as a component of a multi-modal imaging approach including simultaneous BOLD imaging, ASL may be used to disentangle competing neuronal and vascular contributions to the BOLD signal, allowing quantitative measurement of $CMRO_2$ fluctuations [8,9]. However, ASL suffers from several limitations of its own. Amongst the greatest limitations of this technique is the intrinsically low signal-to-noise ratio of the ASL signal, which is largely due to the small amount of labeled arterial blood that can be delivered during the longitudinal relaxation time of the blood. To compensate, quantitative measurements of CBF using ASL are often made with lower spatial and temporal resolution than standard BOLD-fMRI studies, and are primarily used to measure baseline blood flow. Dynamic measurements of blood flow typically require significant trial averaging over repeated stimuli and spatial averaging over a selected region of interest [4,10–12].

While such studies provide useful insights into differences in cerebral perfusion and metabolic requirements between nominal states of "control" and "activity", the methods they employ can say little about the role of functional hyperemia in everyday neural processing. Current methods of quantitatively estimating CBF and $CMRO_2$ fluctuations associated with more natural neural tasks, which could include watching a film, listening to music, or simply lying quietly in the scanner, are inadequate in large part because the underlying stimulus driving hemodynamic and metabolic changes cannot be defined, making it difficult to identify and average measurements corresponding to the same physiological state. Here we examined the feasibility of estimating fluctuations in CBF and $CMRO_2$ without *a priori* knowledge of the temporal pattern of neural activity by combining the CBF information contained in simultaneously acquired BOLD and ASL measurements. We hypothesized that because the BOLD signal is strongly driven by CBF, simultaneous measurement of ASL and BOLD fluctuations via a combined BOLD-ASL imaging experiment could be used to model an improved estimate of the "true" CBF signal even in the presence of significant noise in both the BOLD and ASL measurements. Further, we hypothesized that under the conditions of a calibrated BOLD experiment, information about fluctuations in $CMRO_2$ could also be extracted from the information contained in the combined BOLD-ASL data. Importantly, we hypothesized that correction of the CBF signal could be accomplished without explicit, *a priori* knowledge of the stimulus presented, opening up a path towards the quantitative study of how cerebral blood flow is modulated to meet the metabolic demands of the neural processing that occurs in response to natural stimuli or at rest. We call this combination of BOLD and ASL image data BOLD-Constrained Perfusion (BCP) estimation to emphasize that our criteria for distinguishing CBF signal fluctuations from noise is that they be simultaneously reflected in the BOLD signal.

The outline of this paper is as follows. We begin with a short theoretical discussion of our motivation for pursuing the BCP estimation approach, which we illustrate schematically in Figure 1. We then present empirical results that demonstrate that the BCP approach can both increase the precision of dynamic CBF estimates and, under the conditions of a calibrated experiment, provide information about the coupling of CBF and $CMRO_2$ without *a priori* knowledge of the stimulus driving neural activity. In order to be able to validate the results of the BCP analysis, we analyzed data that were previously acquired and reported as a calibrated BOLD study [8], using a stimulus with well-understood temporal characteristics: a simple block-design visual task. Our rationale for choosing such a simple stimulus was two-fold. First, to determine whether the influence of noise on the estimated dynamic CBF time series was decreased by BCP analysis, we needed to be able to predict with some confidence what the CBF time series should be in the absence of noise. Second, in order to be able to verify that we could accurately estimate the coupling of CBF and $CMRO_2$ we needed to choose an experimental design for which traditional calibrated BOLD analysis could also be performed.

Theory

Signal and Noise in Simultaneous BOLD-ASL Imaging

In a dual-echo, simultaneous BOLD-ASL acquisition scheme, "tag" images, in which the magnetization of inflowing arterial blood is inverted, and "control" images, in which the magnetization of arterial blood is not inverted, are acquired in an interleaved fashion, typically with an echo-planar or spiral gradient recalled echo (GRE) readout. The echo time (TE) of the first echo is chosen to be as short as possible in order to minimize sensitivity to fluctuations in R_2^* decay, while the second echo is chosen to have a longer TE, so as to maximize BOLD sensitivity. From the measured time series two new time series are constructed by surround subtraction and surround addition, in which the voxel signal at one time point is appropriately combined (subtracted or added) with the average value of the preceding and following time points. Surround subtraction of sequential images acquired at the first echo time produces the ASL time series of images, in which the intensity of each voxel is weighted by the local rate of cerebral blood flow. Surround addition of sequential second echo images produces the BOLD time series of images, with little CBF weighting but considerable BOLD sensitivity [13].

However, in addition to CBF and blood oxygenation, the instantaneous magnitudes of the surround subtraction and surround addition signals, respectively, are sensitive to several sources of noise. This noise may be attributable to the scanner itself, to subject motion and cardiac pulsatility, or to instabilities in the magnetic field due to changes in the size of the thoracic cavity associated with the breathing cycle. Several methods have been developed for identifying and removing the signal contributions from some of these noise sources, in particular, subject motion, cardiac and respiratory activity, and scanner drifts [14–19]. Often, one or more of these methods is used to reduce the noise in the BOLD and ASL signals before quantitative analysis is performed. However, in general, none of these techniques can perfectly remove all sources of nuisance signal and no technique can remove the random thermal noise inherent in every signal. Thus we must think of our measured BOLD and ASL signals, even after correction for known sources of noise, as discrete time signals that are combinations of both "real" signal fluctuations (that are of interest to us) and noise [13]. We can express this very generically as

$$A[t] = f[t] + \varepsilon_A[t] \tag{1}$$

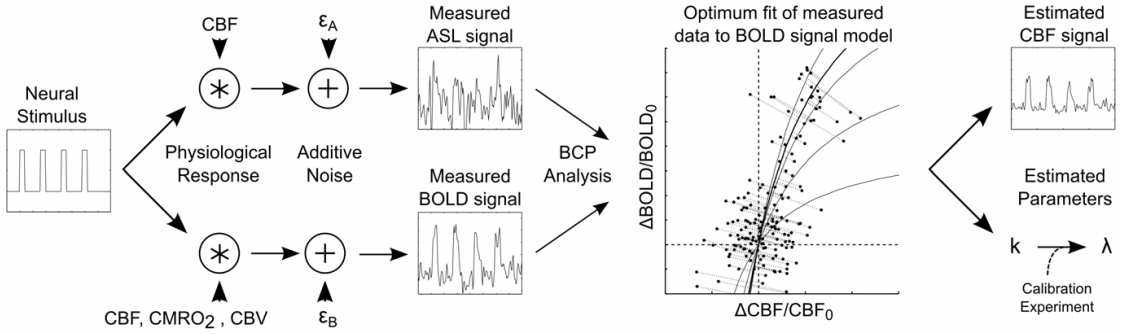

Figure 1. Schematic of the BOLD-constrained Perfusion (BCP) estimation process. When a cognitive task is presented to a subject, induced neural activity evokes both a hemodynamic and a metabolic response. ASL imaging captures principally the evoked changes in CBF while BOLD imaging is sensitive to changes in CBF, $CMRO_2$, and CBV. In addition, both imaging modalities are sensitive to noise of both physiological and mechanical origin (ε_A and ε_B, respectively). The BCP analysis approach is to combine information about CBF fluctuations present in both the BOLD and ASL signals to improve the estimate of dynamic CBF fluctuations. This is accomplished by fitting the measured data to a cost function (Equation 4 in text) that treats the measured time series as noisy representations of two signals that are linked by a simple mathematical model. The output of this process is an improved dynamic estimate of CBF fluctuations. Under the conditions of a calibrated BOLD experiment, an additional estimated parameter of the mathematical model (k) may also provide information about the coupling of $CMRO_2$ and CBF fluctuations (λ). *ASL: Arterial Spin Labeling. CBF: Cerebral Blood Flow. $CMRO_2$: Cerebral Metabolic Rate of Oxygen Metabolism. CBV: Cerebral Blood Volume.*
doi:10.1371/journal.pone.0054816.g001

$$B[t] = b[t] + \varepsilon_B[t] \tag{2}$$

where $A[t]$ and $B[t]$ are the measured ASL and BOLD signals, respectively, $f[t]$ represents a low-pass filtered representation of the CBF at sample t scaled by a constant related to imaging parameters and experimental conditions, $b[t]$ represents a low-pass filtered representation of the instantaneous BOLD signal, and $\varepsilon_A[t]$ and $\varepsilon_B[t]$ capture the contributions of random thermal noise and any physiological sources of noise in the ASL and BOLD signals, that are not completely removed by the methods cited above. The precision of the CBF and BOLD estimates at each time point is then determined by the variances of $\varepsilon_A[t]$ and $\varepsilon_B[t]$, which may still be significant, especially for the ASL signal.

Relating BOLD Fluctuations to Changes in Cerebral Blood Flow

Both $A[t]$ and $B[t]$ are driven by the underlying CBF fluctuations. The former is a direct but noisy reflection of CBF, and the latter is a more sensitive measurement but related to CBF in a nonlinear way. The central idea of BOLD-constrained perfusion (BCP) is to use both signals to make a better estimate of the underlying CBF fluctuations. To utilize the BOLD signal in this way requires a mathematical model that links changes in cerebral blood flow to changes in the BOLD signal. Recently our group developed a detailed numerical model of the BOLD response as a function of changes in $CMRO_2$, CBF, and cerebral blood volume (CBV). The model also includes a number of baseline physiological parameters (microvascular hematocrit, venous and capillary blood volume, baseline oxygen extraction fraction (OEF), etc.) that modulate the magnitude of the BOLD response [20]. Although the detailed model is not in a tractable form for the current application, it nevertheless provides a useful framework for testing the accuracy of much simpler, closed-form models. Recently we used this approach to develop a relatively simple model and test its accuracy through many simulations with the detailed model for different values of the unknown physiological parameters [14]. The form of the model is:

$$\frac{b[t]-b_0}{b_0} = M(1-\alpha_v-\lambda)\left(1-\frac{f_0}{f[t]}\right) = k\left(1-\frac{f_0}{f[t]}\right) \tag{3}$$

In this equation, the parameter M is a scaling factor that absorbs many of the physiological factors that simply scale the BOLD response and depends on the amount of deoxyhemoglobin in the baseline state as well as parameters of the image acquisition (echo time and field strength). We have used the symbol M for this scaling factor in analogy with the Davis model [21], but it should be noted that analyzing data to determine a value of M will yield a different numerical value using Equation 3 than using the original Davis model because of the different mathematical form. The factor α_v is the exponent of a power law relationship between the venous CBV change and the CBF change. The parameter λ is the ratio of the fractional change in $CMRO_2$ to the fractional change in CBF (e.g., a 20% change in $CMRO_2$ with a 40% change in CBF would correspond to $\lambda = 0.5$). Finally, f_0 and b_0 represent the magnitude of the CBF and BOLD signal in the baseline state.

We refer to this model as a *heuristic* model because it clearly shows the basic anatomy of the BOLD response: it is driven by the CBF change, but strongly modulated by the baseline state (M), the venous CBV change (α_v), and the $CMRO_2$/CBF coupling ratio (λ). In addition, though, our comparison tests with the detailed model have shown that the heuristic model is reasonably accurate as well. Previously, the most commonly used closed form model for the BOLD response was the Davis model, and our comparison tests have shown that the accuracy of these two simpler models is similar. However, the particular advantage of the heuristic model is that all of the unknown parameters that modulate the BOLD response can be combined into a single factor, k, scaling a simple nonlinear function of the CBF change. This means that our model connecting $b[t]$ to the underlying CBF fluctuation requires only a single parameter to be determined. (In principle, the BCP approach can be applied using any model that connects the BOLD response to the CBF change, and the Supporting Section and shows a similar analysis based on the Davis model. See the Document S1, Figure S1, and Figure S2 for this analysis).

BOLD Constrained Perfusion Estimation

We now propose that the precision of an estimate of the instantaneous CBF, $\hat{f}[t]$ may be improved by assuming that the expected values of the measured ASL and BOLD signals, $E[A[t]]$ and $E[B[t]]$ are the true underlying CBF and BOLD signals, $f[t]$ and $b[t]$, and that the unknown parameter k of our BOLD model has a constant value over a window of interest T samples in length. The values of $\hat{f}[0],\ldots,\hat{f}[T-1]$ and $\hat{k}$ can then be estimated by minimizing the cost function

$$\min_{\hat{f}[t],\hat{k}} g\left(\hat{f}[t],\hat{k}\right) = \sum_{t=0}^{T-1}\left(\frac{1}{\sigma^2{}_{\varepsilon_B}}\left(B[t]-\hat{b}[t]\right)^2+\frac{1}{\sigma^2{}_{\varepsilon_A}}\left(A[t]-\hat{f}[t]\right)^2\right) \quad (4)$$

under the constraint that $\hat{b}[t]=\hat{k}\left(1-\frac{f_0}{\hat{f}[t]}\right)$ (Equation 3) at every time point in the window. In essence, what we are doing here is finding the values of $\hat{f}[0],\ldots,\hat{f}[T-1]$ and $\hat{k}$ that best fit the measured ASL and BOLD signals to Equation 3 given the assumption that there is noise in both (Figure 1). Note that this is quite different from performing a simple non-linear regression of the two signals based on Equation 3, which would implicitly assume that only one of the signals contained noise and that the other was noise-free. In the cost function represented by Equation 4, the parameters $\sigma_{\varepsilon_A}{}^2$ and $\sigma_{\varepsilon_B}{}^2$ are weighting parameters that reflect the fact that both measured signals contain noise and account for the possibility that the noise variance in $A[t]$ may be different from that of $B[t]$. In this work we have estimated these parameters by measuring the variances of the BOLD and ASL signals in voxels containing cerebral spinal fluid (CSF), which should have no CBF-related ASL or BOLD signal fluctuations [17].

Estimating $CMRO_2$-CBF Coupling for Calibrated Experiments

As stated above, the output of the minimization of Equation 4 is a time series of CBF estimates, $\hat{f}[t]$, which we hypothesize will more precisely approximate the time course of true underlying CBF fluctuations than the time series of ASL measurements $A[t]$. In addition, the minimization of Equation 4 yields an estimate of the parameter k, which links BOLD fluctuations to underlying changes in CBF. Alone, the value of $\hat{k}$ yields very little information of physiological interest. This is because the value of k depends on three parameters, α_v, λ, and M. However, if the values of M and α_v are obtained by other means, then an estimate of k becomes equivalent to an estimate of λ. This is of great physiological interest as it represents the ratio of $CMRO_2$ changes to CBF changes throughout the analysis window. For a typical calibrated-BOLD experiment, the value of α_v is assumed based on literature values. Though there is still some disagreement about the appropriate value to assume for α_v, the most recent estimates suggest that it is approximately 0.2 [22]. Because of the dependence of M on the baseline state, in most cases it must be measured rather than assumed. The most common method of estimating M is through a separate calibration experiment during which simultaneous BOLD and ASL images are acquired while the subject breaths CO_2 enriched air [23]. The underlying assumption of this experiment is that breathing CO_2 increases blood flow without affecting oxygen metabolism ($\lambda = 0$), allowing one to calculate M based on an assumed value of α_v. Of course, the accuracy of the value of λ estimated by this approach will depend on the accuracy of the values obtained for α_v and M. However, under conditions where these values may be obtained, BCP analysis may yield an estimate of $CMRO_2$-CBF coupling in addition to CBF fluctuations.

Potential Sources of Bias in BCP estimates

The BCP approach outlined here relies implicitly on several assumptions about the nature of both the underlying physiology of functional hyperemia and the characteristics of the BOLD and ASL signals that could potentially bias BCP estimates of $f[t]$ and λ. First, the BCP approach assumes that the $CMRO_2$-CBF coupling ratio (λ) varies slowly enough in time that it can be considered constant over a window of several or even many time points. If in reality λ varies significantly over a period of time shorter than the window, the BCP estimates of both λ and $f[t]$ may become less accurate. Related to this is the assumption that the dynamics of the CBF, CBV and $CMRO_2$ responses to neural stimuli are tightly coupled, at least as resolvable at the sampling rate of an ASL experiment. In reality the coupling of these processes may not be strictly tight, as analysis of transient features of the BOLD response have led several investigators to conclude [24–27]. Dynamic mismatch of these processes would effectively produce transient fluctuations in the values of λ or α_v in Equation 3, which again is not currently accounted for in the BCP approach. Finally, the BCP approach is based on the idea that CBF fluctuations may be distinguished from noise by the correlated fluctuations they produce in the ASL and BOLD signals. This implicitly assumes that noise in the ASL and BOLD signals is not correlated in a significant way. If correlated noise in the ASL and BOLD signals is consistent with a similar estimate of k as the physiological fluctuations in CBF and $CMRO_2$, the correlated fluctuations will add noise to the BCP estimation, reducing the ability of BCP estimation to improve the precision of $\hat{f}[t]$. If the correlated noise leads to a shift in the line defining the BOLD-ASL relationship it will likely reduce the accuracy of both $\hat{\lambda}$ and $\hat{f}[t]$ as well as their precisions.

Methods

Ethics Statement

This study was approved by the institutional review board at the University of California San Diego, and written informed consent was obtained from all participants.

Imaging

For the empirical component of this work, we reanalyzed the raw data from a previously published calibrated-BOLD study [8]. Briefly, the study was conducted on 10 healthy adults (mean age 33+/−7 years). Simultaneous BOLD and CBF images were acquired on a GE Excite 3T scanner with a dual-echo arterial spin labeling (ASL) PICORE QUIPSS II sequence [28] with a spiral readout. ASL sequence parameters were six 5-mm slices aligned with the calcarine sulcus, TR 2.5 s, TI1/TI2 600/1500 ms, TE1 2.9 ms, TE2 24 ms, 90° flip angle, FOV 240 mm, matrix 64 × 64. Functional imaging consisted of two scans during which subjects performed a visual task and two calibration scans during which subjects breathed a gas mixture containing 5% CO_2. Each visual task began with 60 seconds of rest followed by four cycles of 20 seconds of stimulus, 60 seconds of rest, and ended with a final 30 seconds of rest. The stimulus consisted of a black and white checkerboard flickering at 8 Hz while numbers appeared in the center of the checkerboard. Throughout scanning, cardiac pulse and respiratory effort data were monitored using a pulse oximeter

(InVivo) and a respiratory effort transducer (BIOPAC), respectively. A high-resolution anatomical image was also acquired at the start of each session, using a magnetization prepared 3D fast spoiled gradient acquisition in the steady-state (FSPGR) sequence (172 sagittal slices, 1-mm slice thickness, TI 450 ms, TR 7.9 ms, TE 3.1 ms, 12° flip angle, FOV 25 cm, matrix 256×256).

Preprocessing

The first four images of each ASL scan were excluded from data analysis to allow the MRI signal to reach steady state. All functional runs were motion corrected and registered to the first functional run using AFNI software [29]. The first echo data was used for the analysis of CBF activity, and the second echo data for the analysis of BOLD activity. To generate a perfusion-weighted signal from the raw ASL images at each time point during the functional scans, the image intensity corresponding to a "tag" image was subtracted voxel-wise from the average intensity of the surrounding two "control" images. Similarly, at each "control" time point, the image intensity was added voxel-wise to the negative average of the surrounding two "tag" images. BOLD-weighted images were obtained by adding the image intensity at each time point (tag or control) to the average of the intensities in the two surrounding time points [13].

ROI Selection

ROI selection was performed on the data from the first visual task using a general linear model (GLM) approach for the analysis of ASL data [8,16]. A stimulus-related regressor in the GLM was obtained by convolving the block design stimulus pattern with a gamma density function [30]. The measured cardiac and respiratory data were included in the GLM as regressors to account for the modulation of the ASL signal caused by physiological fluctuations [15,16] as were regressors related to variations in heart rate and respiratory volume [19]. A constant and a linear term were also included as nuisance regressors to account for scanner drift. Voxels exhibiting CBF or BOLD activation were detected after correcting for multiple comparisons using AFNI AlphaSim [29,31] and setting an overall significance threshold of $p = 0.05$ for CBF and $p = 0.01$ for BOLD given a minimum cluster size of four voxels. For each subject, an active region of interest (ROI) was defined as those voxels exhibiting both BOLD and ASL activation. Subjects were excluded from further analysis if fewer than 50 voxels met these criteria, resulting in the exclusion of three subjects from further study. Following ROI selection, data from the first visual task was excluded from further analysis.

Voxel Scale BCP Analysis

To determine whether BCP estimation could be used to improve the precision of a dynamic CBF time series, BCP analysis was conducted on the measured ASL and BOLD time series obtained from the second visual task on each voxel within the previously defined ROI. Before performing the BCP analysis, known sources of physiological noise and linear scanner drifts were regressed out of the measured CBF- and BOLD-weighted time series [15,16]. For each voxel, estimates of f_0 and b_0 were obtained by averaging the first 20 time points of the measured ASL and BOLD signals. The relative noise weighting terms σ_A^2 and σ_B^2 were estimated for each subject by calculating the mean variance of the measured ASL and BOLD signals (after physiological noise regression) in voxels with a CSF partial volume greater than 95% as estimated by auto-segmentation of the high resolution anatomical image with FSL's FAST image segmentation tool [32]. The value of k that minimized Equation 4 was determined using a Golden-Section search algorithm [33]. This algorithm is initialized by bracketing the expected function minimum between two assumed values (e.g. *a* and *b*). Here we assumed that (corresponding to approximately for and) in order to minimize any *a priori* assumptions about its value. A third point (point *c*) is then chosen that is intermediate to the bracketing values, forming a triplet of test solutions (two brackets and an intermediate value). The minimum of a function is then found by evaluating it at a fourth point (point *d*) located 38.197% of the distance between the intermediate point and the more distant bracket (a fractional distance called the golden section). If the value of the function at *d* is lower than at *c*, then *c* becomes a new bracket point and *d* becomes the new intermediate value. If the value of the function is greater at *d* than at *c*, then *d* becomes the new bracket and *c* remains intermediate. In this way the distance between the brackets is reduced until a specified tolerance is reached. Here the tolerance was set to 0.001. At each test point, Equation 4 was evaluated by mapping each pair of measurements $(\boldsymbol{A}[t],\boldsymbol{B}[t])$ to the closest point $\left(\hat{\boldsymbol{f}}[t],\hat{\boldsymbol{b}}[t]\right)$ on a line defined by Equation 3 and the current value of $\hat{\boldsymbol{k}}$.

To test the effect of voxel-wise BCP estimation, we examined signal-to-noise improvements by measuring the correlation (r^2) of the BCP-estimated CBF signal $\hat{\boldsymbol{f}}[t]$ for each voxel in the active ROI with the stimulus-related regressor used in the GLM analysis and comparing it to the correlations of $\boldsymbol{A}[t]$ and $\boldsymbol{B}[t]$ with the same regressor. In addition, we evaluated the precisions of $\boldsymbol{A}[t]$ and $\hat{\boldsymbol{f}}[t]$ by calculating the standard deviation of each signal during the last 10 seconds of each stimulus, a time period usually assumed to represent a steady state of elevated CBF, and in the period 12.5–22.5 seconds after the cessation of each stimulus, a period of time during the BOLD post-stimulus undershoot. We also assessed whether BCP estimation introduced any bias in the estimate $\hat{\boldsymbol{f}}[t]$ by comparing the ROI-averaged values of $\hat{\boldsymbol{f}}[t]$ and $\boldsymbol{A}[t]$ during the steady state period of activity and during the BOLD post-stimulus undershoot period. Because the hypercapnia calibration experiment used lacks sufficient precision to estimate M at the single voxel scale, we did not attempt to estimate λ for individual voxels.

ROI-scale Analysis

BCP analysis was also conducted at the spatial scale of a region of interest in order to determine the feasibility of estimating the $CMRO_2$-CBF coupling parameter λ with this technique. As described above, estimation of λ is feasible only if M and α_v are known. For this study we used the literature value of $\alpha_v = 0.2$ for the CBF-venous CBV coupling constant [22] and an additional calibration experiment to make an ROI-scale estimate of M for each subject. To determine M, data from the two hypercapnia runs was first corrected for fluctuations due to physiological noise and linear drifts on a voxel-wise basis using a general linear model. Time series were then averaged across each subject's ROI and across the two experiments to produce a single pair of CBF and BOLD time courses for each subject. Estimates of the baseline CBF and BOLD signals were obtained from these time courses by averaging the first 40 data points in the image series. Estimates of the steady-state response to hypercapnia were obtained by averaging the last 40 time points recorded while CO_2 was being administered. The scaling parameter M was then calculated for each subject using the equation

$$M = \frac{\frac{b_{CO_2} - b_0}{b_0}}{(1-\alpha_v)\left(1-\left(\frac{f_0}{f_{CO_2}}\right)\right)} \quad (5)$$

where b_{CO_2} and f_{CO_2} represent the steady state BOLD and CBF responses to hypercapnia, α_v is assumed to be 0.2, and λ is assumed to be zero.

Once values of M were obtained for each subject, the measured ASL and BOLD signals from the second visual task were corrected for fluctuations due to physiological noise and scanner drifts and then averaged-spatially across each subject's ROI. The value of k for the average time courses was then estimated for a window the length of the entire functional run and λ was estimated using the formula $\lambda = 1 - \alpha_v - \frac{k}{M}$. For comparison, λ was also estimated by a method more commonly used in calibrated BOLD studies. To obtain this reference estimate of λ, the measured CBF and BOLD responses of each subject were averaged over the last 10 seconds of each visual task to produce the average steady-state CBF and BOLD estimates f_{vt} and b_{vt}. These estimates were then plugged into the equation

$$\lambda = 1 - \alpha_v - \frac{b_{vt} - b_0}{M\left(1-\frac{f_0}{f_{vt}}\right)} \quad (6)$$

To investigate the possibility that λ or α_v fluctuate through the stimulus cycle, we next divided each subject's ROI-averaged time series into four epochs: a transient active period (first 10 sec. of each stimulus), a steady state active period (last 10 sec. of each stimulus), a transient inactive period (first 10 sec after each stimulus) and a BOLD post-stimulus undershoot period (12.5–22.5 sec after the cessation of each stimulus). We then concatenated the data points corresponding to each of these four epochs, forming four BOLD/CBF time series pairs (per subject), each containing 16 data points from within a single epoch. We then used BCP analysis to estimate $\hat{\alpha}_v + \hat{\lambda} = 1 - \frac{k}{M}$ separately for each time series pair, under the assumption that systematic changes in λ and/or α_v would produce systematic differences in their sum from epoch to epoch.

Results

Voxel Scale BCP Analysis

Application of BCP estimation at the single voxel scale increased the correlation the CBF signal with the stimulus model and increased the precision of our estimates of CBF changes during steady-state active and BOLD-undershoot periods without introducing any apparent bias. Figure 2a displays a representative CBF time course from a single voxel after correction for known sources of physiological noise (blue) and after constraint by BCP analysis (red). For comparison, a scaled and shifted representation of the measured BOLD signal is also shown (gray). Black lines indicate when the visual stimulus was on. Note that the shape of the constrained CBF signal is similar, though not identical, to the BOLD signal, but that proper CBF scaling is maintained at the stimulus peaks. It is also interesting to note that many of the very large fluctuations in the measured CBF signal that occur between peaks are also represented (albeit in a less dramatic way) in the BOLD signal, and are thus attenuated but not eliminated from the constrained CBF signal. Figure 2b displays the mean correlation (r^2) of single voxel time series from within an ROI with a stimulus-related regressor. The height of the blue bars represents the mean r^2 of the measured CBF signal after correction for known physiological noise for each subject. The height of the red bars represents the mean r^2 of the BCP estimated CBF signal. For comparison, the grey bar represents the mean r^2 of the measured BOLD signal after correction for known physiological noise. Across subjects, the mean correlation of the BCP estimated CBF signal with the stimulus related regressor at the single voxel scale was 0.45+/−0.13 (mean +/− std.). This was significantly higher than the mean correlation of the measured CBF signal (0.19+/−0.07, $p<0.01$, pairwise t-test) and the measured BOLD signal (0.42+/−0.12, $p=0.026$, pairwise t-test).

In addition to increasing the correlation of the CBF signal with the stimulus model, BCP estimation increased the precision of estimated changes in CBF during both the steady-state active and BOLD post-stimulus undershoot periods. Across subjects, during the active period, the mean standard deviation of the single voxel CBF signal as a fraction of the baseline was 0.38+/−0.14 for the measured signal and 0.22+/−0.08 for the BCP-estimated signal ($p<0.01$ pairwise t-test). Similarly, during the undershoot period, the mean standard deviation of the single voxel CBF signal was 0.38+/−0.12 for the measured CBF signal and 0.14+/−0.04 for the BCP-estimated signal ($p<0.01$ pairwise t-test). For comparison, the mean value of σ_{ε_A} was 36+/−15% of the baseline ASL signal or 28+/−5 signal units. The mean value of σ_{ε_B} was 0.5% +/−0.2% of the baseline BOLD signal or 56+/−18 signal units across subjects. No bias was observed in the BCP estimated CBF signals during either the steady-state active period or the post-stimulus undershoot period. Figure 2c displays the mean change in CBF as a fraction of baseline CBF signal for each subject during the active (red) and undershoot (blue) periods for the measured (horizontal axis) and BCP estimated (vertical axis) CBF signals. Across subjects the mean change in CBF during the steady-state active period was 0.46+/−0.14 (mean +/− std.) for the measured CBF signal and 0.44+/−0.15 for the BCP estimated CBF signal ($p=0.3$, pairwise t-test). The mean change in CBF during the undershoot period was −0.02+/−0.11 for the measured CBF signal and −0.04+/−0.08 for the BCP estimated CBF signal ($p=0.31$, pairwise t-test). For the measured BOLD signal, the mean change across subjects was 0.014+/−0.004 (mean +/− std.) during the steady-state active period and −0.002+/−0.004 (mean +/− std.) during the undershoot period.

ROI-scale Analysis

BCP estimation at the ROI level yielded estimates of λ in good agreement with those produced by traditional calibrated BOLD techniques despite the blind application of the BCP estimation method to the entire time series. Figure 3 displays the estimates of λ found for each subject by traditional analysis and by BCP analysis using the heuristic model. Figure 3a displays results from a single subject (subject 2), demonstrating the difference between estimating λ by traditional calibrated BOLD methods and by BCP estimation. In traditional calibrated BOLD analysis, BOLD and CBF measurements collected during a period of steady-state activity (red circled dots) are averaged together to produce a single estimate of the change in BOLD and CBF signal associated with the stimulus (red 'X'). The location of this point in the CBF-BOLD plane determines the value of $\hat{\lambda}$. In contrast, with BCP analysis, all (CBF, BOLD) data points from within a chosen time-window, in this case the length of the entire functional run, are fit to a BOLD-CBF relationship defined by a BOLD signal model. The value of $\hat{\lambda}$ that minimizes Equation 4 determines the $CMRO_2$-CBF coupling ratio. Figure 3b displays the value of $\hat{\lambda}$ estimated for each subject

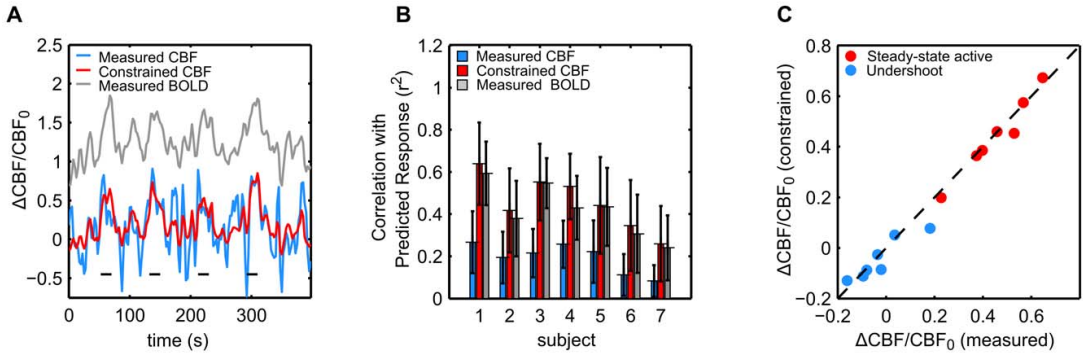

Figure 2. BCP estimation improves precision of CBF estimates without inducing estimation bias. A) Representative CBF time series from a single voxel within the visual cortex before (blue) and after (red) BCP estimation. For comparison, a scaled and shifted version of the measured BOLD signal is displayed in gray. Black lines indicate when the stimulus (8 Hz flashing checkerboard) was on. **B**) BCP significantly reduces the influence of noise on the CBF signal as measured by correlation with a predicted hemodynamic response. Height of the blue bars indicates mean correlation (r^2) for each subject between measured CBF time series (after removal of known sources of physiologic noise) and a predicted CBF time course based on the convolution of the stimulus paradigm with a hemodynamic response function. Height of the red bars indicates mean correlation between BCP estimated CBF time series and the same predicted time course. For comparison, grey bars indicate the correlation between the measured BOLD response (after removal of known sources of physiologic noise) and the predicted time series. Error bars indicate the standard deviations of the calculated r^2 values across the ROI. **C**) BCP estimation produces no detectable bias in CBF estimates of steady-state activation response or post-stimulus undershoot response. Scatterplot shows mean CBF responses for each subject during steady-state activation (red) and undershoot (blue) before (horizontal axis) and after (vertical axis) BCP analysis. No significant difference was observed between pre- and post-BCP estimates. *BCP: BOLD Constrained Perfusion. CBF: Cerebral Blood Flow. ROI: Region of Interest.*
doi:10.1371/journal.pone.0054816.g002

using the BCP or traditional approach. Across subjects the mean value of $\hat{\lambda}$ estimated by BCP analysis of the whole time series was 0.35+/−0.14 (mean +/− std.) and by traditional calibrated BOLD, 0.36+/−0.13 ($p = 0.26$, paired t-test). Across subjects the mean scaling parameter M was found to be 0.11+/−0.04.

As is shown in Figure 3c, there were not any clear systematic differences across subjects in the values of $\lambda + \alpha_v$ estimated at different stages of the stimulus cycle. Across subjects, $\hat{\lambda} + \hat{\alpha}_v$ was estimated to be 0.57+/−0.12 during the transient active period, 0.55+/−0.14 during the steady-state period, 0.53+/−0.15 during the transient off period, and 0.59+/−0.12 during the post stimulus undershoot. Not one epoch was found to produce an estimate of $\alpha_v + \lambda$ that was significantly different from another across subjects ($p > 0.2$ for all pairwise t-tests, even without correction for multiple comparisons).

Discussion

In this study we report a new method of measuring dynamic CBF fluctuations by combining information obtained through simultaneous acquisition of ASL and BOLD image time series. This approach takes advantage of the favorable features of both time series. The ASL measurement is directly proportional to CBF, but the low signal to noise ratio makes it difficult to assess dynamics. The BOLD signal has much better sensitivity, but is related to the underlying CBF fluctuations in a complicated and nonlinear way. To simplify this relationship, we incorporated a recent model of the BOLD effect. The BOLD and ASL signals are then essentially treated as two independent but noisy windows into the same underlying physiological process, so that by constraining the CBF fluctuations to be consistent with the BOLD signal model, we may substantially decrease the influence of noise on the CBF time series and increase the precision of CBF estimates. Importantly, the BOLD constrained perfusion (BCP) estimation procedure does not require any prior knowledge of the stimulus, suggesting that the method may be applicable to complex tasks in addition to conventional block and event-related stimulus designs.

Reducing the Influence of Noise on CBF Estimates and Time Series Measurements

To test the method we used data from a simple, block-design visual task for which we believed we could generate a fairly accurate, *a priori* model of dynamic CBF fluctuations. We then compared the correlation of measured and BCP-estimated CBF time series with the predicted model as a metric for the improvement in SNR. We found that the value of the BCP estimated CBF signal was on average more than 200% that of the measured CBF signal based on ASL alone at the single voxel scale and that it was comparable to, and even slightly greater than, the r^2 value of the measured BOLD signal, suggesting a substantial decrease in the influence of noise on the CBF time series. We noted that the shape of the constrained CBF time series was similar, though not identical, to that of the measured BOLD time series. They are not identical because both the BOLD and CBF signals are assumed to contain some noise, which differentiates BCP estimation from a simple, non-linear regression analysis. However, it is not surprising that the estimated CBF is similar to the measured BOLD, given the higher SNR of the BOLD signal. In addition, we noted that, interestingly, many of the very large, inter-stimulus fluctuations in the measured CBF signal were also present, though to a lesser extent, in the BOLD signal, and were thus reduced in magnitude but not absent in the constrained CBF signal. We cannot conclude definitively whether these correlated fluctuations partly represent real fluctuations in CBF (perhaps related to opening and closing of eyes between stimuli or "resting state" activity) or whether they represent correlated noise in the BOLD and CBF signals. Several features of our image acquisition and processing protocol, however, reduce the likelihood that these fluctuations are pure artifacts. First, the CBF and BOLD signals are acquired from separate spiral readouts, making it unlikely that

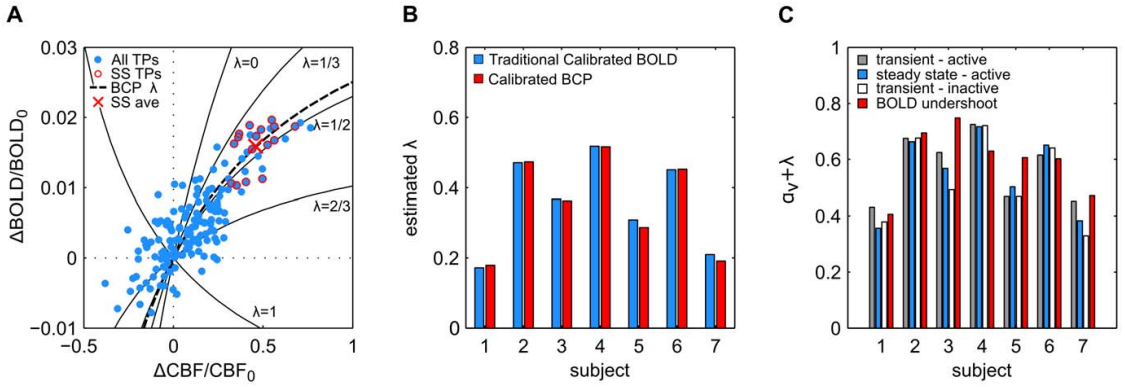

Figure 3. Calibrated BCP allows estimation of $CMRO_2$-CBF coupling without prior knowledge of the stimulus paradigm. A) Representative, ROI-averaged single subject (subject 2) data comparing traditional and BCP approach to estimating λ, the ratio of changes in $CMRO_2$ to changes in CBF evoked by a stimulus. In traditional calibrated BOLD analysis, BOLD and CBF measurements collected at time points (TPs) during which the stimulus response is assumed to be in a steady state (SS). These measurements (red circled dots) are averaged into a single measurement (red 'X'). The location of the 'X' in the BOLD-CBF plane determines the coupling ratio λ. Conversely, calibrated BCP estimation requires no knowledge of the stimulus pattern. All data points within a time window (here, the length of the experiment) are fit to a cost function (Equation 4 in text) using a mathematical model (here Equation 3 in text) to link BOLD and CBF fluctuations. The value of λ that minimizes the difference between the measured and estimated BOLD and CBF values given the relative noise (dashed black line) determines the coupling ratio. **B**) Estimates of λ produced by blind Calibrated BCP analysis agree with those produced by traditional calibrated BOLD analysis. Height of blue bars indicates traditional calibrated BOLD estimate for each subject. Height of red bars indicates the calibrated BCP estimate for a window the length of the full time series. No significant difference between the two was detected. **C**) Epoch-based BCP analysis does not reveal evidence of systematic variation of model parameters with stimulus cycle. Height of bars indicates the estimated sum of the model parameters α_v and λ during the transient active (gray), steady state active (blue), transient inactive (white), and BOLD undershoot periods (red). Considerable differences between steady state and undershoot estimates may be seen in several subjects; however, no systematic differences were detectable across the group. *BCP: BOLD Constrained Perfusion. ROI: Region of Interest. $CMRO_2$: Cerebral Metabolic Rate of Oxygen. CBF: Cerebral Blood Flow.*
doi:10.1371/journal.pone.0054816.g003

random readout noise or k-space spikes would be correlated across the two signals. Second, the surround subtraction procedure used to produce the CBF signal should further reduce the correlation of its noise with that of the BOLD signal. For example, while rapid fluctuations in the static tissue signal that are precisely timed with control images will produce correlated fluctuations in the BOLD and CBF signals, those that are precisely timed with tag images will produce anti-correlated fluctuations, and those that last longer than a tag-control triplet will be preserved in the BOLD but eliminated from the CBF signal. Still, further work must be done to investigate the source of these correlated inter-stimulus fluctuations, and if they prove to be artifacts, to account for them.

We further investigated the effect of BCP analysis on the precision of the CBF signal by measuring the standard deviation of CBF measurements taken during a period of presumably steady-state activity and during the post-stimulus BOLD undershoot. Again, we found that BCP analysis significantly reduced the influence of noise on the measurements, reducing the standard deviation of the measurements by approximately 40% during the active period and by approximately 60% during the undershoot period.

We were concerned that despite the improvement in the precision of our measurement, there might be some bias in the magnitude of the BCP estimated CBF fluctuations as compared to the measured ASL signal, which we assume, on average, reflects the true magnitude of CBF fluctuations. We were particularly concerned about this possibility because we assume in applying the BCP estimation approach that the parameters of our BOLD signal model are fixed throughout the duration of a chosen time window, which in our analysis encompassed the entire experiment. As discussed above, despite the simplicity of our experimental design, the stimulus we chose consisted of several epochs (e.g. rest, activation, post-stimulus BOLD undershoot, and transitions between activity and rest) during which several of our BOLD model parameters (in particular λ and possibly α_v as well) might be expected to change significantly, and we anticipated that the non-stationarity of these parameters might bias the BCP estimate of the CBF signal.

To determine whether bias was significant in the BCP estimated signal, we averaged CBF measurements taken during the steady-state period of activity and during the post-stimulus undershoot period and compared them to average BCP estimates of the same periods. We found that during the steady-state activity period, the average BCP estimate was only 1.6% of the baseline signal lower than the average measurement and that during the undershoot period the average BCP estimate was only 2.1% lower. Neither of these differences was statistically significant. While we cannot conclude definitively from this finding that the BCP estimate is unbiased or that this finding is applicable to all stimulus paradigms, we take it as an encouraging sign that the BCP CBF estimate is reasonably robust despite the potential weakness of the parameter stationarity assumption. Further experiments will be important to test this potential limitation of the method.

Estimating $CMRO_2$-CBF Coupling

BCP estimation with the heuristic model yields a set of CBF estimates as well as an additional parameter estimate, $\hat{k}$. We noted that the value of this parameter alone could not be interpreted in a physiological sense. However, we hypothesized that if values for the CBF-CBV coupling parameter, α_v, and the BOLD model scaling factor, M, could be obtained, then the value of $\hat{k}$ could be used to calculate an estimate of the ratio of fluctuations in $CMRO_2$ to CBF, $\hat{\lambda}$, throughout the analysis window. Because of

the imprecision of the calibration experiment required to estimate M, the test of this hypothesis was conducted at the scale of a region of interest in the visual cortex. To determine whether the blind application of BCP analysis to the complete time series could produce an accurate estimate of λ, we compared estimates of λ produced by a traditional calibrated BOLD technique to estimates produced by BCP analysis of the complete time series. We found that λ estimates were highly consistent between the traditional and BCP estimation techniques, with no significant differences between the two. We then divided the time series into distinct epochs in order to look for systematic differences in the sum of λ and α_v during the steady state active period, the post-stimulus BOLD undershoot period, and the transition periods as the stimulus was turned on and off. We looked at the sum of λ and α_v, rather than λ alone, because in transition periods we cannot be certain that α_v maintains its steady state value. Across subjects, no systematic differences in the sum $\hat{\lambda}+\hat{\alpha}_v$ were found between any epoch pairs. Again, these findings are encouraging, as they suggest that potentially divergent CBF and BOLD dynamic transients are not having a strong biasing effect on our estimates of k; however, more work will be required to determine conclusively whether the apparent lack of systematic difference is attributable to an underlying physiological process or simply to signal noise.

The BOLD Post-stimulus Undershoot

The lack of evidence of systematic bias in the BCP estimates of CBF and k during the BOLD undershoot period is somewhat surprising given our current understanding of its etiology. The origin of the BOLD post-stimulus undershoot has been a topic of considerable debate for nearly two decades. Several studies have found the undershoot to be consistent with a slow return to baseline of $CMRO_2$ compared with CBF [34,35], while others have found it to be consistent with a slow return of venous blood volume [36,37] or a post-stimulus CBF undershoot [37]. Transient uncoupling of CBF and $CMRO_2$ dynamics would result in changes in λ (increased for a slow $CMRO_2$ recovery and decreased for a CBF undershoot at baseline $CMRO_2$). The model for the BOLD signal used in the BCP analysis does not include the possibility of a slow return of blood volume explicitly, so we would expect this effect to appear as a slow recovery of $CMRO_2$ and a correspondingly higher value of λ (i.e., the basic problem is that these two potential effects can produce similar BOLD responses). Each of these potential undershoot mechanisms suggest that k (or $\lambda+\alpha_v$) should be significantly different in the active and undershoot states, and that as a result, our estimate of CBF in the undershoot period should be systematically biased if we blindly apply BCP to a long time series. The reason we do not see this bias may be because the BOLD and CBF fluctuations in the undershoot period are relatively small. As Figure 3a demonstrates, CBF-BOLD contours representing distinct values of λ converge at the origin. As a result, near the origin small deviations in the CBF-BOLD plane produce large changes in λ. Thus in this regime, systematic errors in the estimated CBF signal due to a biased estimate of k are likely to be small, especially compared to the random error due to noise. This has both positive and negative implications for BCP analysis. On the positive side, it suggests that even large changes in λ during an undershoot should not cause dramatic bias in the CBF estimates made in that period, as we have seen here. On the negative side, it suggests that as the magnitude of CBF and BOLD fluctuations within a window of interest decrease, the precision of BCP estimates of λ should decrease as well.

Potential Applications for BCP Analysis

The two principal findings of this work were (1) that the blind application of BCP-analysis to voxel scale CBF time series increased their correlation with the hemodynamic model and increased the precision of CBF estimates both in periods of steady-state activity and post-stimulus undershoot without producing significant estimation bias, and (2) that the blind application of BCP-analysis to ROI-scale BOLD and CBF data produced an estimate of the $CMRO_2$-CBF coupling parameter λ that was highly consistent with one produced by traditional, steady-state calibrated BOLD analysis. These findings are encouraging, as they suggest that transient fluctuations in our BOLD model parameters (λ and α_v) may not dramatically bias our estimates of instantaneous CBF or $CMRO_2$-CBF coupling over a window of time if the underlying hemodynamic and metabolic activity is coupled in a relatively stationary way, as was the case in these experiments. The findings presented here suggest that BCP analysis may be immediately useful in the study of the hemodynamic responses of small regions of interest or even single voxels to simple block-design stimuli, as a way of improving the precision of CBF estimates. Similarly, BCP has the potential to be useful in the study of stimuli that cannot be presented repeatedly or for prolonged periods, either because they are noxious or produce habituation or sensitization. BCP analysis could also be potentially applied to the calibration of the BOLD response by fitting for the parameter k during a CO_2 challenge and calculating M based on the assumption that $\lambda = 0$; however, given the CO_2 challenge often lasts several minutes, BCP may not produce a more precise estimate of M than is achievable with simple temporal averaging.

Looking forward, we hope that BCP analysis will prove to be a useful tool in the quantitative study of hemodynamic and metabolic activity associated with more natural neural tasks, such as watching movies, listening to music, or even rest, tasks that are difficult to study with traditional calibrated BOLD techniques because the temporal pattern of CBF and BOLD fluctuations may not be predicable or replicable with repeated stimuli. To date, neural tasks of this type have typically been studied in a qualitative or semi-quantitative manner. Several groups [38,39] have used BOLD imaging alone to investigate the patterns of neural activity associated with watching popular films and found significantly correlated signal fluctuations not just across regions within a single brain, but across the brains of multiple subjects, suggesting that such natural stimuli might be used to drive blood flow and oxygen metabolism fluctuations throughout the brain, allowing many regions to be studied at once. Similarly, resting state BOLD fMRI has been used extensively to map the spatial and temporal patterns of hemodynamic activity that occur when a subject lies quietly in the MR scanner [40–42]. ASL has also been used for this purpose [43,44] and the two modalities have even been combined in a semi-quantitative fashion to demonstrate that the ratio of BOLD fluctuations to ASL fluctuations at rest is closer to the ratio associated with a visual task than an iso-metabolic breathing task, suggesting a metabolic basis for resting state BOLD fluctuations [45]. The consensus produced by this body of work is that hemodynamic and metabolic activity in the brain is highly coordinated even in nominal states of rest. However the magnitude of this activity, and thus its importance in maintaining homeostasis, remains poorly understood. If BCP estimation may be applied to quantitatively measure the CBF and $CMRO_2$ fluctuations associated with natural neural activity, it could provide important insights into the physiology of complex neural processing and how it is altered by disease.

Potential Limitations and Future Work

Despite the promising results of this proof-of-principle experiment, we acknowledge that the results presented here do not demonstrate conclusively that BCP analysis will prove to be robust under more general experimental conditions, and more study will be necessary before BCP analysis is ready to be used to study the physiology of complex neural processing. A key issue that requires further study is the sensitivity of the BCP estimation approach to the dynamics of the BOLD signal. As discussed above, the BOLD response to neural activity is notable for several transient features that have been observed in various studies including initial dips [26], early overshoots [25], and post-stimulus undershoots [24]. While no definitive dynamic BOLD model has yet been described, both experimental [35,46] and theoretical [27,36,47] analyses agree that these transient features occur due to differences in the dynamic responses of $CMRO_2$, CBF, CBV to neural stimuli. This poses a potential challenge for BCP estimation, as the simplifications made to the BOLD signal model in order to reduce it to a function of CBF and a few unknown parameters implicitly requires the assumption that these physiological variables are dynamically synchronized, at least over the finite length of a window of time and within the temporal resolution of our measurements. In this study we looked for evidence of bias due to this assumption by comparing the mean responses of measured and BCP estimated CBF time series both in the active state and during the post-stimulus undershoot, by comparing estimates of λ produced by blind BCP estimation with those made by traditional calibrated BOLD analysis, and by comparing BCP estimates of the sum $\lambda+\alpha_v$ at different stages of the stimulus cycle. None of these tests revealed evidence of bias, even during the period of the BOLD post-stimulus undershoot. This is quite encouraging, however, the lack of evidence of bias in this study cannot be taken as definitive proof that BCP analysis is robust to these transients, nor does it guarantee that BCP analysis will be robust to transient dynamics under more general experimental conditions. To test this assumption more rigorously, we are currently working to develop visual stimuli that continuously drive CBF and $CMRO_2$ in ways that will allow us to carefully examine how both how the dynamics and amplitudes of CBF and BOLD fluctuations influence the accuracy and precision of BCP estimation. A useful tool in assessing the robustness of BCP analysis under these more general conditions may be ASL with background suppression. Several methods of acquiring background suppressed ASL images have recently been developed [48–50], though they share the common strategy of reducing noise from the static tissue compartment through the application of multiple inversion pulses timed to null the static tissue signal at the time of image acquisition [51]. An advantage of ASL with background suppression is that it achieves SNR gains independently of the BOLD effect, which makes it less vulnerable to the sources of potential bias in BCP analysis. CBF time series produced by background suppressed ASL may thus prove to be useful reference functions for determining BCP estimation bias in future studies.

Conclusions

We have presented here a proof-of-principle demonstration of the feasibility of improving the precision of dynamic estimates of CBF by combining information from simultaneously acquired ASL and BOLD images through a technique we term BOLD Constrained Perfusion (BCP) estimation. Further, we have shown that, under the condition that a calibration experiment is conducted, the BCP approach may be utilized to obtain quantitative information about the coupling of $CMRO_2$ and CBF fluctuations. Importantly, we have demonstrated that this technique may be used without taking into consideration the temporal dynamics of the stimulus presented, suggesting that it may be useful in the quantitative study of hemodynamic and metabolic responses to neural tasks that cannot be easily modeled temporally. Further studies are required to investigate and if necessary correct for the sensitivity of the BCP approach to the dynamics of $CMRO_2$, CBF, and CBV; however, the results presented in this initial test are quite promising and suggest that, despite its simplicity, BCP analysis may improve our ability to estimate CBF and $CMRO_2$ fluctuations under conditions that are currently challenging to study with traditional calibrated BOLD techniques.

Supporting Information

Figure S1 Calibrated BCP Estimation with the Davis model. In this bar chart, the height of blue bars indicates traditional calibrated BOLD estimate of λ, the ratio of evoked changes in $CMRO_2$ to CBF, for each subject. The height of red bars indicates the BCP estimate. Dark colored bars represent estimates based on the Davis model. Light Colored bars represent estimates based on the heuristic model. No significant differences between BCP and traditional estimates produced by the same model were observed. However, a small but significant difference in the estimates produced by the two models was observed, regardless of whether BCP or traditional calibrated BOLD estimation was used. *BCP: BOLD Constrained Perfusion. ROI: Region of Interest. $CMRO_2$: Cerebral Metabolic Rate of Oxygen. CBF: Cerebral Blood Flow.*
(TIFF)

Figure S2 Danger of attributing physiological significance to simultaneously estimated values of λ and M. In the heuristic model (Equation 3 in Text), The $CMRO_2$-CBF coupling parameter, λ, and the scaling parameter, M, may be lumped into a single parameter, *k*, when both of their values are unknown. BCP analysis may then still be used to improve CBF estimates, although *k* has no real physiological meaning. In the Davis model (Equation S1 in Document S1), λ and M cannot be lumped together and must be estimated simultaneously from the data if both are unknown. However, if estimated in this manner, their values will still not be interpretable physiologically because the BOLD-CBF relationship is not uniquely defined. The plot above illustrates this point, displaying two nearly identical BOLD-CBF relationships defined by the Davis model for two very different pairs of λ and M. *BCP: BOLD Constrained Perfusion. $CMRO_2$: Cerebral Metabolic Rate of Oxygen. CBF: Cerebral Blood Flow.*
(TIFF)

Document S1 Discussion of BCP Analysis with Davis model. In theory BCP estimation should be applicable to a variety of mathematical models of the BOLD signal. Here we repeated our analysis using the Davis model (Equation S1 in Document S1) instead of the Heuristic model (Equation 3 in the Text) to constrain the relationship between BOLD and CBF measurements.
(DOC)

Acknowledgments

We would like to thank Nicholas Blockley, Farshad Moradi, David Dubowitz, and Michael Chappell for helpful discussions in preparing this work and Joanna Perthen for the original collection of the data we analyzed.

Author Contributions

Conceived and designed the experiments: ABS RBB. Performed the experiments: ABS. Analyzed the data: ABS. Contributed reagents/materials/analysis tools: VEMG ECW. Wrote the paper: ABS VEMG ECW RBB.

References

1. Iadecola C (2004) Neurovascular regulation in the normal brain and in Alzheimer's disease. Nat Rev Neurosci 5: 347–360. doi:10.1038/nrn1387.
2. Ogawa S, Lee T, Kay A, Tank D (1990) Brain magnetic resonance imaging with contrast dependent on blood oxygenation. Proc Natl Acad Sci USA 87: 9868.
3. Fox PT, Raichle ME (1986) Focal physiological uncoupling of cerebral blood flow and oxidative metabolism during somatosensory stimulation in human subjects. Proc Natl Acad Sci USA 83: 1140–1144.
4. Griffeth VEM, Perthen JE, Buxton RB (2011) Prospects for quantitative fMRI: investigating the effects of caffeine on baseline oxygen metabolism and the response to a visual stimulus in humans. NeuroImage 57: 809–816. doi:10.1016/j.neuroimage.2011.04.064.
5. Detre J, Leigh J, Williams D, Koretsky AP (1992) Perfusion imaging. Magn Reson Med 23: 37–45.
6. Wong EC, Buxton RB, Frank LR (1997) Implementation of quantitative perfusion imaging techniques for functional brain mapping using pulsed arterial spin labeling. NMR Biomed 10: 237–249.
7. Wong EC (2005) Quantifying CBF with pulsed ASL: Technical and pulse sequence factors. J Magn Reson Imaging 22: 727–731. doi:10.1002/jmri.20459.
8. Perthen JE, Lansing AE, Liau J, Liu TT, Buxton RB (2008) Caffeine-induced uncoupling of cerebral blood flow and oxygen metabolism: A calibrated BOLD fMRI study. NeuroImage 40: 237–247. doi:10.1016/j.neuroimage.2007.10.049.
9. Buxton RB (2010) Interpreting oxygenation-based neuroimaging signals: the importance and the challenge of understanding brain oxygen metabolism. Front Neuroenerg. doi:10.3389/fnene.2010.00008.
10. Liau J, Perthen JE, Liu TT (2008) Caffeine reduces the activation extent and contrast-to-noise ratio of the functional cerebral blood flow response but not the BOLD response. NeuroImage 42: 296–305. doi:10.1016/j.neuroimage.2008.04.177.
11. Ances BM, Leontiev O, Perthen JE, Liang C, Lansing AE, et al. (2008) Regional differences in the coupling of cerebral blood flow and oxygen metabolism changes in response to activation: Implications for BOLD-fMRI. NeuroImage 39: 1510–1521. doi:10.1016/j.neuroimage.2007.11.015.
12. Owen DG, Bureau Y, Thomas AW, Prato FS, St Lawrence KS (2008) Quantification of pain-induced changes in cerebral blood flow by perfusion MRI. Pain 136: 85–96. doi:10.1016/j.pain.2007.06.021.
13. Liu TT, Wong EC (2005) A signal processing model for arterial spin labeling functional MRI. NeuroImage 24: 207–215. doi:10.1016/j.neuroimage.2004.09.047.
14. Griffeth VEM, Blockley NP, Buxton RB (2012) A simple heuristic model for the BOLD response (that works remarkably well). Proc Intl Soc Mag Reson Med 20: 1–1.
15. Glover GH, Li TQ, Ress D (2000) Image-based method for retrospective correction of physiological motion effects in fMRI: RETROICOR. Magn Reson Med 44: 162–167.
16. Restom K, Behzadi Y, Liu TT (2006) Physiological noise reduction for arterial spin labeling functional MRI. NeuroImage 31: 1104–1115. doi:10.1016/j.neuroimage.2006.01.026.
17. Behzadi Y, Restom K, Liau J, Liu TT (2007) A component based noise correction method (CompCor) for BOLD and perfusion based fMRI. NeuroImage 37: 90–101. doi:10.1016/j.neuroimage.2007.04.042.
18. Kundu P, Inati SJ, Evans JW, Luh W-M, Bandettini PA (2011) Differentiating BOLD and non-BOLD signals in fMRI time series using multi-echo EPI. NeuroImage: 1–12. doi:10.1016/j.neuroimage.2011.12.028.
19. Chang C, Cunningham JP, Glover GH (2009) Influence of heart rate on the BOLD signal: the cardiac response function. NeuroImage 44: 857–869. doi:10.1016/j.neuroimage.2008.09.029.
20. Griffeth VEM, Buxton RB (2011) A theoretical framework for estimating cerebral oxygen metabolism changes using the calibrated-BOLD method: Modeling the effects of blood volume distribution, hematocrit, oxygen extraction fraction, and tissue signal properties on the BOLD signal. NeuroImage 58: 198–212. doi:10.1016/j.neuroimage.2011.05.077.
21. Davis TL, Kwong KK, Weisskoff RM, Rosen BR (1998) Calibrated functional MRI: mapping the dynamics of oxidative metabolism. Proc Natl Acad Sci USA 95: 1834–1839.
22. Chen JJ, Pike GB (2010) MRI measurement of the BOLD-specific flow–volume relationship during hypercapnia and hypocapnia in humans. NeuroImage 53: 383–391. doi:10.1016/j.neuroimage.2010.07.003.
23. Blockley NP, Griffeth VEM, Buxton RB (2012) A general analysis of calibrated BOLD methodology for measuring CMRO2 responses: Comparison of a new approach with existing methods. NeuroImage 60: 279–289. doi:10.1016/j.neuroimage.2011.11.081.
24. Fransson P, Krüger G, Merboldt KD, Frahm J (1998) Temporal characteristics of oxygenation-sensitive MRI responses to visual activation in humans. Magn Reson Med 39: 912–919.
25. Uludağ K (2008) Transient and sustained BOLD responses to sustained visual stimulation. Magnetic Resonance Imaging 26: 863–869. doi:10.1016/j.mri.2008.01.049.
26. Hu X, Le TH, Ugurbil K (1997) Evaluation of the early response in fMRI in individual subjects using short stimulus duration. Magn Reson Med 37: 877–884.
27. Buxton RB, Wong EC, Frank LR (1998) Dynamics of blood flow and oxygenation changes during brain activation: the balloon model. Magn Reson Med 39: 855–864.
28. Wong E, Buxton R (1998) Quantitative imaging of perfusion using a single subtraction (QUIPSS and QUIPSS II). Magnetic Resonance in
29. Cox RW (1996) AFNI: software for analysis and visualization of functional magnetic resonance neuroimages. Comput Biomed Res 29: 162–173.
30. Boynton GM, Engel SA, Glover GH, Heeger DJ (1996) Linear systems analysis of functional magnetic resonance imaging in human V1. J Neurosci 16: 4207–4221.
31. Forman SD, Cohen JD, Fitzgerald M, Eddy WF, Mintun MA, et al. (1995) Improved assessment of significant activation in functional magnetic resonance imaging (fMRI): use of a cluster-size threshold. Magn Reson Med 33: 636–647.
32. Zhang Y, Brady M, Smith S (2001) Segmentation of brain MR images through a hidden Markov random field model and the expectation-maximization algorithm. IEEE Trans Med Imaging 20: 45–57. doi:10.1109/42.906424.
33. Press WH, Teukolsky SA, Vetterling WT, Flannery BP (2002) Numerical Recipes in C. Second Edition. Cambridge: Cambridge University Press.
34. Lu H, Golay X, Pekar JJ, van Zijl PCM (2004) Sustained poststimulus elevation in cerebral oxygen utilization after vascular recovery. J Cereb Blood Flow Metab 24: 764–770. doi:10.1097/01.WCB.0000124322.60992.5C.
35. Donahue MJ, Blicher JU, Østergaard L, Feinberg DA, MacIntosh BJ, et al. (2009) Cerebral blood flow, blood volume, and oxygen metabolism dynamics in human visual and motor cortex as measured by whole-brain multi-modal magnetic resonance imaging. Journal of Cerebral Blood Flow & Metabolism 29: 1856–1866. doi:10.1038/jcbfm.2009.107.
36. Mandeville JB, Marota JJ, Ayata C, Zaharchuk G, Moskowitz MA, et al. (1999) Evidence of a cerebrovascular postarteriole windkessel with delayed compliance. J Cereb Blood Flow Metab 19: 679–689. doi:10.1097/00004647–199906000–00012.
37. Chen JJ, Pike GB (2009) Origins of the BOLD post-stimulus undershoot. NeuroImage 46: 559–568. doi:10.1016/j.neuroimage.2009.03.015.
38. Hasson U (2004) Intersubject Synchronization of Cortical Activity During Natural Vision. Science 303: 1634–1640. doi:10.1126/science.1089506.
39. Kauppi (2010) Inter-subject correlation of brain hemodynamic responses during watching a movie: localization in space and frequency. Front Neuroinform. doi:10.3389/fninf.2010.00005.
40. Biswal B, Yetkin FZ, Haughton VM, Hyde JS (1995) Functional connectivity in the motor cortex of resting human brain using echo-planar MRI. Magn Reson Med 34: 537–541.
41. Fransson P (2005) Spontaneous low-frequency BOLD signal fluctuations: An fMRI investigation of the resting-state default mode of brain function hypothesis. Hum Brain Mapp 26: 15–29. doi:10.1002/hbm.20113.
42. Fox MD, Snyder AZ, Vincent JL, Corbetta M, Van Essen DC, et al. (2005) The human brain is intrinsically organized into dynamic, anticorrelated functional networks. Proc Natl Acad Sci USA 102: 9673–9678. doi:10.1073/pnas.0504136102.
43. Biswal BB, Van Kylen J, Hyde JS (1997) Simultaneous assessment of flow and BOLD signals in resting-state functional connectivity maps. NMR Biomed 10: 165–170.
44. Zou Q, Wu CW, Stein EA, Zang Y, Yang Y (2009) Static and dynamic characteristics of cerebral blood flow during the resting state. NeuroImage 48: 515–524. doi:10.1016/j.neuroimage.2009.07.006.
45. Fukunaga M, Horovitz SG, de Zwart JA, van Gelderen P, Balkin TJ, et al. (2008) Metabolic origin of BOLD signal fluctuations in the absence of stimuli. Journal of Cerebral Blood Flow & Metabolism 28: 1377–1387. doi:10.1038/jcbfm.2008.25.
46. Vanzetta I, Grinvald A (1999) Increased cortical oxidative metabolism due to sensory stimulation: implications for functional brain imaging. Science 286: 1555–1558.
47. Friston KJ, Mechelli A, Turner R, Price CJ (2000) Nonlinear Responses in fMRI: The Balloon Model, Volterra Kernels, and Other Hemodynamics. NeuroImage 12: 466–477. doi:10.1006/nimg.2000.0630.
48. Günther M, Oshio K, Feinberg DA (2005) Single-shot 3D imaging techniques improve arterial spin labeling perfusion measurements. Magn Reson Med 54: 491–498. doi:10.1002/mrm.20580.
49. Ye FQ, Frank JA, Weinberger DR, McLaughlin AC (2000) Noise reduction in 3D perfusion imaging by attenuating the static signal in arterial spin tagging (ASSIST). Magn Reson Med 44: 92–100.

50. St Lawrence KS, Frank JA, Bandettini PA, Ye FQ (2005) Noise reduction in multi-slice arterial spin tagging imaging. Magn Reson Med 53: 735–738. doi:10.1002/mrm.20396.

51. Dixon WT, Sardashti M, Castillo M, Stomp GP (1991) Multiple inversion recovery reduces static tissue signal in angiograms. Magn Reson Med 18: 257–268.

Acknowledgements

Chapter 5, Section A, in full, is a reprint of material as it appears in NMR Biomed 2012. Blockley, NP, VEM Griffeth, Simon AB, Buxton RB (2012). A review of calibrated blood oxygenation level-dependent (BOLD) methods for the measurement of task-induced changes in brain oxygen metabolism. NMR Biomed. The dissertation author was a supporting investigator and author of this material.

Chapter 5, Section B, in full, is a reprint of material as it appears in Neuroimage 2012. Blockley, NP, VEM Griffeth, Buxton RB (2012). A general analysis of calibrated BOLD methodology for measuring $CMRO_2$ responses: comparison of a new approach with existing methods. Neuroimage 60: 279-89. The dissertation author was a supporting investigator and author of this material.

Chapter 5, Section C, in full, is a reprint of material as it appears in Neuroimage 2013. Blockley NP, Griffeth VEM, Germuska MA, Bulte DP, Buxton RB. (2013). An analysis of the use of hyperoxia for measuring venous cerebral blood volume: Comparison of the existing method with a new analysis approach. Neuroimage 72: 33-40. The dissertation author was a supporting investigator and author of this material.

Chapter 5, Section D, in full, is a reprint of material as it appears in PLoS ONE 2013. Simon AB**,** Griffeth VEM, Wong EC, Buxton RB (2013). A novel method of combining blood oxygenation and blood flow sensitive magnetic resonance imaging techniques to measure the cerebral blood flow and oxygen metabolism responses to an unknown neural stimulus. PLoS ONE 8: e54816. The dissertation author was a supporting investigator and author of this material.

CHAPTER 6 CONCLUSIONS

Why study the BOLD signal?

Functional brain imaging is an exciting field with the potential to provide extensive insight into how the brain works at a macroscopic level. The classic technique of neuroscience is patch-clamp and focuses on how single neurons respond to and interact with the environment around them, but it is also necessary to relate these findings to the global function of the brain. Other electrophysiological techniques and optical two-photon imaging examine populations of neurons, but all require an invasive surgical procedure to gain access to the brain through the skull. Optical techniques are also limited by their ability to penetrate at most the top 1mm of the brain due to scattering of light. Other optical measurements exist, which are non-invasive, and measure both blood velocity and oxygenation, but again these are limited by their inability to penetrate deeply into the brain. Electroencephalography (EEG) and magnetoencephalography (MEG) are non-invasive techniques, which directly measure fluctuations in synchronized neuronal currents that reach the scalp in the form of voltage changes and magnetic fields. Both directly measure the electrical activity in the cortex but EEG is limited by spatial resolution while MEG has low signal magnitude. Positron emission tomography (PET) detects gamma-rays from positron-emitting radionuclide tracers and can measure cerebral blood flow (CBF), glucose metabolism, and oxygen metabolism ($CMRO_2$). A limitation of PET is that it involves exposure to ionizing radiation, especially when combined with computed tomography (CT). Of these techniques, PET is the most similar in what it measures to functional MRI (fMRI).

The advantage of functional fMRI is that it is non-invasive, safe, and can provide information about deep structures of the brain including subcortical structures such as the thalamus. To integrate knowledge gained from all of these modalities in order to gain a better

understanding of how the brain works, it is necessary to understand how the technologies are related. Here I focused on relating the blood oxygenation level dependent (BOLD) fMRI signal to underlying physiological changes, especially CBF and $CMRO_2$ while applying the technique to neurophysiological questions of interest. Of particular interest is the relationship of the BOLD signal to $CMRO_2$, which is related to neural activity through the large energy requirement of pumping ions against their gradient at neural synapses [1,2].

Interpreting changes in the BOLD signal response

Similar to optical techniques measuring blood oxygenation changes, the BOLD signal is not a direct reflection of neural activity but rather depends on the fractional change in hemoglobin oxygen saturation, which is a function of cerebral blood flow (CBF), oxygen metabolism, and the baseline state of the brain. The complexity of the BOLD signal makes interpretation of changes in the response magnitude difficult for two reasons: a change in the BOLD response does not necessarily imply a change in neural activity [3,4], and a lack of a measureable change in the BOLD response does not equate to a constant neural response [5]. Specifically previous studies using acetazolamide and end-tidal carbon dioxide manipulations modulated basal cerebral blood flow thereby producing changes in the BOLD response magnitude despite an expectation that the neural and $CMRO_2$ responses to the stimuli were unchanged [6-9]. Similarly in work presented in this dissertation, I showed that without a measureable change in the BOLD response pre- and post-caffeine, there could still be changes in the underlying neural activity [5]. In other words, both false positives and false negatives are possible when equating changes in the BOLD signal alone to changes in neural activity. The complexity of the BOLD signal, which leads to this conundrum, suggests an approach for measuring how $CMRO_2$ changes with a stimulus or under different baseline conditions. By combining measurements of BOLD with CBF, a measurement of cerebral oxygen metabolism

can be extracted in an approach known as calibrated fMRI [10], thereby providing an indication of the underlying neural activity.

Prospects for quantitative fMRI: neuromodulation due to caffeine

To examine the prospects for quantitative fMRI, I studied the effects of caffeine on BOLD, CBF and $CMRO_2$ in the baseline state and in response to a visual stimulus. Using previously developed acquisition and analysis methods for combined BOLD and arterial spin labeling (ASL) [11,12], I quantitatively measured fluctuations in CBF and R_2*, which is the MR signal decay rate that produces the BOLD signal. By combining these measurements with a calibration experiment to determine the baseline state of the brain, I was able to calculate changes in both baseline $CMRO_2$ and the $CMRO_2$ stimulus response using the Davis model of the BOLD response [10]. I found that caffeine ingestion results in a decrease in baseline CBF and an increase in baseline $CMRO_2$ [5]. Additionally in response to a visual stimulus, the CBF response was blunted by caffeine while the $CMRO_2$ response was increased. Notably these changes in the CBF and $CMRO_2$ stimulus responses combined to produce no change in the BOLD response to the visual stimulus pre- and post-caffeine thus demonstrating how changes in neural activity can be masked by the complexity of this signal.

Limitations of the calibrated fMRI approach

This study clearly shows the dangers of only measuring the BOLD signal when examining interventions affecting the central nervous system. While it is possible to use the BOLD signal directly to examine immediate CNS effects of drugs by infusion while subjects lie in the scanner [13], it is much more difficult to measure the effects when subjects must be removed from the scanner or studied on multiple days. In these types of studies, it is more reliable to calculate the quantitative signal decay rate, R_2*, from the echo decay curve in order

to characterize changes in the BOLD signal [14]. Furthermore changes in the BOLD signal response are confounded by changes in the blood flow response, which necessitates combining BOLD and CBF measurements with a mathematical model to extract information about oxygen metabolism, which is likely to be a better indicator of neural activity. Inherent to this approach are assumptions due to both the mathematical model and the calibration experiment. Classically the Davis model for calibrated fMRI has been used [10], but this model neglects contributions to the BOLD signal from the intravascular compartment [15], incorrectly assumes cerebral blood volume (CBV) changes are distributed equally across the vascular compartments [16-18], and ignores the exchange of blood for tissue as CBV increases with activation [19]. Furthermore it relies on an additional calibration experiment to measure a scaling parameter, which is reflective of the baseline state of the brain. Most often the calibration performed requires subjects to breathe 5% carbon dioxide (combined with 21% oxygen), but this additional experiment is time consuming, uncomfortable for subjects, and impossible in many patient populations. There are also indications that hypercapnia is not isometabolic, a key assumption of the calibration calculation [20,21].

To address these criticisms of the Davis model and further our understanding of the BOLD signal, I developed a detailed mathematical model (DBM) of the BOLD response incorporating factors that affect the baseline brain state and how changes in blood volume depend on changes in blood flow [22]. Using the DBM to test the accuracy of the Davis model [10], I found that the physiological factor having the greatest impact on $CMRO_2$ calculations is the dependence of venous CBV on CBF while variation in hematocrit and oxygen extraction fraction are accounted for by performing a calibration experiment. This result confirmed the potential for error in Davis model calculations due to the underlying assumption that CBV changes are distributed equally, but beyond this variation I determined that the Davis model is

surprisingly accurate in most areas of CBF-$CMRO_2$ coupling. The exception is when CBF and $CMRO_2$ change in opposite directions, which is typical of caffeine ingestion. In this case, optimization of α and β in the Davis model by treating them as free parameters improves the accuracy of the Davis model for calculating $CMRO_2$ changes. While these results address criticism of the mathematical form of the Davis model, the limitations due to calibration (questionable accuracy and limited application in patient populations) remain.

Variation in the coupling of CBF and $CMRO_2$

Calibration of the BOLD signal provides quantitative information about $CMRO_2$ as an indication of the underlying changes in neural activity, but this specific information may not always be necessary to study changes in neural activity using fMRI. In fact by developing techniques independent of calibration, questions regarding the accuracy of the calibration can be circumvented and a more diverse population of subjects can be studied making the possibility of clinical studies more likely. One possibility for identifying changes in the underlying neural activity without a calibration experiment is monitoring how the coupling of CBF and $CMRO_2$ responses change with stimulus intensity or other stimulus characteristics. Supporting this approach are studies indicating that blood flow and energy metabolism respond to different aspects of neural activity. Previously it was believed that energetically expensive increases in neural activity first produced an increase in the metabolic demand, which in turn triggered a rise in blood flow all in a linear fashion [23]. The work of Fox and Raichle questioned this presumption revealing that blood flow and oxygen metabolism are not tightly coupled as brain blood flow increased much more than the change in oxygen metabolism in response to a sensory stimulus [24]. Current thinking is that $CMRO_2$ may simply respond to the net energy demand associated with evoked neural activity (more specifically the energetic cost of pumping sodium and potassium ions against their gradients) [1,25] while changes in CBF are thought to

respond to neuronal signals in a feed-forward manner with the balance of these changes determining the magnitude of the BOLD response [25,26]. The details of these changes and the type of neuronal activity therefore will likely affect the coupling of CBF and $CMRO_2$ changes.

To show that CBF changes are not simply dependent on metabolic signaling molecules, research has focused on determining a direct relationship between neural activity and changes in blood flow. Evidence supporting this hypothesis comes from a diverse group of animal studies using techniques such as electrophysiological recordings, optical imaging, PET, and fMRI. Instead of metabolic signals initiating the blood flow response, *in vitro* research indicates that specific neuronal cell types directly produce the arteriolar response [27-29]. In particular research using patch-clamp recordings coupled to confocal observation of GABA inhibitory interneurons and blood vessels indicate that activation of neurons expressing vasoactive intestinal peptide (VIP) or nitric oxide synthase (NOS) produce vasodilation while those expressing somatostatin and neuropeptide-Y (NPY) elicit vasoconstriction [28]. Related work using infrared videomicroscopy showed that specific cerebellar cell types either dilate (stellate cells) or contract (Purkinje cells) the microvasculature [29]. *In vivo* studies have also linked neuronal inhibition to both vasoconstriction and the negative BOLD response using fMRI or optical imaging combined with electrophysiological recordings [30-32]. Further evidence of blood flow dependence on neural activity rather than on the metabolic consequences of neural activity is the dissociation of glucose metabolism from blood flow; in areas with predominantly neuronal inhibition an increase of glucose consumption was shown to occur in the presence of vasoconstriction [31,33]. Numerous studies also cite a role for astrocytes in the coupling of neural activation and blood flow changes, as astrocytes mediate both vasodilation [34-36] and vasoconstriction [37,38]. These studies in summary provide mechanisms by which neural activity modulates cerebral blood flow independent of metabolic changes in the brain.

To study these changes in CBF and $CMRO_2$ responses in a straightforward manner, I proposed a new heuristic model of the BOLD response, which inspired the "ratio method" for identifying differences in *n* for the same region of interest activated by different stimuli based only on the measured BOLD and CBF signals. My findings indicate that the ratio method performs well at 1.5T and 3T, but caution should be used when applying this method at higher field strengths where the method may predict a change in *n* where one does not exist (Chapter 3). Within the context of a calibrated BOLD experiment, I also demonstrated that the heuristic model performs with accuracy similar to that of the Davis model when changes in CBF and $CMRO_2$ are both positive (Chapter 3). To test the ratio method on experimental data, I applied it to previously published data confirming that as visual stimulus intensity is increased so does *n* for the response in primary visual cortex. The approach using the ratio method is straightforward and simple, but the original analysis was cumbersome as it used the Davis model and multiple calculations assuming a broad range of values for *M*, α and β. In an additional application of this method, I compared a complex movie stimulus to a simple flickering checkerboard and found no difference in the coupling of blood flow and oxygen metabolism. This was in contrast to our hypothesis that more complex stimuli would be associated with lower *n* as additional afferents modified the response of the visual cortex increasing $CMRO_2$ more than CBF. Examining this data further I found that during a movie stimulus the variance of R_2* and CBF in the primary visual cortex is increased over that of the baseline and that the correlation of the CBF and R_2* responses to a long movie stimulus is higher across subjects watching the same movie than it is within the same subject watching different movies (Chapter 4). These results were in line with our hypothesis and existing data that the brain responds in a consistent manner to a complex stimulus even across subjects [39-41].

Improving calibrated BOLD

Returning to discussion of calibrated BOLD, quantitative measurements of $CMRO_2$ using combined CBF and BOLD measurements rely on the accuracy of the calibration experiment used to measure the scaling parameter. Numerous approaches have been proposed for calibration and typically involve inhaled gases (hypercapnia, hyperoxia or some combination). The original and most common calibrated BOLD approach, hypercapnia, assumes that cerebral oxygen metabolism does not change when subjects inhale carbon dioxide, but this assumption has been questioned [9,20,21,42,43]. Gas calibrations are also time-consuming and uncomfortable for subjects. To address these criticisms, some groups have proposed using hyperoxia as an alternative for calibrating the BOLD signal, but an ideal calibrated BOLD experiment would not use an inhaled gas protocol at all and would instead rely on imaging techniques to measure tissue properties reflective of the baseline state of the brain.

We used the DBM to simulate one such gas-free BOLD calibration, the reversible signal decay rate (R_2'), and compared this new calibration method with those using inhaled gases. We simulated whether combining measurements of CBF with BOLD responses scaled by one of the calibration parameters (hypercapnia, hyperoxia or R_2') would be sufficient to distinguish between levels of $CMRO_2$. While both idealized hypercapnia (no metabolic effect) and R_2' methods for calibration distinguished between levels of $CMRO_2$ change, hyperoxia calibration did not, because it is sensitive to fluctuations in baseline CBV, baseline oxygen extraction fraction and subject hematocrit [44,45]. Consistent with previous findings, the physiological factor having the greatest impact on all calibration methods was the dependence of venous CBV on CBF; hypercapnia was the least sensitive to this variation while hyperoxia

and R_2' were more sensitive. These findings support pursuit of a measurement for R_2' as a simple method of calibrating BOLD fMRI studies.

While hyperoxia is not a reliable method for calibrated fMRI, there does appear to be a direct relationship between the BOLD signal change due to hyperoxia and venous CBV [46]. We showed that the existing analysis for determining venous CBV based on dynamic contrast agent experiments has substantial systematic error, because it assumes that the change in the BOLD signal due to hyperoxia depends only on the intravascular signal. Instead a new method relating the BOLD signal change directly to venous CBV is more reliable and consistent with the limited literature in this area. Quantitative measurements of venous CBV are important, because there may be important differences in the venous vasculature between the healthy brain and disease state. Venous CBV also strongly influences the magnitude of the BOLD response, so these measurements may be useful when controlling for differences across subjects and in disease.

Improving noise limitations of ASL CBF measurements

A limitation of the combined measure of CBF with R_2* is the low signal to noise ratio of the blood flow measurement, which is a result of the small amount of tagged blood that can be delivered to a brain region during the imaging period. To overcome this, CBF imaging is often performed with lower spatial and temporal resolution than standard BOLD imaging. Significant averaging (spatially over a region of interest and temporally over repeated stimuli) is also used to acquire dynamic measurements of CBF. The BOLD signal has a much higher signal to noise ratio and is strongly weighted by the blood flow signal, suggesting a method called BOLD Constrained Perfusion, which combines information in the two signals to improve the precision of the CBF signal [47]. This work was done in collaboration using the DBM and heuristic model, which makes BCP work more cleanly and straightforwardly than the Davis

model. It is advantageous over other analysis methods because it does not require repeated temporal measurements making it possible to study more natural stimuli that cannot be easily repeated or averaged.

In total these results confirm the limitations of the BOLD signal while demonstrating that combined quantitative acquisition of R_2* with CBF provides a significant improvement to our ability to relate the BOLD signal to neural activity through changes in $CMRO_2$. Without a calibration experiment, a simple comparison of the BOLD response ratio and non-linear CBF response ratio permits comparison of CBF-$CMRO_2$ coupling for different stimuli. If specific information about $CMRO_2$ or if response comparison across regions of interest is necessary, then a calibration experiment is required. While hypercapnia appears to be the most reliable gas-based method as long as it is iso-metabolic, the gas-free measurement of R_2' holds promise for the future.

Future studies: The neurological basis of CBF-$CMRO_2$ coupling changes

Recent findings from our group and others suggest that the coupling of blood flow and oxygen metabolism in the brain is not constant but rather depends both on the state of the brain [5,14,48] as well as the stimulus [49,50]. Caffeine has been shown to alter the baseline state of the brain by decreasing CBF and increasing $CMRO_2$ [5,14]. When the response to a simple visual stimulus was examined, the absolute $CMRO_2$ change to the same stimulus was increased by 61% after caffeine ingestion resulting in a lower *n* and suggesting increased neuronal excitability. This is consistent with the idea that adenosine (as an inhibitory neuromodulator) is blocked by caffeine thereby relieving the inhibition [5,14]. Modulations of attention appear to have a similar effect on the response to a visual stimulus as increasing attention to a stimulus produces a lower *n* in response [48]. On the other hand adaptation to a stimulus appears to

decrease the metabolic response relative to the vascular response resulting in a higher *n* (Moradi, submitted). Modulations to the stimulus itself have also been shown to alter the physiological response: increasing either the stimulus frequency [50] or characteristic intensity [49] results in a higher *n*. In sum these studies are consistent with the idea that changing stimulus strength modulates CBF more than $CMRO_2$, while changing the brain state so that it responds differently to the same stimulus modulates $CMRO_2$ more than CBF. These findings are closely related to the studies discussed earlier showing the regulation of cerebral blood flow and metabolism are driven in parallel by separate mechanisms.

Examining these results closely a pattern emerges, which suggests a new hypothesis: CBF and $CMRO_2$ coupling reflects the underlying balance of excitatory and inhibitory activity with larger increases in excitatory activity leading to relatively larger $CMRO_2$ responses while larger increases in inhibitory activity lead to larger relative CBF responses (Figure 1). This hypothesis is based on three ideas. First excitation is always coupled to inhibition because of the wiring of cortical circuits [51]. Second acute increases in CBF are thought to be driven by fast glutamate-mediated neural signaling (associated with excitatory activity) and also GABA interneurons, which may either increase or decrease CBF depending on the signaling molecule released [25,26,28,52]; decreases in CBF are due in part to somatostatin- and NPY-positive interneurons while increases in CBF are due to VIP- and NOS-positive interneurons. Astrocytes play a secondary role during prolonged activation integrating signals from multiple sources [25,28,53]. Third $CMRO_2$ is a reflection of the overall evoked neural activity (associated with action potentials, postsynaptic effects of glutamate, and the cost of transporting ions), and is likely to be dominated by excitatory activity with only a small component due to inhibitory activity [2,54]. In sum CBF and $CMRO_2$ are driven in parallel by separate mechanisms integrating signals from both excitatory and inhibitory activity to different degrees based on the

stimulus type. This hypothesis would suggest that when stimulus intensity increases inhibitory activity increases more than excitatory activity such that the CBF response increases more than the $CMRO_2$ response leading to a larger *n* with increasing stimulus intensity.

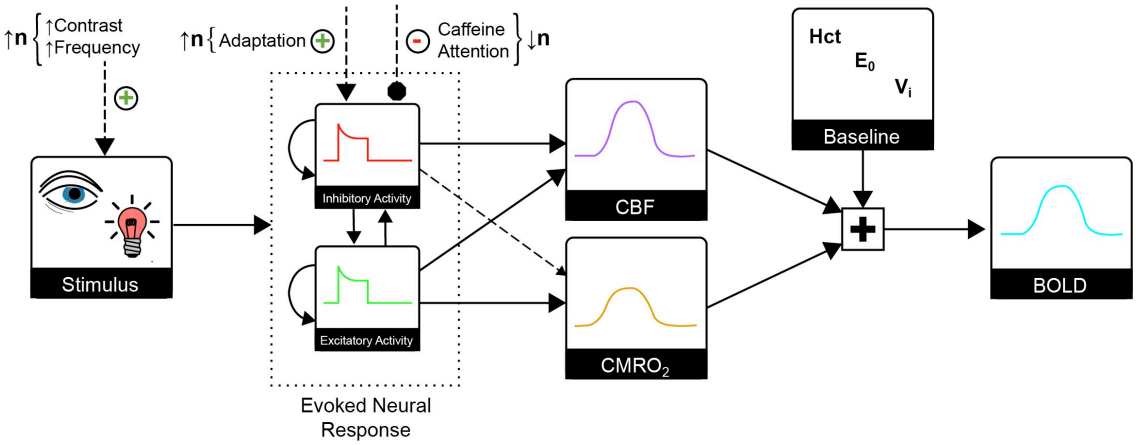

Figure 6.1. Illustration of the physiological relationship between BOLD, CBF, $CMRO_2$ and neural activity.
A stimulus results in activation of both excitatory and inhibitory neurons. Excitatory neuronal activity (green) produces increases in both CBF and $CMRO_2$ while inhibitory neuronal activity (red) directly tends to decrease CBF but also has an indirect effect on coupling by decreasing excitatory activity. The combined changes typically lead to the uncoupling of CBF and $CMRO_2$ such that the blood flow response tends to be much greater than the metabolic response. This is the phenomenon underlying the BOLD signal, which is also scaled by the baseline state of the brain. Factors altering these responses include direct actions on the stimulus, which tend to increase *n* as the stimulus intensity is increased, and modulations of the underlying neural activity by factors such as caffeine, subject attention and adaptation to prolonged stimuli.

On the other hand neuromodulation by caffeine is thought to impact inhibitory activity directly. Caffeine is a non-selective antagonist of adenosine receptors, particularly types A_1, A_{2A} and A_{2B} [55,56]. In the brain adenosine acts to inhibit the release of excitatory neurotransmitters at A1 receptors, so by blocking these receptors caffeine diminishes inhibitory activity leading to an increase in the neuronal firing rate [55,57]. Additionally caffeine acts as a vasoconstrictor by blocking A_{2A} and A_{2B} receptors [56,58]. Our hypothesis is that this combination of changes due

to caffeine leads to more excitatory activity than inhibitory activity relative to the pre-caffeine state thereby producing a larger $CMRO_2$ response relative to CBF resulting in a lower *n* [59].

Studies examining the effects of attention have shown that neurons increase their firing rates in response to a stimulus when it is attended [60-63], while there is only moderate attentional modulation of the BOLD signal [64-67]. However recent findings from my group indicate that attention strongly modulates the $CMRO_2$ response [48]. This not only emphasizes the importance of combining BOLD and CBF measurements but also shows a decrease in *n* with attention. Interestingly modulation of visual cortex V1 firing activity by attention is shown to be much weaker than the effect on $CMRO_2$, and the source of this large mismatch is unknown [48,68]. One possible reason for this discrepancy is the balance of excitatory and inhibitory activity: if both types of activity increase, then $CMRO_2$ would be expected to increase as well because of the energy costs of transporting ions while the firing rate of particular neurons would depend instead on the balance of excitatory and inhibitory activity [48]. The decrease in CBF-$CMRO_2$ coupling could then be explained by an increase in excitatory activity more than that of inhibitory activity leading to a modulation of $CMRO_2$ that is greater then the CBF modulation.

Possibilities for modulation of *n*

Future studies will focus on examining this relationship in detail through experiments modulating both the stimulus intensity and neural response to stimuli. One possibility is testing the effect of finger tapping frequency on *n* to examine whether changing stimulus frequency affects coupling in areas of the brain other than the visual cortex, although one previous study did not show a difference [69]. Another possibility is testing the neuromodulatory effects of nicotine. Nicotine is a nicotinic acetylcholine receptor agonist that acts within both the adrenal

medulla and the central nervous system (CNS). In the CNS, nicotine produces an increase in the release of many neurotransmitters including dopamine, norepinephrine, acetylcholine, serotonin, γ-aminobutyric acid (GABA) and glutamate [70]. Excitatory glutaminergic projections and inhibitory GABA projections alter the level of dopamine release such that the overall effect of nicotine (whether it is a stimulant or sedative) is dependent on the balance of glutamate and GABA [71]. While the effect of nicotine on brain metabolism will also depend on this balance, there are indications that nicotine enhances alertness, arousal and cognition through stimulation of nicotinic cholinergic receptors [72,73]. PET studies have indicated increases in cerebral glucose consumption after administration of nicotine [73,74] as well as cerebral blood flow in certain areas of the brain [75]. Magnetic resonance methods have also shown increases in blood flow and metabolism [76,77]. These neuromodulatory effects make nicotine a fascinating candidate for a calibrated BOLD experiment that parallels the previous study of caffeine, and I would hypothesize that nicotine would decrease the coupling of CBF and $CMRO_2$ in response to a stimulus due to its the stimulatory effects. In particular both the visual cortex and the left inferior frontal cortex were stimulated by nicotine, so a task incorporating both a visual stimulus and either go/no-go decision making or semantic working memory could be interesting [74]. In short, our caffeine study can serve as a prototype for other studies of neuromodulation.

Neuromodulatory effects of exercise

Recently I proposed to study the neurophysiological effects of exercise, which is interesting due to its beneficial effects on physical health, mental health and disease prevention [78-81]. With increasing sedentary lifestyle, there is an increased risk of depression, cardiovascular disease, diabetes, cancer, and hypertension as well as lowered general wellbeing [81-83], but how exercise modulates brain physiology specifically is less clear. Exercise increases CBF and metabolic rate during exercise while decreasing glucose uptake and

increasing CBF post-exercise [84-87]. How exercise modulates local metabolic rate and $CMRO_2$ is not known, and how these physiological changes may be related to "that warm fuzzy feeling" after exercise [88] is of additional interest. The ability to measure local changes in CBF and $CMRO_2$ continuously over a period of time using the techniques discussed in this dissertation will provide insight into the neural effects of exercise, whether these changes may be localized to specific areas, and how exercise may modify the brain's response to stimuli.

I started work on this project and have collected data from ten subjects. Over the next few months I will analyse this data in order to determine whether exercise affects baseline CBF and $CMRO_2$ or alters the stimulus response by studying subjects' R_2* and CBF responses before and after 30 minutes of exercise at 60% of their maximum VO_2. Like caffeine, exercise has been shown to impact adenosine levels. However, exercise increases adenosine [89,90] while caffeine decreases adenosine effects [55]. Since exercise increases adenosine, it would be expected to have the opposite effect as caffeine on CBF and $CMRO_2$, increasing baseline CBF and decreasing baseline $CMRO_2$. However, exercise has many other effects which could dominate these anticipated adenosine effects. Past experiments have shown exercise increases CBF and metabolism during an exercise task [84,86] while glucose uptake is decreased in the 90 minutes post-exercise [87]. Anecdotally, exercise increases alertness and may increase baseline $CMRO_2$, so we are very interested in the outcome of this experiment.

With regard to the effect of exercise on the neurological response to different stimuli, my work on the effects of caffeine demonstrated the importance of measuring not only the BOLD response to a stimulus but also the CBF and $CMRO_2$ responses. In the case of caffeine, both the baseline state (decreased CBF with increased $CMRO_2$) and the evoked response to a standard stimulus (a larger increase of $CMRO_2$ relative to CBF after caffeine) were altered with the result being no change in the BOLD response. Considering the impact of exercise on

increasing adenosine levels, it would be expected to decrease the $CMRO_2$ response to the stimulus relative to the CBF response. However as noted above, exercise mediates many other effects increasing both $CMRO_2$ and CBF during exercise, but how this will impact neurophysiology post-exercise is not known. Anecdotally, exercise increases alertness, which may result in increased $CMRO_2$ responses to the stimuli.

The experimental approach developed here lays the groundwork for future studies by establishing a tool for probing the physiological effects of exercise directly. My long-term goal is to build on the proposed studies of acute effects of exercise in order to study brain responses after modifications of daily exercise regimens.

References

1. Attwell D, Laughlin SB (2001) An energy budget for signaling in the grey matter of the brain. J Cereb Blood Flow Metab 21: 1133-1145.

2. Attwell D, Iadecola C (2002) The neural basis of functional brain imaging signals. Trends Neurosci 25: 621-625.

3. Cohen ER, Ugurbil K, Kim SG (2002) Effect of basal conditions on the magnitude and dynamics of the blood oxygenation level-dependent fMRI response. J Cereb Blood Flow Metab 22: 1042-1053.

4. Brown GG, Eyler Zorrilla LT, Georgy B, Kindermann SS, Wong EC, et al. (2003) BOLD and perfusion response to finger-thumb apposition after acetazolamide administration: differential relationship to global perfusion. J Cereb Blood Flow Metab 23: 829-837.

5. Griffeth VE, Perthen JE, Buxton RB (2011) Prospects for quantitative fMRI: Investigating the effects of caffeine on baseline oxygen metabolism and the response to a visual stimulus in humans. Neuroimage 57: 809-816.

6. Vorstrup S, Henriksen L, Paulson OB (1984) Effect of acetazolamide on cerebral blood flow and cerebral metabolic rate for oxygen. J Clin Invest 74: 1634-1639.

7. Kety SS, Schmidt CF (1948) The Effects of Altered Arterial Tensions of Carbon Dioxide and Oxygen on Cerebral Blood Flow and Cerebral Oxygen Consumption of Normal Young Men. J Clin Invest 27: 484-492.

8. Okazawa H, Yamauchi H, Sugimoto K, Toyoda H, Kishibe Y, et al. (2001) Effects of acetazolamide on cerebral blood flow, blood volume, and oxygen metabolism: a positron emission tomography study with healthy volunteers. J Cereb Blood Flow Metab 21: 1472-1479.

9. Sicard KM, Duong TQ (2005) Effects of hypoxia, hyperoxia, and hypercapnia on baseline and stimulus-evoked BOLD, CBF, and CMRO2 in spontaneously breathing animals. Neuroimage 25: 850-858.

10. Davis TL, Kwong KK, Weisskoff RM, Rosen BR (1998) Calibrated functional MRI: mapping the dynamics of oxidative metabolism. Proc Natl Acad Sci USA 95: 1834-1839.

11. Liu TT, Wong EC (2005) A signal processing model for arterial spin labeling functional MRI. Neuroimage 24: 207-215.

12. Wong EC, Buxton RB, Frank LR (1998) Quantitative imaging of perfusion using a single subtraction (QUIPSS and QUIPSS II). Magn Reson Med 39: 702-708.

13. Chen Y, Parrish TB (2009) Caffeine dose effect on activation-induced BOLD and CBF responses. Neuroimage 46: 577-583.

14. Perthen JE, Lansing AE, Liau J, Liu TT, Buxton RB (2008) Caffeine-induced uncoupling of cerebral blood flow and oxygen metabolism: a calibrated BOLD fMRI study. Neuroimage 40: 237-247.

15. Boxerman JL, Hamberg LM, Rosen BR, Weisskoff RM (1995) MR contrast due to intravascular magnetic susceptibility perturbations. Magn Reson Med 34: 555-566.

16. Kim T, Kim SG (2006) Quantification of cerebral arterial blood volume using arterial spin labeling with intravoxel incoherent motion-sensitive gradients. Magn Reson Med 55: 1047-1057.

17. Chen JJ, Pike GB (2009) BOLD-specific cerebral blood volume and blood flow changes during neuronal activation in humans. NMR Biomed 22: 1054-1062.

18. Hillman EM, Devor A, Bouchard MB, Dunn AK, Krauss GW, et al. (2007) Depth-resolved optical imaging and microscopy of vascular compartment dynamics during somatosensory stimulation. Neuroimage 35: 89-104.

19. Obata T, Liu TT, Miller KL, Luh WM, Wong EC, et al. (2004) Discrepancies between BOLD and flow dynamics in primary and supplementary motor areas: application of the balloon model to the interpretation of BOLD transients. Neuroimage 21: 144-153.

20. Xu F, Uh J, Brier MR, Hart J, Jr., Yezhuvath US, et al. (2011) The influence of carbon dioxide on brain activity and metabolism in conscious humans. J Cereb Blood Flow Metab 31: 58-67.

21. Zappe AC, Uludag K, Oeltermann A, Ugurbil K, Logothetis NK (2008) The influence of moderate hypercapnia on neural activity in the anesthetized nonhuman primate. Cereb Cortex 18: 2666-2673.

22. Griffeth VE, Buxton RB (2011) A theoretical framework for estimating cerebral oxygen metabolism changes using the calibrated-BOLD method: modeling the effects of blood volume distribution, hematocrit, oxygen extraction fraction, and tissue signal properties on the BOLD signal. Neuroimage 58: 198-212.

23. Roland PE, Skinhoj E, Lassen NA, Larsen B (1980) Different cortical areas in man in organization of voluntary movements in extrapersonal space. J Neurophysiol 43: 137-150.

24. Fox PT, Raichle ME (1986) Focal physiological uncoupling of cerebral blood flow and oxidative metabolism during somatosensory stimulation in human subjects. Proc Natl Acad Sci USA 83: 1140-1144.

25. Devor A, Boas D, Einevoll G, Buxton R, Dale A (2012) Neuronal Basis of Non-Invasive Functional Imaging: From Microscopic Neurovascular Dynamics to BOLD fMRI. In: Choi I-Y, Gruetter R, editors. Neural Metabolism In Vivo: Springer US. pp. 433-500.

26. Cauli B, Hamel E (2010) Revisiting the role of neurons in neurovascular coupling. Front Neuroenergetics 2: 9.

27. Hamel E (2004) Cholinergic modulation of the cortical microvascular bed. Prog Brain Res 145: 171-178.

28. Cauli B, Tong XK, Rancillac A, Serluca N, Lambolez B, et al. (2004) Cortical GABA interneurons in neurovascular coupling: relays for subcortical vasoactive pathways. J Neurosci 24: 8940-8949.

29. Rancillac A, Rossier J, Guille M, Tong XK, Geoffroy H, et al. (2006) Glutamatergic Control of Microvascular Tone by Distinct GABA Neurons in the Cerebellum. J Neurosci 26: 6997-7006.

30. Shmuel A, Augath M, Oeltermann A, Logothetis NK (2006) Negative functional MRI response correlates with decreases in neuronal activity in monkey visual area V1. Nat Neurosci 9: 569-577.

31. Devor A, Hillman EM, Tian P, Waeber C, Teng IC, et al. (2008) Stimulus-induced changes in blood flow and 2-deoxyglucose uptake dissociate in ipsilateral somatosensory cortex. J Neurosci 28: 14347-14357.

32. Devor A, Tian P, Nishimura N, Teng IC, Hillman EM, et al. (2007) Suppressed neuronal activity and concurrent arteriolar vasoconstriction may explain negative blood oxygenation level-dependent signal. J Neurosci 27: 4452-4459.

33. Lindauer U, Leithner C, Kaasch H, Rohrer B, Foddis M, et al. (2010) Neurovascular coupling in rat brain operates independent of hemoglobin deoxygenation. J Cereb Blood Flow Metab 30: 757-768.

34. Zonta M, Angulo MC, Gobbo S, Rosengarten B, Hossmann KA, et al. (2003) Neuron-to-astrocyte signaling is central to the dynamic control of brain microcirculation. Nat Neurosci 6: 43-50.

35. Mulligan SJ, MacVicar BA (2004) Calcium transients in astrocyte endfeet cause cerebrovascular constrictions. Nature 431: 195-199.

36. Takano T, Tian GF, Peng W, Lou N, Libionka W, et al. (2006) Astrocyte-mediated control of cerebral blood flow. Nat Neurosci 9: 260-267.

37. Blanco VM, Stern JE, Filosa JA (2008) Tone-dependent vascular responses to astrocyte-derived signals. Am J Physiol Heart Circ Physiol 294: H2855-2863.

38. Metea MR, Newman EA (2006) Glial cells dilate and constrict blood vessels: a mechanism of neurovascular coupling. J Neurosci 26: 2862-2870.

39. Hasson U, Malach R, Heeger DJ (2010) Reliability of cortical activity during natural stimulation. Trends Cogn Sci 14: 40-48.

40. Lahnakoski JM, Salmi J, Jaaskelainen IP, Lampinen J, Glerean E, et al. (2012) Stimulus-related independent component and voxel-wise analysis of human brain activity during free viewing of a feature film. PLoS One 7: e35215.

41. Kauppi JP, Jaaskelainen IP, Sams M, Tohka J (2010) Inter-subject correlation of brain hemodynamic responses during watching a movie: localization in space and frequency. Front Neuroinform 4: 5.

42. Bolar DS, Rosen BR, Evans KC, Sorensen AG, Adalsteinsson E. Depression of cortical gray matter CMRO2 in awake humans during hypercapnia; 2010 2010. pp. 516.

43. Jones M, Berwick J, Hewson-Stoate N, Gias C, Mayhew J (2005) The effect of hypercapnia on the neural and hemodynamic responses to somatosensory stimulation. Neuroimage 27: 609-623.

44. Blockley NP, Griffeth VE, Buxton RB (2012) A general analysis of calibrated BOLD methodology for measuring CMRO2 responses: comparison of a new approach with existing methods. Neuroimage 60: 279-289.

45. Blockley NP, Griffeth VE, Simon AB, Buxton RB (2012) A review of calibrated blood oxygenation level-dependent (BOLD) methods for the measurement of task-induced changes in brain oxygen metabolism. NMR Biomed.

46. Blockley NP, Griffeth VE, Germuska MA, Bulte DP, Buxton RB (2013) An analysis of the use of hyperoxia for measuring venous cerebral blood volume: Comparison of the existing method with a new analysis approach. Neuroimage 72: 33-40.

47. Simon AB, Griffeth VE, Wong EC, Buxton RB (2013) A novel method of combining blood oxygenation and blood flow sensitive magnetic resonance imaging techniques to measure the cerebral blood flow and oxygen metabolism responses to an unknown neural stimulus. PLoS One 8: e54816.

48. Moradi F, Buracas GT, Buxton RB (2012) Attention strongly increases oxygen metabolic response to stimulus in primary visual cortex. Neuroimage 59: 601-607.

49. Liang CL, Ances BM, Perthen JE, Moradi F, Liau J, et al. (2013) Luminance contrast of a visual stimulus modulates the BOLD response more than the cerebral blood flow response in the human brain. Neuroimage 64: 104-111.

50. Lin AL, Fox PT, Hardies J, Duong TQ, Gao JH (2010) Nonlinear coupling between cerebral blood flow, oxygen consumption, and ATP production in human visual cortex. Proc Natl Acad Sci U S A 107: 8446-8451.

51. Lefort S, Tomm C, Floyd Sarria JC, Petersen CC (2009) The excitatory neuronal network of the C2 barrel column in mouse primary somatosensory cortex. Neuron 61: 301-316.

52. Hamel E (2006) Perivascular nerves and the regulation of cerebrovascular tone. J Appl Physiol 100: 1059-1064.

53. Nizar K, Uhlirova H, Tian P, Saisan PA, Cheng Q, et al. (2013) In vivo stimulus-induced vasodilation occurs without IP3 receptor activation and may precede astrocytic calcium increase. J Neurosci.

54. Buxton RB (2010) Interpreting oxygenation-based neuroimaging signals: the importance and the challenge of understanding brain oxygen metabolism. Front Neuroenergetics 2: 8.

55. Fredholm BB, Battig K, Holmen J, Nehlig A, Zvartau EE (1999) Actions of caffeine in the brain with special reference to factors that contribute to it widespread use. Pharmcological reviews 51: 83-133.

56. Pelligrino DA, Xu HL, Vetri F (2010) Caffeine and the control of cerebral hemodynamics. J Alzheimers Dis 20 Suppl 1: S51-62.

57. Dunwiddie TV, Masino SA (2001) The role and regulation of adenosine in the central nervous system. Annu Rev Neurosci 24: 31-55.

58. Kusano Y, Echeverry G, Miekisiak G, Kulik TB, Aronhime SN, et al. (2010) Role of adenosine A2 receptors in regulation of cerebral blood flow during induced hypotension. J Cereb Blood Flow Metab 30: 808-815.

59. Fredholm BB (1995) Adenosine, adenosine receptors and the actions of caffeine. Pharmacology and Toxicology 76: 93-101.

60. Ito M, Gilbert CD (1999) Attention modulates contextual influences in the primary visual cortex of alert monkeys. Neuron 22: 593-604.

61. McAdams CJ, Reid RC (2005) Attention modulates the responses of simple cells in monkey primary visual cortex. J Neurosci 25: 11023-11033.

62. Motter BC (1993) Focal attention produces spatially selective processing in visual cortical areas V1, V2, and V4 in the presence of competing stimuli. J Neurophysiol 70: 909-919.

63. Yoshor D, Ghose GM, Bosking WH, Sun P, Maunsell JH (2007) Spatial attention does not strongly modulate neuronal responses in early human visual cortex. J Neurosci 27: 13205-13209.

64. Brefczynski JA, DeYoe EA (1999) A physiological correlate of the 'spotlight' of visual attention. Nat Neurosci 2: 370-374.

65. Buracas GT, Boynton GM (2007) The effect of spatial attention on contrast response functions in human visual cortex. J Neurosci 27: 93-97.

66. Gandhi SP, Heeger DJ, Boynton GM (1999) Spatial attention affects brain activity in human primary visual cortex. Proc Natl Acad Sci U S A 96: 3314-3319.

67. Tootell RB, Hadjikhani N, Hall EK, Marrett S, Vanduffel W, et al. (1998) The retinotopy of visual spatial attention. Neuron 21: 1409-1422.

68. Chen Y, Martinez-Conde S, Macknik SL, Bereshpolova Y, Swadlow HA, et al. (2008) Task difficulty modulates the activity of specific neuronal populations in primary visual cortex. Nat Neurosci 11: 974-982.

69. Kastrup A, Kruger G, Neumann-Haefelin T, Glover GH, Moseley ME (2002) Changes of cerebral blood flow, oxygenation, and oxidative metabolism during graded motor activation. Neuroimage 15: 74-82.

70. Benowitz NL (2008) Clinical pharmacology of nicotine: implications for understanding, preventing, and treating tobacco addiction. Clin Pharmacol Ther 83: 531-541.

71. Mansvelder HD, Keath JR, McGehee DS (2002) Synaptic mechanisms underlie nicotine-induced excitability of brain reward areas. Neuron 33: 905-919.

72. Rusted J, Graupner L, O'Connell N, Nicholls C (1994) Does nicotine improve cognitive function? Psychopharmacology (Berl) 115: 547-549.

73. Parks RW, Becker RE, Rippey RF, Gilbert DG, Matthews JR, et al. (1996) Increased regional cerebral glucose metabolism and semantic memory performance in Alzheimer's disease: a pilot double blind transdermal nicotine positron emission tomography study. Neuropsychol Rev 6: 61-79.

74. Domino EF, Minoshima S, Guthrie SK, Ohl L, Ni L, et al. (2000) Effects of nicotine on regional cerebral glucose metabolism in awake resting tobacco smokers. Neuroscience 101: 277-282.

75. Domino EF, Minoshima S, Guthrie S, Ohl L, Ni L, et al. (2000) Nicotine effects on regional cerebral blood flow in awake, resting tobacco smokers. Synapse 38: 313-321.

76. Hyder F, Kennan RP, Kida I, Mason GF, Behar KL, et al. (2000) Dependence of oxygen delivery on blood flow in rat brain: a 7 tesla nuclear magnetic resonance study. J Cereb Blood Flow Metab 20: 485-498.

77. Pettegrew JW, Panchalingam K, McClure RJ, Levine J (2001) Brain metabolic effects of acute nicotine. Neurochem Res 26: 181-185.

78. Carek PJ, Laibstain SE, Carek SM (2011) Exercise for the treatment of depression and anxiety. Int J Psychiatry Med 41: 15-28.

79. Diehl JJ, Choi H (2008) Exercise: the data on its role in health, mental health, disease prevention, and productivity. Prim Care 35: 803-816.

80. Salmon P (2001) Effects of physical exercise on anxiety, depression, and sensitivity to stress: a unifying theory. Clin Psychol Rev 21: 33-61.

81. Warburton DE, Nicol CW, Bredin SS (2006) Health benefits of physical activity: the evidence. CMAJ 174: 801-809.

82. Kocer O, Wachter M, Zellweger M, Piazzalonga S, Hoffmann A (2011) Prevalence and predictors of depressive symptoms and wellbeing during and up to nine years after outpatient cardiac rehabilitation. Swiss Med Wkly 141: w13242.

83. Bauman AE (2004) Updating the evidence that physical activity is good for health: an epidemiological review 2000-2003. J Sci Med Sport 7: 6-19.

84. Ide K, Secher NH (2000) Cerebral blood flow and metabolism during exercise. Prog Neurobiol 61: 397-414.

85. Smith JC, Paulson ES, Cook DB, Verber MD, Tian Q (2010) Detecting changes in human cerebral blood flow after acute exercise using arterial spin labeling: implications for fMRI. J Neurosci Methods 191: 258-262.

86. Querido JS, Sheel AW (2007) Regulation of cerebral blood flow during exercise. Sports Med 37: 765-782.

87. Kemppainen J, Aalto S, Fujimoto T, Kalliokoski KK, Langsjo J, et al. (2005) High intensity exercise decreases global brain glucose uptake in humans. J Physiol 568: 323-332.

88. Lowry CA, Lightman SL, Nutt DJ (2009) That warm fuzzy feeling: brain serotonergic neurons and the regulation of emotion. J Psychopharmacol 23: 392-400.

89. Marshall JM (2007) The roles of adenosine and related substances in exercise hyperaemia. J Physiol 583: 835-845.

90. Costa F, Heusinkveld J, Ballog R, Davis S, Biaggioni I (2000) Estimation of skeletal muscle interstitial adenosine during forearm dynamic exercise in humans. Hypertension 35: 1124-1128.